UNIVERSITY OF SOUTHAMPTON

FACULTY OF MEDICINE

Cancer Sciences Unit

Volume 1 of 1

Exploring the efficacy of anti-GD2 and anti-4-1BB monoclonal antibody therapy for the treatment of neuroblastoma

by

Carol Wareham BSc. (Hons), MRes.

Thesis for the degree of Doctor of Philosophy

September 2014

UNIVERSITY OF SOUTHAMPTON

ABSTRACT

FACULTY OF MEDICINE

CANCER SCIENCES UNIT

Thesis for the degree of Doctor of Philosophy

EXPLORING THE EFFICACY OF ANTI-GD2 AND ANTI-4-1BB MONOCLONAL ANTIBODY THERAPY FOR THE TREATMENT OF NEUROBLASTOMA

Carol Wareham BSc. (Hons) MRes.

Neuroblastoma is the most common solid malignancy of childhood. The majority of children present with metastatic disease, for which the prognosis remains poor despite intensive multi-modal conventional therapies. Monoclonal antibody (mAb) therapy targeting GD2, expressed on the surface of neuroblastoma cells, has shown considerable promise in these children. A 2009 study reported a significant survival benefit in children with high risk neuroblastoma receiving the antibody in addition to standard therapy. Anti-GD2 was administered in combination with the cytokines IL-2 and GM-CSF, with the aim of augmenting Natural Killer (NK) cell effector function. Although these results are encouraging, the immunotherapy was associated with considerable toxicity and a large proportion of patients still died from their disease.

An alternative strategy may be to combine anti-GD2 antibody with an immunostimulatory mAb. Rather than directly targeting tumour cells, such mAb enhance immune function by binding to co-stimulatory molecules within the immune system. Here I explore the effects of combining anti-GD2 with antibodies targeting the co-stimulatory molecule 4-1BB, which is up regulated on NK cells following Fc receptor engagement. Others have demonstrated that anti-4-1BB can be used to synergistically enhance the effects of other tumour targeting mAbs (rituximab, trastuzumab, cetuximab) in lymphoma, breast and epidermal growth factor receptor $(EGFR)^{+}$ carcinoma models respectively.

In this thesis I examine whether agonistic anti-4-1BB mAb can be used to enhance the efficacy of anti-GD2 in pre-clinical models. In both syngeneic and spontaneous murine neuroblastoma models, anti-GD2 plus anti-4-1BB mAb therapy was found to confer a significant survival advantage over mice receiving either mAb alone. Significant up-regulation of 4-1BB was observed on human NK cells following co-culture of peripheral-blood mononuclear cells with anti-GD2 opsonised neuroblastoma cells. Together these results support a novel immunotherapeutic approach in which antibodies can be used to target neuroblastoma cells and enhance the host immune response.

Table of contents

List of tables

List of figures

DECLARATION OF AUTHORSHIP

I, ...[please print name]

declare that this thesis and the work presented in it are my own and has been generated by me as the result of my own original research.

[title of thesis] .....

.....

I confirm that:

1. This work was done wholly or mainly while in candidature for a research degree at this University;
2. Where any part of this thesis has previously been submitted for a degree or any other qualification at this University or any other institution, this has been clearly stated;
3. Where I have consulted the published work of others, this is always clearly attributed;
4. Where I have quoted from the work of others, the source is always given. With the exception of such quotations, this thesis is entirely my own work;
5. I have acknowledged all main sources of help;
6. Where the thesis is based on work done by myself jointly with others, I have made clear exactly what was done by others and what I have contributed myself;
7. None of this work has been published before submission.

Signed:.....

Date:.....

Acknowledgements

I would like to thank the following people:

My supervisors Dr Juliet Gray and Professor Martin Glennie for their support, advice and guidance throughout this project. Dr Ferdousi Chowdhury for her day to day advice and support. Mr Stuart Dunn for his technical assistance processing and running samples. Professor Mark Cragg for his continual input and guidance, particularly throughout the first year of lab rotation projects.

The staff in the BRF Lisa Dunning, Vicky Field, Sam Martin, Charlotte Dunning and Mel Dunscombe for their technical assistance. A special thank you to Vicky for her patience when training me to handle – I was not 'a natural'.

Dr Claude Chan and Mrs Chris Penfold for producing several of the antibodies used throughout this project.

Everyone in the Antibody and Vaccine group for making the lab such a nice place to work.

Finally my husband, Toby for his patience and support.

Definitions and Abbreviations

ADCC	Antibody-dependent cellular cytotoxicity
ADCP	Antibody-dependent cellular phagocytosis
APC	Antigen presenting cell
BMDMs	Bone marrow-derived macrophages
Calcein-AM	Calcein-acetoxymethyl ester
$CD4^+$ T cell	CD4 positive T cell
$CD8^+$ T cell	CD8 positive T cell
CDC	Complement-dependent cytotoxicity
CDRs	Complementarity-determining regions
CFSE	Carboxyfluorescein succinimidyl ester
CLIP	Class II associated Ii peptide
COG	Children's Oncology Group
cSMAC	Central supramolecular activation complex
CTLs	Cytotoxic lymphocytes
DAMPs	Damage-associated molecular patterns
DAF	Decay-accelerating factor
EFS	Event free survival
EGFR	Epidermal growth factor receptor
ER	Endoplasmic reticulum
ERAD	ER-associated protein degradation
Fab	Antigen binding fragment
Fc	Constant fragment
FcγR	Fcγ receptor
FDA	Food and Drug Administration
GM-CSF	Granulocyte-macrophage colony stimulating factor
HAMA	Human anti-mouse antibodies
HEV	High endothelial venules
HLA	Human leucocyte antigen
HRP	Horseradish peroxidase
IFN-γ	Interferon-γ
Ig	Immunoglobulins
Ii	Invariant chain
IL	Interleukin
IL-7Rα	Interleukin-7 receptor-α

ILL	Innate-like lymphocytes
INSS	International Neuroblastoma Staging System
i.p.	Intraperitoneal
ITAM	Immunoreceptor tyrosine based activatory motif
ITIM	Immunoreceptor tyrosine based inhibitory motif
i.v.	Intravenous
KIRs	Killer cell immunoglobulin-like receptors
LFA-1	Leucocyte functional antigen-1
LRS	Leucocyte reduction system
mAb	Monoclonal antibodies
MAC	Membrane attack complex
MCP	Membrane cofactor protein
MDMs	Monocyte-derived macrophages
MDSCs	Myeloid-derived suppressor cells
MHC	Major histocompatibility complex
MICA	MHC class I chain related ligand A
MICB	MHC class I chain related ligand B
MIIC	MHC class II compartment
MRD	Minimal residual disease
MTOC	Microtubule organising centre
NK cell	Natural killer cell
NKT cells	Natural killer T cell
OMS	Opsoclonus-myoclonus syndrome
OVA	Ovalbumin
PAMPs	Pathogen-associated molecular patterns
PCD	Programmed cell death
PH	Pleckstrin homology
PI3-K	Phosphatidylinositol-3-kinase
PIP_2	Phosphatidylinositol 3,4-bisphosphate
PIP_3	Phosphatidylionositol 3,4,5-triphosphate
PS	Phosphatidylserine
pSMAC	Peripheral supramolecular activation complex
RAE-1	Retinoic acid early inducible-1-like transcript
S1P	Sphingosine 1-phosphate
SIOPEN	Society of Paediatric Oncology European Neuroblastoma Group
TAAs	Tumour-associated antigens

TAM	Tumour-associated macrophages
TAP	Transporter of antigen processing
TCR	T cell receptor
TH	Tyrosine Hydroxylase
TILs	Tumour-infiltrating lymphocytes
TLR (s)	Toll-like receptor (s)
Tregs	Regulatory T cells
ULBP	UL16 binding proteins
α-GalCer	α-galactosylceramide
β_2m	β_2 microgobulin

Chapter 1: Introduction

1.1 Neuroblastoma: An overview of the disease

After domestic accident, neuroblastoma is the second most frequent cause of mortality and the most common solid malignancy occurring in children under five (1). Neuroblastoma is a cancer of the sympathetic nervous system, arising from primordial neural crest cells. Unfortunately, over half of all cases present with disseminated disease (2) with metastasis to the lymph nodes, liver, bone or bone marrow. In terms of treatment the therapeutic strategy applied depends on disease stage and patient risk group. Following surgical resection, disease stage is determined in accordance with the International Neuroblastoma Staging System (INSS) developed in 1986 (3) and revised in 1993 (4). Using this system patients are assigned to one of four distinct prognostic groups, referred to as stage I, II, III and IV. The INSS disease stage, along with age at diagnosis, plus certain clinical/ biological features and prognostic variables are factors used to form a risk based schema, that in turn is used to assign patients to a risk group, namely low, intermediate, or high, and ultimately dictates the treatment schedule. Whilst the factors selected by the different co-operative groups, such as the Society of Paediatric Oncology European Neuroblastoma Group (SIOPEN) and the Children's Oncology Group (COG) are not standardised (5), children diagnosed with stage III or IV neuroblastoma, particularly those greater than one year of age, are generally assigned to an intermediate, or high risk group, especially if they have an amplified MYCN status (5). Amplification of the MYCN oncogene is an important prognostic marker in neuroblastoma, as high copy number, typically greater than ten copies per cell, is associated with rapid disease progression and an unfavourable clinical outcome (6, 7).

Prognosis is good for children assigned to the low risk group and this subset of patients often require limited therapeutic intervention (8-11), whereas assignment to the high risk group normally necessitates intensive multi-modal treatment regimens. Standard treatment for high risk neuroblastoma involves induction chemotherapy plus surgery and/or radiotherapy to eradicate gross residual disease, followed by myeloablative chemotherapy with autologous bone marrow transplantation and 13-cis-retinoic acid (isotretinoin). This

therapeutic strategy was established based on the results of a randomised, controlled trial published by Matthey *et. al.* in 1999 (12). Patients recruited onto this study all received the same induction chemotherapy before being randomly assigned to a further treatment group. Patients that went on to receive myeloablative chemotherapy with autologous bone marrow transplantation showed a significant improvement in event free survival (EFS) compared to patients that received a further three cycles of intensive chemotherapy (12). Subsequent administration of 13-cis-retinoic acid, which has been shown to reduce proliferation and induce differentiation of neuroblastoma cell lines including some established from refractory tumours (13-16), was also associated with a significant improvement in EFS regardless of prior therapy (12). Many high risk neuroblastoma patients achieve clinical remission as a result of this intensive multi-modal treatment regimen; however, toxicity is significant. Matthay *et al.* reported grade 3 or 4 toxic effects based on the National Cancer Institute toxicity criteria as a result of induction therapy alone, with further complications, such as interstitial pneumonitis and veno-occulsive disease arising as a consequence of myeloablative therapy (12). Sadly 5–8 % of patients die from treatment related causes (12). Despite many children achieving clinical remission following therapy long term prognosis remains poor, with the three year EFS among high risk patients reported to be as low as 30-40 % (17, 18). Poor prognosis is attributed to residual tumour cells that survive therapy and eventually give rise to recurrent refractory disease (19). The ability to eradicate these residual tumour cells, termed minimal residual disease (MRD), and maintain disease remission remains a major challenge that needs to be overcome in order to improve long term survival in high risk neuroblastoma patients.

The adverse effects associated with treatment of high risk neuroblastoma are already severe and often dose limiting. Hence there is little scope for introducing more aggressive therapies; instead there is an urgent requirement for more efficacious, less toxic therapeutic strategies that confer long term survival. Immunotherapies, particularly in the form of monoclonal antibodies (mAb) that target tumour-specific antigens, represent an attractive alternative to current treatment. Immunotherapy is a method of treating disease using components of the immune system to induce, enhance, or suppress normal immune effector function. Anti-cancer immunotherapies aim to destroy and eradicate tumour cells and in some cases may be able to promote long term

anti-tumour immunity, *i.e.* a memory response, to protect against regrowth. The genetic aberrations that occur as cancer develops can result in the expression of proteins, or tumour-associated antigens (TAAs) on the cell surface that differ from normal cells and therefore have the potential to be recognised as foreign (20). Additionally, the abnormal expression of self-antigens on tumour cells may also alert the immune system to potential danger. An ideal immunotherapy would target an antigen that is expressed exclusively, or almost exclusively, on tumour cells. A number of TAAs are reportedly expressed in neuroblastoma (as summarised in table 1) and may represent suitable targets for immunotherapy.

Table 1-1. Tumour-associated antigens reported to be expressed by human neuroblastoma tumours

Antigen	Nature of antigen	Tumour expression	Normal tissue expression
MYCN	Transcription factor and proto-oncogene	Over expression in > 40 % of patients with metastatic disease	Minimal beyond foetal development
Disialoganglioside GD2	Glycolipid	100 % patients	CNS neurons and peripheral nerve fibres
Tyrosine hydroxylase	Catecholamine biosynthesis	100 % samples	Adrenal medulla and CNS dopaminergic neurons
Hu antigens	Neuronal-specific RNA binding proteins	80 % patients express HuD	Central and peripheral nervous tissue
Survivin	Inhibitor of apoptosis	Expression in 26/26 high risk patients	Low or absent in normal tissue
Melanoma antigen A (MAGE) family	Cancer germline antigens	8/10 patients express at least one MAGE family antigen	Little expression in normal tissue other than testis
NY-ESO-1	Cancer germline antigen	18/22 (82 %) samples	Normal tissue expression restricted to testis
Preferentially expressed Antigen in Melanoma (PRAME)	Cancer germline antigen	87/94 (93 %) samples	Normal tissue expression restricted to testis
Anaplastic lymphoma kinase	Receptor tyrosine kinase	Expression in 14/16 samples	Limited expression on neuronal tissue

Table taken from (21), reproduced with kind permission from Dr Juliet Gray

In summary there are two major goals of anti-cancer immunotherapy. Firstly, immunotherapies aim to mimic the exquisite specificity cells of the immune system have for their target antigen, thus permitting recognition and subsequent elimination of tumour-antigen bearing cells, whilst innocent bystander cells (*i.e.* healthy cells) escape unscathed. Secondly, immunotherapies may trigger the generation of immunological memory towards the tumour, which would provide long term protection against

recurrence and may improve survival. Taken together the potential for immunotherapies to offer a more specific, less toxic treatment strategy and confer immunological memory, thus improving long term survival means there is considerable interest in the use of immunotherapies for the treatment of high risk neuroblastoma.

1.2 Cancer immunotherapy and the immune system

Immunotherapy is a method of treating disease using components of the immune system. By inducing, or enhancing immune effector function, cancer immunotherapies aim to destroy and clear tumour cells, and in some cases may be able to promote long term anti-tumour immunity to protect against re-growth. There are two clinically relevant categories of immunotherapy used to target malignancy, these immunotherapeutic agents can be classified as either passive, or active. Passive immunotherapies are not dependent on the host's own immune system to attack disease, instead immune components created outside the body, *i.e.* in a laboratory, are administered to the patient. Direct targeting mAb, such as trastuzumAb (Herceptin®), cetuximab (Erbitux®) and rituximab (Rituxan®) are examples of passive immunotherapies. In contrast, active immunotherapies effectively hijack the patient's own immune system to promote an immune response against the tumour cells. More recently a new group of mAb that can be classified as active immunotherapies have been introduced, rather than directly targeting TAAs these immunomodulatory mAb recognise key receptors on the surface of immune cells. Immunomodulatory mAb therefore potentiate T cell responses by acting as surrogate ligands for these co-stimulatory molecules and provide agonistic or counter-inhibitory signals. Figure 1.1 summarises the main passive and active immunotherapy approaches that have been applied for the treatment of cancer.

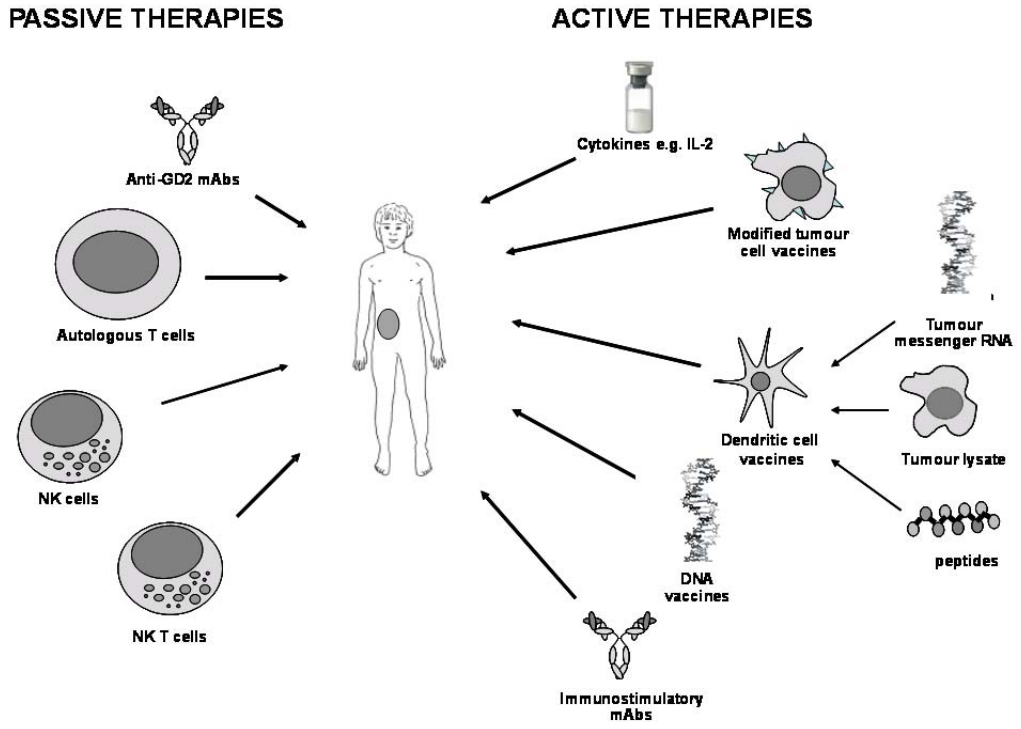

Figure 1-1. Passive and active immunotherapy approaches for the treatment of cancer.
Figure taken from (21), kindly provided by Dr Juliet Gray.

The rational design of immunotherapeutic approaches for the treatment of cancer requires a detailed understanding of how the immune system functions under normal physiological conditions and how it responds to cancer.

1.2.1 The immune system

The main function of the immune system is to defend the body against infectious agents that, if left unchecked, would cause disease. These immune responses are classified as either innate, or adaptive. Innate immune responses are front line non-specific defence mechanisms that are immediately available upon exposure to pathogens but do not usually impart lasting immunity. Cells of the innate immune system express a number of germline encoded pattern recognition receptors, called Toll-like receptors (TLRs) due to their similarity to the Toll receptor originally identified in *Drosophila* (22). The mammalian homologue of *Drosophila* Toll receptor was first identified in 1997 (23) and was quickly followed by the discovery of a whole family of proteins structurally related to *Drosophila* Toll (24). The TLRs recognise and bind to highly conserved, invariant (within a given class of organism) pathogen-associated molecular patterns (PAMPs), including but not limited to, peptidoglycan and

lipopolysaccharide (LPS), *i.e.* the components of Gram positive and Gram negative bacterial cell walls, as well as double-stranded RNA and unmethylated CpG motifs frequently found in bacterial DNA (25). Once the immune system is alerted to the presence of infection the innate response is initiated within minutes and proceeds for the first few hours and days of infection. However, if the innate immune response is unable to clear the infection a more sophisticated adaptive immune response is generated, which takes several days to evolve. Adaptive immune responses are acquired throughout an individual's lifetime in response to infection with a certain pathogen and are highly antigen-specific. They also confer immunological memory resulting in an enhanced immune response upon subsequent exposure, thus providing lifelong protection against re-infection with the same pathogen. Adaptive immune responses are initiated when a lymphocyte bearing receptors with unique specificity for a target antigen encounter that antigen. Upon antigen recognition the activated lymphocyte starts to divide, producing a clone of identical progeny all bearing receptors specific for the same target antigen (26, 27). Clonal expansion of the antigen-specific B (*b*one marrow-derived) and T (*t*hymus-derived) lymphocytes gives rise to the humoral and cell-mediated components of the adaptive immune response respectively. In general, humoral, *i.e.* antibody, responses protect against extracellular bacteria and toxins, whereas cell-mediated responses provide protection against intracellular bacteria and viruses.

Pathogen specificity and immunological memory are two key features of the adaptive immune response that distinguish it from innate responses. However, these two branches of the immune system work closely together to eradicate infection and prevent disease. Recognition of PAMPs alerts the immune system to both the presence, and nature of the pathogen, resulting in the production of cytokines and up regulation of co-stimulatory molecules (25). These in turn activate T cells, which are involved in both the killing of infected cells and the provision of essential signals required for the production of antibody by antigen stimulated B cells, thus bridging the gap between innate and adaptive responses.

1.2.1.1 Humoral immunity

The term 'humoral' is used to describe the non-cellular components of the blood, thus humoral immunity was so called because it involves immunologic responses mediated by non-cellular molecules, such as secreted antibodies, or complement proteins. Antibodies are the secreted form of the membrane bound immunoglobulins (Ig) located on the B cell surface, which are involved in antigen recognition and referred to as the B cell receptor. Immunoglobulins of the same antigen specificity are secreted as 'antibodies' by terminally differentiated B cells, *i.e.* the plasma cells.

Antibody structure and function

Antibodies have two distinct functions, the first is to bind to their specific antigen, which is produced by the pathogen that elicited the immune response, and the second is to recruit immune cells and molecules responsible for the destruction of the pathogen. The basic structure of an antibody comprises of four polypeptide chains joined together by disulphide bonds (28). The basic structure of a human IgG antibody is illustrated in figure 1.2. Each IgG antibody comprises of two identical heavy and two identical light chains containing several Ig domains that are held together by disulphide bonds and non-covalent interactions. The light chains fold to form one variable (V_L) and one constant (C_L) domain, whereas the heavy chains comprise of one variable (V_H) and three constant (C_H) domains (29). The variable regions of the heavy and light chains combine to form the antigen binding (Fab) fragment. The variable regions of the heavy and light chains each contain three hyper variable regions that are brought together when the chains combine to form a single hyper variable point and the tip of each arm, thus creating two identical antigen binding sites. The regions between the hyper variable regions provide the framework allowing the hyper variable regions to combine to form six hyper variable loops that determine antigen specificity. These six hyper variable loops form a surface complementary to the antigen and are known as the complementarity-determining regions (CDRs). Whilst the Fab fragment determines antigen specificity, the constant (Fc) fragment, which comprises of the two heavy chains, determines the Ig isotype. There are five Ig isotypes, IgM, IgD, IgG, IgA and IgE, and the heavy chain of each isotype is denoted μ, δ, γ, α, and ε respectively. IgG is the most abundant isotype in humans and can be further divided into one of four different subclasses, namely IgG1–4. Four

different subclasses also exist in mice, known as IgG1, IgG2a, IgG2b and IgG3 (30). Once bound to its target antigen on the cell surface via CDR interactions the Fc portion of the antibody interacts with a variety of effector cells and molecules through which it exerts its effector function.

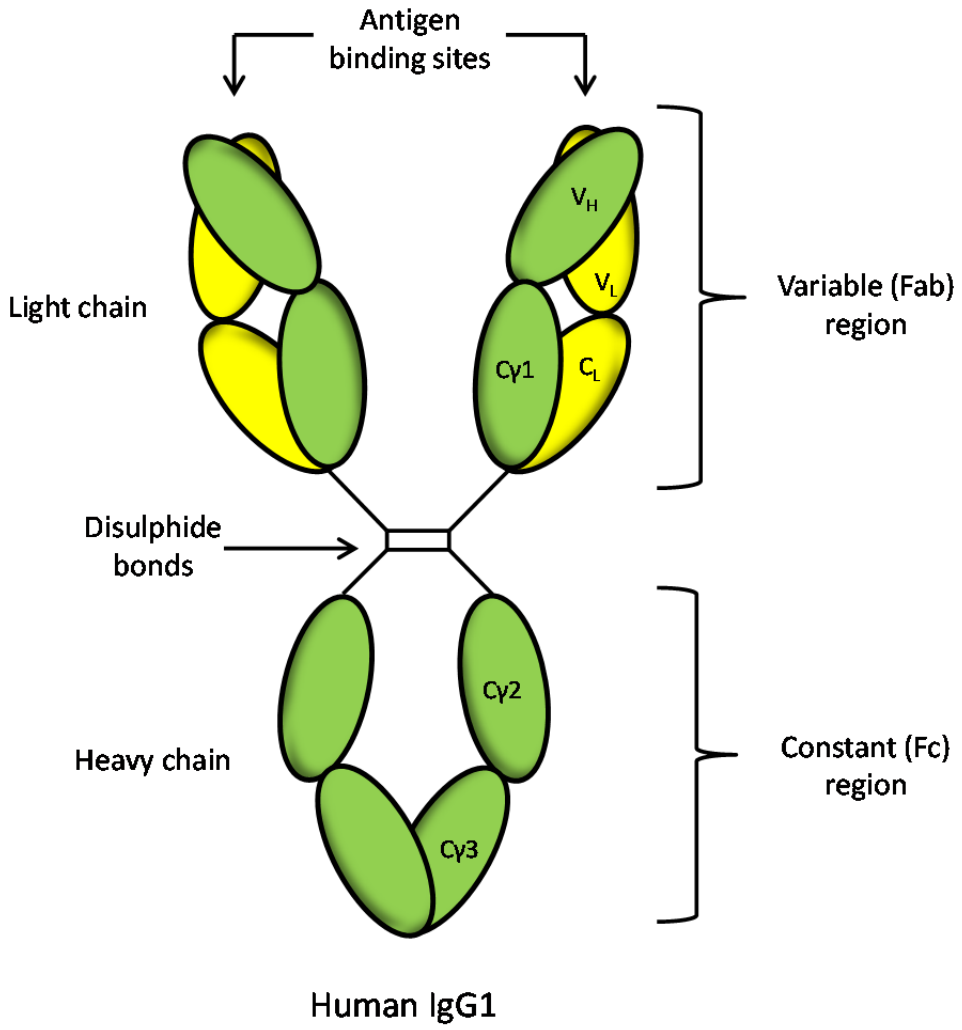

Figure 1-2. The basic structure of an antibody. Each antibody is composed of two identical heavy and light chains joined together by disulphide bonds and non-covalent interactions. Both the heavy and the light chains combine to form the variable (Fab) region that contains the antigen binding sites and the two heavy chains combine to form a constant (Fc) region that determines effector function.

The Fcγ receptor family

The Fcγ receptors (FcγRs) are a group of surface glycoproteins belonging to the Ig receptor superfamily that bind the Fc portion of IgG. The various FcγR subtypes are differentially expressed on the surface of leucocytes and each receptor preferentially recognises one, or more, of the different IgG heavy

chain isotypes. Hence the antibody isotype determines which effector cells are initiated in the immune response. In humans three different classes of FcγR have been described, known as FcγRI (CD64), FcγRII (CD32) and FcγRIII (CD16). FcγRII and FcγRIII can be further subdivided into their different isoforms: two isoforms of FcγRII have been identified, referred to as FcγRIIA and FcγRIIB, along with three isoforms of FcγRIII, referred to as FcγRIIIA, FcγRIIIB and FcγRIIIC. Additionally, four different classes of FcγR have been described in mice, known as FcγRI, FcγRII, FcγRIII and FcγRIV. Mouse FcγRIV is considered to be the orthologue of human FcγRIIIA, whereas mouse FcγRIII is most closely related to human FcγRIIA (30).

Classification of the FcγR is determined by the affinity for the Fc fragment of the antibody to which they bind and the signalling pathways this promotes. FcγRI is the only high affinity receptor in both humans and mice and binds to the IgG1 and IgG3 subclasses in humans, or the IgG2a subclass in mice with an affinity of 10^8–10^9 M^{-1} (30). The other FcγR have much lower affinity (in the low to medium micromolar range) and a more general subclass specificity (30). The mouse medium affinity FcγRIV selectively interacts with mouse IgG2a and IgG2b, which are the most pro-inflammatory IgG molecules and show greater activity than mouse IgG1 and IgG3 in many *in vivo* model systems (31). In normal physiological situations the relatively low affinity of the FcγR is functionally important as it reduces the likelihood of monomeric antibody molecules, which are naturally present as high concentrations in the serum, from binding FcγR thus promoting non-specific activation of pro-inflammatory responses. FcγRIIB, which is conserved between humans and mice is the only known inhibitory FcγR and comprises of a single chain bearing an immunoreceptor tyrosine based inhibitory motif (ITIM) in its cytoplasmic region, through which it exerts an inhibitory signal. All other FcγR are activatory and, excluding human FcγRIIIB, activate signalling pathways through the immunoreceptor tyrosine based activatory motif (ITAM) contained in their cytoplasmic region. FcγR are widely expressed on cells of the haematopoietic system, although there is little evidence to suggest they are present on T cells (30). Innate immune effector cells, such as dendritic cells, monocytes, macrophages, basophils and mast cells all express both activatory and inhibitory FcγR. However, natural killer (NK) cells solely express FcγRIIIA (CD16) suggesting these cells might be potent mediators of antibody-dependent cellular cytotoxicity (ADCC), whereas B cells only express the inhibitory

receptor FcγRIIB, thus regulating activatory signals generated by the B cell receptor (30).

1.2.1.2 Cell mediated immunity

In contrast to humoral immunity, which involves the non-cellular components of the immune system e.g. antibodies and complement proteins. Cell mediated immunity, as the name suggests, involves the activation of a variety of cells of the immune system, including NK cells, phagocytes and antigen-specific $CD8^+$ T cells. Therefore, like humoral immunity cell mediated immune responses fall under both the innate and adaptive arms of the immune system.

Natural killer cells

NK cells are a subset of lymphocytes that arise from the common lymphoid progenitor and circulate in the blood. NK cells represent the third major lineage of lymphocytes (32), the other lineages being the antibody producing B cells briefly mentioned in the previous section, and the T cells. Human NK cells can be distinguished from other lymphocytes on the basis of their expression of the adhesion molecule CD56 and lack of surface CD3. Murine NK cells do not express CD56; instead they are usually identified by their expression of the integrin α-subunit CD49b. However, like their human counterpart, murine NK cells also lack surface CD3 (33). NK cells possess cytotoxic granules in their cytoplasm and are capable of killing virally infected and/ or tumour cells, through the release of toxic substances, such as perforin and the serine protease granzymes. NK cells can exert their cytotoxic effect without the need for prior immunisation, or activation and are therefore considered to be part of the innate immune system. The ability of NK cells to distinguish virally infected and/ or tumour cells from normal healthy cells can be explained by the 'missing, or altered-self' hypothesis formulated by Klas Kärre (34), following the observation that NK cells have the ability to lyse major histocompatibility class (MHC) I negative target cells (35). The missing-self hypothesis predicted that NK cells express inhibitory receptors that recognise and bind self MHC class I molecules (or the equivalent, human leucocyte antigen (HLA) class I molecules), which are present on the surface of all nucleated cells. As illustrated in figure 1.3 under normal physiological conditions engagement of these inhibitory receptors by self MHC/ HLA class I molecules overrides any activating signals received by the NK cells, allowing them to tolerate healthy

cells (see figure 1.3 a). Both virally infected, and tumour cells typically express little to no MHC/ HLA class I molecules, either as a consequence of disrupted protein synthesis, or as a mechanism of evading cytotoxic CD8+ T cells, and as a consequence of this 'missing-self' the inhibitory signal is lost, rendering these cells susceptible to NK cell mediated killing (36) (see figure 1.3 b).

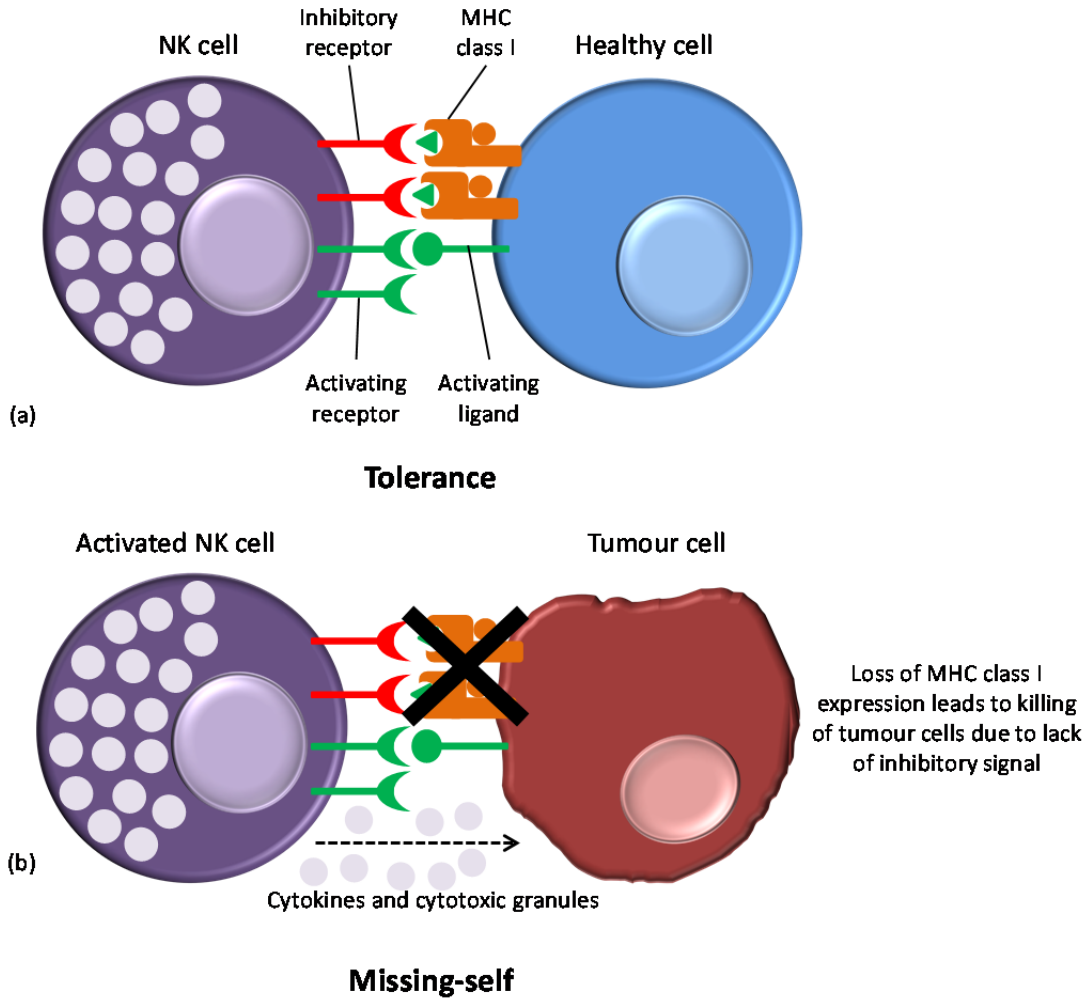

Figure 1-3. The missing-self hypothesis. Natural killer cells are able to tolerate healthy cells as any activating signals they receive upon encounter are overridden following the engagement of inhibitory receptors by self MHC/ HLA class I molecules, which are expressed on all nucleated cells (a). Both virally infected and tumour cells lack MHC/ HLA class I molecules and as a consequence of this 'missing-self' the overriding inhibitory signal is lost, rendering these cells susceptible to NK cell mediated killing (b). Figure adapted from (36).

NK cell receptors

NK cells detect changes in expression of MHC, or HLA class I molecules by integrating signals from two different types of cell surface receptor, which work together to fine tune their cytotoxic activity (37). These cell surface receptors are classified as either activatory, or inhibitory. The activatory and inhibitory receptors that recognise MHC, or HLA class I molecules, thus regulating NK cell activity, belong to two large families that contain numerous other receptor types. These include the killer lectin-like receptors (KLRs), which are homologous with the C-type lectins, and killer cell immunoglobulin-like receptors (KIRs). KIRs are type-I transmembrane glycoproteins with two to three immunoglobulin-like domains that have either long cytoplasmic tails containing ITIMs, or short cytoplasmic tails containing ITAMs, and are encoded by the leucocyte receptor complex located on chromosome 19 (33). The majority of KIRs are inhibitory and the interaction between a self-specific KIR and its cognate HLA class I ligand is fundamentally important for a process called licensing (38) a critical stage in the functional development of NK cells. Licensed NK cells that express inhibitory KIR for self-specific HLA class I ligands have a higher capacity for response than unlicensed NK cells, which do not recognise self-specific HLA class I ligands. Unlicensed NK cells, such as those found in MHC or HLA class I deficient mice, or patients, are hyporesponsive *in vitro*. Additionally, these individuals do not develop autoimmune disorders (39-41), which is seemingly at odds with the missing-self hypothesis. The observation that NK cells arising in mice that express MHC class I are responsive, whilst those arising in MHC class I deficient mice are hyporesponsive led to the proposal of two opposing models known as the ‘arming’ and ‘dis-arming models’ (42). The arming model hypothesized that functional maturation of NK cell pre-cursors requires interaction with cognate MHC class I positive cells, thus NK cells that do not encounter their cognate MHC class I ligand remain unarmed and therefore hyporesponsive (43). The dis-arming model proposes that high functional responsiveness is acquired by default; however, NK cell are prevented from acquiring, or retaining full responsiveness when an encounter with other self-cells results in over-stimulation (43). Over-stimulation can occur in the absence of MHC class I expression, as the NK cell does not receive an overriding inhibitory signal and will ultimately become functionally anergic (43). Several studies have acquired data that supports the dis-arming model (44-46). However, the possibility that

functionally mature, licensed NK cells that recognise self-specific MHC class I ligands may be subsequently inactivated cannot be ruled out.

Mice lack KIRs, instead they express functionally equivalent C-type lectin-like Ly49 receptors encoded by the NK gene complex located on chromosome 6. Different isoforms of the Ly49 receptor exist (33), including the activatory LY49D, H and P (32), although the majority of the Ly49 receptors are inhibitory and recognise the classical MHC class I molecules H2-K and D/L (33). Some of the key activatory and inhibitory NK cell receptors and their cognate ligands are summarised in figure 1.4.

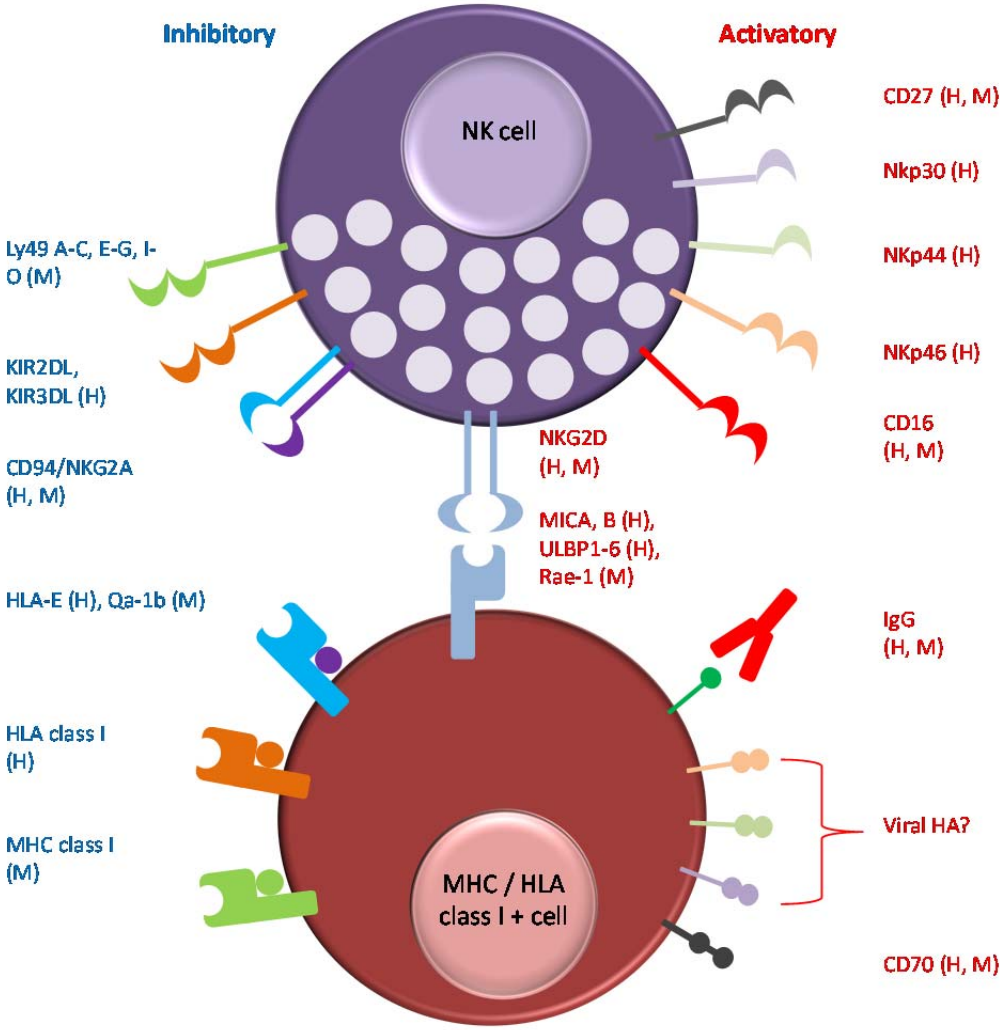

Figure 1-4. Key activatory and inhibitory NK cell receptors and their cognate ligands in humans (H) and mice (M). Figure adapted from (47).

The NKG2 receptors

Both human and murine NK cells express the C-type lectin-like heterodimer CD94/NKG2, this receptor interacts with non-polymorphic HLA-E in humans, and Qa-1 in mice. These MHC-like molecules bind to leader peptide fragments from other MHC class I molecules, allowing the CD94/NKG2 heterodimer to detect many different MHC class I molecules (33). The NKG2 family comprises of several members including NKG2A, B, C, D, and E. NKG2A and B are inhibitory receptors, whereas NKG2C and D are activatory receptors. NKG2D is distinct from the rest of the family as it does not dimerise with CD94, it also differs in terms of the signalling pathway it triggers within the cell. Once activated NKG2D binds to the adaptor molecule DAP10, which does not contain an ITAM, instead it activates the intracellular lipid modifying enzyme phosphatidylinositol-3-kinase (PI3-K), leading to localised production of phosphatidylionositol 3,4,5-triphosphate (PIP_3) via phosphorylation of phophatidylinositol 3,4-bisphosphate (PIP_2). PIP_3 subsequently recruits signalling proteins that contain pleckstrin homology (PH) domains, such as Akt, to the plasma membrane.

NK cell activation

All mature NK cells constitutively express FcεR1-γ, CD3-ζ and DAP12 transmembrane bound proteins, that form homodimers, or in the case of FcεR1-γ and CD3-ζ heterodimers, that contain ITAMs in their cytoplasmic domains (48). Activatory receptors are associated with these adaptor molecules and upon receptor engagement the ITAMs are phosphorylated by Src family kinases. This leads to the recruitment of intracellular tyrosine kinases, such as Syk or Zap-70, and triggers a cascade of downstream signalling events culminating in the re-organisation of the actin cytoskeleton, which is required for cell polarisation and release of cytotoxic granules by exocytosis, as well as transcription of a variety of cytokine and chemokine genes (48). The cytotoxic granules contain perforin and the serine protease granzymes. Upon release perforin undergoes calcium-dependent polymerisation and forms pores in the target cell membrane, facilitating delivery of the granzymes into the target cells and trigger apoptosis by caspase-dependent and independent means.

One activatory receptor of note is CD16 whose γ-chain is directly associated with the FcεR1-γ and CD3-ζ heterodimer. Consequently, whereas most NK cell

activatory receptors require antibody to crosslink pairs, or combinations of receptors simultaneously to achieve a critical threshold of activation, the engagement of CD16 by the Fc portion of an antibody is sufficient to elicit cytotoxic activity, or cytokine secretion, (48). Hence NK cells are considered to be important mediators of ADCC.

T cells

Adaptive cell mediated immune responses occur following the clonal expansion of antigen-specific T cells. T cells are a subset of lymphocytes that arise from the common lymphoid progenitor cells in the bone marrow and mature in the thymus. T cells can be identified by their expression of antigen-specific receptors located on the cell surface, known as T cell receptors (TCRs). TCRs recognise specific antigen peptide fragments bound to MHC molecules, so as to form a peptide: MHC complex and presented to them by the host's own cells (49). T cells can be divided into two distinct classes based on their expression of two usually mutually exclusive membrane glycoproteins, known as CD8 and CD4 co-receptors. The CD8 and CD4 co-receptors have a key role in T cell activation through their ability to recognise MHC class I and MHC class II molecules respectively. CD8 positive ($CD8^+$) T cells recognise antigenic peptide fragments derived from intracellular (endogenous) pathogens presented to them via MHC class I molecules. Whereas, CD4 positive ($CD4^+$) T cells are involved in recognition of antigenic peptide fragments derived from extracellular (exogenous) pathogens, presented to them via MHC class II. Upon recognition of their specific antigen, naïve $CD8^+$ and $CD4^+$ are induced to differentiate into effector cells with distinct immunological functions designed to facilitate removal of antigen. The processes involved in antigen recognition, generation of effector cell populations and the subsequent removal of antigen will be summarised in the following sections.

The T cell receptor

The specificity a T cell has for its target antigen is conferred by the TCR. The TCR is a heterodimeric surface bound molecule comprised of two different polypeptide chains, denoted either α and β, or γ and δ, joined together by a disulphide bond. The vast majority of T cells possess TCRs comprising of the α:β heterodimer but a small subset possess the γ:δ heterodimer. Each T cell bears approximately 30,000 identical TCRs on its surface, which are

responsible for antigen recognition. However, the TCR does not bind antigen directly, instead it recognises specific peptide fragments of antigenic proteins, which are bound to MHC molecules expressed on the surface of other host cells. The TCR heterodimer is expressed in conjunction with four invariant polypeptide chains (denoted ε, δ, and γ), which together with the disulphide linked homodimer ζ-chain is collectively known as the CD3 complex as shown in figure 1.5.

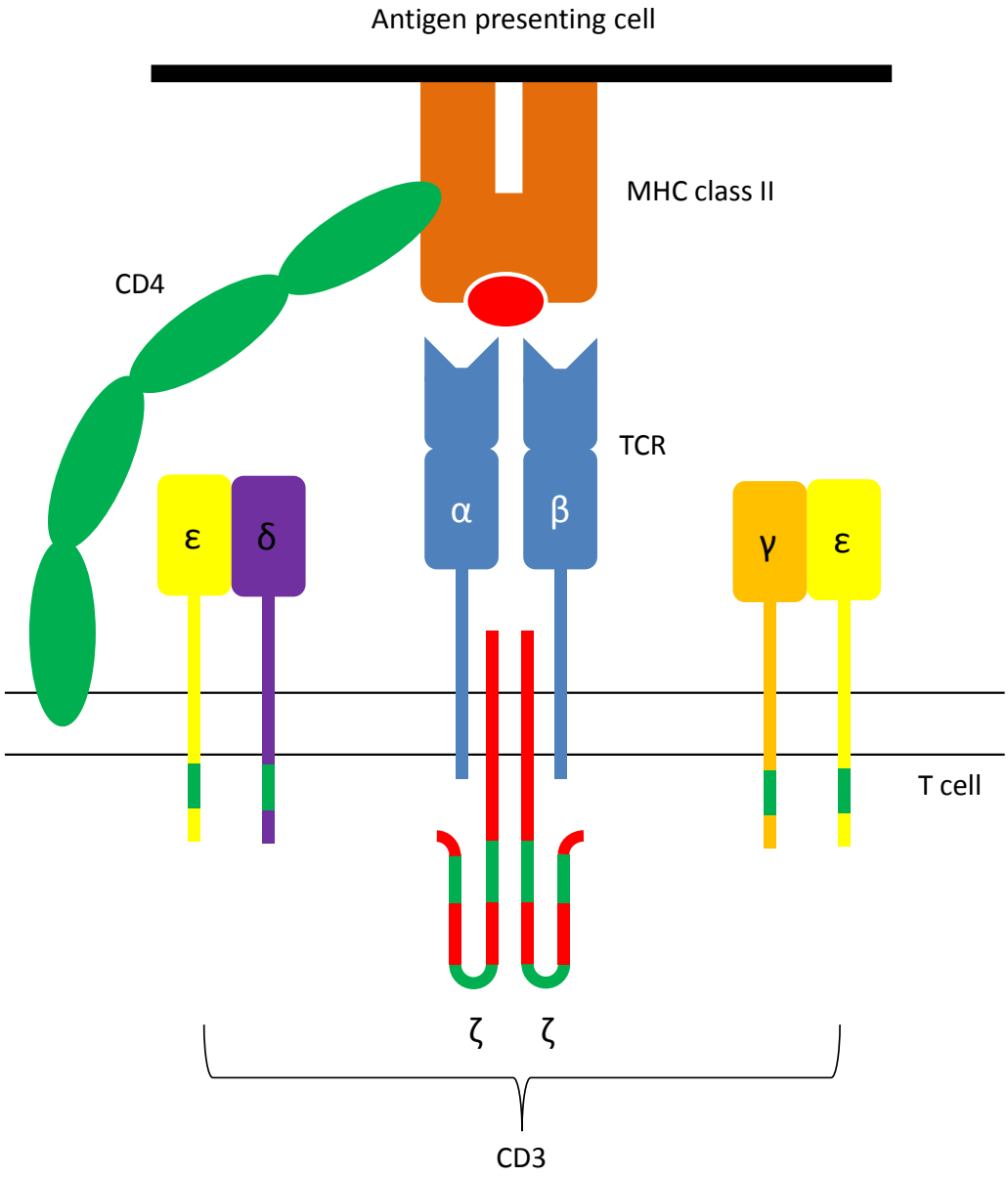

Figure 1-5. A schematic representation of the T cell receptor CD3 complex. An antigenic peptide fragment is presented by an MHC class II molecule on the surface of an antigen presenting cell. The CD4 co-receptor, which is associated with the TCR CD3 complex binds to an invariant region of the MHC class II molecule. The CD3 complex itself comprises of five invariant polypeptide chains made up of two heterodimers (γε and δε) plus a homodimer of two ζ-chains. The TCR CD3 complex contains a total of ten ITAMs (shown in green), which are involved in signal transduction.

The CD3 complex is involved in signal transduction upon recognition of antigen by the TCR and contains a total of ten ITAMs, one in each of the four polypeptide chains and six in total (three per chain) in the ζ-chain homodimer. Hence TCR signalling is initiated following phosphorylation by Src family kinases.

Antigen processing and presentation

MHC class restriction means that mature, naïve T cells only recognise their specific peptide antigen when it is presented to them in the form of a peptide MHC complex. Consequently, before an antigen can be presented to a T cell it must first be processed into peptide fragments and loaded onto MHC molecules. Almost all nucleated cells express MHC class I and are able to present antigenic peptide fragments to primed $CD8^+$ T cells making them potential targets for cytotoxic lymphocytes (CTLs). Expression of MHC class II molecules, involved in presentation of antigenic peptides to $CD4^+$ T cells, is limited to professional antigen presenting cells (APCs), namely dendritic cells, B cells and macrophages. Early investigations found that endogenous antigens were processed in the cytosol and presented by MHC class I molecules, whereas exogenous antigens were taken up and processed by endocytic pathways before presentation by MHC class II molecules. However, work published in the mid-1970s confirmed that this distinction was not absolute, as exogenous antigens can also be expressed by MHC class I molecules and this phenomenon was termed cross-presentation (50).

Presentation of endogenous antigen by MHC class I

Endogenous antigens of cytosolic, or nuclear origin are broken down into peptide fragments containing 8-10 amino acids that preferentially fit within the antigen binding groove of MHC class I molecules, resulting in the formation of peptide-MHC complexes. These proteins are cleaved into the appropriate sized peptide fragments by large cylindrical complexes of proteases called proteasomes. The peptide fragments are subsequently translocated into the rough endoplasmic reticulum (ER) by the transporter of antigen processing (TAP). In the ER the MHC class I heterodimer is formed, comprising of a polymorphic heavy chain, and a light chain called β_2 microglobulin (β_2m). In the absence of peptide the MHC class I molecules are stabilised by ER chaperone proteins, such as calrecticulin, ERp57, protein disulphide isomerase (PDI) and tapasin (51). Tapasin interacts with TAP combining peptide translocation into the ER with peptide delivery to MHC class I molecules. Once peptides bind MHC class I molecules the chaperone proteins are released, and the fully assembled peptide: MHC class I complexes leave the ER and are presented on the cell surface. A large proportion of the MHC class I proteins do not bind antigenic peptides (52) and they are subsequently

degraded (along with any misfolded MHC class I molecules) by the ER-associated protein degradation (ERAD) system. This system involves the retro-translocation of the MHC class I molecules from the ER into the cytosol, where they are ubiquitinated, thus targeting them for degradation by the proteasome (53). A schematic representation of the steps involved in endogenous antigen processing and presentation is shown in figure 1.6.

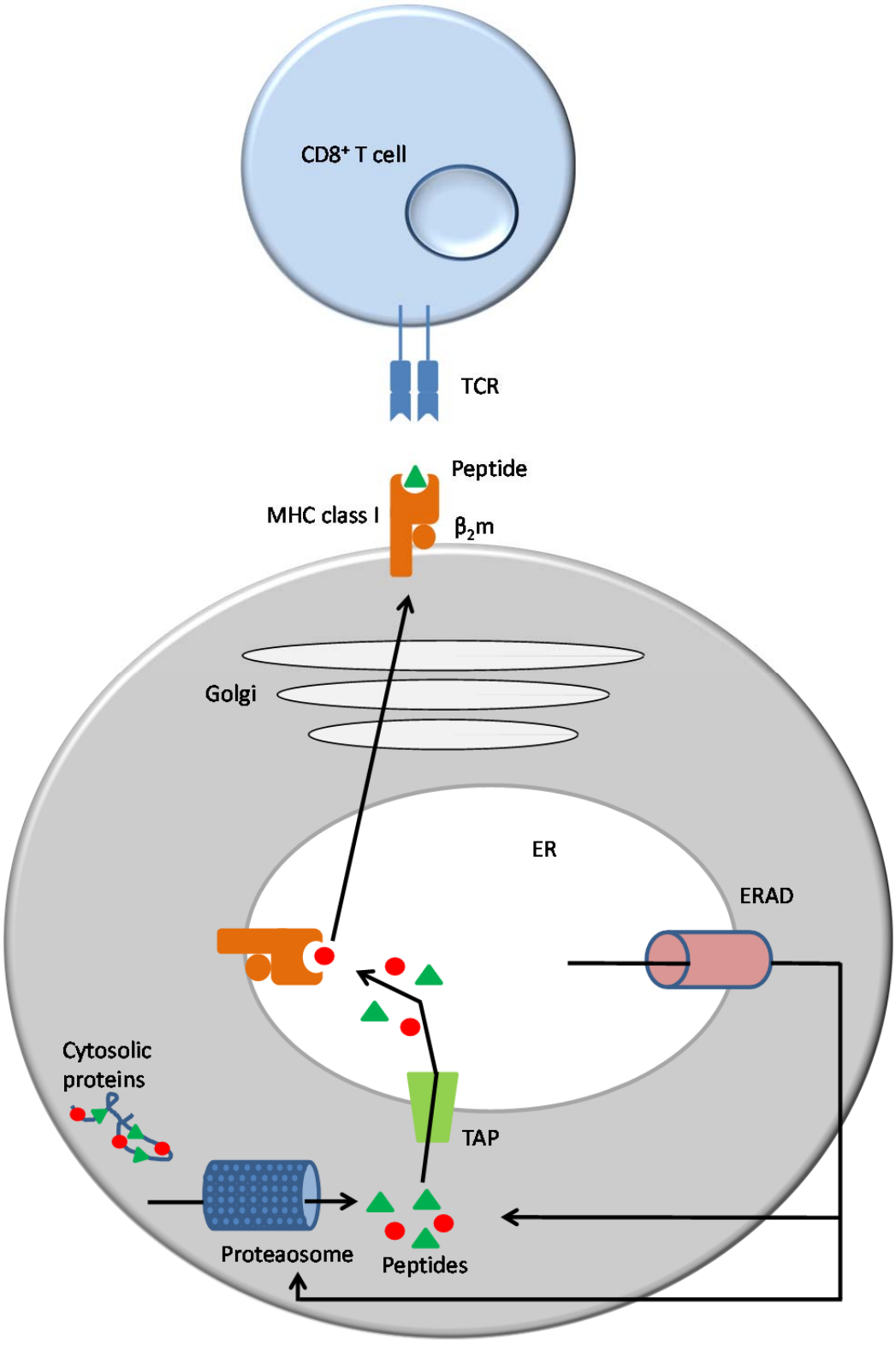

Figure 1-6. Endogenous antigen presentation by MHC class I. Presentation of endogenous antigenic peptides to $CD8^+$ T cells occurs in a step wise process. First, antigens are degraded by the proteasome, the resulting antigenic peptide fragments are transported by the transporter associated with antigen presentation (TAP) into the endoplasmic reticulum (ER) and loaded onto MHC class I molecules. Peptide: MHC complexes are subsequently released from the ER and transported via the golgi to the plasma membrane, where they are presented to $CD8^+$ T cells. Figure adapted from (51).

Presentation of antigen by MHC class II

Once taken up by professional APCs by phagocytosis, or endocytosis, exogenous antigens are degraded in the endocytic compartment by proteases. The transmembrane α and β chains of MHC class II are assembled in the ER and associate with a trimeric protein, known as the invariant chain (Ii), which occupies the binding groove of the MHC class II molecule and thus prevents binding of endogenously synthesised peptides (54). The resulting Ii-MHC class II complex is transported to a late endosomal compartment, known as the MHC class II (MIIC) compartment. Ii is digested in the MIIC leaving a residual class II associated Ii peptide (CLIP) in the antigen binding groove. Exchange of CLIP for a specific peptide derived from a protein degraded in the endocytic compartment is facilitated by HLA-DM in humans or H2-DM in mice (51). Once the exchange has taken place MHC class II molecules are subsequently transported to the plasma membrane to present peptide to $CD4^+$ T cells. A schematic of the steps involved in exogenous antigen processing and presentation is shown in figure 1.7.

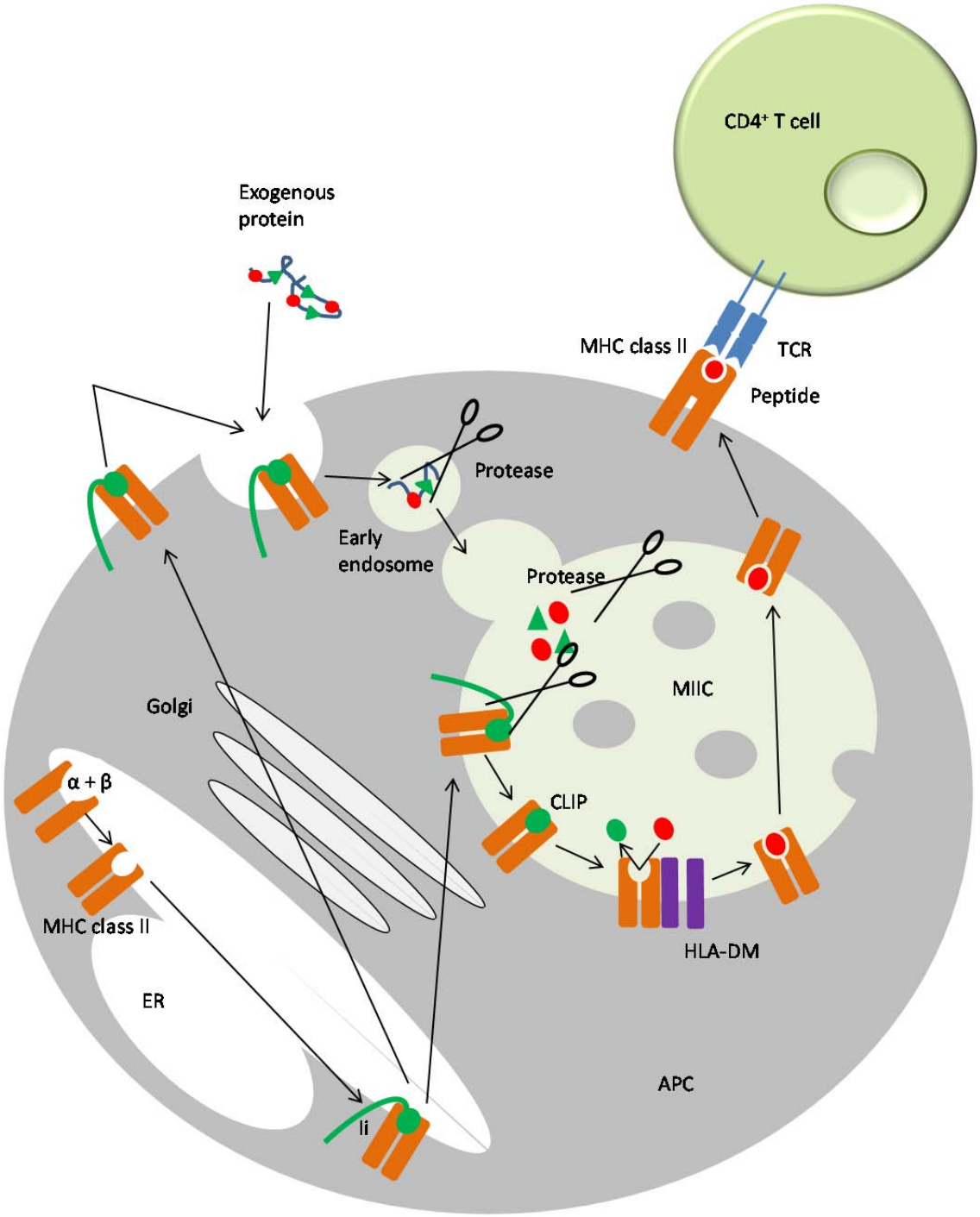

Figure 1-7. Exogenous antigen presentation by MHC class II. MHC class II α and β chains come together in the ER and form a complex with the invariant chain Ii. The Ii-MHC class II heterotrimer is transported via the golgi to the MHC class II compartment (MIIC) directly, or via the plasma membrane. Endocytosed proteins and Ii are degraded by proteases present in the MIIC. The class II associated Ii peptide (CLIP) fragement of Ii remains in the antigen binding groove of the MHC class II dimer until it is exchanged for an antigenic peptide. The exchange is facilitated by the chaperone protein HLA-DM (H2-DM in mice). MHC class II molecules are then transported to the plasma membrane where they present antigen to $CD4^+$ T cells. Figure adapted from (51).

Cross presentation of exogenous antigen by MHC class I

Under normal homeostatic conditions cross presentation of self-antigens runs the risk of autoimmunity and must be strictly controlled. Consequently, cross presentation of exogenous antigen is confined to a specific subset of dendritic cells. The phagocytic capacity of dendritic cells makes it difficult to discriminate between endogenous and exogenous antigen, hence dendritic cells are capable of presentating both endogenous and exogenous antigen via MHC class I molecules. All MHC class I positive cells can present antigenic peptide fragments to CTLs, however, only dendritic cells are able to prime naïve T cells (55) thus preventing the initiation of immune responses against viruses, or tumour cells that do not affect dendritic cells. The ability to cross present exogenous antigen via the MHC class I pathway is relevant for a number of cell-associated antigens in various disease states, including viral, self and tumour-associated antigens (56). Cross presentation is largely confined to $CD8\alpha^+$ dendritic cells in mice (57) and $CD141^+$ dendritic cells in humans (58-61). These subsets of dendritic cells take up apototic, necrotic and live cell fragments, as well as particulate, and soluble antigens via phagocytosis, receptor-mediated endocytosis, or macropinocytosis for presentation to class I and class II restricted T cells.

Since the proteasome is a key component of the classical MHC class I presentation pathway, its role in cross presentation was assessed using proteasome selective inhibitors. These investigations found that both proteasome-dependent (62) and independent antigen processing (63, 64) occurred in cross presentation model systems. So far experimental evidence has been obtained to support two pathways leading to antigen cross presentation, these are the cytosolic and vacuolar pathways, The cytosolic pathway advocates that endocytosed antigen is transported to the cytosol, where it undergoes proteasome, or cytosolic peptidase mediated degradation before entering the conventional MHC class I pathway. It is hypothesized that phagosomes containing exogenous protins fuse with the ER derived vesicles containing newly synthesized MHC class I molecules, TAP, tapasin, calreticulin and ERp57. The phagocytosed proteins are thought to be transported to the adjoining cytosol via Sec-61, a multimolecular channel in the ER membrane (55). Once in the cytosol the peptides are degraded by proteasomes and transported back into the phagosome via the TAP complex and loaded on the

MHC class I molecules. Experimental evidence in support of the cytosolic pathway in antigen cross presentation was provided by the phagosome-to-cytosol translocation of ovalbumin (OVA)-beads (62) OVA-IgG, and horseradish peroxidase (HRP)-IgG complexes (65). Once translocated to the cytosol both the proteasome and amino-/ caroboxy-peptidases process the antigen into peptide fragments (66, 67). TAP then translocates these peptides into the ER where they are processed as normal via the MHC class I pathway (68).

The vacuolar pathway proposes that antigen processing is carried out by proteases situated within endosomes (69). In contrast to the cytosolic pathway, the vacuolar pathway does not require phagosome-to-cytosol translocation, instead it relies on endosomal proteases for the generation of antigenic peptides (70, 71), which are loaded onto recycled MHC class I molecules. Shen *et al.* demonstrated that within a population of dendritic cells, cell associated OVA can be degraded either by cathepsin S in the endosome, or by the cytosolic proteasome (63) suggesting that proteosome independent and cytosolic pathways may co-exist. Further evidence to support this hypothesis is provided by reports that demonstrate the plasmacytoid dendritic cells cross present in both proteasome-dependent and indpendent pathways (71, 72). In short, the process of cross presentation is dependent on antigen processing by proteolytic enzymes, which may occur in the endosomal compartment itself, as well as in the cytosol. Figure 1.8 summarises the cytosolic and vacuolar pathways in the context of antigen cross presentation.

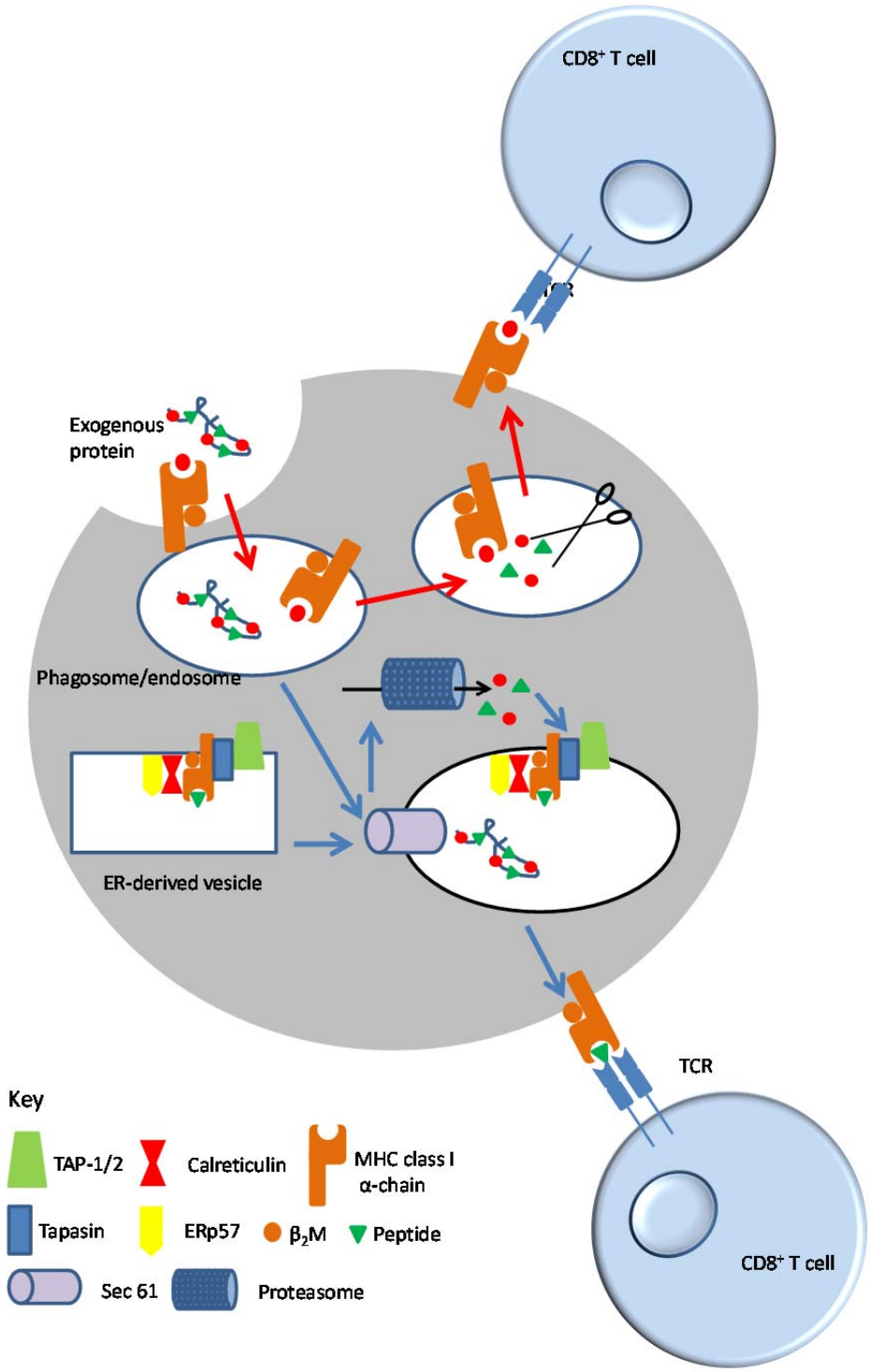

Figure 1-8. The proposed pathways for cross presentation of exogenous antigen by MHC class I. The vacuolar pathway (red arrows) proposes antigen is taken up and processed in the endocytic compartmentand loaded onto recycled MHC class I molecules. The cytosolic pathway (blue arrows) proposes that endogenous antigen undergoes phagosome-to-cytosol translocation, where it is subject to proteosome, or cytosolic pepitdase mediated degradation, prior to entering the conventional MHC class I pathway.

T cell priming

Activation of a naïve T cell upon enocounter with its specific antigen, and the subsequent proliferation and differentiation into an effector T cell consitutes a primary cell-mediated immune response. Hence the first encounter between a naïve T cell and its specific antigen is known as T cell priming. Three distinct signals control the clonal expansion and differentation of naïve T cells following activation (73). Signal one is provided by the interaction between antigen peptide: MHC complex and the TCR, additional co-stimulatory signals, referred to as signal two, promote or inhibit survival and expansion of T cells and finally signal three directs differentiation into effector T cells.

Signal one: The interaction between peptide: MHC complexes and the TCR

Mature naïve T cells circulate in the blood until they reach a peripheral lymphoid organ, such as a lymph node, at which point they leave the blood and migrate through the lymphoid tisse, where they sample antigenic peptide fragments presented by mature dendritic cells via MHC. The selectins are responsible for guiding leucocytes into specific tissues, a process known as leucocyte homing. L-selectin, also known as CD62L, expressed on the surface of naïve T cells guides their entry into the lymph nodes by binding to the vascular addressins CD34 and GlyCAM-1, expressed on vascular endothelial cells, such as the high endothelial venules (HEV) of the lymph nodes. This interaction enables the T cells to roll along the HEV where they encounter the chemokine CCL21 present at the HEV surface. The binding of CCL21 to the chemokine receptor CCR7, expressed on the surface of T cells, activates the integrin leucocyte functional antigen-1 (LFA-1), another T cell surface marker, increasing its affinity for the adhesion molecule ICAM-1 expressed on the venule endothelium. The strong interaction that occurs between LFA-1 and ICAM-1 facilitates T cell entry into the lymph node via a process called dipedesis. As the naïve T cells migrate through the lymph node they transiently bind each dendritic cell they encounter, during which time they sample the antigenic peptides presented by the MHC molecules. Recognition of its specific antigen peptide fragment by the TCR induces a conformational change that increases the affinity between LFA-1 on the T cell and the adhesion molecules on the surface of the APC stabilising the interaction, whilst the naïve T cells proliferate and differentiate into effector T cells. Naïve T cells that do not encounter their specific antigen return to the blood via the lymphatics. This

process is mediated by sphingosine 1-phosphate (S1P), a lipid molecule with chemotactic properties. Naïve T cells expressing the S1P receptor ($S1P_1$) are drawn out of the lymphoid tissues, down the concentration gradient thought to exist between the lymphoid tissues and the blood. Activated T cells internalise $S1P_1$ via the early activation marker CD69 hence they are retained in the lymphoid tissue. After several days of proliferation and differentiation CD69 expression wanes, $S1P_1$ returns to the cell surface and the T cells are once again drawn out of the lymph node and into the blood via S1P.

Signal two: Co-stimulatory signals promote survival and expansion

It has long been estabilished that recognition of a specific antigenic peptide: MHC complex by the TCR alone is insufficient to induce T cell activation. Additional co-stimulatory signals independent of antigen are required to ensure T cell survival and proliferation. These signals are also important for the generation of memory T cell responses. Co-stimulatory signals have a synergistic effect when combined with signal one but do not have the capacity to stimulate T cells in their own right. In the absence of co-stimulation engagement of the TCR will result in apoptosis, or alternatively anergy, which may render the T cell non-responsive and refractory to re-stimulation (74).

Co-stimulation is provided by ligands, such as the B7 molecules CD80 and CD86, expressed on the surface of APCs. These homodimeric molecules are members of the Ig superfamily and interact with the co-stimulatory receptor CD28 constitutively expressed on the surface of T cells. Engagement of the TCR in the presence of the appropriate co-stimulatory signal induces synthesis of the α-chain of the IL-2 receptor, known as CD25. The IL-2 receptor comprises of three chains, α, β, and γ. Resting T cells constitutively express the β- and γ-chains; however, association of the α-chain increases the affinity of the receptor for IL-2. Binding of IL-2 to the high affinity receptor enables the T cell to divide two to three times a day for several days resulting in clonal expansion. Thus, the most important function of signal two is to promote IL-2 production. Once activated a naïve T cell expresses a number of proteins in addition to CD28 that sustain or modify the co-stimulatory signals that drive clonal expansion and differentiation. The majority of these molecules belong to the Ig superfamily, or the tumour-necrosis factor receptor (TNFR) family and are summarised in figure 1.9.

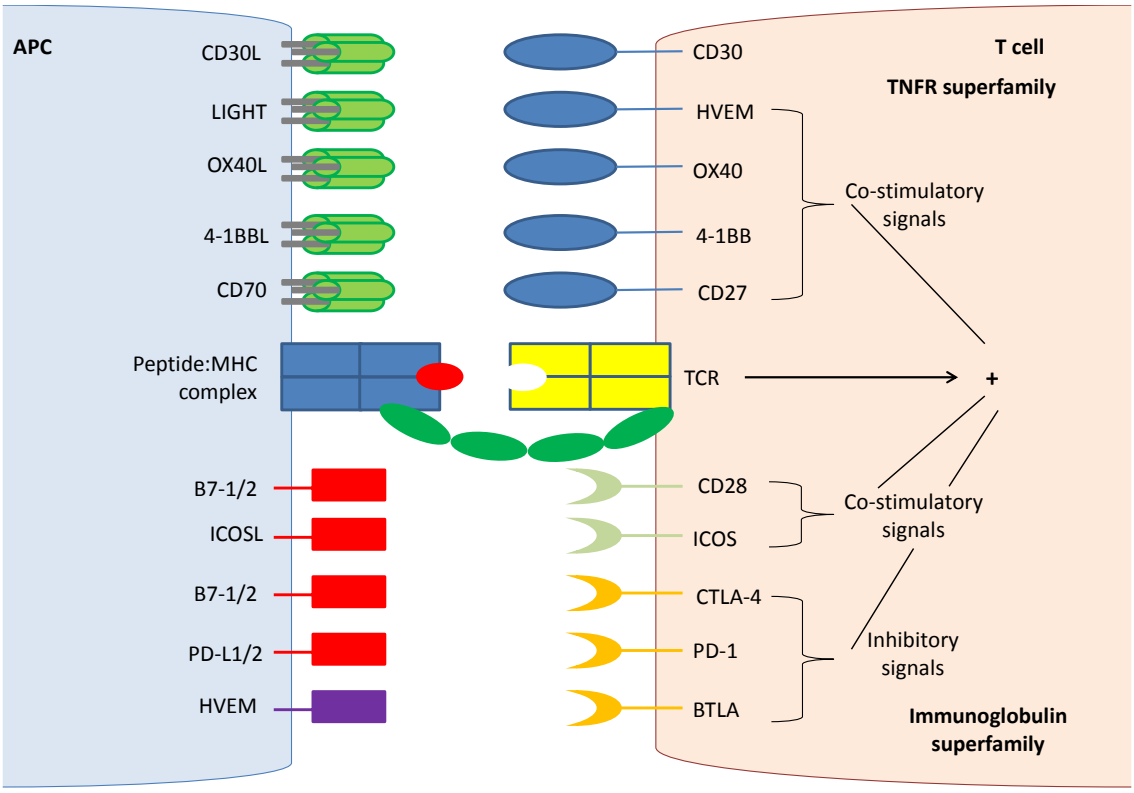

Figure 1-9. T cell co-stimulatory and inhibitory molecules involved in T cell activation following antigenic stimulation. The signals generated following ligation of members of the TNFR and Ig superfamilies by their respective ligands augment, or inhibit signals provided upon antigenic stimulation of the TCR. Figure adapted from (75).

Co-stimulatory signals are not a prerequisite for T cell responses, instead the requirement for co-stimulation varies and depends on the strength of the TCR signal. Low affinity interactions, such as those produced in the presence of limited concentrations of antigen, require more co-stimulation to promote effective T cell responses. Different co-stimulatory molecules may be important at different stages of the T cell response (76, 77), for example constitutively expressed CD28 is important early on for primary T cell expansion but is less important during effector T cell and memory responses (78). Whereas, data suggests 4-1BB and OX40, which are up regulated post T cell activation, are more important for maintenance of the expanded T cell population and for ensuring survival and responsiveness of memory T cells (77, 79, 80).

Signal three: Differentiation into effector T cells

After four to five days of IL-2 induced proliferation activated T cells differentiate into effector T cells. Once generated effector T cells do not require co-stimulation and can kill their target cells upon recognition of

specific antigen via the TCR alone. Effector T cells downregulate CD62L and ultimately cease to circulate through the peripheral lymphoid organs. $CD8^+$ T cells proliferate and differentiate into CTLs upon encounter with their specific antigen and the appropriate co-stimulatory signal. This effector cell population has an important role in the destruction of virally infected and malignant cells. CTLs are class I restricted, which means they have the potential to target any nucleated cell. $CD8^+$ T cells require strong co-stimulation to drive them to become effector cells, most likely due to the destructive nature of CTLs, which is provided in one of two different ways. Firstly, $CD8^+$ T cells are activated by mature dendritic cells, which have high intrinsic co-stimulatory activity, kickstarting the production of IL-2 and formation of the IL-2 receptor. Secondly, $CD4^+$ T cells can provide additional help. $CD4^+$ effector T cells are recruited to the $CD8^+$ T cell: dendritic cell complex and CD40L expressed on the $CD4^+$ T effector cell engages CD40 on the dendritic cell. This interaction leads to up regulation of the B7 molecules CD80 and CD86, which subsequently bind CD28 on the $CD8^+$ T cell thus inducing proliferation and differentiation. The $CD4^+$ effector cells may also provide additional IL-2.

CTL mediated destruction of target cells

CTLs are responsible for killing of virally infected and malignant cells through the calcium-dependent release of the cytotoxic proteins perforin and serine protease granzymes in a manner that is analogous to NK cells as previously discussed. These cytotoxic proteins are synthesised *de novo* and packaged into cytotoxic granules upon ligation of the CTL TCR. Release of perforin and granzymes must be tightly regulated as their cytotoxic activity is non-specific, which means these substances will penetrate the lipid bilayer and trigger apoptosis in any cell they encounter. The initial interaction between a CTL and a potential target is mediated by the binding of LFA-1 on the T cell surface and the adhesion molecule ICAM-1 on the target cell. This allows the T cell to scan the target for its specific antigen presented as a peptide: MHC complex. If the CTL does not recognise its specific antigen then the two cells dissociate and the CTL moves on to another potential target. However, upon recognition of its specific antigen the peptide: MHC complexes rapidly coalesce to form a *central* supramolecular activation complex (*c*SMAC) within which the TCR and its co-receptors cluster at the site of cell-cell contact. The adhesion molecule ICAM-1 also clusters here and interactions between LFA-1 and ICAM-1 results in the

formation of a tight *peripheral* ring junction (81), known as the *p*SMAC, which surrounds the cSMAC creating a molecular seal to ensure that cytotoxic granule release is confined to the CTL: target cell interface, thus sparing innocent bystander cells. The structure of this interface therefore resembles a 'bullseye' and has been termed the immunological synapse (82, 83). Cytotoxic granules are released at a specialised secretory domain within the immunological synapse. This process occurs when the CTL polarises towards its target as a result of the re-organisation of the actin cytoskeleton, this in turn triggers a re-orientation of the microtuble-organising centre (MTOC) allowing it to transiently make contact with the plasma membrane at the cSMAC and focuses granule exocytosis at the site of CTL: target cell contact (84).

Generation of effector memory cells

The developmental fate of naïve $CD8^+$ T cells is not pre-programmed (85), each cell is immunologically pluripotent and can give rise to an array of distinct subsets. During the primary response the majority of $CD8^+$ T cells expand and terminally differentiate into end stage effectors that are short-lived but highly functional, whereas a small percentage of the naïve cells differentiate into memory-pre-cursor cells that have the potential to complete transition into fully fledged memory cells and provide long term immunity (86, 87). Increased expression of IL-7 receptor-α (IL-7Rα), also known as CD127, can be used to differentiate between memory pre-cursor cells and terminally differentiated short-lived effector cells and is functionally important for their long term survival (88, 89). Memory cells that descend from the IL-7Rα population display distinct memory cell properties, such as increased proliferative response to antigen, production of IL-2 and the ability to self-renew (86). Several factors are thought to determine which $CD8^+$ T cells die out and which develop into memory cells, such as the strength and duration of TCR stimulation, inflammatory cytokines, transcriptional regulation and metabolic switches. Co-stimulatory signals are also required to ensure maximal maintenance of T cell memory. Both IL-7 and IL-15 are required for the homeostatic turnover of memory T cells and have been reported to up regulate the expression of the co-stimulatory TNFR family members OX40 and 4-1BB respectively, which may provide additional survival signals to memory $CD8^+$ T cells (87).

The innate-like lymphocytes

The innate-like lymphocytes (ILL) are a type of lymphocyte that express a limited set of antigen receptor genes, hence they possess somewhat invarient antigen receptors. ILL do not have to undergo clonal expansion and therefore have a role in the early stages of infection. The ILL comprise of natural killer T (NKT) cells and γδ T cells.

NKT cells

NKT cells are a subset of T lymphocytes that express both the TCR αβ-chains and NK cell receptors. NKT cells recognise glycolipid antigens presented by the MHC class I-like molecule CD1d expressed on the surface of various APCs. The majority of mouse NKT cells can be identified using CD1d tetramers loaded with the prototypic antigen α-galactosylceramide (α-GalCer). These α-GalCer reactive type I NKT possess a unique invariant TCR α-chain, called Vα14Jα18 in humans, with limited variability in TCR β-chain usage; hence they are a fairly homogeneous population. Upon stimulation with α-GalCer these type I NKT cells produce large quantities of the T helper-1 cytokine IFN-γ and the T helper-2 cytokines IL-4 and IL-13. Another type of CD1d-restricted NK cells has been identified in mice, these type II NKT cells do not express Vα14Jα18 and represent a more heterogenous population than type I. Investigations reported on the function of type II NKT cells is limited (90).

γδ T cells

The γδ T cells are a minor subset of T cells possessing a distinct TCR composed of a γ-chain and a δ-chain, as opposed to the more typical α- and β-chains. Unlike the majority of T cells, γδ T cells are not dependent on antigen processing and MHC mediated presentation for antigen recognition, instead they can recognise their antigen directly.

Phagocytes

Phagocytosis is defined as the engulfment of large particulate matter (≥ 5 μm). The engulfment and subsequent destruction of evading microorganisms by professional phagocytes, such as macrophages, neutrophils and dendritic cells, is an important function of the innate immune response. Phagocytes are also involved in the clearance of apoptotic bodies, which means they have an essential role in the process of tissue remodelling and homeostasis.

Phagocytes have a key role in the initiation of adaptive immune responses through the release of pro-inflammatory cytokines. However, upon phagocytosis of apoptotic bodies, phagocytes release anti-inflammatory cytokines to prevent further tissue damage.

Phagocytosis is a receptor mediated process; however, due to the wide range of particles that can be taken up by this process, several different receptor subtypes are involved. For example the PAMPs introduced at the start of section 1.2.1 are recognised by some phagocytic receptors, including the mannose receptor CD206 (91), which recognises polysaccharides present on yeast cells, and scavenger receptor A (CD204), which recognises the LPS component of Gram negative bacterial cell walls (92). Foreign particles can also be recognised by soluble molecules, such as antibodies, or components of the complement cascade, once bound to a foreign particle these soluble molecules, termed opsonins, engage receptors on the surface of phagocytes. Opsonic receptors include the FcγR (introduced in section 1.2.1.1) that bind to the Fc portion of antibodies and the CR3 receptors that bind the complement component iC3b. Phagocytosis of apoptotic bodies is a normal physiological process with up to ten billion health cells undergoing apoptosis each day (93). The phagocytosis of apoptotic cells is regulated by a series of 'find me' and 'eat me' signals (93). Cells undergoing apoptosis release molecules such as ATP, lysophosphatidylcholine, fractalkine and S1P (94), these soluble 'find me' signals have chemoattractant properties and recruit phagocytes to the site of apoptotic cells. The apoptotic cells themselves display molecules on the surface that provide 'eat me' signals to phagocytes, such as phosphatidylserine (PS), which under normal circumstances is generally restricted to the inner cell membrane and is only widely displayed on the cell surface during apoptosis. Multiple phagocytic receptors recognise and bind PS, including those belonging to the T cell immunoglobulin mucin (TIM) family, BAI1 and stabilin (95-97).

Whilst the receptors involved in initiating phagocytic responses vary the outcome is essentially the same. The internalisation process results in the formation of a membrane bound vacuole, called the phagosome. The membrane of the phagosome itself resembles the plasmalemma from which it was derived and its fluid phase contents are similar to the extracellular milieu, hence phagocytosis *per se* does not trigger destruction of the engulfed foreign

particle. Once cleaved from the membrane the phagosome undergoes a series of biochemical modifications, termed phagosome maturation. During this process the phagosome first fuses with the early endosome, giving rise to the early phagosome, which subsequently fuses with the late phagosome, or lysosome, resulting in formation of the late phagosome/ phagolysosome. Once the maturation process is complete, the phagosome becomes markedly acidic, highly oxidative, and enriched with the hydrolytic enzymes that ultimately degrade its contents (93).

1.3 The immune system and cancer

Tumour progression from a single transformed cell to a detectable malignant mass is a complex multistep process that occurs over a period of months, or even years (98). The genetic aberrations that drive the transformation of healthy cells towards malignancy can result in the production of proteins not usually present under normal physiological conditions. These abnormal proteins are the TAAs briefly introduced in section 1.1 and have the potential to be recognised by the immune system as foreign. The TAAs expressed by neuroblastoma were summarised in table 1; however, a wide range of TAAs with the potential to be recognised by T cells have been discovered for a variety of different cancers (20, 99, 100). Therefore, in addition to conferring protection against infection, the immune system can also recognise and eliminate nascent tumour cells, thus providing protection against malignancy; a concept referred to as cancer immunosurveillance (101).

1.3.1 The immune surveillance hypothesis

The concept that the host immune system could provide protection against what would otherwise result in an ‘overwhelming frequency’ of neoplastic disease was first postulated by Paul Ehrlich in 1909. Nevertheless, it was Sir Macfarlane Burnet who went on to formalise the immune surveillance hypothesis in 1970 (102). Burnet’s theory was that sentinel thymus dependent cells surveyed host tissues looking for early transformed cells, which were subsequently eliminated (102). What followed was a series of experiments designed to test this hypothesis by investigating tumorigenesis in immunocompromised mice, reviewed in (101). In these early experiments immunosuppression was induced by neonatal thymectomy, heterologous anti-

lymphocyte serum, or by pharmacological means and the results obtained from these experiments were inconsistent (103). Extensive investigations subsequently performed by Osias Stutman utilised an athymic nude mouse model to explore immune surveillance in the physiological setting and concluded that CBA/H nude mice did not develop chemically induced tumour at a greater frequency, nor did they demonstrate reduced latency when compared to wild type mice (104). Little was known about the immunological defects in the nude mouse models available at the time, hence the data reported by Stutman and others was deemed convincing (101). Ultimately, the immune surveillance hypothesis was abandoned due to the absence of strong evidence in its favour (101). There were several attempts to revive the immune surveillance hypothesis throughout the next two decades. However, a real resurgence came about in the mid- to late-1990s with the discovery that transplanted immunogenic fibrosarcomas grew more efficiently in mice that had be treated with neutralising antibodies specific for interferon- γ (IFN-γ) (105). Plus immunodeficient mice that overexpress a dominant-negative mutant of the IFN-γ receptor-α subunit (IFNGR1), or lacking an intact T cell compartment were demonstrably more susceptible to methylcholanthrene (MCA) induced sarcomas (105-107). An abundance of data has since been published by numerous laboratories demonstrating unequivocally that the immune system provides protection against a variety of primary and transplantable tumours in *in vivo* mouse models (105, 106, 108-112). Additionally, it has been established that the immune surveillance hypothesis only adequately describes one aspect of the complex relationship that exists between the host immune system and cancer (101, 103). A key paper published by Shankaran *et. al* in 2001 demonstrated that the immune system can also promote the emergence of primary tumours that have reduced immunogenicity and therefore the ability to avoid immune recognition and destruction (108). These findings led to the more current concept of immunoediting, which encompasses both the protective and tumour enhancing properties of the immune system (101).

1.3.2 The 'three Es' of cancer immunoediting

The concept of cancer immunoediting, first proposed in the early 2000s (101, 108) and reviewed in detail in (103), can be divided into three phases, referred to as the 'three Es of cancer immunoediting', these are: elimination,

equilibrium and escape. The elimination phase incorporates the original immune surveillance hypothesis, and assuming the immune system successfully identifies and destroys the developing tumour cells, represents the entire immunoediting process without progression to the later stages of equilibrium and escape (103). The disruption to normal tissue architecture when a developing tumour starts to invade its surroundings induces an inflammatory response that leads to the recruitment of a variety of innate and innate-like immune cells, including NK cells, macrophages, dendritic cells, NKT cells and γδ T cells, as well as the production of IFN-γ. The production of IFN-γ may have a direct effect on the developing tumour due to its anti-proliferative properties and ability to induce apoptosis. Moreover, any anti-tumour effects of IFN-γ are likely to be amplified as it induces local production of chemokines that serve to recruit more immune effector cells (103). Tumour cell debris generated either as a direct, or indirect consequence of IFN-γ production, is ingested by dendritic cells, which subsequently migrate to the draining lymph nodes where they may initiate TAA-specific adaptive immune responses.

Tumour cells that survive elimination then enter the equilibrium phase. During this phase the immune system exerts a selective pressure on the tumour cells, which is sufficient to contain but not eradicate the tumour cells. This dynamic process may continue for years. However, the original tumour cells that were able to avoid elimination are gradually destroyed and replaced by new variants carrying different genetic mutations conferring increased resistance to immune responses. The tumour cells that have acquired increased resistance to immune cell mediated destruction continue to accumulate in an uncontrolled manner, eventually resulting in the clinical presentation of disease, which represents the escape phase.

Finally, the developing tumour has the ability to recruit immunosuppressive mechanisms that can foil attempts to eliminate malignant cells and foster a state of immune tolerance (113), thus adding a further layer of complexity to the relationship between the immune system and cancer, which implies that the tumour itself is in fact the executor of immune unresponsiveness.

1.3.3 Humoral immunity and cancer

Immune responses against self-antigens can occur in cancer patients. These responses may originate in the tumour itself due to alterations and aberrations that increase the immunogenicity of self-antigens. Alternatively, these responses may be specific for TAAs that have little to no expression on normal tissues and arise through several different mechanisms, for example coding DNA mutations that cause new epitopes to be expressed by proteins, post-translational modifications that have immunological relevance, and altered tissue specific patterns, or expression levels resulting in presentation of antigens such as NY-ESO-1 normally only found at immune privileged sites (99). Spontaneous adaptive immune responses against TAAs have been reported in cancer patients; however, at present there are no standard protocols for the detection of a humoral immune responses against TAAs (114). Following a systematic review of the literature in 2009 Reuschenbach *et al.* concluded that whilst auto-antibodies against TAAs have been detected in cancer patients, most are merely markers of antigen exposure and have no functional activity (114). TAA specific antibodies may provide useful tools for early cancer detection, prognosis, or post-treatment surveillance; however, data on pre-diagnostic antibody levels is scarce, so it is unclear what the predictive value of these humoral immune responses may be (114). In summary, endogenous humoral immune responses are not thought to play a major role in the control of tumour growth.

1.3.4 Cell mediated immunity and cancer

The term cell mediated immunity was introduced in section 1.2.1.2 to describe both the innate and adaptive immune responses that are executed by the various cells of the immune system, many of which have been implicated in the immune response to cancer. These include NK cells, T cells, ILL and macrophages.

1.3.4.1 Natural killer cells and cancer

The ability to kill tumour cells *in vitro* without the need for prior sensitisation is what led to the discovery of NK cells (115-118) and this anti-tumour activity has also been demonstrated *in vivo* using mouse models (119). A number of studies have revealed an important role for NK cells in the immune response

against cancer. Intra-tumoral NK cells have been identified in a variety of cancers, including colorectal, gastric, and squamous cell lung cancer, and their presence positively correlates with survival (120-123). NK cells participate in antibody mediated anti-tumour responses (*i.e.* ADCC) following engagement of the FcγR CD16 on the NK cell surface. Additionally, the activating NKG2D receptor can also contribute to the anti-tumour immune response. The ligands for NKG2D include MHC class I related (MIC) A/B and the UL16 binding proteins (ULBP) in humans, as well as the retinoic acid early inducible-1-like transcript (RAE-1) and the minor histocompatibility complex H60 in mice (33). These ligands are not generally expressed on healthy cells, instead they are up regulated as a consequence of cellular stress (124, 125). MICA/B are differentially expressed on a variety of primary carcinomas including lung, breast, kidney, ovary, prostate, colon (126) and melanoma (127), thus targeting these cells for NK mediated destruction upon ligation of NKG2D. A number of other cell types also express the NKG2D receptor these include NKT cells, γδ T cells and $CD8^+$ T cells.

1.3.4.2 T cells and cancer

The first evidence that T cells were able to recognise and respond to malignant cells was provided towards the end of the 1980s/ early 1990s by Wolfel *et al.*, who discovered tumour-infiltrating lymphocytes (TILs) that could kill autologous tumour cells in a HLA-restricted manner (128), and Kawakami *et al.* who characterised the requirements for HLA restriction (129). Contemporaneously, Van der Bruggen *et al.* completed the molecular characterisation of the first TAA recognised by T cells (130). Development of effective strategies to identify TAA recognised by specific T cells resulted in characterisation of several families of MHC class I related TAA (131) and just a decade after Van der Bruggen *et al.* published their findings more than 60 TAA had been identified (99, 100). Naturally occurring adaptive immune responses in the form of $CD8^+$ T cells that recognise specific TAAs are often identified in cancer patients (131) and clinical studies have shown that immunisation with peptides derived from TAAs leads to the generation of high levels of TAA-specific $CD8^+$ effector T cells in cancer patients (132). Thus, tumour-specific $CD8^+$ T cells may represent the most important component of the host anti-tumour immune response and the ability to either enhance the activity of naturally occurring tumour-specific $CD8^+$ T cells, or induce their production

may be integral to the provision of long term immunity against malignant disease.

1.3.4.3 Innate-like lymphocytes and cancer

The two types of ILL that have been implicated in the immune response to cancer are the NKT cells and the γδ T cells. The prototypic NKT cell antigen α-GlyCer was originally isolated from marine sponge as a potential anti-tumour compound. Consequently, the role of α-GlyCer activated type I NKT cells in anti-tumour immunity has been studied in depth. The anti-tumour effects of α-GlyCer has been attributed to the Th1-skewed cytokine production profile of activated type I NKT cells and production of IL-12 by dendritic cells, which is required for the activation of NKT cells. The co-stimulatory molecules CD28 and CD40L may also contribute to anti-tumour immunity by augmenting NKT cell recognition and activating dendritic cells (133). Additionally, as mentioned previously some NKT cells also express the activatory NK cell receptor NKG2D, which may facilitate NKT cell mediated tumour cell recognition and destruction upon ligation with the stress induced molecules MICA and MICB up regulated by a variety of tumours (126, 127). The γδ T cells are thought to recognise MICA and MICB by their antigenic receptor. However, they also express the activatory NK cell receptor NKG2D, which may further enhance their ability to recognise and destroy tumour cells.

1.3.4.4 Phagocytes and cancer

Of all the professional phagocytes, macrophages in particular have been implicated in cancer. So called tumour-associated macrophages (TAM) represent the major inflammatory component of the tumour stroma in a host of malignancies (134). Broadly speaking macrophages can be classified as one of two types: M1 and M2 as illustrated in figure 1.10.

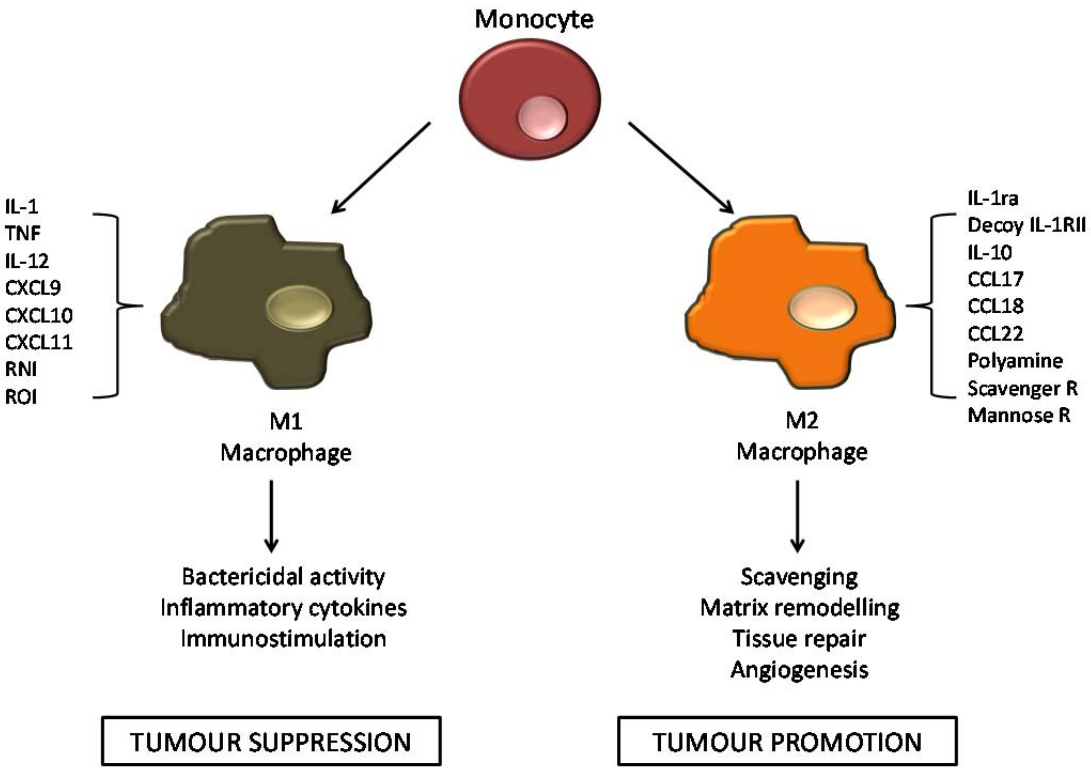

Figure 1-10. The macrophage subtypes. Macrophages can be classified as one of two subtypes. The M1 subtype has a pro-inflammatory phenotype and is involved in the response to microbial products, whereas the M2 subtype is more anti-inflammatory and has a role in tissue re-modelling and repair.

M1-like macrophages are said to be pro-inflammatory. Activation of M1-like macrophages occurs in response to microbial products, such as LPS a component of Gram negative bacterial cell walls, or IFN-γ produced by NK cells and T cells (135). M1-like macrophage activation results in the production of toxic substances, such as nitric oxide or reactive oxygen species, M1-like macrophages are thought to be capable of killing tumour cells. M2-like macrophages on the other hand scavenge debris and promote angiogenesis, as well as tissue re-modelling and repair. M2-like macrophages have been implicated in tumour promotion (135). TAM, which are associated with poor prognosis are said to have an M2-like phenotype (135).

1.4 The immune response to neuroblastoma

The first evidence of an immune response to neuroblastoma was obtained in the 1960s when Hellstrom *et al.* demonstrated that lymphocytes and serum obtained from the blood of neuroblastoma patients inhibited colony formation of both autologous and allogeneic neuroblastoma cells (136). Around the same time TILs were identified in resected neuroblastoma tumours and their

presence was considered indicative of favourable prognosis (137, 138). TILs are most prominent among a small subset of patients that present with both neuroblastoma and opsoclonus-myoclonus (OMS) syndrome, a rare paraneoplastic disorder indicative of naturally occurring anti-tumour immunity (139). More than 50 % of cases of OMS occur in children with neuroblastoma (140). The pathogenesis of OMS is not fully understood; however, it has been hypothesized that anti-tumour immune responses against neuronal antigens found on both tumour cells and normal neuronal tissue trigger an autoimmune mediated neurodegenerative disease (141). Apoptotic tumour cells are internalised by dendritic cells, which subsequently migrate to the lymphoid tissues where they activate T cells, these activated T cells that specifically target the common antigen then cross the blood brain barrier and attack neurons, cumulating in the clinical manifestation of neuronal degeneration (142). In the case of OMS symptoms include rapid, irregular eye movements and may be accompanied by polymyoclonia, ataxia, jerking of the limbs and behavioural disturbances (143). One retrospective study reported that ninety percent of neuroblastoma patients presenting with OMS were found to have non-metastatic disease and the estimated three year survival among these patients was one hundred percent compared to seventy seven percent (p 0.0222) for similar disease matched patients that did not have OMS (144). Whilst it is tempting to attribute the favourable prognosis to the immune responses observed in this subset of patients, many presented with low grade, well differentiated tumours (145), both well-established good prognostic markers, making it difficult to determine how much the immune responses actually contributed to improved survival.

Clinical and pre-clinical studies have identified peptides from the TAA survivin, an inhibitor of apoptosis, which is widely expressed in neuroblastoma (see table 1, section 1.1 for a list of TAA expressed in neuroblastoma) as targets for CTLs (146, 147). In one study survivin-specific CTL were detected in the blood of eight out of nine high risk neuroblastoma patients at diagnosis (147). Whilst these circulating TAA-specific CTL were clearly unable to suppress tumour progression, they were functional with the majority exerting cytotoxic activity against autologous and HLA-matched neuroblastoma cells when stimulated with survivin *in vitro* (147).

NK cells are the other main subset of lymphocyte involved in tumour specific immune responses. Neuroblastoma cells are potentially good targets for NK cells as they express little to no MHC/ HLA class I molecules on their surface (148). The net result being that NK cells have the ability to recognise and destroy neuroblastoma cells even without prior sensitisation in accordance with the missing-self hypothesis introduced in section 1.2.1.2. NKT cells have also been implicated in the immune response to neuroblastoma and their presence in the immune infiltrate positively correlates with disease free survival (149). The presence of NKT cells in the tumour immune infiltrate is thought to be due to the secretion of the chemokine MCP-1/ CCL2. Expression of CCL2 inversely correlates with MYCN proto-oncogene amplification and expression (149) thus, infiltrating NKT cells might not be as apparent in high risk neuroblastoma. Additionally, NKT cells can only exert a cytotoxic effect if they recognise a glycolipid antigen presented to them via the MHC class I-like molecule CD1d expressed on the tumour cell surface, and neuroblastoma cells lack this surface molecule. However, stimulated NKT cells can secrete IL-2 hence any observed anti-tumour mediated effect is potentially indirect rather than tumour specific (149).

1.4.1 Mechanisms of immune evasion in neuroblastoma

Whilst there is sufficient evidence to support the generation of tumour-specific immune responses in neuroblastoma, the clinical manifestation of the disease confirms that these tumour-specific immune responses are insufficient to control tumour progression. The inability of the host immune system to eradicate tumour and the subsequent disease presentation represents the final stage of the immunoediting process, namely immune escape, a concept that was introduced in section 1.3.2. In order to improve long term survival in high risk neuroblastoma patients through the use of immunotherapeutic strategies it is necessary to have a thorough understanding of the mechanisms responsible for immune evasion.

1.4.1.1 Host related mechanisms of immune evasion

Some of the barriers to achieving effective therapy are due to the limitations of the immune system itself, for example T cell activation requires antigen to be captured by an APC and transported to the lymph nodes for presentation to a TCR. This process is relatively inefficient when an antigen is present in limited

concentrations and TAAs in particular need to be expressed at high levels if they are to be cross presented (150). As discussed in section 1.2.1.2 T cell activation is dependent on both antigen recognition and the binding of additional co-stimulatory molecules. If these co-stimulatory signals are lacking then engagement of the TCR results in anergy, or apoptosis, this process forms part of the normal immune regulatory response required to prevent activation of T cells specific for self-antigens. APCs only up regulate these co-stimulatory molecules when they encounter noxious stimuli, such as inflammatory cytokines, thus in the somewhat non-inflammatory tumour microenvironment T cell activatory signals are likely to be suboptimal and T cell may become anergic (151).

Regulatory T cells

Regulatory T cells (Tregs) may contribute to tolerance to tumour antigen. These inhibitory T cells are present under normal physiological conditions and exert an immunosuppressive effect, so as to prevent autoimmunity. Tregs can be subdivided into two subsets: those that develop in the thymus and are involved in regulating normal immune responses, and the adaptive variants that develop in the periphery. The number of Tregs is often increased in patients with malignancy; however, they have not been evaluated in human primary neuroblastoma, or at metastatic disease sites (152). Nevertheless, Tregs secrete immunosuppressive cytokines TGFβ1 and IL-10, which have been detected in neuroblastoma patients with stage IV disease (152). Whilst clinical data is limited, murine models have shown that depletion of Tregs enhanced vaccine induced immunity to neuroblastoma (153).

Myeloid-derived suppressor cells

Myeloid-derived suppressor cells (MDSCs) are a heterogeneous population of immature myeloid-derived cells that do not have a distinct phenotype *per se*, perhaps due to the fact they accumulate in response to tumour-secreted and pro-inflammatory factors. Consequently, their exact phenotype may depend on the specific combination of factors generated by a particular tumour. In cancer patients MDSCs are present in the blood and are generally characterised as $CD11b^{+}CD33^{+}CD34^{+}CD14^{-}HLA\text{-}DR^{-}$ but may vary in their expression of other surface markers. The variation in phenotype is consistent with the observation that MDSCs comprise a heterogeneous population of myeloid-derived cells that

are at different stages along their differentiation pathway. A consequence of this heterogeneity is that no single marker, or combination of markers may exist that precisely defines MDSCs, hence their immunosuppressive ability is considered to be their defining characteristic. MDSCs have been identified in the blood of neuroblastoma patients (154), whether these cells have suppressive function and the implications this has on disease stage and treatment outcome has yet to be elucidated.

1.4.1.2 Tumour-derived mechanisms of immune evasion

In addition to the host related factors neuroblastoma cells themselves have acquired mechanisms of evading the immune system. Two of the main strategies employed by neuroblastoma cells to facilitate immune escape include down regulation of MHC/ HLA class I molecules and down regulation of the ligands for the activatory NK cell receptor NKG2D.

Down regulation of MHC / HLA class I molecules

Studies have shown neuroblastoma cells express little to no surface MHC/ HLA class I molecules (148), which renders them unable to present TAA to CTL (155). The lack of MHC/ HLA class I expression can be attributed to defects in β2-m, HLA class I heavy chain and TAP1 gene expression, which in human neuroblastoma cell lines can be corrected by treatment with IFN-γ (155). Conversely, as previously mentioned the lack of MHC/ HLA class I does mean neuroblastoma cells are more susceptible to NK cell mediated killing.

Down regulation of the ligands for the activatory NKG2D receptor

The down regulation and/ or specific release of NKG2D ligands in neuroblastoma has been proposed as another immune evasion strategy (156). Surface expression of the NKG2D receptor ligands MICA, MICB, ULBP-1, ULBP-2 and ULBP-3 was assessed on a variety of primary neuroblastoma, tumours and cells lines. MICA, MICB and ULBP-1 were detected on all primary neuroblasts and ULBP-2 and ULBP-3 were also present in 50 % of cases. However, analysis of the primary tumours revealed that the only NKG2D ligands expressed were MICB and ULBP-2 (156). MICB was present in the cytosol of the majority of the neuroblastoma cell lines tested and surface expression of MICA, ULBP-2, or ULBP-3 was observed on a number of the cells lines tested, whereas ULBP-1 was notably absent on all cell lines (156). Soluble

MICA and MICB is released into the sera of patients with a host of different malignancies and has been shown to down regulate NKG2D on the associated effector cells (157, 158). Moreover, soluble MICA was found to be much higher in the sera of neuroblastoma patients compared to healthy donors, and when NK cells were pre-incubated with sera containing soluble MICA from neuroblastoma patients NKG2D mediated lysis was reduced. (156).

1.5 Immunotherapy for neuroblastoma

As mentioned in section 1.1 the potential for immunotherapies to offer a more specific, less toxic treatment strategy and potentially confer immunological memory, means there is considerable interest in the use of immunotherapies for the treatment of high risk neuroblastoma. A number of passive and active immunotherapeutic strategies have undergone trials for the treatment of neuroblastoma, reviewed in (21); however, passive therapies in the form of mAb have undoubtedly been the most successful, especially when combined with active cytokine therapy.

1.5.1 Monoclonal antibody therapy

Since Köhler and Milstein developed the hybridoma technique for the production of mAb in the 1970s (159) an array of mAb based therapies have entered the clinic to treat a wide range of diseases. As of 2012 there are twelve Food and Drug administration (FDA) approved mAb used clinically in the treatment of cancer patients, these are summarised in table 2.

Table 1-2. FDA approved mAb used clinically to treat cancer.

Antibody	Target	FDA approved indication	Mechanism of action
Trastuzumab (Herceptin®) humanised IgG1	HER2 (Erb2)	HER2-positive breast cancer, both as a single agent and in combination with chemotherapy for (i) adjuvant or (ii) palliative treatment; HER2-positive gastric, or gastroesophageal junction carcinoma, as first line treatment in combination with cisplatin and capecitabine/5-FU	Inhibition of HER2 signalling
Bevacizumab (Avastin®) humanised IgG1	VEGF	Palliative treatment of colorectal cancer, non-small cell lung cancer, glioblastoma, or renal cell carcinoma	Inhibition of VEGF signalling
Cetuximab (Erbitux®) chimeric IgG1	EGFR (ErbB1)	In combination with radiation therapy for the initial treatment of locally, or regionally advanced squamous cell cancer of the head and neck (SCCHN); a single agent for SSCHN patients when prior platinum based therapy failed; palliative treatment of pre-treated metastatic EGFR-positive colorectal cancer	Inhibition of EGFR signalling; ADCC
Pantitumumab (Vectibix®)* human IgG2	EGFR (ErbB1)	A single agent for the treatment of pre-treated EGFR-expressing metastatic colorectal carcinoma	Inhibition of EGFR signalling
Ipilimumab (Yervoy®) IgG1	CTLA-4	For the treatment of unresectable, or metastatic melanoma	Inhibition of CTLA-4 signalling
Rituximab (Rituxan® and Mabthera®) chimeric IgG1	CD20	For the treatment of CD20 positive B cell non-Hodgkin lymphoma (NHL) and chronic lymphocytic leukaemia (CLL) and for maintenance therapy of untreated follicular CD20 positive NHL	ADCC; direct induction of apoptosis; CDC
Alemtuzumab (Campath®) humanized IgG1	CD52	As a single agent treatment for B cell CLL	Direct induction of apoptosis; CDC
Ofatumumab (Arzerra®) human IgG1	CD20	Treatment for patients with CLL refractory to fludarabine and alemtuzumab	ADCC; CDC
Gemtuzumab ozogamicin	CD33	For the treatment of patients with CD33-positive acute myeloid leukaemia in first	Delivery of toxic payload,

Antibody	Target	FDA approved indication	Mechanism of action
(Mylotarg®) humanized IgG4		relapse who are ≥ 60 years of age and not considered eligible for other cytotoxic chemotherapy – Withdrawn June 2010	calicheamicin toxin
Brentuximab vedotin (Adcetris®) chimeric IgG1	CD30	For the treatment of relapsed or refractory Hodgkin lymphoma and systemic anaplastic lymphoma	Delivery of toxic payload, auristatin toxin
^{90}Y-Ibritumomab Tiuxetan (Zevalin®) murine IgG1	CD20	Treatment of relapsed refractory low-grade, or follicular B cell NHL in patients who achieve a partial complete response to first-line chemotherapy	Delivery of the radio-isotope yttrium-90
^{131}I-Tositumomab (Bexxar®) murine IgG2	CD20	Treatment of patients with CD20-antigen expressing relapsed or refractory low-grade, follicular, or transformed NHL	Delivery of the radio-isotope iodine-131; ADCC; direct induction of apoptosis

*Not recommended in colorectal cancer patients whose tumours express mutated Kras

Table reproduced from (160).

1.5.1.1 Monoclonal antibody production

The first mAb produced using hybridoma technology (159) involved the fusion of splenocytes harvested from a mouse that had been immunised with the desired antigen, with an immortalised myeloma cell line to produce the hybridoma. Individual hybridoma cells were then selected and cloned to ensure they produce single antibody specificity, directed towards a unique region of the immunised substance known, as the epitope (159). The hybridoma cells were subsequently screened and those producing the desired antibody cloned by growing up from a single antibody producing cell, hence the term 'monoclonal antibody'. Whilst the process of mAb production was successful in terms of proof or principle, the mAb produced were less successful in terms of promoting a therapeutic benefit. The lack of clinical effect was attributed to the production of human anti-mouse antibodies (HAMA), which are responsible for the rapid clearance of the therapeutic mAb and the termination of therapy.

With time, the advent of molecular biology techniques allowed the development of chimeric, humanised and more recently fully human, mAb with less associated immunogenicity. First came the chimeric mAb, in 1986 the Winter group produced a chimeric murine mAb with human Fc domains (161). These mAb, which were approximately 70 % human and 30 % mouse, retained the binding specificity of the original mAb but were less immunogeneic. Other therapeutic benefits of chimeric mAb include a longer half-life and more effective engagement of human effector cells (162). In 1988 Riechmann put forward the notion of humanising mAb by grafting the CDRs of rat mAb onto human framework (163) and by 1990 this same group had produced a humanised anti-tumour necrosis factor-α mAb using phage display technology (164, 165). By using bacteria to randomly generate human antibody chains that are subsequently selected through their specific binding properties *in vitro*, phage display technology bypasses the need for animal immunisation and therefore issues associated with self-tolerance (164, 165). Other humanisation techniques include CDR grafting and the immunisation of genetically modified mouse strains that only possess human IgG genes, thus producing similarly humanised re-agents.

1.5.1.2 Direct targeting mAb

Monoclonal antibodies that directly target TAA are an attractive alternative to traditional chemotherapies, as their exquisite specificity for their target antigen mimics Ehrlich's 'magic bullet', in the sense that mAb can be targeted to TAA expressing cells specifically, thus minimising the damage to healthy cells. Once bound to its target antigen via the Fab region the Fc portion of the mAb is able to interact with FcγR expressed on a variety of immune effector cells and molecules, through which the antibody exerts its therapeutic effect.

Mechanisms of action for direct targeting mAb based therapy

As mentioned previously once bound to its target antigen via CDR interactions the Fc portion of the mAb engages FcγR expressed on immune effector cells and molecules. The Fc: FcγR interaction initiates immune effector mechanisms, such as ADCC and phagocytosis. Additionally, the binding of a mAb to its target antigen may also trigger signalling pathways that result in complement-dependent cytotoxicity (CDC) and programmed cell death (PCD), whereas other

clinically approved mAb, such as Herceptin, are able to perturb survival signalling. These effector mechanisms are summarised in figure 1.11.

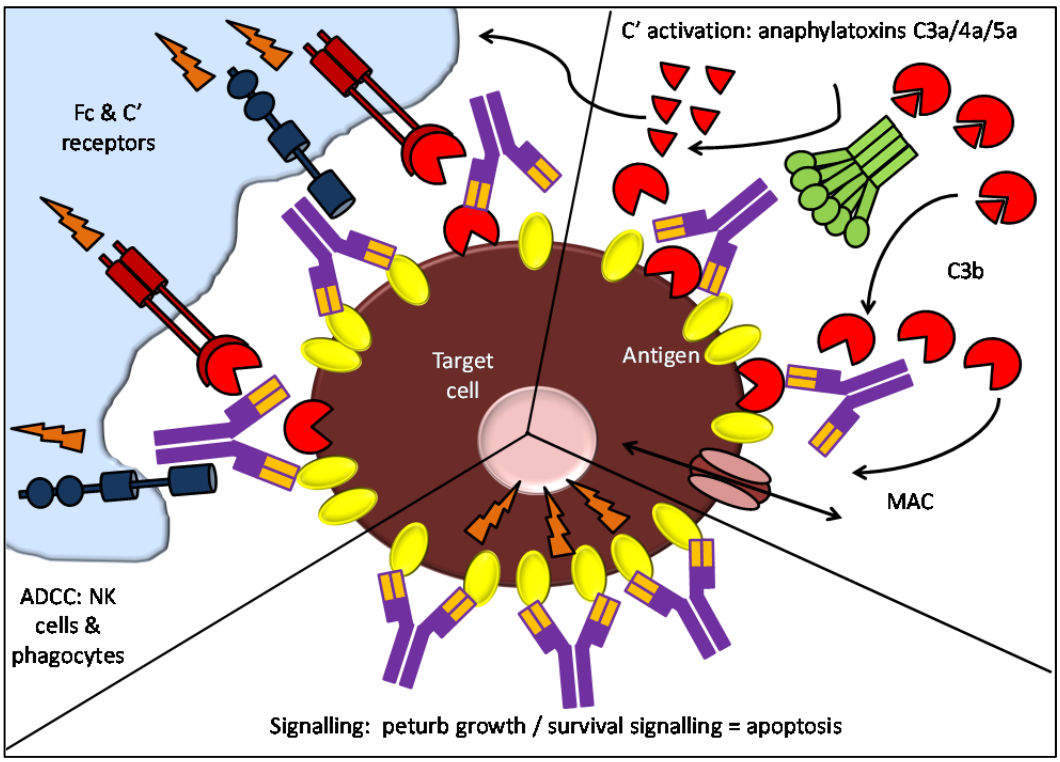

Figure 1-11. Mechanisms of action for direct targeting mAb. Upon binding its target antigen a direct targeting mAb can mediate killing via antibody dependent cellular toxicity/ phagocytosis, complement-dependent cytotoxicity, or though initiation/ disruption of signalling pathways to trigger apoptosis/ perturb survival signalling.

Antibody dependent cellular cytotoxicity/ phagocytosis

ADCC is initiated when the Fc portion of a mAb bound to its target antigen engages an activatory FcγR expressed on the surface of an effector cell, such as NK cells, macrophages, or activated granulocytes, resulting in release of cytotoxic granules, reactive oxygen species, or phagocytosis (166). ADCC can occur when the Fc portion of the mAb engages the FcγR CD16, which is expressed on the surface of human and murine NK cells. As discussed in section 1.2.1.2. the γ-chain of CD16 is associated with the FcεR1-γ-CD3-ζ heterodimer, hence engagement of CD16 triggers the release of the cytotoxic granules perforin and granzymes and results in destruction of the antibody labelled target cell. Macrophages also elicit ADCC, a phenomenon known as antibody-dependent cell mediated phagocytosis (ADCP), consequently the engagement of FcγR expressed on the surface of macrophages results in the physical engulfment of the antibody coated target cell via receptor mediated phagocytosis.

Complement-dependent cytotoxicity

Complement-dependent cytotoxicity (CDC) is initiated when several mAb are bound to multiple sites on the target cell surface in close proximity. To activate the classical complement pathway, two or more of the six globular heads of the C1q molecule must bind an Fc domain, thereby initiating a cascade of events culminating in the lysis of the antibody labelled target cell. The early events of complement activation lead to the production of C3 convertases, these enzymes go on to produce large amounts of C3a and C3b. C3b opsonises target cells and triggers phagocytosis through the engagement of the CR3 receptor and is also involved in the formation of C5 convertases. The C5 convertase produces large volumes of C5a and C5b, the latter of which initiates the late events of complement activation, resulting in the formation of the membrane attack complex (MAC) that is thought to contribute to the lysis of the target cells. Additionally, both C5a and C3a are potent inflammatory mediators and may augment cytotoxicity through the recruitment of phagocytes. Complement is not only initiated upon recognition of antigen: antibody complexes. The lectin pathway can be initiated when mannose binding lectin binds to mannose containing carbohydrates expressed by bacteria and viruses. Additionally, the alternative pathway is initiated following spontaneous hydrolysis of C3, which is abundant in the plasma. Each pathway leads to the production of C3 convertases and kick starts the complement cascade.

Perturbing growth and survival signals: induction of apoptosis

The binding of direct targeting mAb to cell surface receptors can trigger signalling cascades that lead to cell death. Alternatively, mAb may also perturb activation signals required for proliferation, or maintaining viability, by depleting the natural ligand from the circulation, blocking or modulating the receptor, or preventing ligand induced dimerization (166). Examples include mAb that bind HER1 (EGFR or c-*erb*-1) and HER2 (*neu* or c-*erb*-2). Anti-EGFR mAb are competitive agonists and bind the receptor with greater affinity than the endogenous ligand, preventing the ligand from binding and subsequently down regulating EGFR expression, hence inhibiting the signal that would, in the absence of mAb, drive tumour growth (167). Similar mechanisms have been described for mAb that target HER2, such as Herceptin (168). These mAb

can also block homodimerisation with other HER2 receptors and heterodimerisation with other members of the receptor family (169).

Inducing adaptive immunity

Regardless of the killing mechanism evoked mAb based therapy will result in the release of lysed tumour cell contents (antigenic material) into the surrounding microenvironment. These particulate or soluble antigens, along with apoptotic/ necrotic cell fragments are likely to be engulfed by professional APCs, such as dendritic cells and macrophages. Engulfment of the antigenic material by specialised $CD8\alpha^+$ (mouse), or $CD141^+$ (human) subsets of dendritic cells that were introduced in section 1.2.1.2. may result in cross presentation of the tumour-derived antigens to naïve $CD8^+$ T cells, and the subsequent generation of tumour-specific CTLs and effector memory cells. The ability of dendritic cells to acquire antigen from dying tumour cells and elicit $CD8^+$ T cell responses has been demonstrated *in vitro* (170-172). Moreover, the cross presentation of tumour-derived antigenic fragments and the subsequent generation of adaptive T cell responses is also likely to account for the vaccine-like effect of rituximab therapy reported in lymphoma patients (173).

1.5.1.3 Monoclonal antibody therapy for the treatment of neuroblastoma

Although not yet clinically approved the advent of direct targeting mAb based therapies that recognise and bind to the disialoganglioside GD2, a TAA located on the outer membrane of neuroblastoma cells, was an exciting new development in the treatment of neuroblastoma.

The disialoganglioside GD2 as a tumour-associated antigen

GD2 is a complex acidic glycolipid that is ubiquitously expressed on the surface of tumour cells of neuroectodermal origin, such as neuroblastoma and the majority of melanomas (174, 175). Under normal physiological conditions GD2 expression is primarily restricted to the central nervous system (CNS), peripheral nerve fibres and skin melanocytes (175-178). This relatively tumour-selective expression of GD2 makes it an ideal target for mAb based therapy, particularly as there is evidence to suggest that GD2 expression is not

modulated at the cell surface upon mAb binding and levels remain persistent post therapy (179).

Anti-GD2 mAb

At present there are three clinically relevant anti-GD2 mAb that have been used to treat children with neuroblastoma; two murine mAb, namely 3F8 and 14G2a, and the chimeric mAb ch14.18. These mAb have all shown considerable promise in the MRD setting.

3F8

The murine based IgG3 mAb 3F8 was developed in 1985 by Cheung *et al.* at the Memorial Slone Kettering Cancer Centre (MSKCC) (174). This mAb has undergone extensive pre-clinical and clinical testing and was the first anti-GD2 mAb to be given to patients (180). Initial *in vitro* experiments suggested that activation of the complement system was the most likely mechanism responsible for 3F8 mediated tumour cell killing (174). Further evidence for the role of complement was provided in a subsequent paper, which demonstrated that human complement could be used to purge the bone marrow (a common site of metastatic disease) of neuroblastoma cells *in vitro* (181) and the results from the first phase I trial of 3F8 subsequently concluded that the antibody was most likely to be effective in the MRD setting (180). Whilst administration of 3F8 treatment for MRD was found to be effective, there were a number of limitations associated with the therapy. Firstly, severe pain was reported as a major side effect of treatment with 3F8 and this is thought to be due to cross reactivity with GD2 on peripheral nerve fibres. The associated pain can be successfully managed; however, it is still considered to be a dose limiting factor. Secondly, 3F8 is a murine IgG3 mAb therefore it can promote the production of HAMA, which subsequently neutralise the mAb and terminate its therapeutic effect, although paradoxically this has been associated with improved survival (182).

14G2a

The murine IgG2a mAb 14G2a is a class switch variant of the IgG3 anti-GD2 mAb 14.18 developed by Reisfeld's group in 1986 (183). The 14G2a class switch was originally developed to investigate the relative contributions of the Fab and Fc domains of the mAb to the overall anti-tumour effect (184). The

14G2a mAb was found to be more effective compared to 14.18 at inducing ADCC *in vitro* at the same concentration and effector: target ratio, consequently 14.18 never underwent clinical testing. 14G2a has been shown to suppress tumour progression in xenograft models using nude mice (184). Whereas other investigations have shown 14G2a may be able to induce apoptosis in a caspase-dependent and independent manner and may also enhance the killing potential of several commonly prescribed chemotherapeutic agents (185). A number of phase I clinical trials have been performed with 14G2a (186-188); however, issue with HAMA responses ultimately led to the development of ch14.18.

ch14.18

The chimeric anti-GD2 mAb ch14.18 was developed in an attempt to reduce the HAMA responses observed with its murine counterpart 14G2a. ch14.18 comprises of the variable Fab region of the original 14.18 mAb and the constant Fc region of human IgG1 (189). Consequently, ch14.18 should retain the specificity of 14G2a but be less immunogenic. Direct comparisons of the ch14.18 and 14G2a mAb found that ch14.18 was more effective at inducing NK cell mediated ADCC *in vitro* using effector cells obtained from both healthy volunteers and stage IV neuroblastoma patients (minimum four weeks post-therapy (190). Having previously undergone phase I and II trials as a single agent (191, 192), ch14.18 was administered alongside the cytokine IL-2 and granulocyte-macrophage colony stimulation factor (GM-CSF) in a phase III trial conducted by the COG, the results of which were published in 2010 (193). Following standard induction therapy patients recruited onto the trial were subsequently assigned to treatment groups and received either 13-cis-retinoic acid alone, or in combination with ch14.18 plus alternating cycles of IL-2 and GM-CSF. Randomisation was stopped early when interim analysis revealed that the immunotherapy based regimen was associated with a significant increase in event free survival, 66 % versus 46 % as reported for patient receiving standard maintenance therapy. The overall survival rate was also significantly superior among patients receiving the immunotherapy based regimen but did not meet the statistical criteria for stopping early.

The results of the COG trial provide some of the most persuasive and compelling evidence for the inclusion of immunotherapy as part of the standard treatment for high risk neuroblastoma patients, particularly in the

MRD setting; however, this trial was not without its limitations. Firstly, as all the patients receiving the anti-GD2 mAb ch14.18 also received IL-2 and GM-CSF, it was not possible to ascertain the relative contributions of the antibody and cytokines to the overall therapeutic effect. This is potentially significant as previous studies have been performed using IL-2 alone to stimulate the immune system and enhance endogenous anti-tumour immune responses with some success (194, 195). Secondly, the immunotherapy regimen was associated with considerable toxicity. The toxic effects observed were attributed to the mode of action for the therapy itself, for example pain, as a consequence of the antibody cross reacting with GD2 expressed on peripheral nerve fibres (196, 197), cytokine mediated capillary leak syndrome (198) and complement activation. Thirdly, despite the fact the immunotherapy regimen conferred a significant survival advantage; a considerable number of patients remained uncured. Hence further work is still required to optimise the immunotherapeutic strategy and maximise the therapeutic benefit. Finally, the *in vivo* mechanisms of action for this immunotherapeutic regimen are poorly characterised, making it difficult to rationally optimise therapy.

Mechanisms of action for anti-GD2 mAb based therapy

Much of the early *in vitro* mechanistic data obtained suggests that CDC and ADCC are likely to be responsible for the therapeutic effect of anti-GD2 mAb (181, 184, 199). However, a number of immune effector cells have been implicated in anti-GD2 tumour cell destruction, including lymphocytes (199), granulocytes (200) and macrophages (201) and there seems to be some debate in the literature regarding the relative contributions of the different effector cell types to the therapeutic effect of anti-GD2 mAb.

Lymphocytes

Of the early papers implicating lymphocytes the general consensus seems to be that NK cells rather than T cells are responsible for the therapeutic effect of anti-GD2 (202). This was perhaps due to the fact neuroblastoma cells express markedly reduced levels of MHC class I molecules, rendering them less susceptible to MHC restricted CTL killing (148). Further evidence to support the role of NK cells *in vivo* was provided when Lode *et al.* reported that their ch14.18-IL-2 fusion protein could effectively clear liver and bone marrow metastasis in C.B17 SCID mice, which are deficient in T and B cells (203). Lode

et al. also reported that the ability to eradicate metastatic disease was abrogated when the same therapy was administered to tumour bearing SCID/BEIGE mice, which are also deficient in NK cells. However, therapy could be restored when SCID/BEIGE mice were reconstituted with NK cells harvested from the spleen of naïve A/J mice. Moreover, the therapeutic effect of ch14.18-IL-2 was also abrogated following depletion of NK cells in tumour bearing A/J mice, whereas depletion of $CD8^+$ T cells had no effect on therapy.

Two recent studies have provided clinical evidence for the contribution of NK cells to the therapeutic effect of anti-GD2 mAb. Firstly, a subset of patients being treated for relapsed, or refractory neuroblastoma who possessed a genetic polymorphism resulting in KIR-HLA mismatch experienced either a complete response, or significant improvement in their disease following immunotherapy (204). Secondly, a separate study found KIR and HLA polymorphisms that resulted in patients missing at least one cognate HLA class I ligand for its associated inhibitory KIR had a 40 % lower risk of death and a 34 % lower risk of disease progression at three years following haematopoietic stem cell transplant compare to patients with all HLA ligands present for their inhibitory KIR (205). This so called 'missing ligand effect' and the therapeutic benefit it confers has been attributed to ADCC mediated by unlicensed NK cells (206). This phenomenon is illustrated in figure 1.12.

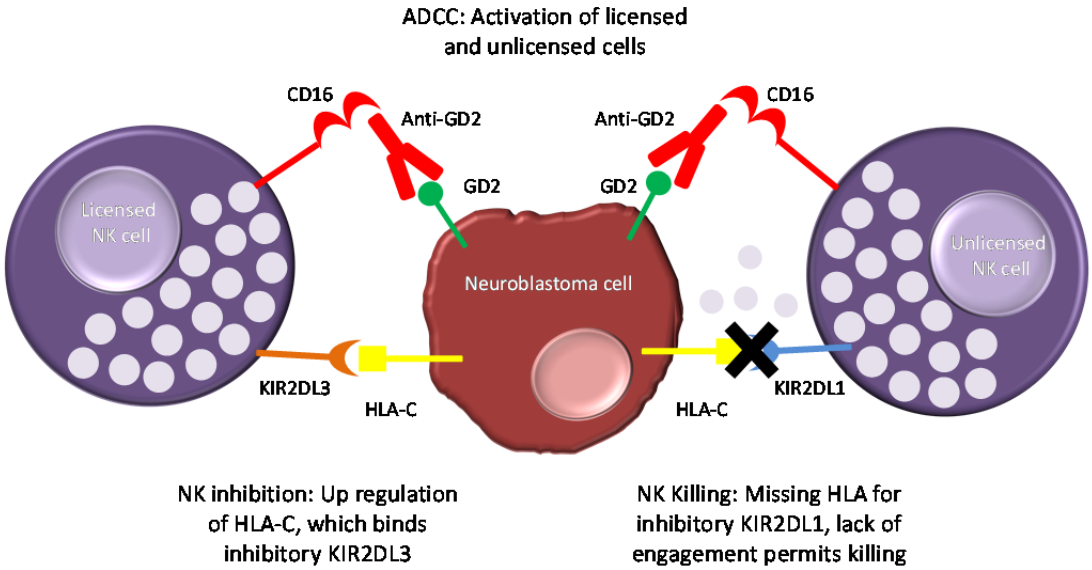

Figure 1-12. The missing-ligand effect. Anti-GD2 mAb activates both licensed and unlicensed NK cells via CD16, the resulting cytokine release triggers up regulation of HLA class I molecules by neuroblastoma cells. The interaction between HLA and its inhibitory KIR on the surface of licensed NK cells prevents further activation. Unlicensed NK cells do not receive the inhibitory signal and continue to mediate ADCC.

Anti-GD2 mAb activates both licensed and unlicensed NK cells via CD16, which triggers ADCC and release of IFN-γ. IFN-γ induces up regulation of HLA molecules on the surface of the neuroblastoma target cells, which subsequently binds to the associated inhibitory KIR expressed by licensed NK cells and prevents further activation. However, the unlicensed NK cells which express inhibitory KIR specific for the missing HLA ligand subtype are not inhibited. Unlicensed NK cells are thought to be responsible for the majority of the anti-GD2 mediated ADCC within the subset of patients missing cognate HLA ligands, which may account for the apparent survival advantage (206).

Granulocytes and macrophages

Investigations carried out by Kushner and Cheung at MSKCC reported that granulocytes were responsible for anti-GD2 mediated ADCC *in vitro* (200). Chromium release assays were performed using purified granulocyte populations obtained from peripheral blood as effectors and 3F8 opsonised human neuroblastoma cells lines as targets. ADCC was instigated following the engagement of the Fc portion of the mAb to FcγRIII (presumably FcγRIIIB, which is expressed on the surface of neutrophils). Tumour cell lysis was reduced when assays were performed used a F(ab')2 3F8 antibody, anti-GD2 mAb of a different isotype, namely the IgM mAb 3G6, or an anti-CD16 mAb 3G8, suggesting granulocyte mediated ADCC was Fc-FcγR dependent. Moreover, the addition of GM-CSF to these *in vitro* ADCC assays was observed to increase tumour cell lysis at least ten-fold. Clinical evidence for the involvement of granulocytes and macrophages in the anti-tumour activity of anti-GD2 mAb was obtained in 2006 following publication of the results from a clinical trial (207). One hundred and thirty six patients were recruited onto this trial; 130 patients had metastatic stage IV disease and the remaining 6 had high risk stage III disease. Of the 135 patients successfully assessed for polymorphism, 30 were found to possess the FcγRIIA (R/R) genotype, which correlated with superior progression free survival (median 47.0 months) following treatment with 3F8 plus GM-CSF. This FcγR subtype is expressed on neutrophils and macrophages and suggests a role for FcγRIIA in phagocyte mediated ADCC.

Conflicting evidence has been published by Raffaghello *et al.* who concluded that neither NK cells, nor macrophages were likely to play a major role in the anti-tumour activity of anti-GD2 mAb (208). Their conclusion was based on experiments performed in SCID/BEIGE mice bearing human neuroblastoma

xenografts that had been depleted of splenic and intraperitoneal macrophages following the administration of dichloromethylene disphosphate (clodronate) liposomes, in which a total dose of 4 mg/kg 14G2a was still observed to have a protective effect. This observation led the authors to conclude that either CDC, or granulocyte-mediated tumour cell lysis was most likely to be responsible for the anti-tumour activity of anti-GD2, although due to the technical difficulties of depleting complement and/ or granulocytes in immunodeficient mice this was not explored further.

It is clear from the above section that the mechanisms of action responsible for the therapeutic effect of anti-GD2 mAb have yet to be clearly defined. The dogma within the scientific community may be that tumour cell killing is largely NK cell mediated; however, considerable evidence has been provided to suggest a role for other immune effector cell types, namely macrophages and neutrophils. Much of the mechanistic characterisation work performed to date has been carried out *in vitro* or *in vivo* using immunodeficient mouse models and human neuroblastoma xenografts, which does not permit study of endogenous immune response to tumour. Consequently, detailed characterisation of both the immune response to tumour and the effector mechanisms responsible for the anti-tumour activity of anti-GD2 mAb in fully immunocompetent mouse models is still required in order to fully understand the complex relationship that occurs between the developing tumour and the immune system and to rationally design new strategies to improve existing therapy.

1.6 Immunomodulatory antibodies

As discussed in section 1.2.1.2 antigenic stimulation alone is generally insufficient to activate naïve T cells, hence additional co-stimulatory signals are required. The first co-stimulatory molecule discovered was CD28 (209) and since then a host of co-stimulatory receptor-ligand pairs have been identified and these were summarised in figure 1.9. T cell responses can be enhanced by altering expression of either member of the receptor-ligand pair, or through the use of inhibitory molecules that block the normal receptor-ligand interaction (75). Immunomodulatory mAb represent a new approach to mAb based therapy, as instead of directly targeting TAA and initiating host effector mechanisms these mAb can be used as surrogate ligands for the co-

stimulatory molecules, thus augmenting T cell proliferation and survival. Replicating the interaction that normally occurs between the co-stimulatory molecule 4-1BB and its natural ligand 4-1BBL using agonistic anti-4-1BB antibodies is of particular interest for this investigation.

1.6.1 Expression of 4-1BB and its natural ligand 4-1BBL

4-1BB, also known as CD137 or tumour necrosis factor receptor superfamily member 9 (TNFRSF9) is a surface glycoprotein expressed on the surface of activated T cells. 4-1BB was first identified as a cDNA selectively expressed in activated but not resting murine T cells (210). The cDNA was found to map to chromosome 4, where the 4-1BB gene spans approximately 13 kb and comprises of 10 exons, two of which are in the 5' untranslated region and eight in the coding region (211). Analysis of the nucleotide sequence uncovered a single open reading frame encoding a 256 amino acid polypeptide, with a calculated molecular mass of 27.5 kDa. The human 4-1BB gene resides on chromosome 1p36 with a cluster of related genes, including TNFR2, CD30 and OX40, which have been shown to be mutated in numerous malignancies (212). Human 4-1BB comprises of 255 amino acids, with a calculated molecular mass of 27 kDa (213) and has 60 % homology with the murine counterpart (214). The extracellular portion of the 4-1BB molecule contains four cysteine rich TNFR motifs, a short transmembrane region and a cytoplasmic tail containing four potential phosphorylation sites (215). The 4-1BB molecule is typically found as a 55 kDa dimer on the surface of T cells (215). Once expression has been induced surface levels increase slowly, peaking at around 60-hours and can still be detected up to 96-hours post-stimulation (215). In addition to expression on activated T cells, activation induced functional 4-1BB surface expression has been reported for NK cells and NKT cells, as well as a number cell types of myeloid lineage, including monocytes, neutrophils, mast cells and eosinophils (216). Moreover, 4-1BB is constitutively expressed on $CD11c^{+}$ dendritic cells and $CD4^{+}CD25^{+}FoxP3^{+}$ Tregs.

Both humans and mice possess a natural high affinity ligand for 4-1BB, known as 4-1BBL (214, 217). 4-1BBL is a type II transmembrane glycoprotein homologous to other members of the TNF ligand family, such as TNF, CD27 ligand and CD40 ligand. 4-1BBL is constitutively expressed at a low level on B

cells, macrophages and dendritic cells (218), and activation of these cells can lead to increased 4-1BBL expression.

1.6.2 4-1BB ligation and T cell function

The discovery that 4-1BB expression is up regulated by activated, rather than resting T cells suggested that 4-1BB may be involved in modulating T cell responses. Numerous studies have been performed to assess the role of 4-1BB using anti-4-1BB antibodies, soluble 4-1BBL, or 4-1BBL$^+$ cell lines in combination with anti-TCR antibodies, and the co-stimulatory effects induced upon 4-1BB ligation have been well characterised. Ligation of 4-1BB in the absence of TCR stimulation has no effect on T cell activity; however, ligation of 4-1BB in conjunction with TCR engagement can have a profound effect on T cell proliferation, survival, cytokine secretion and cytotoxic effector function. Whilst initial reports suggested that proliferation of CD8$^+$ T cells was preferentially induced following 4-1BB stimulation (219), more recent evidence has shown that the enhanced proliferative effect is observed to a similar extent in both CD4$^+$ and CD8$^+$ T cells (220). Improved T cell survival is associated with increased expression of the anti-apoptotic genes *bcl-X*$_L$ and *bfl-l* in response to 4-1BB mediated NF-κB activation, thus preventing activation-induced cell death (AICD) (221). Another co-stimulatory effect of 4-1BB ligation is enhanced cytokine production, with CD4$^+$ T cells producing more IL-2 and IL-4, and CD8$^+$ T cells producing more IFN-γ in response to 4-1BB ligation (222). Moreover, anti-4-1BB mAb can also enhance CTL activity by increasing the number of T cells with full effector function both *in vitro* and *in vivo* (223, 224).

1.6.2.1 The effect of 4-1BB ligation on other cell types

The effects of ligation of 4-1BB expressed on the surface of several cell types, other than T cells, has also been explored. Agonistic anti-4-1BB mAb have been shown to increase murine NK cell proliferation and IFN-γ production, as well enhance their ability to prime CD8$^+$ T cells; however, their cytotoxic capacity remained unaltered (225). Ligation of 4-1BB expressed on the surface of dendritic cells has resulted in up regulation of the B7 molecules CD80 and CD86, as well as increased production of the cytokines IL-6 and IL-12 (226). Additionally, increased proliferation of functionally suppressive 4-1BB$^+$ Tregs has been reported in response to 4-1BB ligation (227).

1.6.3 Anti-4-1BB mAb and cancer

The first evidence that anti-tumour effects could be evoked through 4-1BB signalling was provided in 1997 when Melero *et al.* demonstrated that administration of agonistic anti-4-1BB mAb could significantly inhibit tumour cell growth in mice bearing either Ag104A sarcoma, or P815 mastocytoma (228). The anti-tumour activity was attributed to the generation of a tumour-specific CTL response that was sufficient to eradicate even established disease (228). Subsequent depletion experiments confirmed that the anti-tumour effects of anti-4-1BB mAb in these murine models were dependent on both $CD4^+$ and $CD8^+$ T cells, as well as NK cells. However, since P815 tumour cells are resistant to NK cell mediated lysis *in vitro* the abrogated anti-tumour effect of anti-4-1BB following NK cell depletion was attributed to a potential loss of immunoregulatory signals involved in the generation of CTLs responses, rather than an anti-4-1BB induced cytolytic effector function (229).

Anti-4-1BB mAb have since been shown to induce tumour-specific CTL responses that are capable of eradicating tumour in a number of syngeneic mouse models, including the CT26 colon epithelial tumour, A31 B cell lymphoma, B10.2 fibrosarcoma, K1735 melanoma, MCA205 sarcoma, GL261 glioma and NS0 myeloma (230-234). In general the more immunogenic tumours were associated with more effective generation of tumour-specific CTL responses. Additionally, tumour burden can have influence the generation of a CTL response. In one study involving mice bearing B10.2 fibrosarcoma administration of anti-4-1BB on day 3 and 6 post-inoculation was observed to have a curative effect in 50 % of cases. However, when therapy was delayed until day 13 and 16 post-inoculation the curative effect was observed in 80 % cases, the superior response was attributed to the increased antigenic load associated with the greater tumour burden (232, 233).

The sequence of events originally postulated in 1997 for the anti-tumour effect of anti-4-1BB mAb therapy were as follows: T cells up regulate 4-1BB in response to TCR stimulation by tumour antigens, the systemically administered anti-4-1BB mAb ligates 4-1BB expressed on the surface of these T cells and provides co-stimulatory signals that promote the effector functions of tumour-specific CTLs and drive expression of anti-apoptotic genes to prevent AICD (228). However, the precise mechanism for the generation of the anti-tumour effects of anti-4-1BB mAb still remains unclear, whilst $CD4^+$ T cells and NK

cells appear to have a role in the induction of anti-tumour immunity, it is apparent that tumour-specific CTLs are the main effector subtype involved. Regardless of the mechanisms responsible for therapy, sufficient pre-clinical data demonstrating the therapeutic effect of anti-4-1BB mAb has been provided and these mAb have entered clinical trials for the treatment of several solid tumours, including melanoma, renal carcinoma and ovarian cancer (235).

1.6.4 Combining anti-4-1BB mAb with direct targeting mAb for the treatment of cancer

The ability of NK cells to induce surface expression of 4-1BB upon activation was first reported by Melero *et al.* in 1998 (229). However, more recently surface 4-1BB up regulation by NK cells has been reported post FcγR triggering (236). This observation led Levy and co-workers to formulate their hypothesis that if FcγR triggering results in 4-1BB up regulation by NK cells, subsequent ligation of 4-1BB by agonistic anti-4-1BB mAb may enhance NK cell killing by ADCC. Levy *et al.* went on to propose a novel combinatorial therapeutic approach for the treatment of lymphoma, which involved the administration of a direct targeting mAb, alongside an agonistic anti-4-1BB mAb (237). The direct targeting mAb, namely anti-CD20, is known to exert its therapeutic effect at least in part via ADCC through the engagement of FcγRIII (CD16) and therefore should induce 4-1BB up regulation by NK cells. Consequently, subsequent administration of an anti-4-1BB mAb will ligate 4-1BB on the NK cell surface, providing a co-stimulatory signal resulting in enhanced effector function. Levy's group went on to test their theory using both *in vitro* and *in vivo* model systems. Their work published by Kohrt *et al.* (237) demonstrated that 4-1BB expression could be up regulated by NK cells isolated from the peripheral blood of healthy donors following 24-hour co-culture with $CD20^+$ cell lines and anti-CD20 mAb. Moreover, when these NK cells were recovered and used as effector cells in ADCC assays combined treatment with both anti-CD20 and anti-4-1BB mAb resulted in a significant increase in $CD20^+$ target cell lysis beyond that observed for either mAb alone . Kohrt *et al.* also tested the effect of anti-CD20 and anti-4-1BB mAb therapy *in vivo* using both syngeneic murine and xenotransplanted human models. In both cases the combination therapy was associated with tumour regression and significantly improved survival compared to mice receiving control, or single mAb therapy. The sequence of administration was found to be important as the most potent

anti-lymphoma effect was observed when anti-4-1BB was administered 24-hours post anti-CD20. Additionally, depletion studies also suggested NK cells and macrophages were responsible for the anti-lymphoma effect as depletion of these cells abrogated therapy, whereas depletion of $CD8^+$ T cells did not.

Levy's group have gone on to explore the effects of other direct targeting mAb when administered in combination with anti-4-1BB. Kohrt *et al.* have published another two papers in which they have investigated trastuzumab (Herceptin®) plus anti-4-1BB for the treatment of $HER2^+$ cell lines and primary breast cancer, and cetuximab plus anti-4-1BB for the treatment of $EGFR^+$ cells lines, including the SCC4 and SCC6 upper aerodigestive tract squamous cell carcinomas and the PC1 pancreatic adenocarcinoma (238, 239). In both cases the combination therapy was associated with potent NK cell mediated anti-tumour effects both *in vitro* and *in vivo* using xenotransplanted models.

1.6.5 Combining anti-4-1BB mAb with direct targeting anti-GD2 mAb for the treatment of neuroblastoma

The observation that 4-1BB expression is up regulated by human NK cells following FcγRIII (CD16) engagement (236) was of considerable interest in terms of this project. The tumour effects of anti-GD2 mAb are often attributed to NK cell induced ADCC, therefore this observation highlighted the potential for anti-GD2 plus anti-4-1BB combination therapy. The rational for this novel combinatorial approach was further strengthened by the more recent work published by Kohrt *et al.* (237-239) who have clearly demonstrated that combining direct targeting mAb with anti-4-1BB mAb has a potent anti-tumour effect in a number of different models. The ability to enhance ADCC in this manner may provide a method for enhancing the efficacy of anti-GD2 mAb whilst avoiding the toxicity associated with systemic cytokine administration.

1.7 Summary

In summary, there is strong evidence to support the routine use of immunotherapy in addition to the standard therapeutic regimen in high risk neuroblastoma patients at risk of relapse. However, substantial work is still required to optimise this treatment strategy. The purpose of this thesis is therefore two-fold. Firstly, I intend to characterise both the immune response

to tumour and the immune effector mechanisms responsible for anti-GD2 mAb therapy. Secondly, I intend to explore the potential of anti-GD2 plus anti-4-1BB mAb based therapy to determine whether this novel combinatorial approach can provide a more efficacious, and potentially less toxic, immunotherapy regimen for the treatment of high risk neuroblastoma, which will hopefully inform the design of future clinical trials.

1.8 Hypothesis, aims and objectives

1.8.1 Hypothesis

The *in vivo* efficacy of anti-GD2 mAb therapy can be enhanced for the treatment of neuroblastoma in murine syngeneic and spontaneous models when administered in combination with anti-4-1BB mAb.

1.8.2 Aims

This research project aims to characterise the cell mediated immune effector mechanisms thought to be responsible for the anti-tumour effects of anti-GD2 mAb and explore methods of enhancing the anti-tumour effect. More specifically this project aims to investigate the efficacy of anti-GD2 plus anti-4-1BB combined therapy using translatable murine models of neuroblastoma.

1.8.3 Objectives

1. Characterise the immune effector mechanisms responsible for the anti-tumour effects of anti-GD2 mAb therapy.
    a. Investigate the relative contributions of CDC, ADCP and ADCC following in response to administration of anti-GD2 mAb *in vitro.*
    b. Characterise the effector mechanisms responsible for anti-GD2 mAb therapy *in vivo.*
    c. Characterise the immune response to tumour in the syngeneic NXS2 mouse model.

2. Investigate the efficacy of anti-GD2 plus anti-4-1BB mAb therapy
    a. Investigate the ability of anti-GD2 mAb to induce 4-1BB expression on murine NK cells *in vivo.*
    b. Optimise the therapeutic strategy for investigating anti-GD2 plus anti-4-1BB mAb therapy *in vivo* using syngeneic murine models
    c. Translate the anti-GD2 plus anti-4-1BB mAb to the human setting using human neuroblastoma cell lines and peripheral blood mononuclear cells from healthy donors.

3. Investigate whether anti-GD2 plus anti-4-1BB mAb combination therapy enhances survival in the spontaneous TH-MYCN transgenic mouse model of neuroblastoma.
    a. Characterise the endogenous immune response to tumour in the TH-MYCN transgenic mice.
    b. Establish a model of MRD using TH-MYCN transgenic mice to facilitate the investigation of GD2 targeted immunotherapeutic strategies.
    c. Test the efficacy of the anti-GD2 plus anti-4-1BB immunotherapeutic regimen in an MRD setting using TH-MYCN transgenic mice.

Chapter 2: Materials and methods

2.1 Animals and cells

2.1.1 Animals

The therapeutic effects of anti-GD2 mAb can be studied *in vivo* using either syngeneic or spontaneous models of neuroblastoma. The syngeneic murine model of neuroblastoma developed by Ralph Reisfeld's group in 1997 utilises a GD2+ murine neuroblastoma cell line NXS2, which can be transplanted into syngeneic A/J mice subcutaneously or intravenously, to induce solid neuroblastoma tumour or metastatic-like disease (240). The transgenic TH-MYCN mice developed by Weiss *et. al.* overexpress human MYCN under the control of the rat tyrosine hydroxylase promoter, causing these mice to spontaneously develop tumours within several months of birth (241). Both the in-bred A/J mice syngeneic for the NXS2 cell line and the TH-MYCN transgenic mice on the 129/SvJ background were supplied by Harlan UK Ltd (Blackthorn, Oxon, UK). All animals used in throughout this project were maintained in local animal house facilities in accordance with Home Office regulations. All procedures have been approved by a local ethics committee and were performed in accordance with the Animals (Scientific Procedures) Acts 1986 as set out in the Project Licence.

The TH-MYCN transgenic mice were regularly examined for palpable abdominal masses and other visual signs of distress, including isolation, hunching and piloerection. The decision to cull a tumour bearing mouse was made by an independent assessor, *i.e.* an experienced animal technician, based on the size of the tumour, the physical appearance and behaviour of the animal.

2.1.2 Cell lines

The murine neuroblastoma cell lines Neuro2a and NXS2 were used throughout this investigation, alongside the human neuroblastoma cell lines Lan-1 and IMR-32. The Neuro2a, Lan-1 and IMR-32 cell lines were obtained from the ECACC, whereas the NXS2 cell line was kindly provided by Prof. Dr. med. Holger Lode (Medical University of Greifsweld). Both the Neuro2a and NXS2 cell

lines were cultured in Dulbecco's modified Eagles medium (DMEM) (Life Technologies) supplemented with 10% heat-inactivated foetal calf serum (FCS) (Lonza), 2 mM glutamine (Life Technologies) and 0.1 mM non-essential amino acids (NEAA) (Life Technologies), herein referred to as complete DMEM. The Lan-1 cell line was cultured in Eagle's minimal essential medium (EMEM) (Lonza) supplemented with 10% FCS, 2mM glutamine and 0.1 mM NEAA and Ham's F-12 nutrient medium (Sigma-Aldrich), supplemented with 10% FCS, 2 mM glutamine and 0.1 mM NEAA, in a 1:1 ratio. The IMR-32 cell line was cultured in EMEM supplemented with 10% FCS, 2 mM glutamine and 0.1 mM NEAA. All neuroblastoma cell lines are adherent and were harvested by gentle scraping (murine cell lines) or using trypsin-ethylenediaminetetraacetic acid (TE) (Lonza) (human cell lines). Murine neuroblastoma cell lines were maintained at 37°C and 5% CO_2 and human neuroblastoma cell lines were maintained at 37°C and 10% CO_2.

Other cell lines used throughout this investigation as either a positive or negative control include the human Burkitt's lymphoma Raji cell line (ATCC). Raji cells were cultured in RPMI-1640 (Life Technologies) supplemented with 10 % FCS, 2 mM glutamine and 1 mM pyruvate, herein referred to as complete RPMI, and maintained at 37°C and 5% CO_2.

2.1.3 Primary cells

Murine bone marrow-derived macrophages

Murine bone marrow-derived macrophages (BMDMs) were isolated from the bone marrow of the femur and tibia of A/J mice and homogenised to obtain a single cell suspension. Cells were cultured in complete RPMI supplemented with penicillin and streptomycin (pen-strep) (Life Technologies) both at 100 ng/mL, plus 10 % L929 cell conditioned medium (see below). BMDMs were maintained at 37°C and 5% CO_2 in 6-well plates seeded at $5x10^6$ cells per well and fed every 2–3 days with complete RPMI plus pen-strep and 10 % L929 conditioned medium. BMDMs were cultured for seven to fourteen days prior to use. BMDMs were harvested from 6-well plates by first washing twice with 2 mL sterile PBS (Severn Biotech) prior to a 10 minute incubation at 37°C with pre-warmed TE. A cell scraper was then used to gently detach the cells from the plate surface. The BMDMs were washed twice in complete RPMI plus pen-strep by centrifuging at 1500 rpm for 5 minutes, before being re-suspended in

complete RPMI plus pen-strep prior to use. Cell viability was determined by trypan blue exclusion and was routinely greater than 90 %.

The murine L929 cell line (ATCC) was cultured in complete RPMI at 37°C and 5 % CO_2 in tissue culture flasks. Once the cells reached confluence the supernatant was collected and sterile filtered using a Millex 0.22 µm PES membrane filter (Fisher Scientific) and stored at -20°C until required. The supernatant collected from the L929 cells contains macrophage colony-stimulating factor (M-CSF) and was used to supplement the media in which the BMDMs were maintained in order to induce macrophage differentiation.

Human peripheral blood mononuclear cells

Human peripheral blood mononuclear cells (PBMCs) were used as a source of effector cells in several different assays throughout this investigation. Human PBMCs were harvested from fully anonymised Trima leucocyte reduction system (LRS) cones collected from healthy adult volunteers. The LRS cones themselves were obtained from the National Blood Transfusion Service, Southampton, UK. The PBMCs were harvested using Lymphoprep™ density gradient medium (Axis-Shield). Briefly, the blood from the LRS cone was diluted in PBS supplemented with 2 mM EDTA and 10% FCS to give a final volume of 50 mL. The diluted blood was then split equally across two 50 mL Falcon tubes each containing 12.5 mL of Lymphoprep™. The balanced Falcon tubes were centrifuged (with the break turned off) at 800 g for 20 minutes, after which time the PBMCs were carefully removed from the interphase layer using a Pasteur pipette and transferred to a fresh Falcon tube. The PBMCs were subsequently washed three times in PBS + 2mM EDTA by centrifuging at 300 g for 5 minutes. The PBMCs were subsequently re-suspended in complete RPMI plus pen-strep if required for immediate use, or RPMI-1640 plus 2 mM glutamine, 1 mM pyruvate, penicillin and streptomycin (both at 100 ng/mL) and 1 % human serum (Sigma) for use as a source of monocyte-derived macrophages (MDMs) (see below).

Human monocyte-derived macrophages

Human PBMCs suspended in RPMI-1640 2 mM glutamine, 1 mM pyruvate, penicillin and streptomycin (both at 100 ng/mL) and 1 % human serum were incubated at 37°C and 5 % CO_2 in 6-well plates seeded at $2x10^7$ cells per well, for a minimum of 2 hours to allow the monocytes to adhere to the tissue

culture plastic. After the incubation period the media was removed and the cells washed in PBS to remove any non-adherent cells. Fresh complete RPMI plus pen-strep was to each well and cells were maintained at 37°C and 5 % CO_2. To induce differentiation into macrophages 100 ng/mL M-CSF was added to each well on day one of culture *i.e.* 24-hours post-harvest. The cells were fed on days 3 and 6 with complete RPMI plus pen-strep, on each occasion fresh M-CSF was added to each well to achieve a final concentration of 100 ng/mL. The MDMs were cultured for a minimum of seven days prior to use in *in vitro* assays. To harvest the MDMS the culture media was removed from each well and replaced with ice cold PBS. The MDMs were subsequently incubated on ice for 15 minutes and then gently detached using a cell scraper. The MDMs were then washed by centrifuging at 1500 rpm for 5 minutes and re-suspended in complete RPMI plus pen-strep prior to use. Cell viability was determined by trypan blue exclusion and was routinely greater than 90 %.

2.2 Antibodies

The anti-GD2 mAb 14G2a and ch14.18 were used routinely throughout this investigation. The 14G2a secreting hybridoma HB9118 was kindly provided by Prof. Dr. med. Holger Lode (Medical University of Greifsweld) and the ch14.18/CHO mAb was kindly provided by Apiron Biologics (Vienna, Austria). Herceptin®, the humanised IgG1 mAb specific for the human epidermal growth factor receptor 2 (HER2) and Rituxan® (Rituximab) the chimeric IgG1 mAb specific for human CD20 was kindly provided by Southampton General Hospital Oncology Pharmacy.

2.2.1 In house produced antibodies

A number of in house mAb produced by Mrs Chris Penfold and Dr Claude Chan were used throughout this investigation, the details of which are shown in table 2.1. All in house IgG mAb were produced from antibody-secreting hybridoma cell lines in tissue culture and purified from supernatant using Protein A columns (GE Healthcare).

Table 2-1. In house produced mAb.

Antigen	*Clone name*	*Reactivity*	*Isotype*	*Fluorescent conjugate*
4-1BB	LOB12.3	Mouse	Rat IgG1	N/A
4-1BB	SAP3/28	Human	Mouse IgG1	N/A
CD20	Ritm2a	Human	Mouse IgG2a	N/A
CD37	WR17	Human	Mouse IgG2a	N/A
NK1.1	PK136	Mouse (C57Bl/6)	Mouse IgG2a	Unlabelled & FITC
CD32	AT130-1	Mouse	Mouse IgG1	N/A
CD16	3G8	Human	F(ab)2	FITC & APC
CD3	OKT3	Human	Mouse IgG2a	FITC

2.2.2 Commercially sourced antibodies

The details of the commercially sourced antibodies used throughout this investigation are summarised in table 2.2.

Table 2-2. Commercially sourced mAb.

Antigen	*Clone name*	*Reactivity*	*Isotype*	*Fluorescent conjugate*	*Supplier*
CD3	17A2	Mouse	Rat IgG2b	V450	BD Biosciences
CD4	RM4-5	Mouse	Rat IgG2a	FITC	eBioscience
CD8α	53-6.7	Mouse	Rat IgG2a	APC-Cy7	BD Biosciences
CD11b	M1/70	Mouse	Rat IgG2b	PerCP-Cy5.5	BD Biosciences
CD11c	N418	Mouse	Ar. Ham. IgG	efluor450	eBioscience
CD25	PC61.5	Mouse	Rat IgG1	APC	eBioscience
CD27	LG.3a10	Mouse	Ar. Ham IgG1	APC	BD Biosciences
CD44	IM7	Mouse	Rat IgG2b	PE	BD Biosciences
CD45	30F11	Mouse	Rat IgG2b	APC	Miltenyi Biotec
CD49b	DX5	Mouse	Rat IgM	PE	BD Biosciences
CD62L	MEL-14	Mouse	Rat IgG2a	PerCP-Cy5.5	BD Biosciences
CD137	17B5	Mouse	Sy. Ham IgG	APC & efluor450	eBioscience
TCRβ chain	H57-597	Mouse	Ar. Ham. IgG2	APC	BD Biosciences
TCRγδ	GL3	Mouse	Ar. Ham. IgG2	FITC	BD Biosciences
FoxP3	FJK16s	Mouse	Rat IgG2a	PE	eBioscience
NKG2ACE	20d5	Mouse	Rat IgG2a	PE	Novus Biologicals
F4/80	C1:A3-1	Mouse	Rat IgG2b	APC	AbD Serotec
CD3	OKT3	Human	Mouse IgG2a	V450	eBioscience
CD56	CMSSB	Human	Mouse IgG1	PE	eBioscience
CD137	4B4-1	Human	Mouse IgG1	APC	BD Biosciences

2.3 Flow cytometry

Both indirect and direct staining methods were used when performing flow cytometry to determine expression of cell surface molecules.

2.3.1 Direct staining

Routinely, $1x10^6$ cells in 100 µL PBS were incubated at 4 °C in the dark for 30 minutes with the fluorescently conjugated antibodies of choice, typically at a final concentration of 10 µg/mL (unless titrated down). Where required red blood cells were lysed using ACK red blood cell lysis buffer for 5 minutes at room temperature. Cells were then washed twice in FACS wash buffer comprising of PBS plus 1 % Bovine Serum Albumin fraction V (BSA) (Wilfred

Smith Ltd) and 20 mM sodium azide (NaN_3) and re-suspended in 100 µL PBS prior to analysis.

2.3.2 Indirect staining

$1x10^6$ cells in 100 µL PBS were incubated at 4°C for 30 minutes with the unlabelled antibody of choice, at a final concentration of 10 µg/mL. Cells were then washed twice in FACS wash buffer and re-suspended in 100 µL PBS before a second 15 minute incubation at 4°C in the dark with a (1:100 dilution) PE-conjugated secondary antibody directed against the first unlabelled mAb. Following the secondary staining step the cells were washed once with FACS wash buffer. Routinely the PE-conjugated $F(ab')_2$ fragment goat anti-mouse IgG Fcγ fragment specific antibody, or the PE-conjugated $F(ab')_2$ fragment goat anti-human IgG Fcγ fragment specific antibody (both from Jackson ImmunoResearch Laboratories Inc.) were used for indirect staining.

2.3.3 Intracellular staining

Intracellular staining was performed to assess regulatory T cells (Tregs) using the mouse regulatory T cell staining kit in accordance with the manufacturer's protocol.

2.3.4 Flow cytometry analysis

Analysis was performed on the FACSCantoII™ flow cytometer (BD Biosciences-Immunocytometry Systems, CA). Routinely, 10,000–50,000 live cell events were collected, as identified by the FSC-H and SSC-H threshold parameters. V450 was excited at 404 nm with emission intensity being recorded at 448 nm wavelength; AM-CYAN was excited at 457 nm with emission intensity being recorded at 491 nm wavelength; FITC was excited at 494 nm with emission intensity being recorded at 520 nm wavelength; PE was excited at 496 nm with emission intensity being recorded at 578 nm wavelength; PerCP-Cy5.5 was excited at 482 nm with emission intensity being recorded at 695 nm wavelength; APC was excited at 650nm with emission intensity being recorded at 660nm wavelength; APC-Cy7 was excited at 650nm with emission intensity being recorded at 660nm wavelength. Samples were analysed using FACSDIVA™ software (BD Biosciences-Immunocytometry Systems, CA). Fluorescence intensities were assessed in comparison to negative/ isotype

control samples and expressed as histograms of fluorescence intensity versus cell number, or dot plots.

2.4 Magnetic-activated cell sorting (MACS®)

2.4.1 Augmenting GD2 expression by the NXS2 neuroblastoma cell line

High GD2 expressing NXS2 cells were positively selected by magnetic-activated cell sorting (MACS®) using a primary anti-GD2 mAb (14G2a) and anti-mouse IgG2a+b microbeads (Miltenyi Biotec). Routinely, $1x10^7$ cells per mL were labelled with the primary antibody (30 minutes at 4 °C) and washed twice in PBS+ 0.5% BSA +2 mM EDTA (MACS® buffer), prior to the addition of 20 µL microbeads per 10^7 cells. Cells were incubated for 15 minutes at 4°C and washed twice before magnetic separation as per the manufacturer's instructions. The magnetically labelled cells were eluted from the column once it had been removed from the magnetic field. The high GD2 expressing NXS2 cells were then washed and re-suspended in complete DMEM and maintained at 37°C and 5 % CO_2 to facilitate expansion.

2.4.2 NK cell isolation

NK cell isolation was achieved by negative selection using the human NK cell isolation kit or the mouse NK cell isolation kit II (both Miltenyi Biotech). PBMCs (human) or splenocytes (mouse) were centrifuged at 300g for 10 minutes and the supernatant aspirated completely. Cell pellets were re-suspended in 40 µL MACS® buffer per 10^7 cells and 10 µl NK cell biotin-antibody cocktail was added per 10^7 total cells. Cells were mixed well and incubated for 5 minutes at 4°C. A further 30 µl MACS® buffer was added per 10^7 cells followed by 20 µL NK cell microbead cocktail per 10^7 total cells. Cells were mixed well and incubated for 10 minutes at 4°C. Meanwhile LS columns were prepared by flushing through with 3 ml MACS® buffer. The volume of the cell suspension was adjusted to 500 µL by adding MACS® buffer and added to the column. Once NK cells had passed through the column was rinsed a further two times with 3 mL MACS buffer, allowing column to empty completely each time. The NK cells were washed and re-suspended in complete RPMI for used as required. The columns were removed from the magnets and flushed through to

collect the non-NK cell fragment. Purity was assessed by flow cytometry using direct staining methods (see section 2.3.1).

2.5 Calcein-release based cytolytic assays

The 'gold standard' for measuring ADCC traditionally involved the use of radioactive chromium (^{51}Cr) release assays developed by Brunner *et. al.* in 1968 (242). The assay relies upon the passive internalisation and binding of ^{51}Cr from sodium chromate by target cells, which upon effector mediated lysis is released into the cell culture supernatant and can be detected using a γ-counter. Whilst these assays are reproducible and easy to perform there are a number of disadvantages, such as poor labelling and/ or high spontaneous ^{51}Cr release by some cell lines, inter assay variability and the biohazards associated with the disposal of radioactive materials, which has ultimately led to the development of a number of non-radioactive based assays (243). One example of a non-radioactive based ADCC assay utilises calcein-acetoxymethyl ester (calcein-AM), a membrane permeable non-fluorescent molecule that passively diffuses into cells. Once inside calcein-AM is converted to calcein, a green fluorescent dye, following the hydrolysis of the acetoxymethyl ester by intracellular esterases. Calcein is retained within the cell provided the cell membrane is intact; however, when a cell is lysed calcein is released into the cell culture supernatant and can be detected using a fluorescence plate reader, in this respect the calcein release assay is analogous with the ^{51}Cr release assay but bypasses the need for radioactive materials. Both complement-dependent cytotoxicity (CDC) and antibody-dependent cellular cytotoxicity (ADCC) were measured throughout this investigation using the calcein-release based assay.

2.5.1 Complement-dependent cytotoxicity assay

Target neuroblastoma cell lines were harvested, washed and re-suspended at $2x10^6$ per mL in 1 mL PBS, 10 µL of calcein-AM (Sigma-Aldrich) was subsequently added and the cells were incubated at 37 °C for 30 minutes in the dark with periodic mixing. The calcein-AM labelled cells were then washed 3 times, re-suspended in serum free RPMI and the concentration adjusted to $1x10^5$ cells per mL. Fifty microliters of the calcein-AM labelled target cells were seeded per well in 96-well round bottom plates and the cells were incubated with either PBS alone, the anti-GD2 mAb (14G2a or ch14.18), or an appropriate

irrelevant isotype matched control, at a final concentration of 10 µg/mL for 30 minutes at 37°C in the dark. Fifty microliters of human serum, or heat-inactivated serum diluted 1:2 in serum free RPMI, or serum free RPMI alone was added to each well as required. To facilitate analysis the following control samples were included each time the experiment was performed: calein-AM labelled targets alone (to measure spontaneous release), calcein-AM labelled targets treated with 4 % Triton X-1000 lysis buffer (to measure maximum release). Final well volume was made up to 200 µL as required with serum free RPMI or lysis buffer. The plates were briefly centrifuged for 1 minute at 100 g and the cells were cultured for 4-hours at 37 °C in the dark. After 4 hours the plates were centrifuged again for 5 minutes at 200 g and 60 µL of supernatant was transferred from each well to a 96-well white walled plate and fluorescence was measured at 495nm using a Varioskan flash plate reader.

2.5.1.1 Processing, storage and heat-inactivation of human serum

Human AB serum (Sigma-Aldrich) was filtered sterilised upon receipt and divided into separate batches. The first batch was immediately transferred to -80°C for storage, the second batch was heated to 56 °C for one hour to destroy complement proteins and was subsequently stored at –80°C until required.

2.5.2 Antibody-dependent cellular cytotoxicity assay

Target neuroblastoma cell lines were labelled with calcein-AM, seeded in 96-well plates and opsonised with antibody as described in section 2.5.1. Mouse splenocytes, human PBMCs, or mouse/ human whole blood was used as a source of effector cells. Spleens were harvested from syngeneic A/J mice and homogenised to obtain a single cell suspension, whereas PBMCs were isolated from LRS cones as described in section 2.1.3. The effector cell population was adjusted to $2x10^6$ per mL and 100 µL was added to each well as required to obtain an effector: target ratio of 40:1, unless otherwise stated. Triplicate wells were prepared for each condition. To facilitate analysis the following control samples were included each time the experiment was performed: calein-AM labelled targets alone (to measure spontaneous release), calcein-AM labelled targets treated with 4 % Triton X-1000 lysis buffer (to measure maximum release) and calcein-AM labelled targets plus the mAb being tested (to measure the effects of antibody alone in the absence of effectors). Final well

volume was made up to 200 µL as required with media alone, or lysis buffer. The plates were briefly centrifuged for 1 minute at 100 g and the cells were cultured for 4-hours at 37°C in the dark. Following incubation the plates were centrifuged and supernatant harvested for analysis as described in section 2.5.1.

2.5.3 Quantifying calcein release

Firstly, the mean spontaneous calcein release from triplicate samples was subtracted from the test, control and maximum lysis samples. Calcein release for the control conditions (T only+mAb) was then subtracted from the test conditions (E+T+mAb) and the corrected calcein release for the test condition was calculated as a percentage of maximal calcein release:

$$Calcein\ release\ (\%\ maximal) = \frac{(E + T + mAb) - (T\ alone + mAb)}{maximum\ calcein\ release}\ x\ 100$$

In order to calculate antibody-induced calcein release the value obtained for the effectors and targets alone was subtracted from the effectors and targets plus mAb and expressed as a percentage of maximum lysis.

$$Antibody\ induced\ calcein\ release\ (\%\ maximal) = \frac{(E + T + mAb) - (E + T\ alone)}{maximum\ calcein\ release}\ x\ 100$$

2.6 Antibody-dependent cell mediated phagocytosis assay

A phagocytosis assay developed by Dr Ruth French was adapted to investigate the ability of murine BMDMs/ human MDMs to phagocytose opsonized neuroblastoma cells via Fc:FcγR mediated interactions and therefore determine the proportion of neuroblastoma cells that undergo antibody dependent cell-mediated phagocytosis *in vitro*. BMDMs/ MDMs were harvested as described in section 2.1.3, the concentration was adjusted to 5 x 10^5 cells per mL and 100 µL of cells (5 x 10^4) were seeded per well in a 96-well flat bottom plate and left to adhere overnight. The following day target cells were harvested, washed and re-suspended in PBS at 1.5–2.5x10^7 cells/mL and labelled with carboxyfluorescein succinimidyl ester (CFSE) (Sigma-Aldrich) to facilitate their identification by flow cytometry. The target cells were incubated with 5 µM CFSE for 10 minutes at room temperature in the dark. An equal volume of heat

attenuated FCS was subsequently added to quench CFSE labelling and cells were washed twice in complete RPMI, prior to incubation with the antibody of interest at 10 µg/mL for 30 minutes at room temperature in the dark. One hundred microliters of CFSE labelled target cells at $2.5x10^6$ cells per mL were then added to the adherent BMDMs/ MDMs to obtain a target: effector ratio of 5:1 and the cells were co-incubated for 1 hour at 37°C and 5 % CO_2. Each sample was prepared in triplicate. Ten microliters of 1:10 diluted stock APC conjugated anti-F4/80 (AbD Serotec), or APC conjugated anti-CD16 (3G8) was added to each well and cells were incubated for 15 minutes at room temperature in the dark. Non-adherent cells were removed using a pipette and cells were washed twice with room temperature PBS-BSA-Azide buffer. Two hundred microliters of chilled (4°C) PBS-BSA-azide buffer was added to each well and cells were incubated at 4°C for 15 minutes in the dark. To harvest the cells a pipette tip was used to scrape the plate surface and the cells were transferred to a FACS™ tube (BD Biosciences) containing 100 µL of 1 % paraformaldehyde to fix the cells. Cells were washed once in 3 mL PBS-BSA-azide buffer prior to analysis on the FACS Canto II™ (BD Biosciences). The macrophage population was identified by the FSC-H and SSC-H threshold parameters and 20,000 events were collected.

Phagacytosis was determined by the number of F4/80-APC+ (FL-4) and CFSE+ (FL-1) double positive events and per cent phagocytosis was calculated as follows:

$$\%\ Phagocytosis = \frac{(No.F4/80 + CFSE + events)}{(Total\ F4/80 + events)}\ x\ 100$$

2.7 NK cell and macrophage depletion

2.7.1 NK cell depletion

NK cells were depleted by i.p. injection of 20 µL anti-asialo GM1 (polyclonal rabbit anti-asialo GM1, Wako Chemicals). Injections were administered 48–96 hours apart.

2.7.2 Macrophage depletion

Macrophage depletion was achieved using clodronate (dichloromethylene bisphosphonate), which belongs to a class of drugs known as the bisphosphonates used to treat bone disorders, such as osteoporosis. Macrophage depletion can be achieved using clodronate encapsulated into liposomes, a method that was originally described by van Rooijen and van Nieuwmegan (244). Clodronate in its free form is non-toxic as free clodronate cannot penetrate the phospholipid bilayer and therefore does not readily enter cells, hence the need to encapsulate the drug into liposomes (245), which are often used as a method of drug delivery. Once injected *in vivo* liposomes are ingested by macrophages and subsequently degraded by lysosomal phospholipases, thus releasing free clodronate within the cell. The inability of clodronate in its free form to cross cell membranes means it is retained within the macrophage, consequently free clodronate accumulates and once a certain intracellular concentration is achieved the macrophage will undergo apoptosis (246). Free clodronate also has a very short half-life in the circulation, thus any drug released by dead/ dying macrophages is rapidly removed from the system (247). Depletion of specific macrophage groups can be achieved using particular routes of administration and liver and splenic macrophages in particular can be depleted by administering clodronate liposomes via the i.v. route (248, 249). To deplete macrophages in the liver and spleen 400 µL total clodronate liposomes were administered i.v. to age and sex matched A/J mice 48 hours apart (*i.e.* day -3 and day -1). Depletion occurs within 24 hours and lasts for approximately one week. Liposomes were prepared in house as described by van Rooijen and van Nieuwmegan (244) using phosphatidylcholine (Sigma P3556 Lα PSC Type XV1-E 99 % TLC) and cholesterol (Sigma C3045 ≥ 99 % TLC).

2.7.3 Confirming NK cell and macrophage depletion

To confirm macrophage/ NK cell had been effectively depleted control mice were culled at the required time point and livers and/ or spleens were harvested. The liver was chopped into ca. 1 mm^2 sections and transferred to a falcon tube containing RPMI plus 10% FCS, 25 mM HEPES and 1 mg/mL collagenase D. Samples were incubated for 45 minutes at 37°C. Both the liver and spleens were passed through a 100 µm cell strainer to obtain a single cell

suspension. Cells were subsequently washed and counted in preparation for analysis by direct immunofluorescence. Macrophages were detected as $F4/80^{+}CD11c^{+}CD11b^{-}$ and NK cells were detected as $NKG2ACE^{+}CD49b^{+}$.

2.8 The syngeneic NXS2 mouse model of neuroblastoma

2.8.1 Inducing metastatic-like disease

Age (minimum 8 weeks) and sex matched mice were injected intravenously (i.v.) with $1x10^{6}$ freshly prepared NXS2 cells (>90 % viability by trypan blue staining) in 100 µL PBS on day 0 to induce metastatic-like disease. Therapy commenced 24 hours later (day 1). Treated mice received 10 µg 14G2a plus 30,000 IU recombinant human IL-2 (Novartis) (diluted in PBS) administered i.v. This was followed by a once daily intraperitoneal (i.p.) injection at the same dose on day two through to six. Naïve control mice received i.v. or i.p injection of an equivalent volume of PBS alone. Mice were either culled on day 21 and the liver was removed, photographed and weighed to document the extent of the metastases in the different treatment groups, or monitored for survival.

2.8.2 Subcutaneous tumours

Age (minimum 8 weeks) and sex matched mice were injected subcutaneously with $2x10^{6}$ freshly prepared NXS2 cells (>90 % viability by trypan blue staining) in 100 µL PBS on day 0. Therapy was administered as detailed in the individual experiments. Tumour diameter was measured a minimum of three times a week and mice were culled when a cross-sectional area exceeded 225 mm^{2}.

2.9 Tissue processing

Tumours were harvested from A/J or TH-MYCN transgenic mice and processed using the mouse Tumour Dissociation Kit (Miltenyi Biotec). Tumours and spleens were harvested from tumour bearing mice. The tumour was cut into pieces measuring approximately 2–4 mm^{2} and approximately one quarter was transferred into a 50 mL falcon tube containing the Tumour Dissociation Kit enzyme mix comprising of 2.35 mL PBS, 100 µL solution 1, 50 µL solution 2 and 12.5 µL solution 3. Samples were incubated for 40 minutes at 37°C with continuous rotation and subsequently passed through a 100 µm cell strainer to

obtain a single cell suspension. Spleen samples were manually disaggregated and passed through 100 µm cell strainer to obtain a single cell suspension. Cells were transferred to falcon tubes and washed twice in PBS prior to staining for flow cytometry.

2.10 Measuring 4-1BB expression by murine NK cells *ex vivo*

Mice were inoculated with NXS2 cells as described in section 2.8.2. Tumour growth was monitored and when a cross-sectional area had reached a minimum of 70 mm^2 but did not exceed 100 mm^2 mice were treated with 50–150 µg anti-GD2 mAb (14G2a), or the irrelevant isotype matched control Ritm2a (which is specific for human CD20), or vehicle alone (PBS) as described. Mice were terminally bled (blood was collected in tubes containing heparin) 24-hours later and tumour, spleen and blood samples were analysed by flow cytometry as described.

2.11 Inducing 4-1BB expression on human NK cells

Lan-1 cells (viability > 90 % by trypan blue) were harvested, washed and re-suspended in complete RPMI at $1x10^5$ cells per mL. Fifty microliters of cells ($5x10^3$) were added to each well of a round bottom 96-well plate, followed by 50 µL PBS alone, Herceptin, or ch14.18 diluted in PBS to achieve a final concentration of 10 µg/mL. based on a final well volume of 200 µL. Cells were incubated for 30 minutes at 37°C. Human PBMCs harvested from LRS cones were re-suspended at $2x10^6$ per mL in complete RPMI and 100 µL ($2x10^5$) of PBMCs were added to each well to achieve a 40:1 effector: target ratio unless otherwise stated. The plate was centrifuged for 1 minute at 100g and the cells incubated at 37°C and 5 % CO_2 for the required duration. Following incubation cells were screened for 4-1BB (and CD16 where stated) expression by direct staining. Baseline expression levels were assessed at the beginning of the experiment.

2.11.1 Inducing 4-1BB expression prior to ADCC assays

Lan-1 cells (viability > 90 % by trypan blue) were harvested, washed and re-suspended in complete RPMI at $2x10^6$ cells per mL. Cells were subsequently

irradiated at 50 Gy. Five hundred microliters of cells ($1x10^6$) were added to each well of a 24-well plate, followed by 15 µL PBS alone, Herceptin, or ch14.18 diluted in PBS to achieve a final concentration of 10 µg/mL. based on a final well volume of 1500 µL. Cells were incubated for 30 minutes at 37°C. Human PBMCs harvested from LRS cones were re-suspended at $1x10^7$ per mL in complete RPMI and 1000 µL ($1x10^7$) of PBMCs was added to each well to achieve a 10:1 effector: target ratio. The plate was centrifuged for 1 minute at 100g and the cells incubated at 37°C and 5 % CO_2 for 16 hours duration. Following incubation cells were screened for 4-1BB expression by direct staining. Baseline expression levels were assessed at the beginning of the experiment. NK cells were subsequently purified (see section 2.4.2) and used as effector cells in calcein release based ADCC assays (see section 2.5.2).

2.12 Testing anti-GD2 plus anti-4-1BB mAb in the TH-MYCN transgenic mouse model

Upon presentation with palpable tumour mice were weighed and treated with 40 mg/kg of freshly prepared cyclophosphamide (Sigma-Aldrich), which was injected i.p. in 200 µL PBS. Mice received either cyclophosphamide alone, mAb alone, or a combination of both as described. 150 µg anti-GD2 mAb (14G2a) or anti-4-1BB mAb (LOB12.3) was injected i.p. in 200 µL PBS. Mice were palpated regularly for signs of tumour regression and re-presentation and culled either once tumour was considered terminal (as described in section 2.1.1) or 100 days post-therapy when the experiment ended.

2.13 Statistics

All statistical differences were assessed by unpaired t tests unless otherwise stated. Survival differences were analysed by Log Rank tests. Differences were considered significant when $p < 0.05$ (in the text * $p < 0.05$, ** $p < 0.01$, *** $p < 0.001$ and **** $p < 0.0001$.

Chapter 3: Exploring the immune effector mechanisms responsible for the anti-tumour effect of anti-GD2 mAb

3.1 Chapter introduction

Although anti-GD2 mAb have shown considerable promise in clinical trials the majority of children with high risk neuroblastoma still relapse and ultimately die from their disease. Enhancing the efficacy of anti-GD2 mAb is key to improving long term survival of high risk patients. Since many mAb based therapeutic strategies have been developed empirically (166), their mechanisms of action are not fully understood. Consequently a thorough understanding of the effector mechanisms responsible for the anti-tumour effects of anti-GD2 mAb is crucial for the rational design of improved therapeutic strategies. As discussed in section 1.5.1.3 the mechanisms of action responsible for the therapeutic effect of anti-GD2 mAb have yet to be fully elucidated. Whilst it is generally accepted that tumour cell destruction is achieved via NK cell mediated ADCC, other mechanisms are likely to contribute. The lack of syngeneic GD2+ murine neuroblastoma models available when anti-GD2 mAb were first introduced in the mid-1980s meant that much of the early mechanistic characterisation was carried out *in vitro*, with *in vivo* investigations reliant on the use of immunodeficient mice and xenotransplantation of human cell lines. Consequently, a more detailed understanding of how murine neuroblastoma cells respond to anti-GD2 mAb therapy and the interactions that occur between the mAb and host immune cells within the tumour microenvironment is still required in order to improve efficacy of the anti-GD2 mAb through enhanced immune effector function.

The main subject of this chapter is the characterisation of the immune effector mechanisms responsible for the anti-tumour effects of anti-GD2 mAb. Four proposed mechanisms of action for direct targeting mAb, such as anti-GD2 were introduced in section 1.5.1.2., to recap these were: direct cell killing, CDC, ADCP and ADCC. Direct killing was not explored in depth in this investigation as whilst it may have a role in the anti-tumour effect of anti-GD2 mAb, it is not widely reported in the literature, and when it has been reported

unfeasibly high concentrations of antibody were used (185). Additionally, anti-GD2 treated neuroblastoma target cells are routinely used a control condition in experiments widely performed within our group and no sign of killing above background has been observed. The complement system has been thought to contribute to the therapeutic effect of anti-GD2 mAb since the first *in* vitro experiments showed lysis of anti-GD2 opsonised neuroblastoma cell lines could be achieved following the addition of human serum (174, 175, 181). Consequently, the ability to induce anti-GD2 mediated CDC using murine neuroblastoma cell lines and serum has been investigated for completeness.

One mechanism of action that has been explored in depth is ADCP. ADCP is triggered when the Fc portion of a mAb, such as anti-GD2, engages an Fcγ receptor expressed on the surface of a phagocytic cell, such as a macrophage, or a neutrophil. To reiterate the points raised in section 1.5.1.3 evidence to suggest that macrophages and/ or neutrophils may contribute to anti-GD2 mediated tumour cell killing was provided when the results of a clinical trial were published in 2006 (207). This study reported that neuroblastoma patients with the FcγRIIA (R/R) genotype exhibited superior progression free survival following treatment with the murine IgG3 anti-GD2 mAb 3F8 plus GM-CSF (207). This observation is significant because FcγRIIA is expressed by cells of myeloid lineage, such as macrophages and neutrophils, rather than NK cells, suggesting that the apparent survival advantage may be attributed to enhanced ADCP in these patients (207). To date ADCP has been poorly characterised as an effector mechanism both *in vitro*, and *in vivo* mouse models of neuroblastoma. The other mechanism of action explored in depth was NK cell mediated ADCC, which is considered to be one of the major mechanisms responsible for the therapeutic effect of anti-GD2 mAb. As discussed in section 1.5.1.3 the lack of MHC class I molecules on the surface of neuroblastoma cells (148) renders them prime targets for NK cell mediated destruction in accordance with the missing-self hypothesis and the data obtained following several early *in vitro* and *in vivo* investigations seems to support this (184, 199, 203). Additionally, as discussed in section 1.5.1.3 more recent investigations have demonstrated the importance of NK cell mediated ADCC in the clinical setting (204-206).

The data presented in this chapter was largely performed using the GD2+ murine neuroblastoma cell line NXS2 and syngeneic murine A/J mice. The GD2

negative Neuro2a cell line was used as a negative control. The NXS2 model developed by Reisfeld's group was the first syngeneic murine model of neuroblastoma that permitted study of anti-GD2 mAb *in vivo* using fully immunocompetent mice (240). This model uses the hybrid neuroblastoma cell line NXS2, which is a sub line of the NX-31T28 cell line (240). The NX-31T28 cell line is a hybrid of the GD2 negative murine neuroblastoma cell line C1300, which is on the A/J background, and dorsal root ganglion cells harvested from C57BL/6 mice. The NX-31T28 cell line was not developed specifically to facilitate neuroblastoma research, instead it was designed to provide a model system for the study of synapse function and other neural properties (250). Sympathetic dorsal root ganglia were chosen as a source of neurons as they contain relatively few types of neuron, all of which had been well characterised previously (250). The C1300 neuroblastoma cells were chosen as the other parent because of their neural properties and the fact that they are embryonically similar to sympathetic ganglion neurons (250). The resultant NX-31 hybrids closely resembled sympathetic ganglion interneurons as characterised by their high dopamine secretion (250). To generate the NXS2 sub-line Reisfeld's group incubated NX-31T28 cells with the murine IgG2a isotype anti-GD2 mAb 14G2a. The subset of cells expressing a high level of surface GD2 were subsequently positively-selected out using anti-mouse IgG2a microbeads and magnetic activated cell sorting (MACS®) (240). The NXS2 cell line differs from the parental neuroblastoma C1300 cell line in terms of increased, yet heterogeneous, GD2 expression, surface expression of the neuronal adhesion molecule L1, and the presence of dense catecholamine storage vesicles, all common features of human neuroblastoma (240). Since the parental cell types used in the initial hybridisation were from two H2 incompatible mouse strains, namely A/J and C57BL/6, major histocompatibility complex antigen expression on the NXS2 cells was also determined and found to be $H2K^{k}$ positive and $H2K^{b}$ negative *i.e.* a match for the A/J strain (240). All of the *in vitro* mechanistic investigations were performed in parallel to experiments using the human neuroblastoma cell lines Lan-1 and/or IMR-32 in order to recapitulate what has been reported in the literature and assess the similarities and differences between murine and human model systems. The Lan-1 human neuroblastoma cell line was established from bone marrow metastasis taken from a 2 year old male with stage IV disease (251), whereas the IMR-32 cell line was established from an abdominal mass of a 13 month

old Caucasian male (252). In contrast to the murine hybrid NXS2 neuroblastoma cells the ganglioside GD2 is endogenously expressed by human neuroblastoma tumours. Ubiquitous GD2 expression has been reported on 100 % of human neuroblastoma tumours in the order of $5x10^6$–$1x10^7$ molecules per cell (253).

3.2 Results

3.2.1 Surface GD2 expression on neuroblastoma cell lines

Prior to commencing *in vitro* characterisation of anti-GD2 mAb effector mechanisms the neuroblastoma cell lines were assessed for surface GD2 expression by flow cytometry using the FITC conjugated anti-GD2 mAb 14G2a, the results of which are shown in figure 3.1.

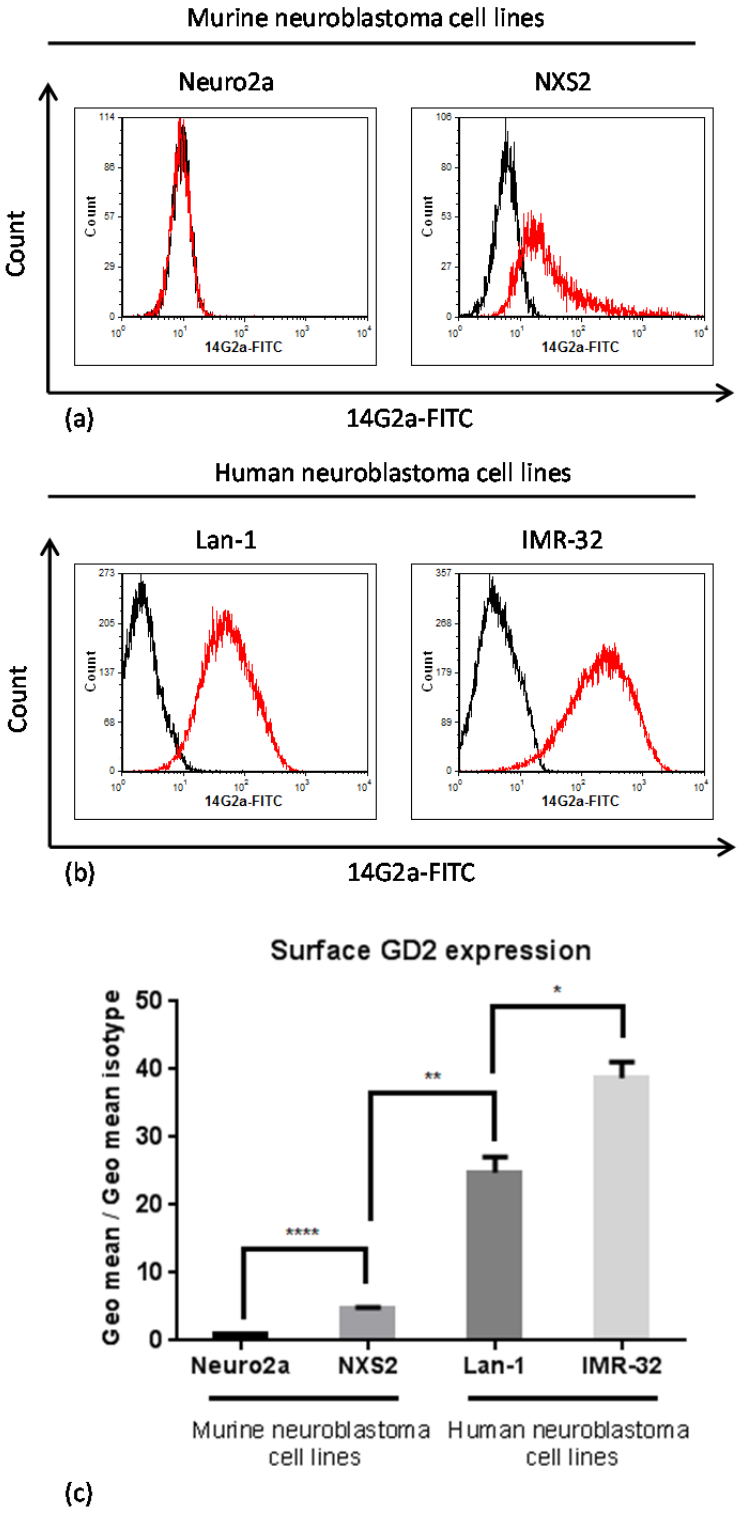

Figure 3-1. Surface GD2 expression on murine and human cell lines. Surface GD2 expression was quantified using the FITC conjugated anti-GD2 mAb 14G2a-FITC and assessed by flow cytometry. A representative flow cytometry histogram shows the mean fluorescence intensity (MFI) obtained using both an irrelevant isotype matched control PK136 (black line), or 14G2a-FITC (red line) for the murine neuroblastoma cell lines Neuro2a and NXS2 (a), plus the human neuroblastoma cell lines Lan-1 and IMR-32 (b). The mean fold change relative to the isotype control for three triplicate repeats is shown in (c) error bars = S.E.M. and * p = 0.0137, ** p = 0.0010 and **** p = <0.0001.

Figure 3.1 (a) firstly confirms that the murine neuroblastoma cell line Neuro2a is negative for surface GD2 and secondly demonstrates the heterogeneous nature of GD2 expression by the NXS2 cell line. Only a small proportion of the NXS2 cells express a high level of surface GD2 as characterised by the shoulder observed on the NXS2 histogram. Conversely, a distinct shift in the entire population relative to the isotype control is observed for both the human cell lines Lan-1 and IMR-32, as shown in figure 3.2 (b). Figure 3.1 (c) demonstrates the fold-change in MFI relative to the isotype control for each cell line confirming that the human cell lines express significantly more surface GD2 than the NXS2 cells and that the IMR-32 cell line has the high surface GD2 expression of all the cell lines screened. The low level GD2 expression by NXS2 cells compared to human neuroblastoma cell lines has been documented in the literature. Scatchard analysis performed by others using iodine-125 labelled 14G2a calculated GD2 expression, in terms of the number of binding sites, for NXS2 and IMR-32 cells as $1.3x10^6$ and $12.6x10^6$ per cell respectively (254).

3.2.2 Augmenting surface GD2 expression by the murine NXS2 neuroblastoma cell line

The data presented in figure 3.1 (a) and (b) confirms that a large proportion of the NXS2 cells express a low level of surface GD2, at least in comparison to the human neuroblastoma cell lines Lan-1 and IMR-32. Low level surface GD2 expression may have implications for this investigation as it may render the NXS2 cell line less susceptible to anti-GD2 mAb mediated tumour cell destruction, in comparison to the human neuroblastoma cell lines. Since the NXS2 sub-line was originally generated by positively-selecting high GD2 expressing NX-31T28 hybrid cells by MACS® it was hypothesized that surface GD2 expression by NXS2 cells could be augmented by the same method. The murine anti-GD2 mAb 14G2a was used to label the NXS2 cells, which were subsequently selected using anti-mouse IgG2a+b microbeads to facilitate cell sorting as previously described (240). Figure 3.2 shows the level of surface GD2 expression by NXS2 cells both pre- and post-selection by MACS® as quantified by flow cytometry using the FITC conjugated anti-GD2 mAb 14G2a.

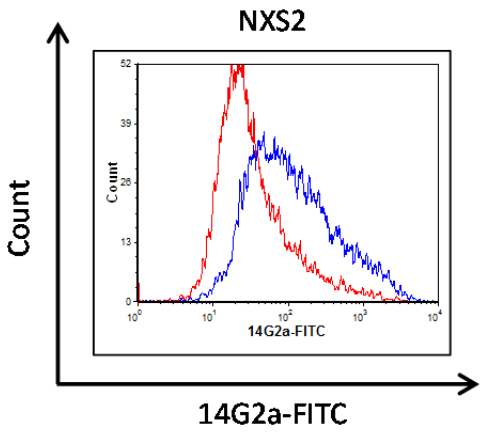

(a)

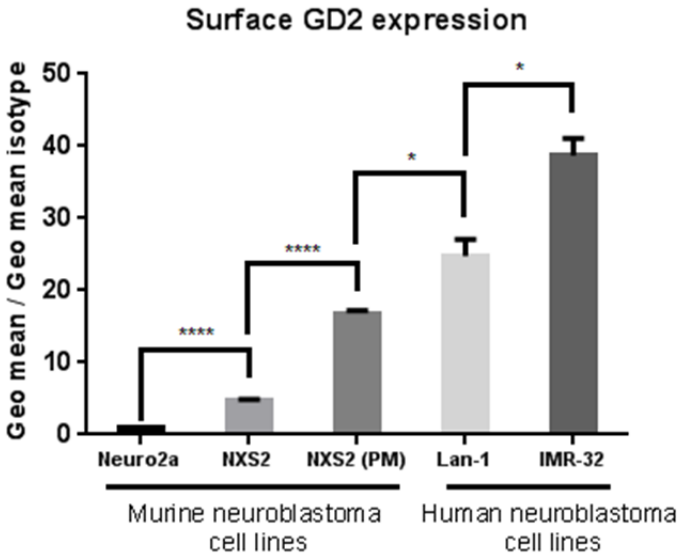

(b)

Figure 3-2. Surface GD2 expression on the murine NXS2 neuroblastoma cell line before and after MACS®. Surface GD2 expression was quantified using the FITC conjugated anti-GD2 mAb 14G2a-FITC, or a FITC conjugated irrelevant isotype matched control (PK136) and assessed by flow cytometry both prior to and after selection by MACS®. A representative flow cytometry histogram illustrating the increase in mean fluorescence intensity (MFI) post-selection (blue line) compared to pre-selection (red line) is shown in (a). The mean fold change relative to the isotype control for the three triplicate repeats post-selection by MACS® (NXS2 PM) was added to the previous screening data (shown in figure 3.1 c) for comparison (b), where error bars = S.E.M. and * p = 0.0280 (for NXS2 PM vs Lan-1), * p = 0.0137 (for Lan-1 vs IMR-32) and **** p = <0.0001.

Figure 3.2 (a) shows the surface GD2 expression on the NXS2 cell line pre- (red line) and post- (blue line) positive selection by MACS®, the post-selection histogram has less of a shoulder, which is indicative of a comparatively more uniform GD2 expression post-selection. The fold-change in MFI relative to the isotype control for the NXS2 cell line post-MACS® (PM) was added to the previous screening data obtained for the murine and human neuroblastoma

cell lines (shown in figure 3.1 c) for comparison. Figure 3.2 (b) shows that despite a significant increase in surface GD2 expression by the NXS2 cell line post-MACS®, surface GD2 expression by the human neuroblastoma cell lines Lan-1 and IMR-32 remains significantly higher.

3.2.3 Characterising the mechanisms responsible for anti-GD2 mediated killing: Complement-dependent cytotoxicity

Several early publications suggested the complement system may contribute to the therapeutic effect of anti-GD2 mAb and this was based on the observation that the addition of human serum to anti-GD2 opsonised neuroblastoma cell lines was sufficient to induce between 60-100 % cell lysis (175, 181). A series of *in vitro* calcein release based CDC assays were performed to assess the ability of anti-GD2 mAb to induce CDC using both murine and human neuroblastoma cells as targets.

3.2.3.1 The anti-GD2 mAb 14G2a failed to induce CDC of murine NXS2 cells when cultured with either mouse or rat serum

It is well documented that mouse complement is extremely labile and the levels of CDC achieved are often low compared to experiments performed with complement sourced from other species (255). Therefore both mouse and rat serum (freshly harvested and commercially sourced) was used as a source of complement; however, attempts to induce CDC with the murine NXS2 neuroblastoma cell line were generally unsuccessful. Both the viability probe propidium iodide and calcein release based assays were employed to measure CDC, and at best the reduction in viability that could be attributed to complement was 20 %. This result was achieved with the rat serum; however, it was not reproducible (hence data not shown). In the initial experiments calcein release by NXS2 targets cultured in the presence of serum alone and serum plus 14G2a was equivalent, consequently since complement activation is not solely dependent on recognition of antibody, attempts were made to titrate down the serum concentration in order to identify the concentration associated with minimal calcein release in the absence of antibody. However, even at serum concentrations as low as 2.5 % the level of CDC achieved in the test conditions remained equivalent to level observed in the control conditions (i.e. matched samples cultured with heat inactivated serum), regardless of the analysis method used.

3.2.3.2 The anti-GD2 mAb ch14.18 induces CDC when human neuroblastoma cell lines are cultured with human serum

The calcein release based assay was used to investigate CDC using the human neuroblastoma cell lines Lan-1 and IMR-32. The cells were opsonised with the anti-GD2 mAb ch14.18 and cultured in the presence of human AB serum. The results from these experiments are summarised in Figure 3.3.

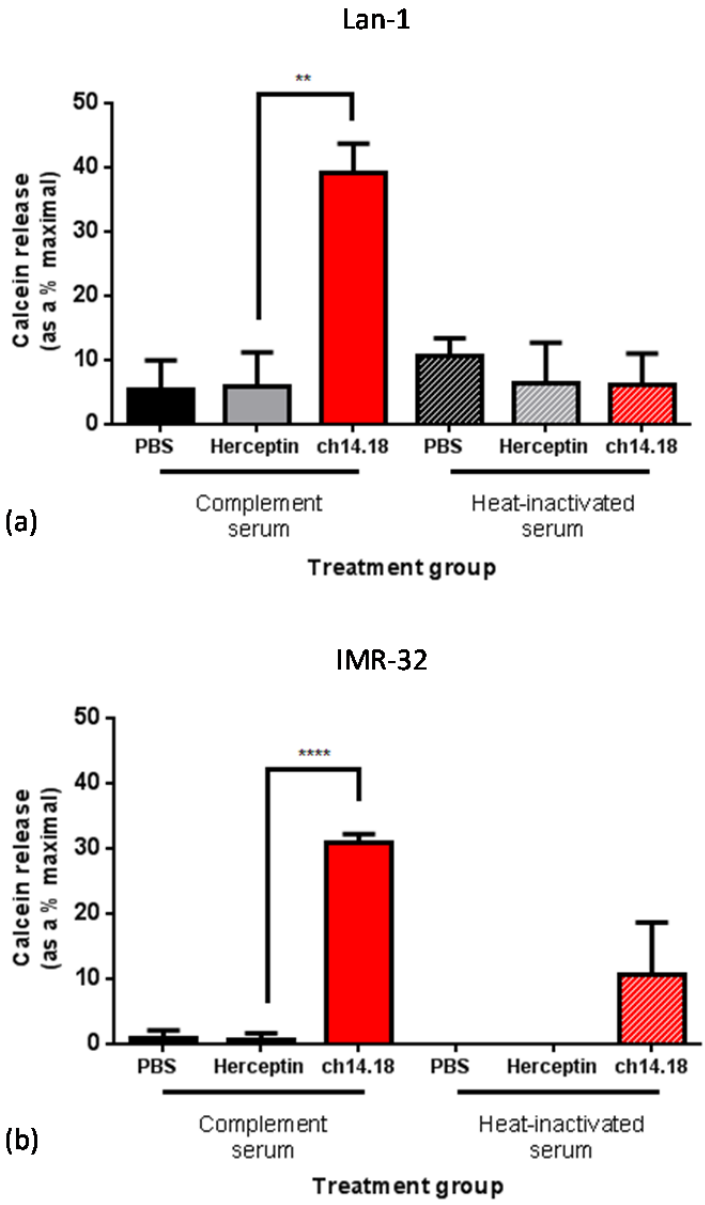

Figure 3-3. Anti-GD2 mediated CDC of the human neuroblastoma cell lines Lan-1 and IMR-32. Calcein-AM labelled Lan-1 (a) and IMR-32 (b) cell lines were treated with PBS alone (black bars), 10 µg/mL irrelevant isotype control Herceptin (grey bars), or 10 µg/mL anti-GD2 mAb ch14.18 (red bars) and cultured with 12.5 % final concentration human AB serum (solid bars), or heat-inactivated human AB serum (striped bars). Data presented as mean ± S.D. from three independent experiments, where ** p = 0.0011 and **** p = < 0.0001.

Figure 3.3 shows that calcein release is significantly increased relative to the isotype control Herceptin when ch14.18 opsonised Lan-1 or IMR-32 human neuroblastoma cell lines are cultured in the presence of human serum. Calcein release is reduced to baseline levels for the Lan-1 cell line, and from 30 % to around 12 % of maximal for the IMR-32 cell line when cultured with matched serum that had been heat inactivated, to destroy complement proteins. Consequently the reduction in calcein release observed when the samples are cultured with heat inactivated serum indirectly implies that antibody induced

complement activation is responsible for the observed calcein release in the assay performed with human serum that had not been heat inactivated.

3.2.4 Characterising the mechanisms responsible for anti-GD2 mediated killing: Antibody-dependent cell mediated phagocytosis

The data presented in this section demonstrates the ability of murine bone marrow-derived macrophages (BMDMs) and human monocyte-derived macrophages (MDMs) to phagocytose anti-GD2 opsonised neuroblastoma cell lines.

3.2.4.1 Obtaining murine bone marrow-derived macrophages

Murine BMDMs were isolated from the bone marrow of the femur and tibia of A/J mice and cultured in the presence of M-CSF (see materials and methods, section 2.3.1). When cultured in this manner murine BMDMs are reported to be fully differentiated by day six of culture and can be used for *in vitro* phagocytosis assay for up to seven days (256). Figure 3.4 illustrates BMDM differentiation as the cells adapt to culture. The supplementation of the growth medium with M-CSF drives the proliferation and differentiation of committed myeloid-derived progenitors into functional macrophages. As shown in figure 3.4 the BMDMs adopt a more stellar-like morphology and adhere to the tissue culture plastic as they differentiate. Other non-adherent cell types harvested from the bone marrow, such as lymphoid progenitors and erythrocytes, are progressively lost each time the media is changed. Hence a purified macrophage population is gradually obtained.

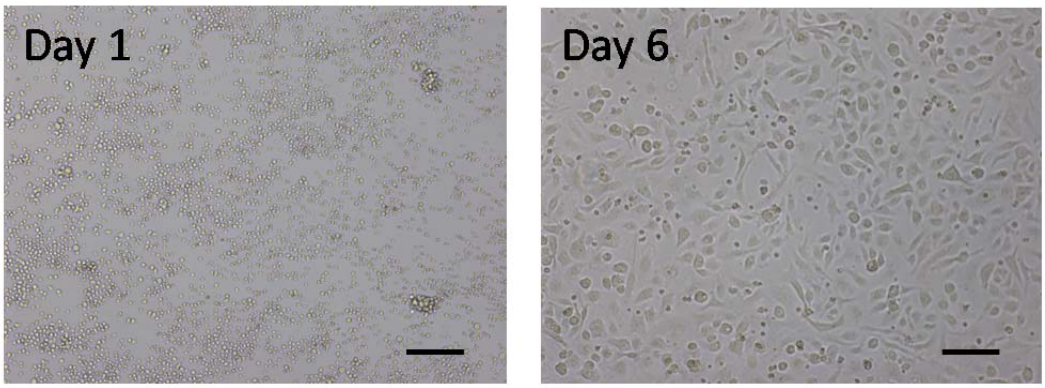

Figure 3-4. BMDM differentiation as cells adapt to culture. Murine BMDMs isolated from the femur and tibia of A/J mice were cultured in complete RPMI and supplemented with 10 % L929 conditioned medium in 6-well tissue culture plates for up to 14-days. Microscopy images were captured at x 10 magnification to demonstrate the change in morphology from day 1 (24-hours post isolation) to day 6 at which point they are reported to be fully differentiated (256).

3.2.4.2 Investigating antibody-dependent cell mediated phagocytosis of the murine NXS2 cell line *in vitro*

A flow cytometry based phagocytosis assay originally developed by Dr Ruth French (257) was adapted to investigate the ability of murine BMDMs obtained from A/J mice to phagocytose anti-GD2 opsonised syngeneic NXS2 neuroblastoma cells. A schematic representation of the steps of the methodology is shown in figure 3.5 (see also materials and methods, section 2.6).

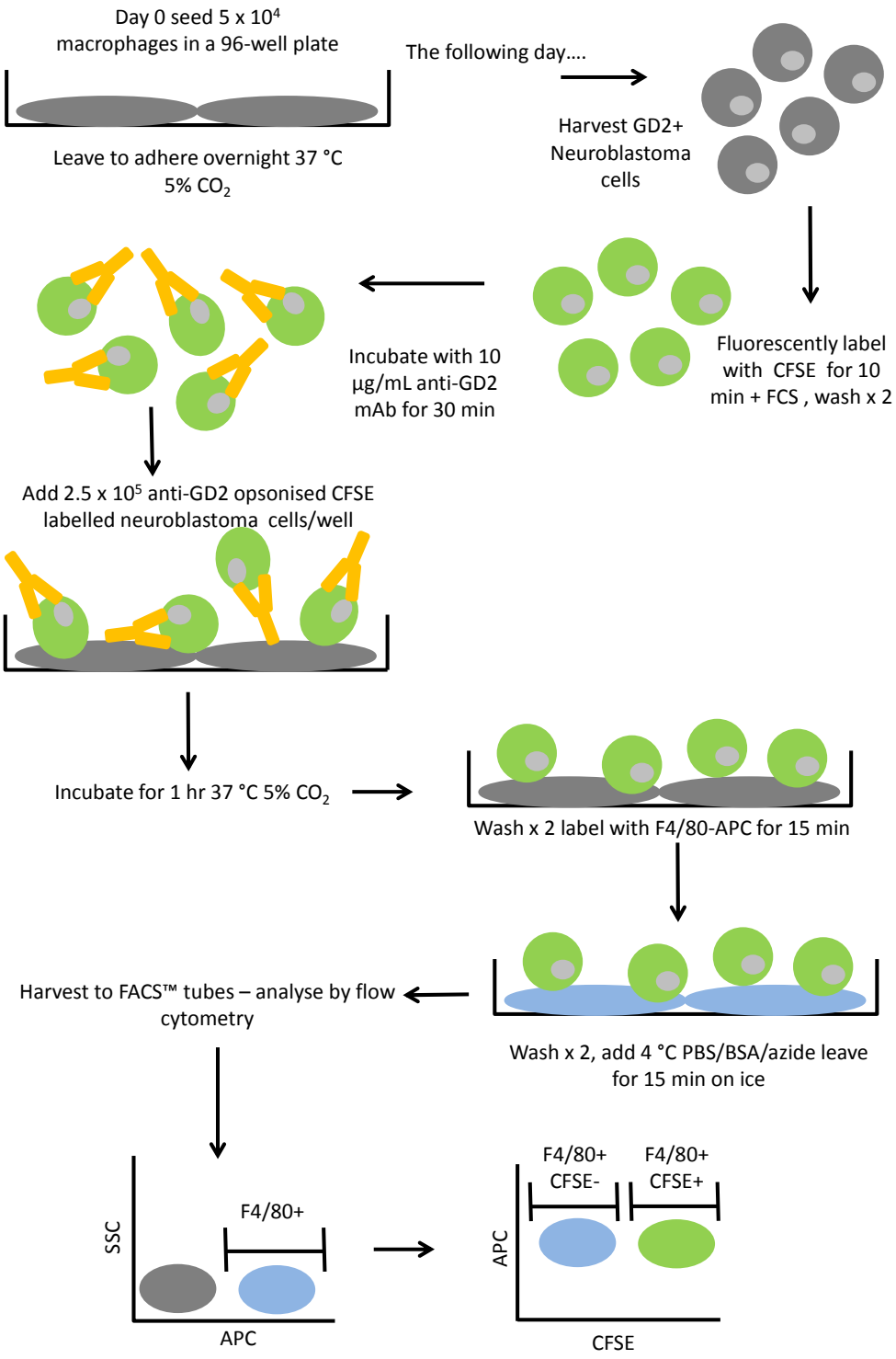

Figure 3-5. Schematic representation of the methodology for the flow cytometry based phagocytosis assay.

Briefly, murine BMDMs were seeded in 96-well plates and left to adhere overnight. The following day NXS2 cells were harvested and labelled with CFSE to facilitate their identification by flow cytometry. The CFSE labelled NXS2 target cells were subsequently opsonised with the anti-GD2 mAb 14G2a, an irrelevant isotype matched control (WR17), or PBS alone. The opsonised NXS2

target cells and BMDMs were subsequently co-cultured for one hour. After the incubation period the non-phagocytosed cells were removed and the BMDMs were labelled using the APC conjugated macrophage marker F4/80. The cells were harvested and analysed by flow cytometry. Phagocytosis was defined as the number of events that stained double positive for CFSE and F4/80 (CFSE+F4/80+), as a percentage of the total F4/80 positive macrophage population. Based on this definition a measure of phagocytosis would incorporate both surface bound and internalised NXS2 cells. Some representative flow cytometry profiles illustrating the gating strategy used to identify the APC labelled macrophages and the CFSE+F4/80+ events is shown in figure 3.6.

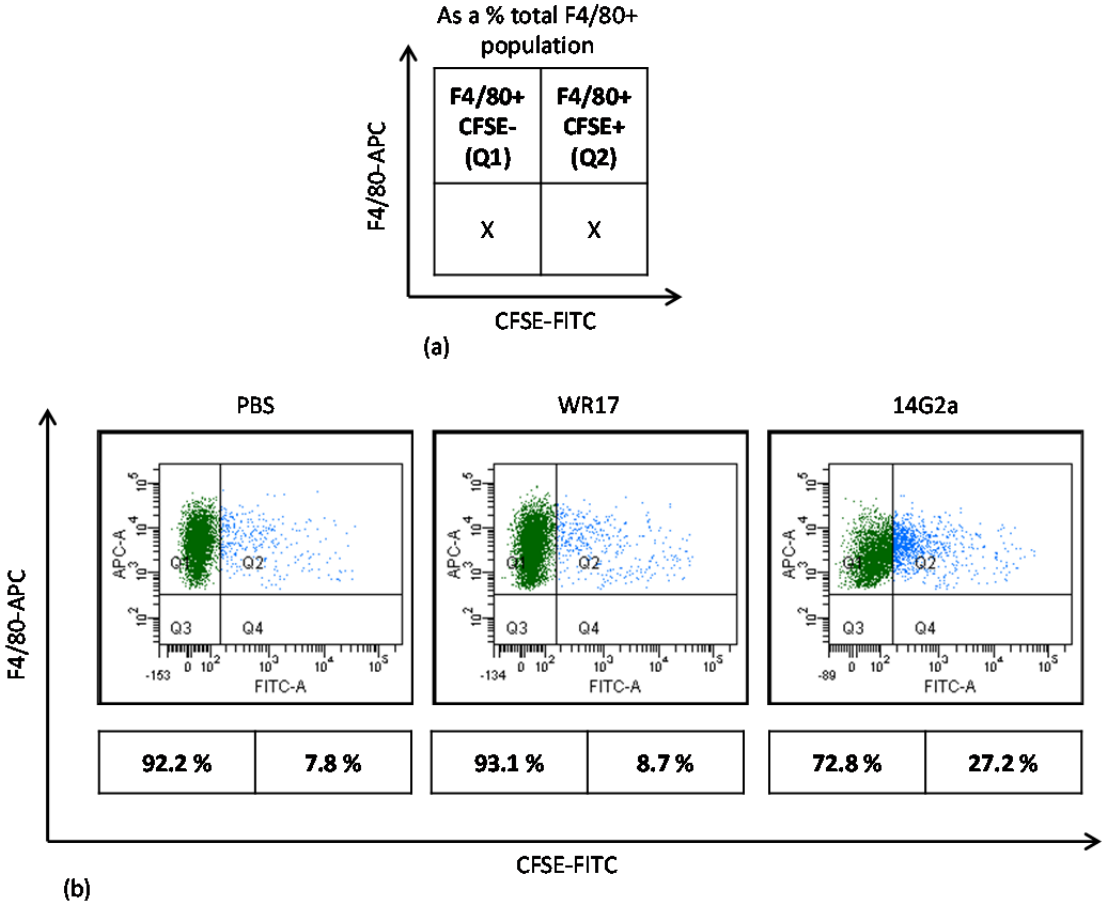

Figure 3-6. Representative flow cytometry profiles illustrating the double positive phagocytosed populations. Schematic representation of the quadrant labels that apply to the statistics displayed beneath each plot (a). Representative flow cytometry profile for each treatment group demonstrating the double positive (CFSE+F4/80+) phagocytosed population when CFSE labelled anti-GD2 opsonised NXS2 cells were co-cultured with F4/80+ BMDMs. (b).

The results of a series of phagocytosis assays performed using BMDMs isolated from A/J mice and the syngeneic NXS2 neuroblastoma cell line are summarised

in figure 3.7. The GD2 negative neuroblastoma cell line Neuro2a, which is also syngeneic for the in-bred A/J strain was used a negative control.

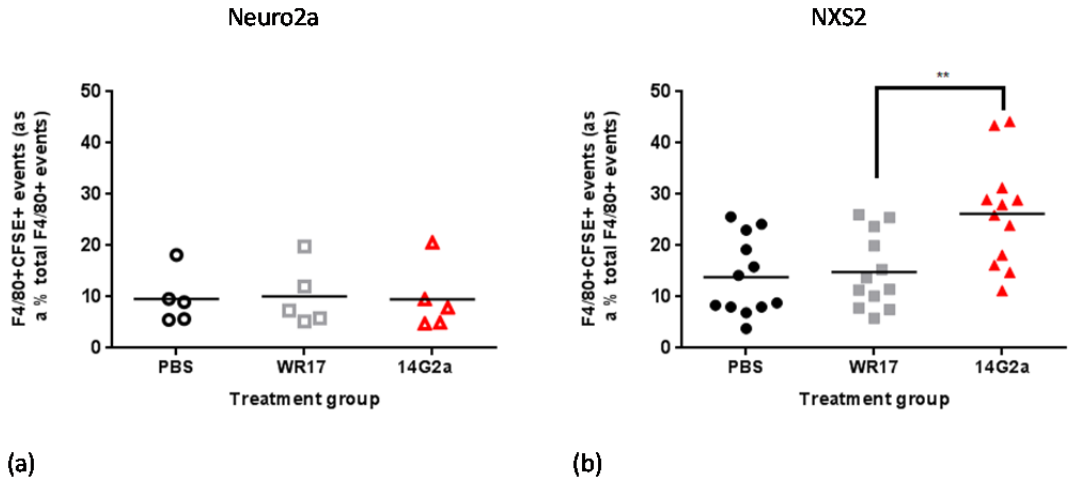

Figure 3-7. Phagocytosis of the murine neuroblastoma cell lines by BMDMs isolated from syngeneic A/J mice. Mean phagocytosis measured as the number of double positive APC-anti-F4/80 macrophages and CFSE labelled targets, as a percentage of the total APC-anti-F4/80 positive macrophage population. Phagocytosis of the GD2 negative Neuro2a cell line following treatment with PBS alone (black open circles), the irrelevant isotype matched control mAb WR17 (grey open squares) and the anti-GD2 mAb 14G2a (red open triangles), where n = 5, (a). Phagocytosis of the GD2 positive NXS2 cell line following treatment with PBS alone (black circles), the irrelevant isotype matched control mAb WR17 (grey squares) and the anti-GD2 mAb 14G2a (red triangles), where n = 12, ** p = < 0.0051 (b).

Figure 3.7 summarises the results of phagocytosis assays performed using the GD2 negative Neuro2a and GD2 positive NXS2 neuroblastoma cell lines. Figure 3.7 (a) clearly shows that when the Neuro2a cells are used as targets the double positive (F4/80+CFSE+) population remains at around 10 % of the total macrophage population despite the addition of the irrelevant isotype matched control mAb WR17, or the anti-GD2 mAb 14G2a. Whereas figure 3.7 (b) shows phagocytosis of the NXS2 cell line is significantly enhanced following the addition of 14G2a compared to the isotype control. On average phagocytosis of the 14G2a opsonised NXS2 cells is around double that observed in the absence of mAb (PBS) or when the isotype control WR17 was added.

3.2.4.3 Investigating antibody-dependent cell mediated phagocytosis of the human Lan-1 neuroblastoma cell line *in vitro*

To confirm whether ADCP as a mechanism also applied to human neuroblastoma cell lines a series of experiments were set up using human monocyte-derived macrophages (MDMs) obtained from PBMCs harvested from leucocyte reduction system (LRS) cones (obtained from the National Blood Transfusion Service) as a source of effector cells and the human Lan-1

neuroblastoma cell line. As with the murine BMDMs, human MDMs were cultured in growth medium supplemented with M-CSF (see materials and methods, section 2.1.3) for a period of seven days to induce macrophage differentiation, from which point they were ready to be used in phagocytosis assays. The phagocytosis assay itself was performed as previously shown in figure 3.6; however, an APC conjugated anti-CD16 mAb was used to identify the macrophage population, instead of the murine macrophage marker F4/80. Consequently, in human phagocytosis assays phagocytosis was defined and the APC-anti-CD16 and CFSE double positive population, as a percentage of the total APC-anti-CD16 positive population. The results from these assays are summarised in figure 3.8.

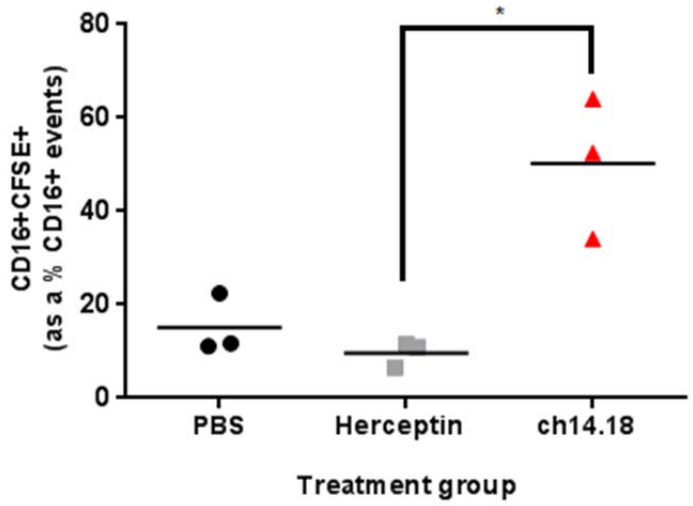

Figure 3-8. Phagocytosis of the human Lan-1 cell line by human MDMs. Human MDMs isolated from leucocyte reduction system cones were cultured for a minimum of 7-days to induce differentiation. Mean phagocytosis measured as the number of double positive APC-anti-CD16 macrophages and CFSE labelled targets as a percentage of the total APC-anti-CD16 positive macrophage population. Phagocytosis of the GD2 positive Lan-1 cell line following treatment with PBS alone (black open circles), the irrelevant isotype matched control mAb Herceptin (grey open squares) and the anti-GD2 mAb ch14.18 (red open triangles), where n = 3, and * p = 0.0101.

Figure 3.8 summarises the results from three separate phagocytosis assays performed using human MDMs harvested from LRS cones and the GD2+ human neuroblastoma cell line Lan-1. The CFSE labelled Lan-1 target cells were treated with either PBS alone, Herceptin, a humanised IgG1 mAb specific for the human epidermal growth factor receptor 2 (HER2), which was used as an irrelevant isotype control, or the anti-GD2 mAb ch14.18. Figure 3.8 shows that phagocytosis is significantly enhanced following the addition of the anti-GD2 mAb ch14.18 compared to the isotype control. On average phagocytosis

of the ch14.18 opsonised Lan-1 cells is around 35–40 % higher than that observed in the absence of mAb (PBS) or following addition of the isotype control Herceptin. The data in figure 3.7 (b) shows that the mean phagocytosis of the murine NXS2 cells following the addition of the anti-GD2 mAb was around 12 % greater than the isotype control, therefore the data in figure 3.8 suggests that a higher proportion of anti-GD2 opsonised human Lan-1 cells are phagocytosed by human macrophages in a similar time frame.

3.2.5 Characterising the mechanisms responsible for anti-GD2 mediated tumour cell killing: antibody-dependent cellular cytotoxicity

The results presented in this section summarise investigations into the ability of NK cells to induce anti-GD2 mediated ADCC *in* vitro using both human and murine target cells and effectors.

3.2.5.1 Comparing ADCC of anti-GD2 opsonised neuroblastoma cell lines using mouse splenocytes and human PBMCs

Anti-GD2 mediated ADCC was assessed *in vitro* using a calcein release based ADCC assay. As discussed in section 2.5 calcein-AM is a membrane permeable molecule that passively diffuses into cells, where it is converted into calcein, a green fluorescent dye, following hydrolysis by intracellular esterases. Calcein is retained within the cell provided the cell membrane remains intact; however, in the event the cell is lysed, calcein is released into the cell culture supernatant and can be detected using a fluorescence plate reader. To investigate anti-GD2 mediated ADCC by calcein release both the murine NXS2 and human Lan-1 cell lines were labelled with calcein-AM, prior to treatment with PBS alone, an irrelevant isotype matched control (PK136 or Herceptin), or the anti-GD2 mAb 14G2a (NXS2) or ch14.18 (Lan-1). The opsonised target cells were subsequently incubated with either syngeneic A/J mouse splenocytes, or human PBMCs, which were used as a source of effector cells. The results of this experiment are shown in figure 3.9.

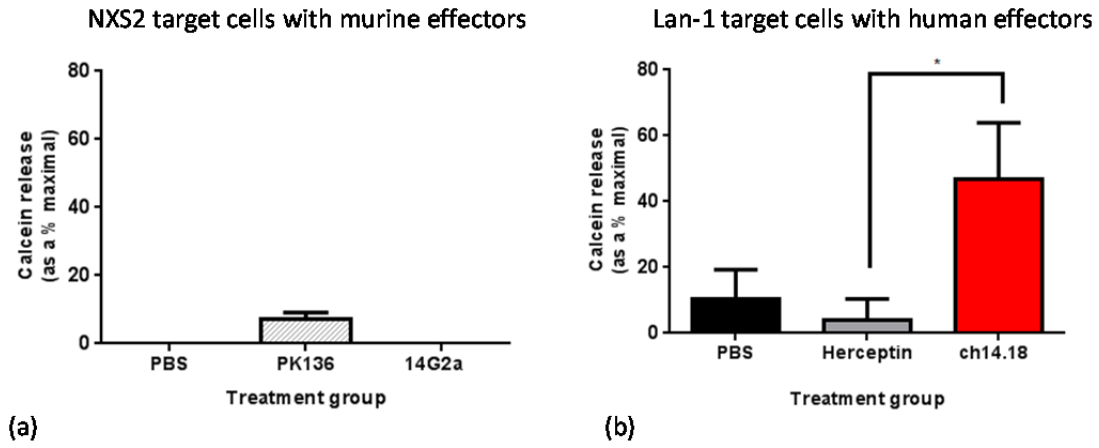

Figure 3-9. Anti-GD2 mediated cytolysis of the murine neuroblastoma cell line NXS2 and the human neuroblastoma cell line Lan-1 using a calcein release based ADCC assay. Calcein-AM labelled murine NXS2 and human Lan-1 neuroblastoma cell lines were treated with either PBS alone (black stripes/ solid bar), an irrelevant isotype matched control, PK136 or Herceptin (grey stripes/ solid bar), or anti-GD2 mAb, 14G2a or ch14.18 (red stripes/ solid bar) and co-cultured with either syngeneic A/J mouse splenocytes (NXS2), or human PBMCs (Lan-1) at an effector: target ratio of 40:1. Calcein release was measured using a Varioskan Flash fluorescence plate reader and calculated as a percentage of maximum lysis. Representative example of the mean + S.E.M calcein release as a percentage of maximal obtained from triplicate repeats for the murine NXS2 cell line (a). Mean + S.D. calcein release as a percentage of maximal obtained from three independent experiments using PBMCs from three separate donors for the human Lan-1 cell line, where * p = 0.0149 (b).

Figure 3.9 (a) shows that treatment with the anti-GD2 mAb 14G2a failed to induce calcein release when murine NXS2 neuroblastoma cells were cultured with murine effector cells. Conversely, figure 3.9 (b) shows that treatment with the anti-GD2 mAb ch14.18 resulted in a significant increase in calcein release, compared to the irrelevant isotype matched control Herceptin when Lan-1 cells were cultured with human effector cells. The failure to induce anti-GD2 mediated specific lysis of NXS2 cells treated with 14G2a and cultured with syngeneic A/J mouse splenocytes, as shown in figure 3.9 (a), can be attributed to either the NXS2 cell line itself, or the source of effector cells, on the basis that figure 3.9 (b) clearly shows the calcein release based ADCC assay can reproducibly detect anti-GD2 mediated specific lysis of the Lan-1 neuroblastoma cell line. Flow cytometry analysis was performed on both the human and mouse effector cells used in these ADCC assays to enumerate NK cell numbers, and assuming NK cells are responsible for anti-GD2 mAb induced ADCC the most likely explanation for the lack of calcein release in the murine ADCC assay is the low number of NK cells in the spleens of A/J mice. Figure 3.10 (a) is a representative flow cytometry profile, which shows that NK cells typically comprise less than 2 % of the lymphocyte population recovered from the spleens of A/J mice, whereas figure 3.10 (b) is a representative flow

cytometry profile, which shows that NK cells can comprise up to 16 % of the total human peripheral blood lymphocyte population recovered from LRS cones. Therefore, although murine effector cells were added at an effector: target ratio of 40:1, based on the NK cell number recovered from the spleens of the A/J mice the actual number of NK cells to NXS2 target cells in the murine ADCC assays was less than 1:1, which may account for the lack of antibody induced calcein release.

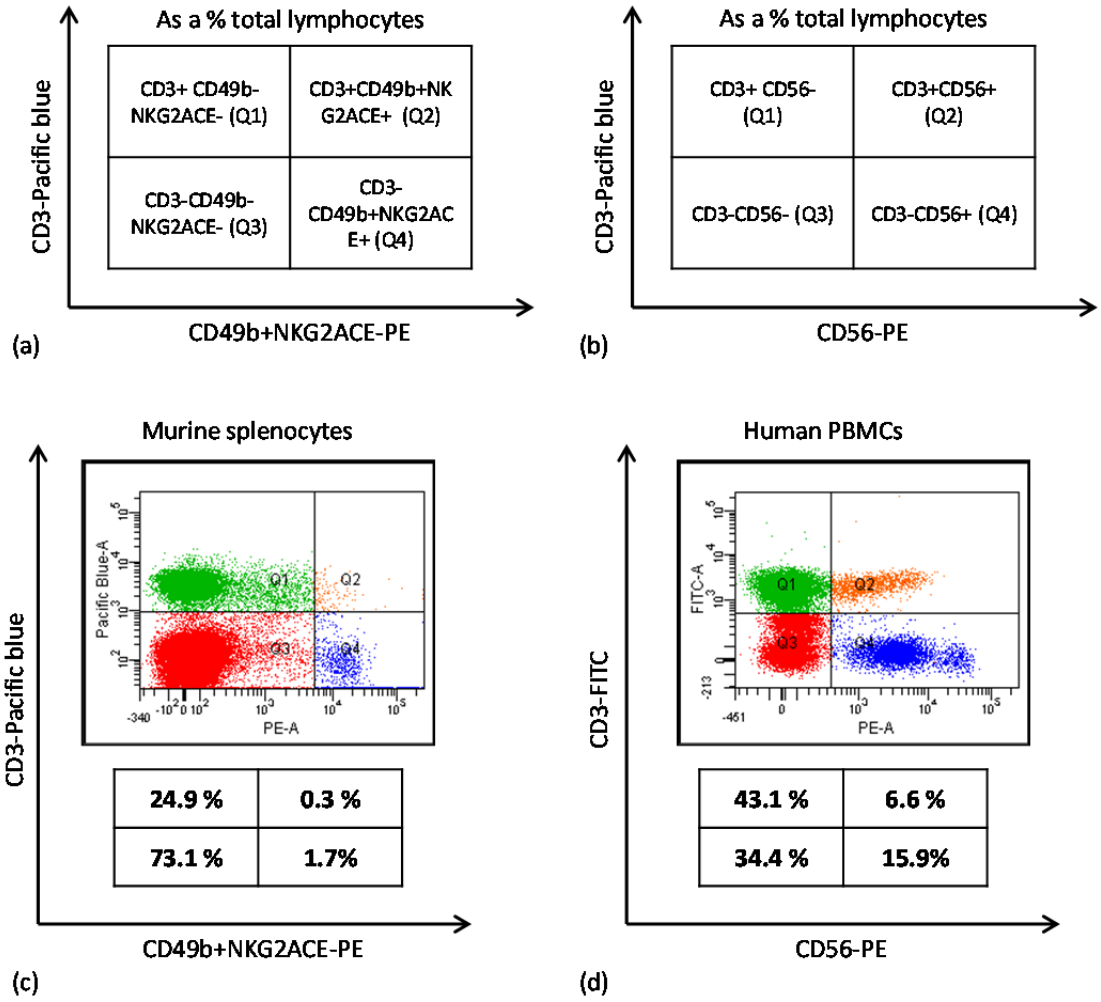

Figure 3-10. The proportion of murine NK cells recovered from the spleen versus human NK cells recovered from LRS cones. The NK cells were assessed by flow cytometry. Schematic representation of the quadrant labels that apply to the quadrant statistics displayed beneath each flow cytometry profile for the murine (a) and human (b) NK cells. The position of the quadrants was based on staining observed using irrelevant isotype controls. Murine CD3-CD49b+NKG2ACE+ NK cells present in the A/J mouse spleen as a percentage of the total lymphocyte population (c). Human CD3-CD56+ NK cells with the human PBMC population isolated from an LRS cone as a proportion of the total lymphocyte population (d).

3.2.5.2 Augmenting murine NK cell numbers prior to use in calcein release based assays

Based on the results in figures 3.9 and 3.10 it was hypothesized that anti-GD2 induced ADCC may still be achieved in the murine NXS2 ADCC assay provided sufficient NK cell numbers could be recovered from the spleens of syngeneic A/J mice. When human PBMCs obtained from LRS cones are used at an effector: target ratio of 40:1 the actual number of NK cells to each neuroblastoma target cell is in the region of 6:1. Whereas murine effector cells recovered from the spleen would have to be added at an effector: target ratio of around 300:1 in order to achieve a similar number of NK cells per neuroblastoma target cell. Therefore, rather than increasing the effector: target ratio to such an extent in the murine assay, attempts were made to increase the number of NK cells recovered by enriching the splenic NK cell fraction post-harvest using an NK cell isolation kit. The results of this experiment are presented in figures 3.11.

A point of note is that whilst Miltenyi Biotec Technical Support Team advise that the mouse NK cell isolation kit should facilitate recovery of an NK cell population that is greater than 90 % pure, the kit was developed using the Balb/c in bred strain. A direct comparison of NK cell purity following isolation of NK cells from the spleens of Balb/c and A/J mice (data not shown) revealed that the NK cells recovered from the spleens of Balb/c mice were typically greater than 80 % pure, whereas less than half of the cells recovered from the spleens of A/J mice were in fact NK cells. Similar observations have been reported by others when assessing the NK cell yield and purity recovered from the spleens of Balb/c mice compared to C57BL/6 mice (258). Consequently, in subsequent experiments involving NK cells harvested from the spleens of A/J mice the NK cell isolation kit has been used to enrich rather than purify the NK cell population.

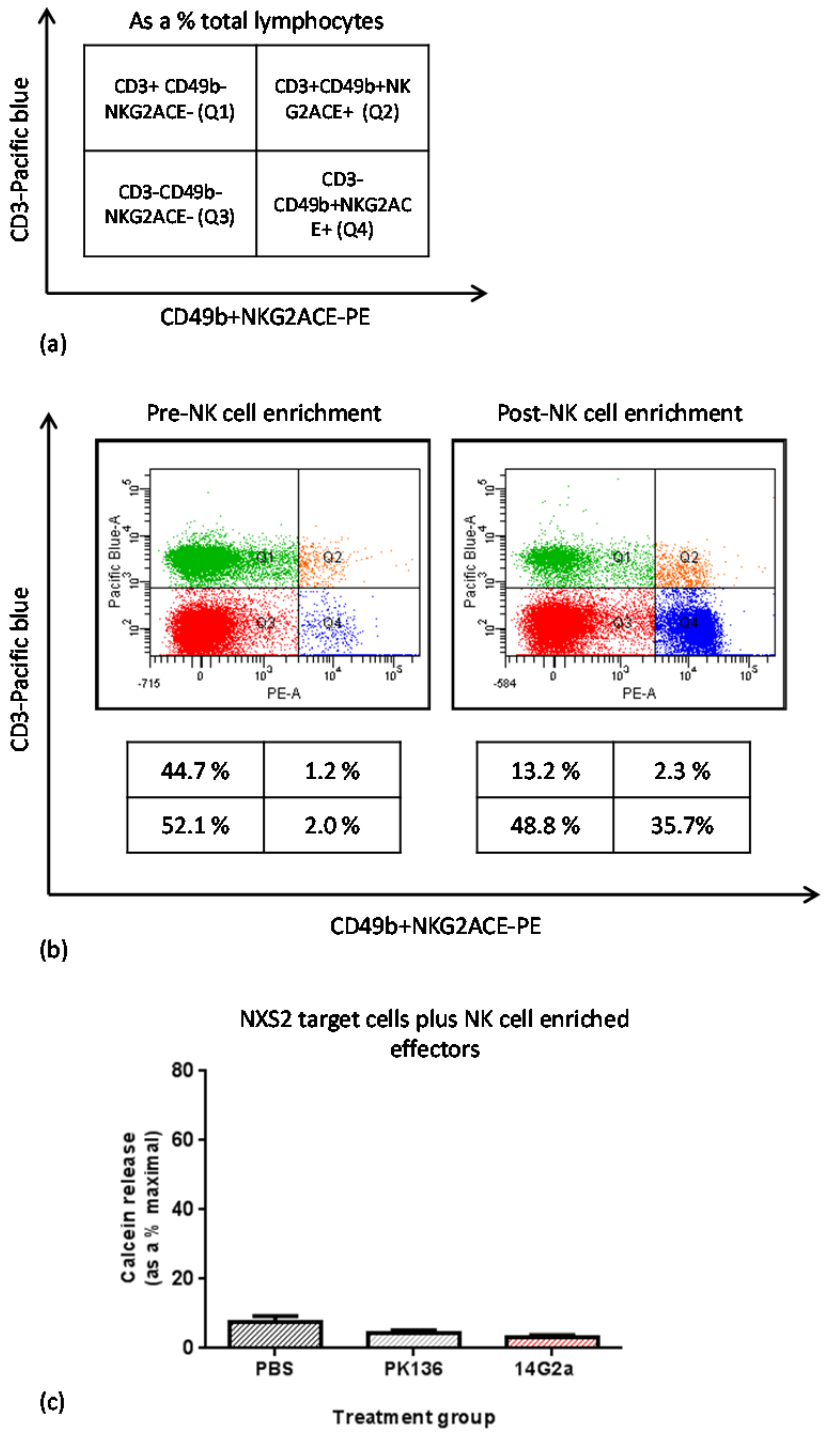

Figure 3-11. Anti-GD2 mediated cytolysis of the murine NXS2 neuroblastoma cell line using A/J splenocytes post-NK enrichment. The proportion of NK cells harvested from the spleen of a syngeneic A/J mouse as a percentage of total lymphocytes was assessed pre- and post-enrichment by flow cytometry. The NK cells recovered were added to calcein-AM labelled NXS2 neuroblastoma cells treated with either PBS alone (black stripes), an irrelevant isotype matched control (grey stripes), or the anti-GD2 mAb 14G2a (red stripes) at a 30:1 effector: target ratio. Calcein release was measured using a Varioskan Flash fluorescence plate reader and calculated as a percentage of maximum lysis. Schematic illustrating the quadrant labels that apply to the individual quadrant statistics displayed beneath each flow cytometry profile for clarity (a) Representative flow cytometry profiles illustrating NK cell numbers pre- and post-enrichment (b). Mean + S.E.M calcein release as a percentage of maximal obtained from triplicate repeats for the murine NXS2 cell line (c).

The data in figure 3.11 (b) shows the NK cell fraction, pre- and post-enrichment. Due to the total number of NK cells recovered following the enrichment step the maximum effector: target ratio that could be achieved in this assay was 30:1. The results of the calcein release based ADCC assay performed using the NK cell enriched effector cells is shown in figure 3.11 (c). As a consequence of NK cell enrichment the actual NK cell: NXS2 target cell ratio achieved when effector cells were seeded at 30:1 was around 10:1. However, despite a 10-fold increase in the number of NK cells to NXS2 targets compared to the previous ADCC assay (see figure 3.9 a) less than 5 % calcein release was achieved following anti-GD2 mAb treatment.

Additional attempts were made to increase the NK cell population *in vivo* prior to harvesting the splenocytes by administering 30,000 IU of recombinant IL-2 to A/J mice per day for a period of five consecutive days. The spleens were subsequently harvested and NK cell enriched, or not prior to use in ADCC assays with murine NCS2 target cells. Despite achieving NK cell: NXS2 target cells ratios in excess of 10:1 the anti-GD2 mAb induced calcein release achieved was consistently less than 5 % of maximal (data not shown).

3.2.5.3 Performing calcein release based ADCC assay using whole blood as a source of effectors.

Natural Killer cells routinely comprise around 10–15 % of the total lymphocyte population recovered from human peripheral blood LRS cones, consequently when used at an effector: target ratio of 40:1 in calcein release based ADCC assays the actual number of NK cells is in the region of 4–6 per target cell. The data in figure 3.9 (b) suggests that this is sufficient to induce anti-GD2 mediated specific lysis. The lack of anti-GD2 mediated specific lysis in figure 3.9 (a) was initially attributed to an insufficient number of murine NK cells per target. However, the results in figure 3.11 and obtained from other experiments (data not shown) imply that even when the NK cell number is increased in the order of 10+ NK cells per target cell (double the number typically used in the human ADCC assay) anti-GD2 mAb induced calcein release remains less than 5 % of maximal.

Since increasing the effector: target ratio failed to make a difference to the level of anti-GD2 mAb induced calcein release in the murine assay, an alternative explanation for the lack of ADCC observed may be that murine

effector cells recovered from the spleen are functionally deficient. In the human ADCC assay the effector cells are recovered from peripheral blood LRS cones, therefore mouse blood may prove to be a better source of effector cells for use in the murine ADCC assay. Consequently, a separate experiment was set up to investigate anti-GD2 mAb induced calcein release using human, or mouse whole blood as a source of effector cells. The human Lan-1 neuroblastoma cell line was chosen as the target cell line in this experiment because figure 3.9 (b) shows these cells are susceptible to anti-GD2 mediated specific lysis. The Lan-1 cells were opsonised with the anti-GD2 mAb ch14.18 when human whole blood was used as a source of effector cells and 14G2a when mouse whole blood was used as a source of effector cells. Mouse whole blood was collected by terminally bleeding A/J mice, whereas human whole blood was obtained from an LRS cone. The results of this experiment are shown in figure 3.12.

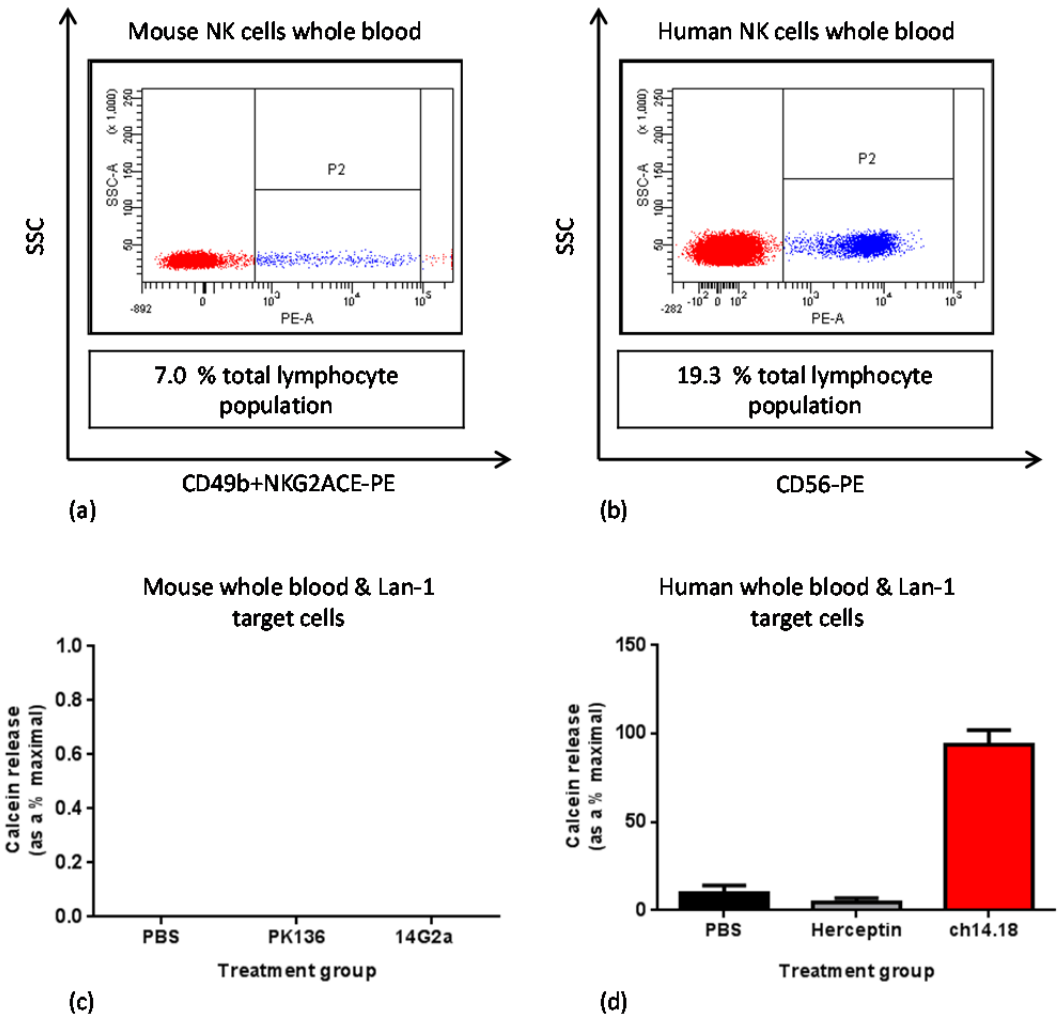

Figure 3-12. Anti-GD2 mediated cytolysis of the human neuroblastoma cell line Lan-1 using whole blood as a source of effectors. Whole blood (diluted 1:2) was added to calcein-AM labelled Lan-1 neuroblastoma cells treated with either PBS alone (black stripes/ solid bar), an irrelevant isotype matched control (grey stripes/ solid bar), or anti-GD2 mAb (red stripes/ solid bar). Calcein release was measured using a Varioskan Flash fluorescence plate reader and calcein release was calculated as a percentage of maximum. Flow cytometry was performed to determine the proportion of NK cells as a percentage of total lymphocytes present in the whole blood. Representative flow cytometry profiles illustrating NK cell number in mouse (a) or human (b) whole blood. Mean + S.E.M calcein release as a percentage of maximal obtained from triplicate repeats using mouse whole blood as a source of effector cells (c). Mean + S.E.M calcein release as a percentage of maximal obtained from triplicate repeats using human whole blood as a source of effector cells (d).

Figure 3.12 (a) and (b) shows the NK cell component of mouse and human whole blood respectively. Based on the lymphocyte counts following red blood cell lysis (which were fairly similar for the mouse and human samples) at 7 % of the total lymphocyte population the NK cell: target ratio in the murine ADCC assay was around 5:1; However, figure 3.12 (c) shows that no anti-GD2 induced calcein release was observed. Based on the human assays this effector: target ratio is assumed to be sufficient to induce killing, therefore the lack of calcein release suggests that peripheral blood NK cells harvested from

A/J mice are no more functionally active than NK cells harvested from the spleen. At around 19 % of the total lymphocyte population the human NK: target cell ratio was around 13:1 and figure 3.12 (d) shows that anti-GD2 induced calcein release was approximately 94 %. This effector: target ratio is much higher than the ratio typically used in ADCC assays, which may account for the particularly high level of calcein release. There may also have been some CDC activity from the serum component of the human whole blood

3.2.5.4 Performing calcein release based ADCC assays using human PBMCs as a source of effectors and murine NXS2 target cells

The failure to induce anti-GD2 mediated ADCC using A/J splenocytes or whole blood alongside both human and murine neuroblastoma target cell lines suggests that the NK cells recovered from A/J mice may be functionally deficient at least *in vitro* and the low lytic activity of NK cells recovered from A/J mice has been reported in the literature (259). Consequently, to confirm that the murine NXS2 neuroblastoma cell line is susceptible to anti-GD2 mAb in calcein release based ADCC assays a series of experiments was set up using the NXS2 neuroblastoma cell line and human PBMCs as a source of effector cells. The results of these experiments are summarised in figure 3.13.

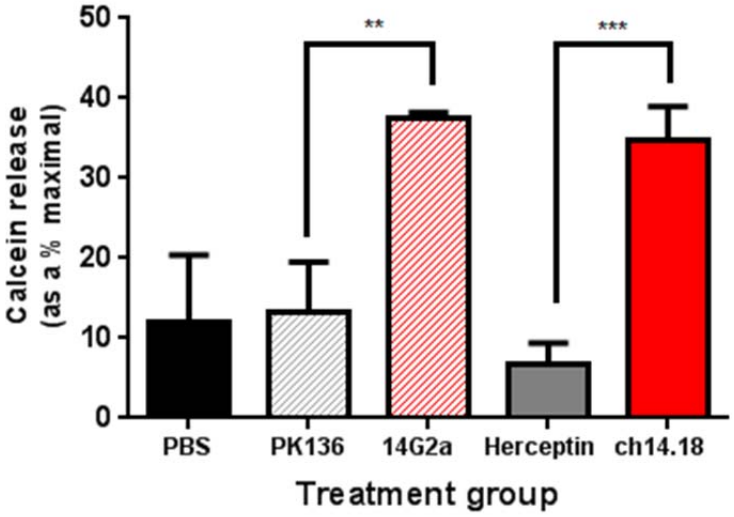

Figure 3-13. Anti-GD2 mediated cytolysis of the murine NXS2 neuroblastoma cell line using human PBMCs as a source of effector cells. Calcein-AM labelled murine NXS2 neuroblastoma cell lines were treated with either PBS alone (black bar), the irrelevant isotype matched controls PK136 (grey striped bar), or Herceptin (grey solid bar), or the anti-GD2 mAb 14G2a (red striped bar), or ch14.18 (red solid bar) and co-cultured with human PBMCs at an effector: target ratio of 40:1. Calcein release was measured using a Varioskan Flash fluorescence plate reader calculated as a percentage of maximum. Mean + S.D. calcein release as a percentage of maximum obtained from three independent experiments using PBMCs from three separate donors, where ** p = 0.0027 and *** p = 0.0007.

The data presented in figure 3.13 suggests that anti-GD2 mAb induced calcein release can be achieved with murine NXS2 targets cells when human PBMCs are used as a source of effectors. Treatment with either the anti-GD2 mAb 14G2a and ch14.18 results in a significant increase in calcein release (at around 36 % of maximal) compared to its respective isotype control.

3.2.5.5 The role of NK cells in anti-GD2 induced specific lysis as determined by calcein release in *in vitro* ADCC assays

NK cell mediated ADCC is considered to be the major effector mechanism responsible for the therapeutic effect of anti-GD2 mAb. The data in figures 3.9 (b) and 3.13 confirms that anti-GD2 induced calcein release by both human and murine neuroblastoma cell lines can be achieved *in vitro* when anti-GD2 opsonised neuroblastoma cells are cultured with human effector cells, *i.e.* PBMCs. However, these results do not confirm whether NK cells are responsible for the anti-GD2 induced calcein release observed. To determine whether anti-GD2 induced calcein release is mediated by NK cells in the *in vitro* ADCC assay a series of experiments were performed using human PBMCs isolated from LRS cones, from which NK cells were subsequently purified using a human NK cell

isolation kit (see materials and methods, section 2.4.2). These ADCC assays were performed using matched PBMCs, purified NK cells and the NK cell depleted fraction isolated from three separate LRS cones. Both the human neuroblastoma cell lines Lan-1 and IMR-32 were used as target cells in these experiments, the results of which are summarised in figures 3.14.

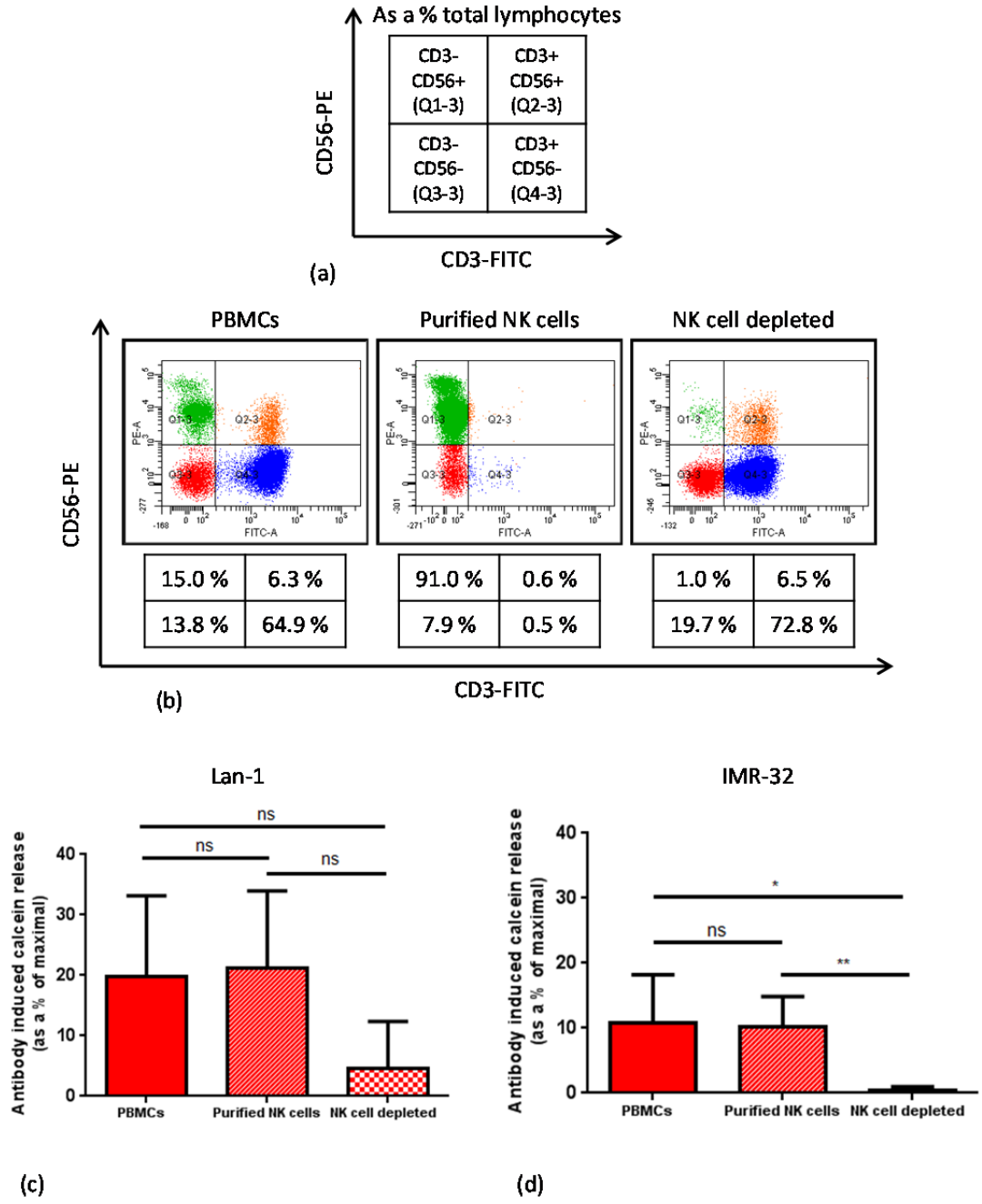

Figure 3-14. Anti-GD2 mediated cytolysis of human neuroblastoma cell lines using PBMCs, purified NK cells or the NK cell depleted fraction as a source of effector cells. PBMCs isolated from human peripheral blood LRS cones were purified using an NK cell isolation kit and assessed by flow cytometry to determine the proportion of NK cells as a percentage of total lymphocytes in the PBMC, purified NK cell and NK cell depleted fractions. The effector cells were then added to calcein-AM labelled anti-GD2 mAb ch14.18 treated Lan-1, or IMR-32 neuroblastoma cells at a 40:1 (PMBCs and NK cell depleted fraction), or 4:1 (purified NK cells) effector: target ratio. Antibody induced calcein release was measured using a Varioskan Flash fluorescence plate reader and calculated as a percentage of maximum. Schematic illustrating the quadrant labels that apply to the individual quadrant statistics displayed beneath each flow cytometry profile for clarity (a) Representative flow cytometry profile illustrating NK cell number in each fraction (b). Mean + S.D antibody induced calcein release as a percentage of maximal obtained following three independent experiments using three separate LRS cones for the Lan-1 (c) and IMR-32 (d) cell lines, where ns = not significant, * p = 0.0326 and ** p = 0.0061.

Figure 3.14 (b) is a series of representative flow cytometry profiles illustrating the NK cell population as a percentage of the total lymphocyte population pre-purification (*i.e.* the PBMCs), post-NK cell purification and in the NK cell depleted fraction (*i.e.* the remainder of PBMCs recovered once the NK cells had been removed). Antibody induced calcein release as a percentage of maximal is shown for the anti-GD2 mAb opsonised Lan-1 cells (c) and IMR-32 cells (d) cultured with PBMCs, purified NK cells, or the NK cell depleted fraction. Antibody induced calcein release was calculated for each cell line by subtracting the calcein release associated with effectors and target cells in the absence of mAb (*i.e.* PBS treated), see materials and methods section 2.5.3. When PBMCs or purified NK cells are used as a source of effector cells the antibody induced calcein release remains equivalent at around 20 % for the Lan-1 cells, and around 10 % for the IMR-32 cells respectively. However, when the NK cell depleted fragment is used as a source of effector cells the anti-GD2 induced calcein release is reduced to less than 5 % for the Lan-1 cells, and less than 1 % for the IMR-32 cells. Although only the reduction observed for the IMR-32 neuroblastoma cell line was statistically significant, taken together the equivalent calcein release observed when PBMCs or purified NK cells are used as effector cells, coupled with the reduction in calcein release observed when the same targets cells are cultured with the NK cell depleted fractions, suggests that the NK cell population is responsible for the anti-GD2 induced calcein release observed in these *in vitro* ADCC assays.

3.2.6 The role of NK cells and macrophages in anti-GD2 mAb therapy *in vivo*

The syngeneic NXS2 model is one of only two murine models of neuroblastoma that permits the study of GD2 targeted immunotherapies in fully immunocompetent mice and will be used extensively throughout this investigation. Since the therapeutic effect of anti-GD2 mAb is widely reported to be NK cell mediated, the failure to induce lysis of the murine NXS2 neuroblastoma cell line following treatment with anti-GD2 mAb was concerning. However, data has been published using this syngeneic model, which confirms that the therapeutic effect of the ch14.18-IL-2 immunocytokine is largely NK cell mediated and can be abrogated following NK cell depletion (203). This suggests that the failure to induce specific lysis of anti-GD2 opsonised NXS2 cells using syngeneic A/J splenocytes, or whole

blood in calcein release based ADCC assays may be due to a functional deficiency *in vitro*. Consequently a preliminary study was set up to assess the *in vivo* functional activity of A/J NK cells by recapitulating the published data as closely as possible. Additionally, since the results in figure 3.7 and 3.8 suggested that ADCP may contribute to the anti-tumour effects of anti-GD2 mAb, the decision was made to include a macrophage depleted group in order to explore the potential role for macrophages in anti-GD2 mAb therapy *in vivo*.

In this experiment syngeneic A/J mice were treated with either anti-asialo-GM1 antisera to deplete NK cells, or clodronate liposomes to deplete macrophages on day -3 and day -1, prior to inoculation with NXS2 neuroblastoma cells on day 0. Mice inoculated with NXS2 cells via the tail vein reportedly develop metastatic-like disease in the liver, lung and bone marrow within 21 days of inoculation (240). Therapy began on day 1 and mice were treated with either PBS alone, or 10 µg anti-GD2 plus 30,000 IU of recombinant IL-2, which provides a dose equivalent to the anti-GD2-IL-2 immunocytokine (203, 260), per day for a period of 6 days. The therapeutic end points included liver weight and the appearance of metastatic foci (as an assessment of tumour burden on day 21) and survival.

3.2.6.1 Depletion of liver and splenic macrophages using clodronate liposomes

Depletion of macrophages cells was achieved by administration of clodronate liposomes on day -3 and day -1 (see materials and methods, section 2.7.2). The data in figure 3.15 shows the deleterious effect of the clodronate liposomes on macrophages in the liver, which is the primary site of tumour burden, and the spleen on day 5 and day 9 post-macrophage depletion.

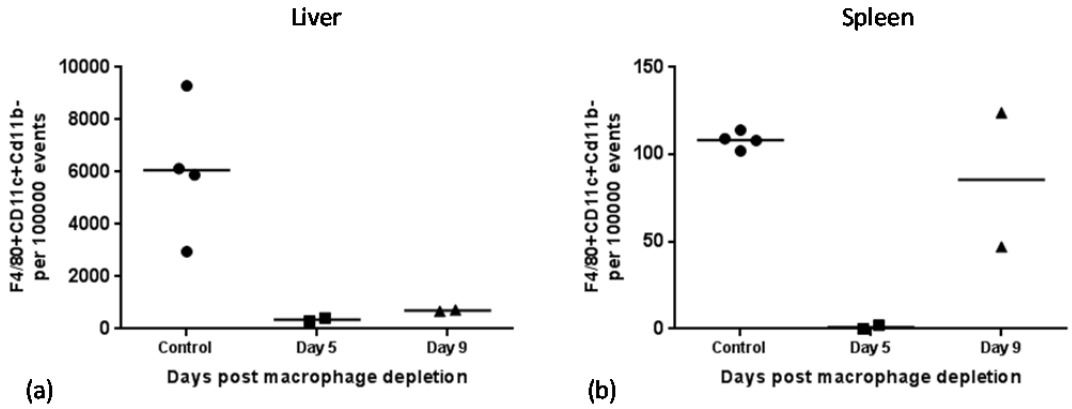

Figure 3-15. Macrophage depletion in the liver and the spleen post-administration of clodronate liposomes. A/J mice were injected 200 µL PBS alone, or 200 µL clodronate liposomes day -3 and day -1 to achieve macrophage depletion. Livers and spleens were harvested on day 5 and 9 post-depletion to confirm depletion by flow cytometry assessment. Number of macrophages per 100,000 events in the liver (a) and spleen (b) relative to naïve control mice.

Figure 3.15 shows clodronate liposome induced macrophage depletion relative to naïve control mice and confirms depletion persists in the liver for at least 9 days post-administration, which covers the duration of therapy; however, splenic macrophages are showing signs of recovery by day 9, therefore further injections of clodronate liposomes are likely to be required in future experiments in order to maintain depletion.

3.2.6.2 The endogenous macrophage response to neuroblastoma

The effect of macrophage depletion on tumour burden and survival is shown in figure 3.16.

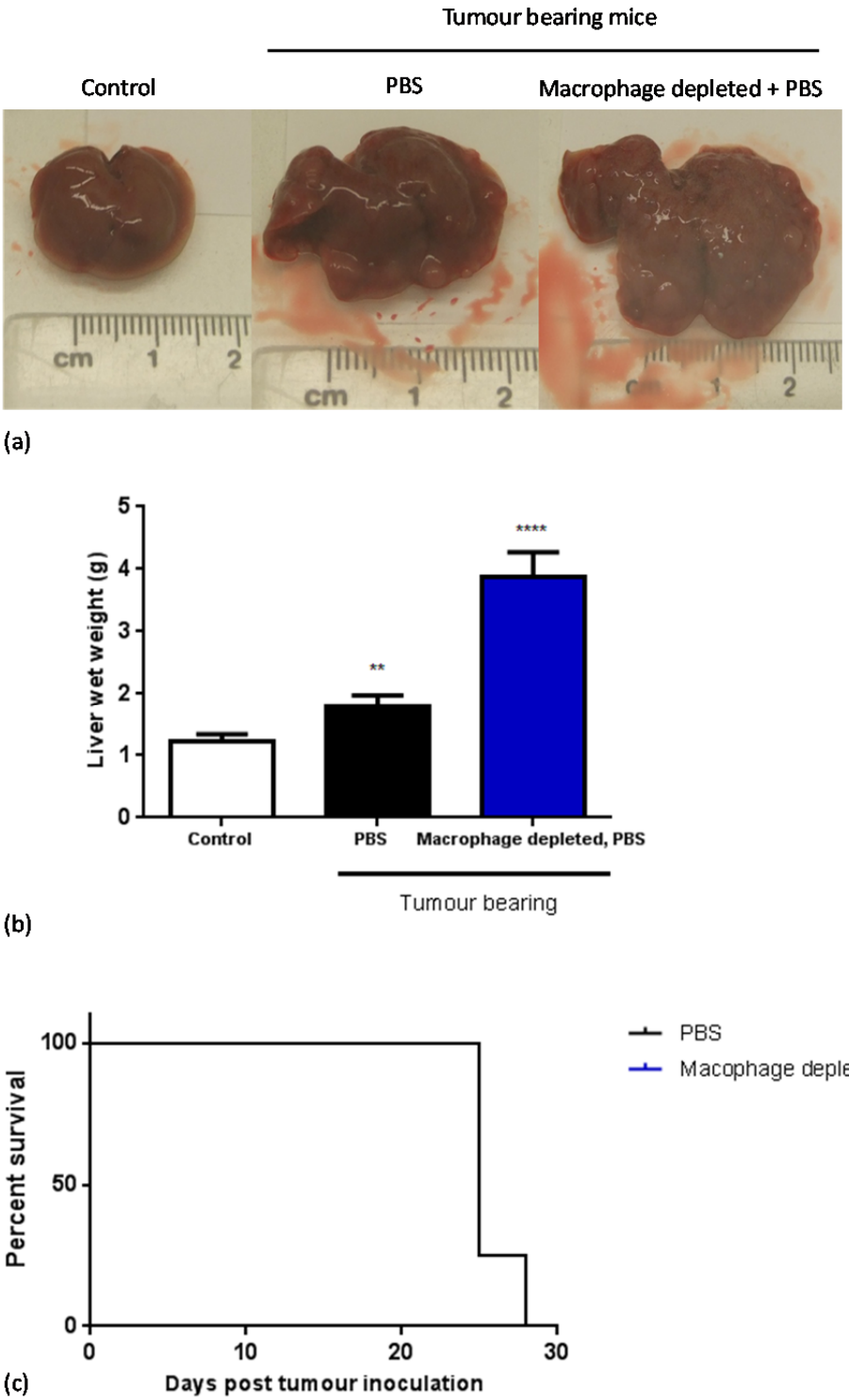

Figure 3-16. The endogenous macrophage response to neuroblastoma. A/J mice were injected with 200 µL PBS alone, or 200 µL (1:10 dilution) clodronate liposomes day -3 and day -1 prior to inoculation with $1x10^6$ NXS2 cells, or PBS alone on day 0. Mice (n = 6 per group, or 3 per group for macrophage depleted, PBS) were culled on day 21 and tumour burden was assessed by the appearance of metastatic foci (a), or liver wet weight (g) (b), ** p = 0.0044 and **** p = < 0.0001. Additional mice (n = 4 per group) were monitored for survival (c).

Figure 3.16 (a) and (b) illustrates the tumour burden as determined by both the appearance of macroscopic foci and the liver wet weight for the tumour-bearing mice (in the absence of therapy) is significantly increased relative to the naïve control mice. The macrophage depleted mice presented with by far the greatest tumour burden at day 21, with liver weights that were more than double those typically recorded amongst the tumour bearing mice (mean 3.9 g vs. 1.8 g). However, survival did not seem to be impaired, as shown in figure 3.16 (c) the survival curves for both tumour bearing untreated groups completely overlap.

3.2.6.3 The effect of macrophage depletion on tumour burden and survival following treatment with anti-GD2 mAb + IL-2

The effect of macrophage depletion on response to treatment with anti-GD2 mAb plus IL-2 in tumour bearing mice is shown in figure 3.17.

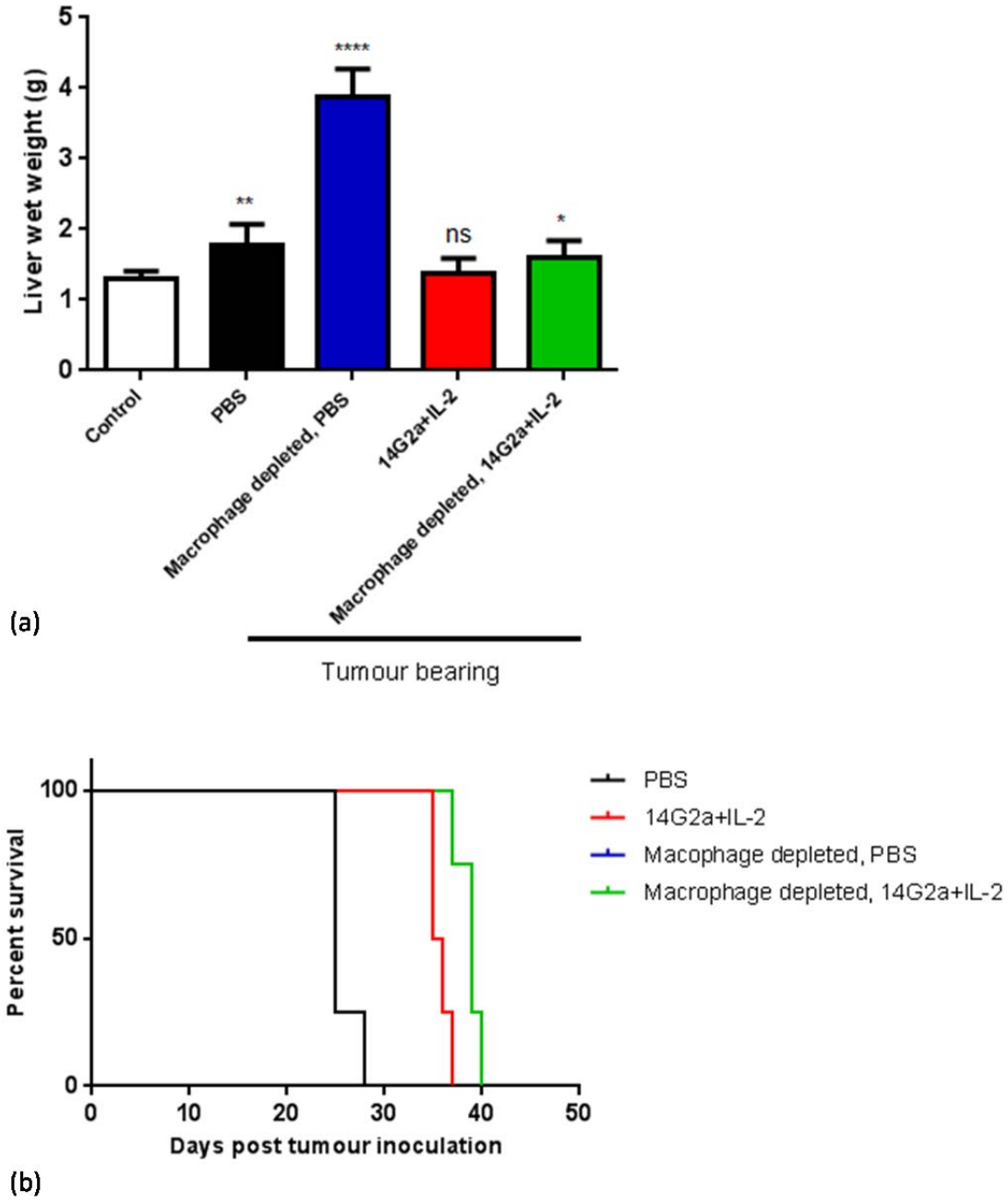

Figure 3-17. The effect of macrophage depletion on anti-GD2 plus IL-2 combination therapy in tumour bearing mice. A/J mice were injected 200 µL PBS alone, or 200 µL clodronate liposomes day -3 and day -1 prior to inoculation with $1x10^6$ NXS2 cells i.v. on day 0. Mice (n = 6 per group, or 3 per group for macrophage depleted, PBS) went on to receive PBS alone or 10 µg anti-GD2 mAb 14G2a plus 30,000 IU recombinant IL-2 for 6 days. Mice were culled on day 21 to assess tumour burden by liver wet weight (g) (a) * p = 0.0199, **** p = <0.0001 and ns = not significant. Additional mice (n = 4 per group) were monitored for survival (b).

Figure 3.17 (a) illustrates that the tumour burden, as determined by the liver weight for tumour bearing mice, is significantly increased in the absence of therapy relative to naïve control mice. The liver weights for the mice receiving 14G2a+IL-2 therapy is comparable to the naïve control; however, the liver

weight for the tumour bearing macrophage depleted group receiving 14G2a+IL-2 remains significantly higher than the naïve control group, suggesting a partial abrogation of therapy. Figure 3.17 (b) shows that despite a potential partial abrogation of therapy macrophage depletion did not reduce survival in the treated mice relative to the treated mice that were not macrophage depleted.

3.2.6.4 Depletion of liver and splenic NK cell using anti-asialo-GM1 antibody

Depletion of NK cells was achieved by administration of anti-asialo-GM1 antibody on day -3 and day -1. The data in figure 3.18 shows the deleterious effect of the anti-asialo-GM1 antibody on NK cells in the liver and spleen on day 5 and day 9 post-NK cell depletion.

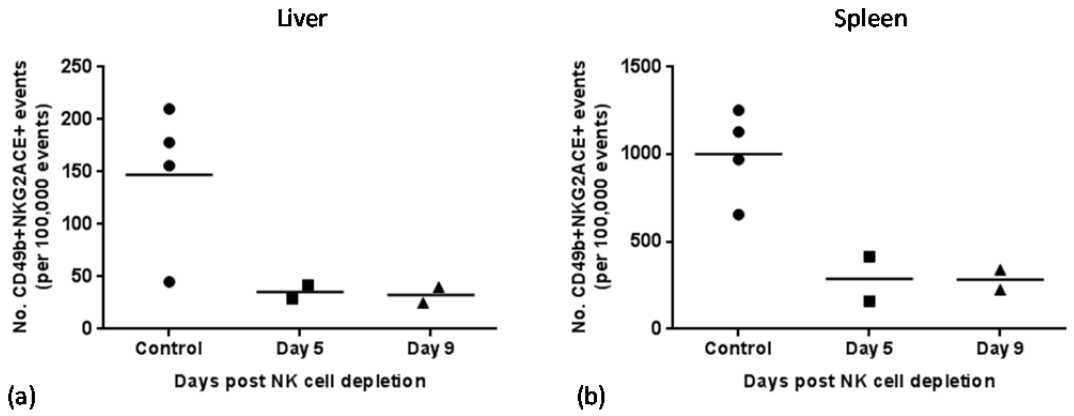

Figure 3-18. NK cell depletion in the liver and spleen post-administration of anti-asialo-GM1. A/J mice were injected 200 µL PBS alone, or 200 µL (1:10 dilution) anti-asialo-GM1 antisera day -3 and day -1 to achieve NK cell depletion. Livers and spleens were harvested on day 5 and 9 post-depletion to confirm depletion by flow cytometry assessment. Number of NK cells per 100,000 events in the liver (a) and spleen (b) relative to naïve control mice.

Figure 3.18 shows anti-asialo-GM1 induced NK cell depletion relative to naïve control mice and confirms depletion persists for at least nine days post-administration, which will cover the duration of therapy.

3.2.6.5 The endogenous NK cell response to neuroblastoma

The effect of NK cell depletion on tumour burden and survival in untreated mice is shown in figure 3.19.

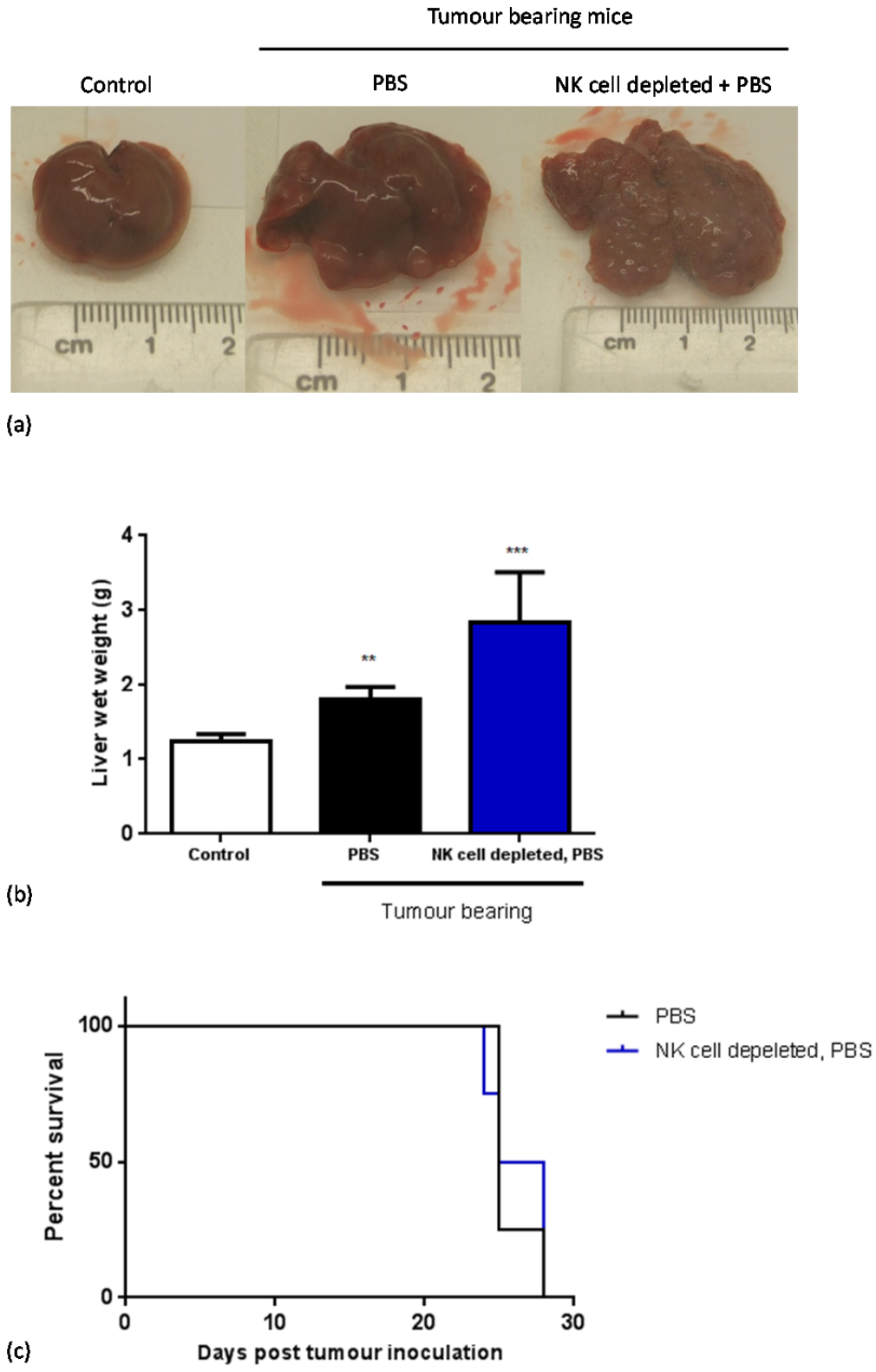

Figure 3-19. The endogenous NK cell response to neuroblastoma. A/J mice were injected with 200 µL PBS alone, or 200 µL (1:10 dilution) anti-asialo-GM1 antisera day -3 and day -1 prior to inoculation with $1x10^6$ NXS2 cells, or PBS alone on day 0. Mice (n = 6 per group, or 3 per group for NK cell depleted group) were culled on day 21 and tumour burden was assessed by the appearance of metastatic foci (a), or liver wet weight (g), ** p = 0.0044 and *** p = 0.0006 (b). Additional mice (n = 4 per group) were monitored for survival (c).

Figure 3.19 (a) and (b) illustrates the tumour burden as determined by both the appearance of macroscopic foci and the liver wet weight for the tumour bearing mice (in the absence of therapy), which in both cases was significantly increased relative to the naïve control mice. As observed in the macrophage depleted mice (see figure 3.16) it is clear that the NK cell depleted mice present with the greatest tumour burden at day 21, with liver weights that were on average more than 1 g heavier than the weight recorded for tumour bearing mice that had not been NK cell depleted and may be indicative of an endogenous NK cell response to neuroblastoma. Survival did not seem to be impaired in untreated NK cell depleted mice relative to untreated mice, as shown in figure 3.19 (c).

3.2.6.6 The effect of NK cell depletion on tumour burden and survival following treatment with anti-GD2 mAb + IL-2

The effect of NK cell depletion on response to treatment with anti-GD2 mAb plus IL-2 in tumour bearing mice is shown in figure 3.20.

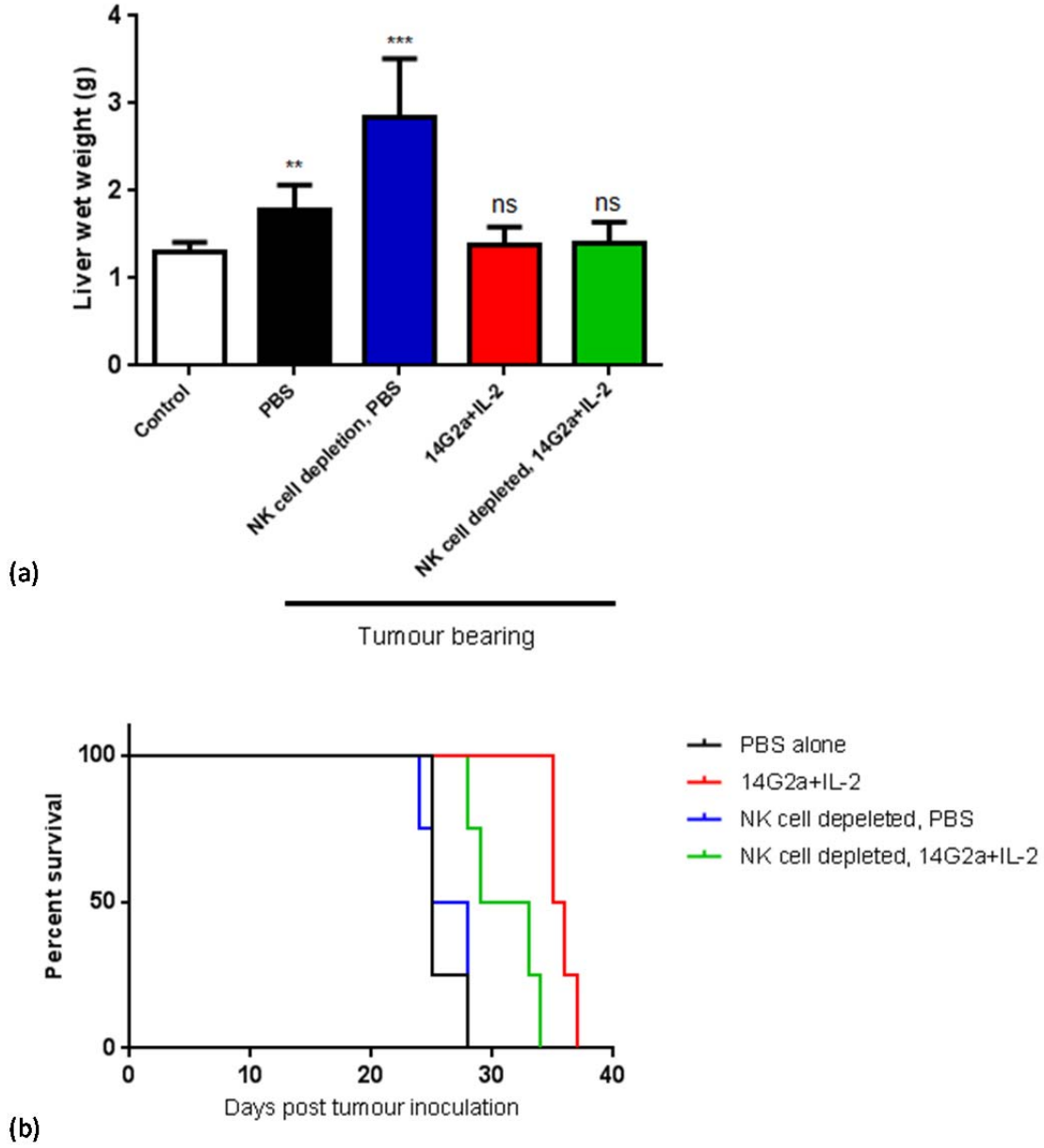

Figure 3-20. The effect of NK cell depletion in anti-GD2 plus IL-2 combination therapy in tumour bearing mice. A/J mice were injected 200 µL PBS alone, or 200 µL (1:10 dilution) anti-asialo-GM1 antisera day -3 and day -1 prior to inoculation with $1x10^6$ NXS2 cells i.v. on day 0. Mice (n = 6 per group, or 3 per group NK cell depleted groups) went on to receive PBS alone or 10 µg anti-GD2 mAb 14G2a plus 30,000 IU recombinant IL-2 for 6 days. Mice (n = 6 per group, or 3 per group NK cell depleted) were culled on day 21 to assess tumour burden by liver wet weight (g) (a), ** p = 0.0044, *** p = 0.0006 and ns = not significant. Additional mice (n = 4 per group) were monitored for survival (b).

Figure 3.20 (a) illustrates that whilst the tumour burden, as determined by the liver weight for the tumour bearing mice, is significantly increased in the absence of therapy relative to the naïve control mice, the liver weights for the mice receiving 14G2a+IL-2 is comparable to the naïve control regardless of NK cell depletion. However, figure 3.20 (b) shows that in terms of survival the NK cell depleted mice receiving 14G2a plus IL-2 reached end point before the

non-NK cell depleted mice receiving the same therapy, suggesting at least a partial abrogation of therapy.

3.2.6.7 NK cell depletion but not macrophage depletion reduces the protective effect of 14G2a+IL-2 treatment in terms of survival

When all the mouse groups receiving 14G2a+IL-2 are compared to the untreated group it is clear that they all benefit from treatment as all the mice survive longer than their untreated counter parts. However, of all the mice receiving therapy the NK cell depleted mice were the first to succumb to their tumour burden, as shown in figure 3.21.

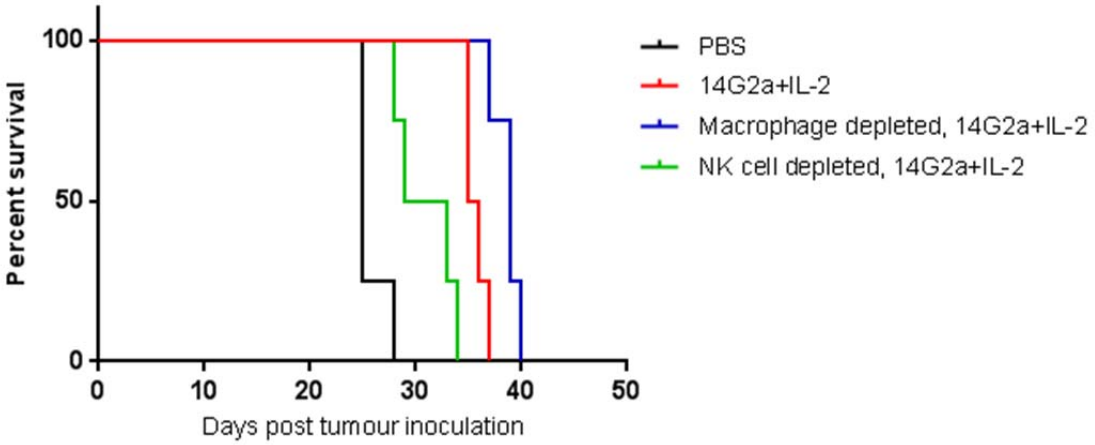

Figure 3-21. The effecto of macrophage or NK cell depletion on anti-GD2 plus IL-2 combination therapy in tumour bearing mice. A/J mice were injected 200 µL PBS alone, 200 µL anti-asialo-GM1, or 200 µL clodronate liposomes day -3 and day -1 prior to inoculation with $1x10^6$ NXS2 cells i.v. on day 0. Mice went on to receive PBS alone or 10 µg anti-GD2 mAb 14G2a plus 30,000 IU recombinant IL-2 for 6 days and were subsequently monitored for survival (n = 4 per group).

These experiments need to be repeated in order to draw any solid conclusions regarding the relative contributions of NK cells and macrophages to anti-GD2 mAb therapy *in vivo*. However, both NK cells and macrophages seem to be important in terms of the response to therapy as depletion of either subtype leads to a partial abrogation of therapy, resulting in either a reduction in survival (as is the case for NK cell depletion), or failure to fully eradicate tumour as determined by liver weight (as is the case for macrophages). Additionally, these experiments confirm that A/J NK cells are functionally active *in vivo*, therefore as anticipated the failure to induce ADCC is likely to be due to a functional deficiency *in vitro.*

3.3 Chapter discussion

The purpose of this chapter was to explore the immune mediated mechanisms of action responsible for the anti-tumour activity of anti-GD2 mAb as a thorough understanding of the mechanisms involved and how they might be enhanced is crucial for the rational design of improved therapeutic strategies. The data presented in this chapter provides some of the first *in vitro* evidence to suggest that macrophages may contribute to the anti-tumour activity of anti-GD2 mAb, in addition to the well-established NK cell mediated ADCC. Furthermore, results obtained from a preliminary experiment using a syngeneic model of murine metastasis suggests a role for macrophages and NK cells in both the endogenous immune response to NXS2 tumour and anti-GD2 mAb therapy *in vivo*, as neither depletion of macrophages nor NK cells alone was sufficient to completely abrogate therapy.

3.3.1 The role of CDC in anti-GD2 mAb therapy

The first immune mediated mechanism explored in this chapter was CDC. As discussed in section 1.5.1.2 CDC is initiated upon binding of the Fc domain of the anti-GD2 mAb engages the globular heads of the C1q molecule, triggering a sequence of events which culminates in the formation of the MAC and results in the death of the target cell. Attempts to investigate CDC using 14G2a opsonised NXS2 cells and mouse, or rat serum as a source of complement were unsuccessful. Mouse complement is extremely labile and often associated with poor lytic activity (255). However, mouse complement-dependent specific lysis has been reported for anti-GD2 opsonised NXS2 targets cells, with approximately 35 % killing observed at mAb concentrations of 5–10 µg/mL (254). At best only 20 % killing of NXS2 targets could be attributed to complement in this investigation using rat serum and this result was not reproducible (data not shown). However, taken together with the published data this does suggest NXS2 cells are susceptible to anti-GD2 mediated CDC *in vitro*. Other groups have investigated the role of CDC as a mechanism of action for the therapeutic effect of anti-GD2 mAb 14G2a *in vivo*, using the murine EL4 metastatic model of disease (255). The EL4 lymphoma cell line is known to express surface GD2 and anti-GD2 mAb have proven effective at eliminating EL4 micrometastases in syngeneic C57Bl/6 mice (261). EL4 cells express *ccry*, a structural analogue of the human complement inhibitors decay-accelerating

factor (DAF) and membrane cofactor protein (MCP) (262, 263) that renders them naturally resistant to CDC. However, *in vitro* data suggests that EL4 cells can be sensitised to CDC following treatment with the anti-GD2 mAb 14G2a. On the other hand EL4/mCD59 cells, which have been stably transfected with mouse CD59 (which is known to interfere with the formation of MAC and inhibit the late phase of complement activation), reportedly remain resistant to CDC despite treatment with 14G2a (255). In a series of *in vivo* experiments performed using the EL4 and the EL4/mCD59 cells the authors found that administration of 100 µg 14G2a 2 days post tumour inoculation was sufficient to eliminate tumour burden. When mice were culled 70 days post challenge both the mice inoculated with the complement sensitised EL4 cells and the complement resistant EL4/mCD59 were found to be tumour free. However, when these cells were administered to FcγRI/III-deficient mice, the protective effect of 14G2a was abrogated and both groups of mice were terminal by day 30. The lack of protection in mice inoculated with the EL4 cell line, which should have been susceptible to CDC even in the FcγRI/III-deficient mice, led the authors to conclude that ADCC is the principle mechanism of action for the anti-GD2 14G2a *in vivo* (255). Additionally, similar experiments performed in C3, or C3 receptor deficient mice had little effect on therapy, except low doses of antibody, which the authors concluded was suggestive of complement-mediated enhancement of ADCC rather than evidence for CDC as a principle mechanism (255). These experiments were performed in the C57Bl/6 strain using EL4 cells, most likely due to the availability of FcγRI/III, C3 and C3 receptor-deficient mice on this background; however, the authors did use the same anti-GD2 mAb 14G2a. Whilst it is likely the effect of therapy may differ between the models, it seems reasonable to suggest that the mechanisms elicited in the *in vivo* setting would be similar between the strains and therefore CDC may not be a major contributor to the therapeutic effect of anti-GD2 mAb *in vivo*.

CDC assays performed using human Lan-1 and IMR-32 neuroblastoma cell lines and human serum confirmed that the addition of the anti-GD2 mAb ch14.18 results in a significant increase in calcein release relative to control mAb, which can be attributed to antibody induced CDC. Anti-GD2 induced CDC has been widely reported for human neuroblastoma cell lines (174, 175, 181) and may be due, at least in part, to the low level surface expression of the complement inhibitors CD59, DAF and MCP by neuroblastoma cell lines

compared to other cancers (264). However, the susceptibility of human neuroblastoma cell lines to antibody induced CDC *in vitro* may be a feature of their adaption to culture. Neuroblastoma cell lines are typically morphologically diverse, comprising of neuroblastic (N-type) cells and non-neuronal Schwann-like (S-type) cells when they are first established; however, with time the N-type cells start to predominate, which is perhaps due to the S-type having less growth potential *in vitro* and *in vivo* (265, 266). Studies performed using matched N-type and S-type clones found that the S-type express significantly increased levels of the complement inhibitors CD59, DAF and MCP, hence this subtype were less susceptible to antibody induced CDC (264). Additionally, the S-type cells were found to express lower levels of GD2 (264). The N- and S-type cells are thought to have *in vivo* correlates, and this implies neuroblastoma cells may not be as susceptible to anti-GD2 induced CDC *in vivo* as the *in vitro* assays performed using cell lines suggest.

The data obtained in the investigation, coupled with the reports in the literature seems to suggest that the classical complement cascade may be initiated by anti-GD2 mAb; however, whether CDC contributes to the overall therapeutic effect of anti-GD2 mAb remains unclear. The observation that anti-GD2 mAb are unable to provide protection in FcγRI/III-deficient mice suggests that CDC as an effector mechanism is unlikely to play a major role in the response to therapy first hand. That said, activation of the classical complement cascade may enhance other immune effector mechanisms, such as phagocytosis, though the deposition of C3b on the tumour cell, which subsequently engages the C3 receptor expressed by macrophages.

3.3.2 The role of ADCP in anti-GD2 mAb therapy

Evidence for a role of ADCP in anti-GD2 mAb therapy was provided by the results of a clinical trial published in 2006 (207) (see section 1.5.1.3). The trial identified a subset of patients who possessed the FcγRIIA (R/R) genotype and went on to demonstrate superior progression free survival, following therapy with the anti-GD2 mAb 3F8 and GM-CSF. This FcγR subtype is expressed on macrophages and neutrophils, rather than NK cells, thus providing indirect evidence that ADCP by these cell types may have contributed to the favourable outcome of these patients. The ability of macrophages to phagocytose tumour cells *in vitro* was described by Bennett *et al.* in 1964 (267), more than 20 years

prior to the development of the first anti-GD2 mAb (174, 183). However, ADCP as a mechanism of action for anti-GD2 mAb is not widely reported in the literature and there have been very few papers in which ADCP has been explored mechanistically. ADCP was proposed as a mechanism of action for the anti-tumour effect of anti-GD2 mAb by Munn and Cheung whilst they were investigating the ability of monocytes cultured with M-CSF to induce ADCC of neuroblastoma cell lines (201). In their 1989 paper the authors reported that significant killing was not observed by chromium release when ADCC assays were performed using anti-GD2 opsonised neuroblastoma target cell lines and human monocytes cultured in the presence of M-CSF for 9–12 days. However, assessment by phase contrast microscopy suggested near complete target cell eradication. Consequently, they developed an ELISA that was capable of detecting viable cells the results of which, when coupled with flow cytometry analysis that facilitated identification of both targets and effectors pre- and post-incubation, correlated with their visual inspection. These observations led Munn and Cheung to conclude that monocyte derived macrophages were capable of eliciting potent anti-tumour effects; however, the physical engulfment of the target cells may prevent radioisotope release, thus masking the true extent of macrophage mediated ADCP in ADCC assays (201). In their follow up paper published in 1990 Munn and Cheung subsequently confirmed by way of electron microscopy that macrophage mediated ADCC was due to phagocytosis of the anti-GD2 opsonised target cells (268).

The data presented in this chapter demonstrates the ability of both murine BMDMs and human MDMs to phagocytose anti-GD2 mAb opsonised neuroblastoma cells. Providing some of the first *in vitro* evidence for macrophage mediated APCP as a mechanism of action in anti-GD2 mAb therapy. Nevertheless, this data is not without its limitations, as previously stated phagocytosis was defined as the number of F4/80+CFSE+, or CD16+CFSE+ events as a percentage of the total macrophage population and will therefore incorporate target and effector cells that are merely surface bound, as well as those that have been fully internalised. Consequently, in order to gain a true measure of phagocytosis additional methods, such as confocal microscopy, need to be employed to distinguish between the cells that are surface bound and those that have been genuinely phagocytosed. Work is ongoing within our research group to develop such methods in order

to fully explore the role of macrophages and the influence of their phenotype in anti-GD2 mAb therapy.

The observation that human macrophages appeared to more effectively phagocytose anti-GD2 opsonised neuroblastoma cells than their murine counterparts may be attributed to the difference in the level of surface GD2 expression between the neuroblastoma cell lines, which will influence the amount of anti-GD2 mAb bound to the surface of the target cell. Internalisation of anti-GD2 opsonised target cells by macrophages can be broken down into three steps: the first step involves the engagement of the FcγR expressed on the macrophage surface; the second step involves FcγR clustering, triggering the downstream signalling cascade that ultimately results in the third step, which is the physical engulfment of the target cell. The effectiveness of this process will be driven by both the affinity of the FcγR for its ligand (and therefore the mAb isotype is important) and the density of both the ligand itself and the FcγR on the macrophage surface (93). Since NXS2 cells have demonstrably less surface GD2 expression than Lan-1 cells, the NXS2 cells are likely to have less surface bound mAb and therefore less available ligand for the macrophage FcγR to bind. Consequently, perhaps only the NXS2 cells with the highest surface GD2 expression are being effectively phagocytosed. It is also possible that murine macrophages express fewer FcγR than the human equivalents and this could be confirmed by flow cytometry.

The contribution of macrophages to the therapeutic effect of anti-GD2 mAb *in vivo* was assessed using a murine metastatic model of neuroblastoma and macrophage depleted mice. Tumour cells establish in the liver in murine metastatic models of cancer, and tumour burden can be assessed by liver weight relative to naïve control mice. Liver weights recorded for the tumour bearing, untreated, macrophage depleted mice were more than double those typically recorded for untreated tumour bearing mice. The dramatic effect of macrophage depletion on tumour burden has been reported in other metastatic models, leading to the suggestion that macrophages may be involved in an endogenous early anti-tumour response (269). Liver weight was significantly increased in untreated, tumour bearing mice relative to naïve controls, and the administration of 14G2a+IL-2 was sufficient to eradicate tumour cells to the extent that there was no difference in liver weight between the mice receiving therapy and naïve controls. However, this effect was

partially abrogated in the macrophage depleted mice. The partial abrogation of therapy did not translate to a reduction in survival. A possible explanation for this is that the macrophages are repopulating. Splenic macrophages show signs of recovery by day 9 post-depletion, which is equivalent to the final day of therapy, and the half-life for murine monoclonal IgG2a antibodies in the mouse is 6-8 days (270). Consequently, anti-GD2 mAb may still be present in the system as late as day 17 by which point the macrophages may have fully recovered. Hence this experiment needs to be repeated in order to draw any definite conclusions regarding the effect macrophage depletion has on survival in 14G2a+IL-2 treated mice.

In short the clinical data published following the 2006 trial provides indirect evidence for the role of macrophages in anti-GD2 mAb therapy and sufficient data has been presented here to suggest that ADCP is a mechanism of action that may contribute to the anti-tumour effect of anti-GD2 mAb. The *in vivo* data obtained following macrophage depletion does suggest macrophages are likely to be involved in the anti-GD2 mAb response; however, this is a fairly artificial system in which 'normal' tissue resident macrophages are depleted prior to tumour inoculation and may not be representative of the M2-like macrophages typically found in the tumour microenvironment (135). With this in mind work is ongoing within the group to investigate both the role of macrophages in anti-GD2 mAb therapy and also the influence their phenotype has on response to therapy.

3.3.3 The role of NK cell mediated ADCC in anti-GD2 mAb therapy

NK cell mediated ADCC is a mechanism widely accepted to contribute to the anti-tumour effects of anti-GD2 mab. The *in vitro* data obtained using human model systems clearly demonstrated that NK cells were responsible for anti-GD2 induced destruction of neuroblastoma target cells in calcein release based ADCC assays. Unfortunately it was not possible to recapitulate these experiments using a murine model system; however, data was obtained confirming murine NXS2 cells are susceptible to anti-GD2 induced ADCC. Interestingly, the murine anti-GD2 mAb 14G2a, which is an IgG2a isotype, was found to be equally capable of inducing ADCC as the anti-GD2 mAb ch14.18, which is a human IgG1 isotype and has previously been reported to be superior

at inducing ADCC *in vitro* using cells from healthy donors and patient samples (190).

Despite their low level lytic activity *in vitro*, A/J NK cells are reportedly responsible for the therapeutic effect of the ch14.18-IL-2 immunocytokine used to treat metastatic disease in the synegeneic NXS2 model (203). The nature of the ch14.18-IL-2 immunocytokine means it is able to deliver a high IL-2 concentration directly to the tumour microenvironment, where it can stimulate a cellular response by activating T cells via their IL-2 receptors and NK cells via both their IL-2 receptors and FcγRIII (CD16). The humanised Hu14.18-IL-2, rather than chimeric form ch14.18-IL-2 form of the immunocytokine has since gone through phase I and phase II clinical trials (271, 272). Lode *et al.* reported that the ch14.18-IL-2 immunocytokine could eradicate established liver and bone marrow metastasis more effectively than equivalent mixtures of the antibody and recombinant IL-2, and that the therapeutic effect of the ch14.18-IL-2 agent was exclusively NK cell mediated (203). The NK cell dependency of this therapeutic strategy was demonstrated in a series of experiments involving SCID, SCID beige, and A/J mice treated with anti-asialo-GM-1 mAb to depleted NK cells. Therapy was effective in the T and B cell deficient SCID mice but not SCID beige mice, which also lack NK cells. However, therapy could be achieved in SCID beige mice when they were reconstituted with A/J splenocytes, yet was abrogated in syngeneic A/J mice following NK cell depletion (203). The observation the A/J splenocytes could be used to achieve therapy in SCID beige mice plus the fact therapy was completely abrogated in NK cell depleted A/J mice suggested that A/J NK cells were functionally active *in vivo*.

The functional activity of A/J NK cells and their role in the anti-tumour effect of anti-GD2 mAb was tested *in vivo* using a murine metastatic model of neuroblastoma and NK cell depleted mice. As observed following macrophage depletion, the depletion of NK cells was associated with a greater tumour burden in untreated mice, with mean liver weight for the NK cell depleted, tumour bearing untreated group exceeding the tumour bearing, untreated group by more than 1 g. Similar effects have been reported previously for Balb/c mice inoculated with C-26 tumour cells following macrophage, or NK cell depletion. In these experiments tumour burden as assessed by liver weight was increased 5-fold and 10-fold compared to control mice in macrophage

and NK cell depleted mice respectively (269). Consequently, both macrophages and NK cells have been implicated in an endogenous early anti-tumour response (269). Liver weight in tumour bearing, untreated mice was significantly increased compared to naïve controls; however, therapy was able to eradicate tumour to the extent that there was no significant difference in liver weight between tumour bearing mice that had received therapy and the naïve controls. Nor was there a significant difference between the NK cell depleted tumour bearing mice treated with 14G2a+IL-2 and the naïve controls. NK cell depletion does seem to have a detrimental effect on survival, as the NK cell depleted group were the first of all the treated groups to reach end point. However, they still had a survival advantage over the untreated control group suggestion some response to therapy. In contrast to the observations reported by Lode *et al.* in our hands NK cell depletion did not seem to completely abrogate therapy, suggesting multiple mechanisms might be at play.

In summary the data presented in this chapter confirms that both macrophage mediated ADCP and NK cell mediated ADCC contribute to the anti-tumour effects of anti-GD2 mAb *in vitro,* in human and murine model systems. Additionally, some evidence has been obtained to suggest that both macrophages and NK cells are important in terms of the response to anti-GD2 mAb therapy *in vivo*, as depletion of neither subtype leads to a complete abrogation of therapy. This is potentially relevant to this investigation as both intra-tumoral macrophages and NK cells express (or can be induced to express) 4-1BB, thus the activity of both effector subtypes may be augmented by anti-GD2 plus anti-4-1BB mAb therapy.

Chapter 4: Exploring the potential of anti-GD2 plus anti-4-1BB mAb therapy for the treatment of neuroblastoma in murine and human model systems

4.1 Chapter introduction

Antibody-dependent cellular cytotoxicity is widely reported to be a major effector mechanism responsible for anti-GD2 mediated tumour cell killing and the results presented in Chapter Three provide further support for this observation. The concept of augmenting ADCC through activation of the NK cells to enhance the clinical efficacy of anti-GD2 mAb is not a new idea, hence the current rationale for administering anti-GD2 mAb along with systemic IL-2. However, the ability to augment ADCC by selectively targeting NK cells at the tumour site, thus avoiding the systemic toxicity associated with global NK cell stimulation represents an attractive alternative strategy. As discussed in section 1.6.4 the discovery that NK cells up regulate the inducible co-stimulatory molecule 4-1BB following FcγR triggering (236) led Levy and co-workers to hypothesize that mAb therapies, such as anti-CD20 (rituximab), that exert their therapeutic effect in part by ADCC upon engagement of FCγRIII (CD16) may induce 4-1BB up regulation by NK cells; hence subsequent administration of anti-4-1BB mAb may ligate 4-1BB expressed on the NK cell surface and provide a co-stimulatory signal, resulting in enhanced effector function. Levy *et al.* have gone on to demonstrate that this novel combinatorial approach enhances the efficacy of several direct targeting mAb, including rituximab, Herceptin® and cetuximab both *in vitro* and *in vivo* using a range of syngeneic and human xenotransplanted models (237-239). This work (published by Kohrt *et al.*) further strengthened the hypothesis that the efficacy of anti-GD2 mAb could be enhanced when administered in combination with anti-4-1BB mAb for the treatment of neuroblastoma, which is explored in this chapter. The data presented here aims firstly to investigate whether expression of the co-stimulatory molecule 4-1BB is induced when murine NK cells encounter anti-GD2 coated tumour cells, and secondly explore the efficacy of anti-GD2 plus anti-4-1BB mAb *in vivo* using the syngeneic NXS2 model of

neuroblastoma. Finally, the data presented towards the end of this chapter will utilise human PBMCs obtained from healthy volunteers, and human cell lines to explore the potential for inducing 4-1BB expression on human NK cells *in vitro* and investigate whether addition of an agonistic anti-4-1BB mAb can enhance anti-GD2 mediated tumour cell killing in *in vitro* ADCC assays.

4.2 Results

The syngeneic NXS2 murine model of neuroblastoma introduced in chapter 3. was used to investigate the effectiveness of anti-GD2 plus anti-4-1BB mAb combination therapy *in vivo*. The ability to induce metastatic-like disease in the liver following i.v. administration of NXS2 cells (240) has already been demonstrated in section 3.2.6. However, liver weight at end point provides a fairly crude (single) measurement of tumour burden and whilst it may be suitable for monitoring differences between treated and non-treated groups, it is unlikely to be sensitive enough to monitor differences between treatment groups. Consequently to assess the efficacy of anti-GD2 mAb administered with and without anti-4-1BB subcutaneous administration of the tumour cells was preferred, as regular measurements can be taken to monitor tumour progression throughout the duration of the experiment.

Prior to performing experiments to investigate whether the addition of anti-4-1BB mAb can enhance the efficacy of anti-GD2 mAb *in vivo*, it was first necessary to determine the composition of the TILs post-antibody therapy, more specifically to confirm whether 4-1BB up regulation was observed on tumour infiltrating NK cells following Fc:FcγR engagement by anti-GD2 coated neuroblastoma cells.

4.2.1 Investigating 4-1BB surface expression on tumour-infiltrating NK cells and T cells post anti-GD2 mAb therapy

In order to complete this investigation syngeneic A/J mice were inoculated with $2x10^6$ NXS2 tumour cells subcutaneously on the lower back. Once the tumour diameter had reached a minimum of 70 mm^2 mice were injected with the anti-GD2 mAb 14G2a, the anti-human CD20 mouse IgG2a irrelevant isotype control Ritm2a, or vehicle alone (PBS) and culled 24-hours later to enumerate tumour infiltrating NK cells and T cells, and quantify 4-1BB surface expression by flow

cytometry. Whole blood and splenocytes were also harvested from each tumour bearing mouse for comparative analysis.

4.2.1.1 Identifying tumour infiltrating NK and T cells among the tumour cell population

Fluorescently conjugated antibodies specific for the common leucocyte antigen CD45 and the ganglioside GD2 (14G2a) were used to separate the tumour infiltrating lymphocytes from GD2+ NXS2 neuroblastoma cells, and aid positioning of suitable gates to facilitate flow cytometry analysis of these subsets. Tumours were harvested 24-hours post-antibody therapy and disaggregated to obtain single cell suspensions. Figure 4.1 illustrates the gating strategy used separate the tumour infiltrating CD45+ leucocytes from the GD2+ tumour cells themselves to facilitate enumeration of infiltrating NK cells and T cells within the tumour cell population.

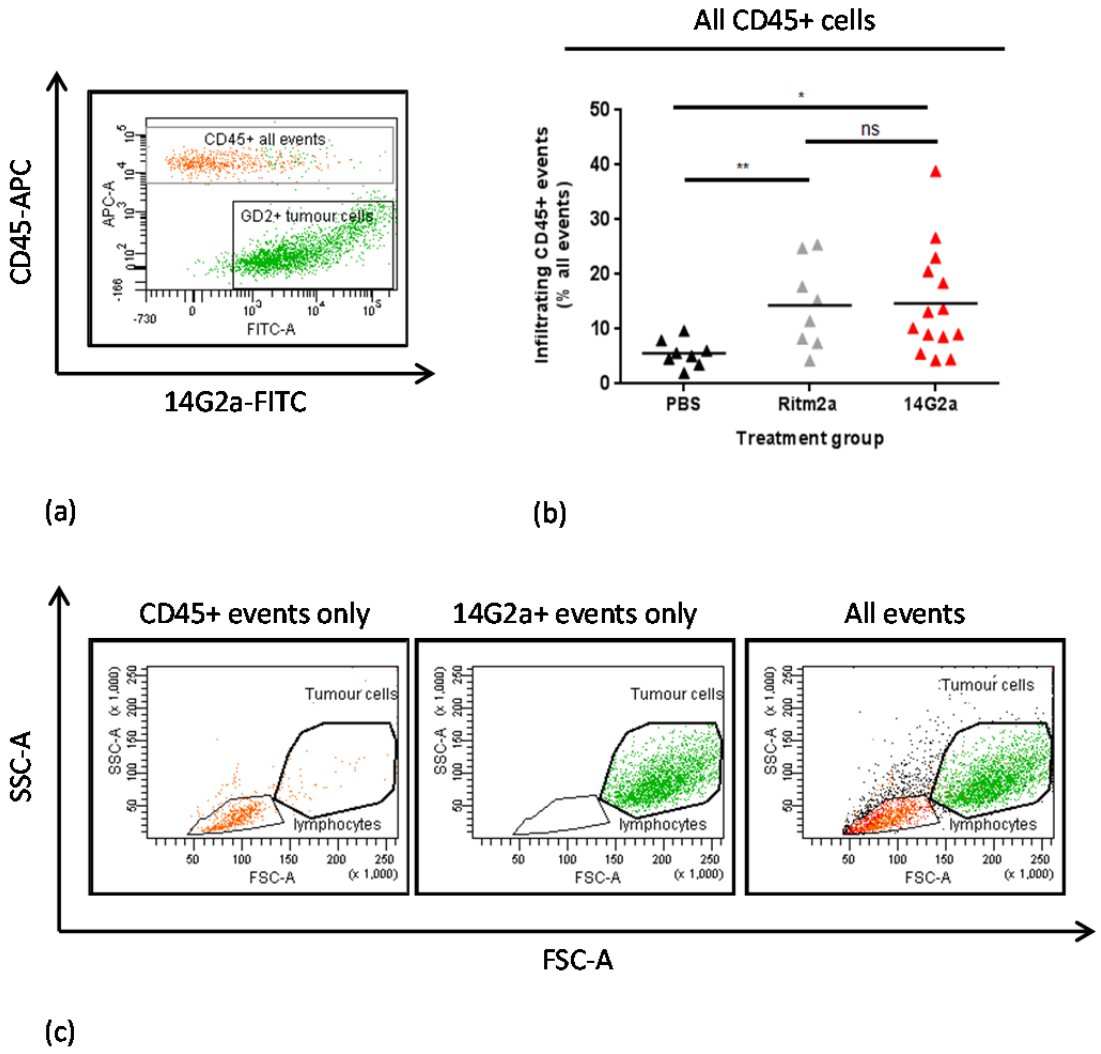

Figure 4-1. Example gating strategy used to identify tumour-infiltrating lymphocytes in subcutaneous NXS2 tumours harvested from syngeneic A/J mice. A representative flow cytometry profile illustrating CD45+ leucocytes and 14G2a+ NXS2 neuroblastoma cells (a). Mean number of tumour infiltrating CD45+ events as a percentage of all events for mice treated with vehicle alone (PBS) (black triangles) n = 8, 150 µg irrelevant isotype control (Ritm2a) (grey triangles) n = 8, or 150 µg anti-GD2 (14G2a) (red triangles) n =14, where * p = 0.0192 and ** p = 0.0095 (b).The CD45+ and 14G2a+ events used to position the lymphocyte and tumour cell gates (c).

The CD45+ and 14G2a+ events were identified as per figure 4.1 (a). As shown in figure 4.1 (b) enumeration of the CD45+ events as a percentage of all events collected revealed significantly more tumour infiltrating CD45+ events in mice treated with antibody versus vehicle alone (PBS). Perhaps surprisingly, this was also seen in mice treated with Ritm2a with the number of CD45+ events in these mice being almost identical to those treated with 14G2a, at 14.35 % versus 14.70 % respectively. It is important to clarify at this stage that the irrelevant isotype control mAb Ritm2a is specific for human CD20 and is used

to treat lymphomas in human CD20 transgenic mice, therefore it does not have a depleting effect on mouse B cells.

Additional tumour samples were prepared and stained with fluorescently conjugated antibodies specific for the surface antigens CD3, CD49b, NKG2ACE, CD8 and 4-1BB (see materials and methods, section 2.2.1). The events that fell within the lymphocyte gate (see figure 4.1 c) were first passed through the pacific blue and PE channels to identify and enumerate any tumour infiltrating CD3+ T cells and CD3-CD49b+NKG2ACE+ NK cells. Figure 4.2 (a) is a representative flow cytometry profile that demonstrates the gating strategy used to identify these subpopulations. Figure 4.2 (b) summarises the mean number of NK cells as a percentage of all events collected for the individual mice belonging to each treatment group 24-hours post-antibody therapy.

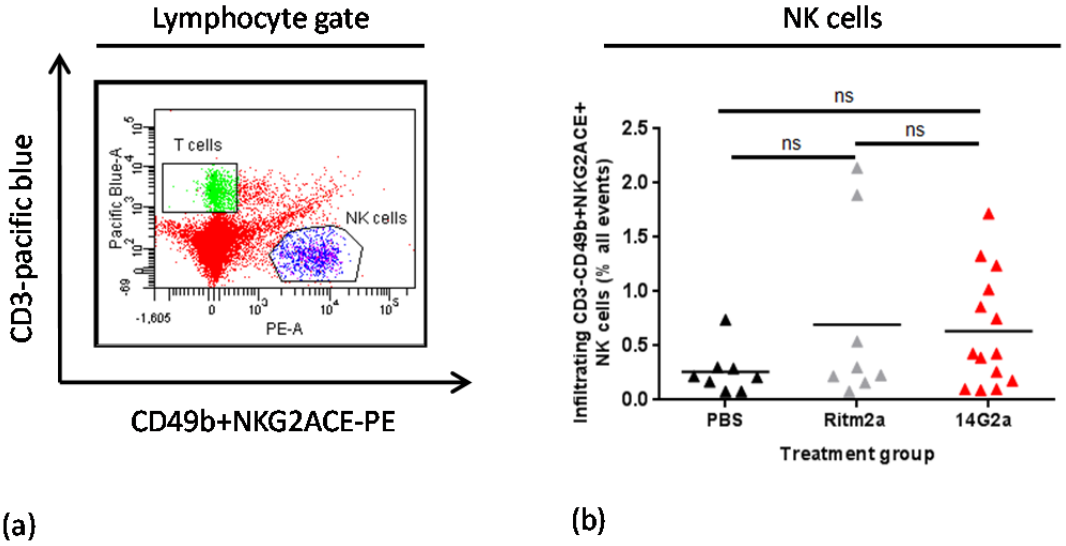

Figure 4-2. Tumour-infiltrating NK cells can be identified and enumerated by flow cytometry. Tumour infiltrating NK cells were identified and enumerated by passing the events in the lymphocyte gate through the pacific blue and PE channels to identify CD3-CD49b+NKG2ACE+ NK cells and CD3+ T cells (a). Infiltrating CD3-CD49b+NKG2ACE+ NK cells as a percentage of all events in mice treated with vehicle alone (PBS) (black triangles), 150 µg irrelevant isotype control (Ritm2a) (grey triangles), or 150 µg anti-GD2 (14G2a) (red triangles) (b), ns = not significant.

The number of tumour infiltrating CD3-CD49b+NKG2ACE+ NK cells (figure 4.2 b) in mAb treated mice are slightly but not significantly increased compared to mice receiving vehicle alone (PBS).

4.2.1.2 4-1BB surface expression by tumour infiltrating NK cells 24-hours post antibody therapy

The CD3-CD49b+NKG2ACE+ tumour infiltrating NK cells were passed through the APC channel to look for surface expression of 4-1BB 24-hours post treatment with vehicle alone (PBS), irrelevant isotype control (Ritm2a), or anti-GD2 (14G2a). Figure 4.3 (a) is a series of example flow cytometry profiles demonstrating surface 4-1BB expression on tumour-infiltrating NK cells for one mouse per treatment group. Figure 4.3 (b) shows the mean number of CD3-CD49b+NKG2ACE+4-1BB+ events as a percentage of all tumour-infiltrating NK cells.

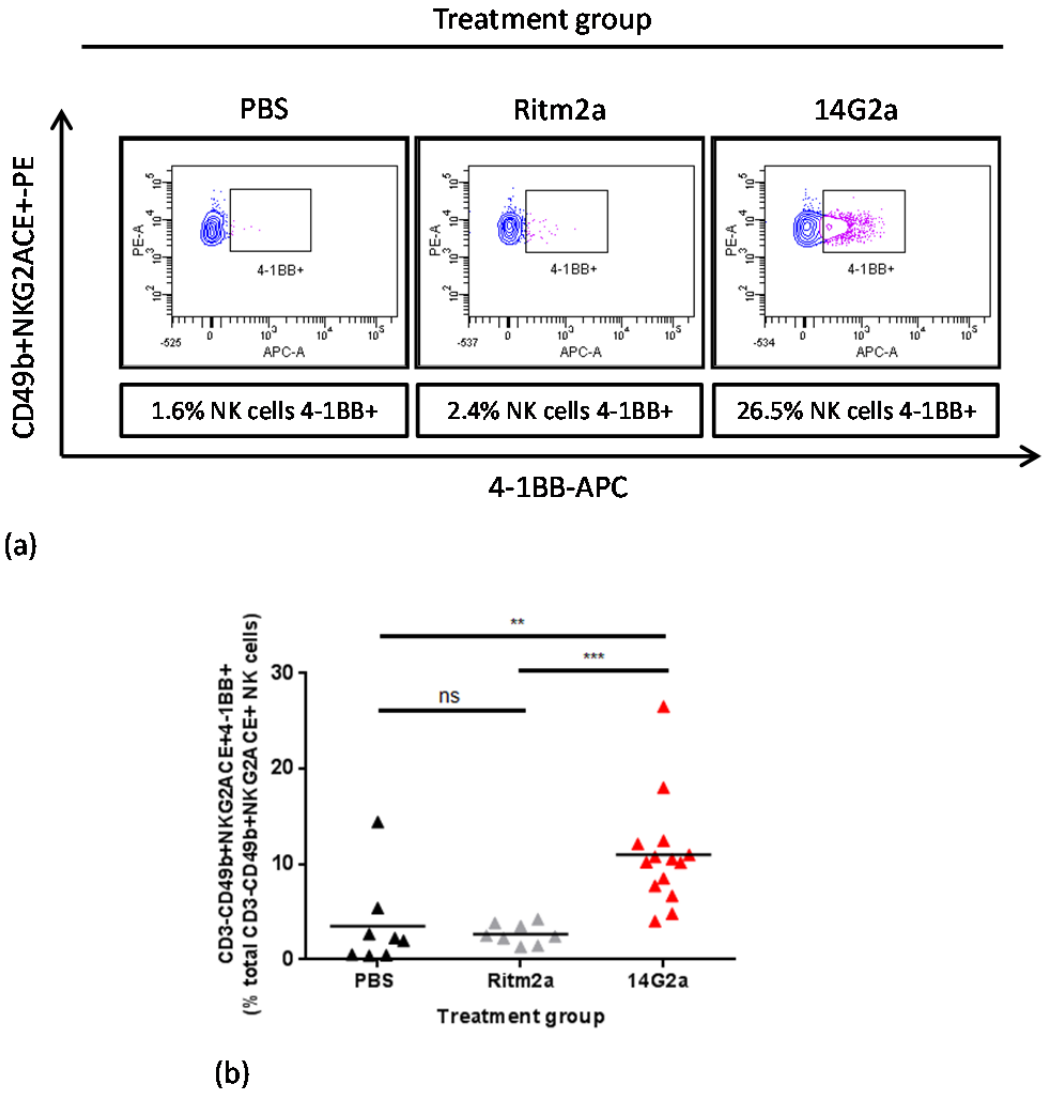

Figure 4-3. Surface 4-1BB expression on tumour-infiltrating NK cells 24-hours post-anti-GD2 mAb therapy. Tumour infiltrating CD3-CD49b+NKG2ACE+ NK cells obtained from A/J mice bearing subcutaneous NXS2 tumours were assessed by flow cytometry for surface expression of 4-1BB 24-hours post-treatment. Flow cytometry profiles showing 4-1BB expression on tumour infiltrating NK cells harvested from PBS, Ritm2a and 14G2a treated mice respectively (a). Mean 4-1BB+ NK cells as a percentage of the total CD3-CD49b+NKG2ACE+ NK cell population 24-hours post-treatment with either vehicle alone (PBS) (black triangles) n = 8, 150 µg irrelevant isotype control (Ritm2a) (grey triangles) n = 8, or 150 µg anti-GD2 (14G2a) (red triangles) n = 14, where ns = not significant ** p = 0.0052 and *** p = 0.0006.

The number of 4-1BB+ NK cells recovered from the tumour bearing mice 24-hours post-14G2a is significantly increased compared to mice receiving PBS or Ritm2a. However, there is some variation in terms of 4-1BB up regulation post-14G2a, with individual responses ranging from 4–26 % of the tumour-infiltrating NK cells recorded as being 4-1BB+. Whilst the data in figure 4.3 suggests this 4-1BB up regulation is anti-GD2 dependent, the data in figure 4.4 suggests that this process requires the presence of both the target antigen and the anti-G2a mAb, as surface 4-1BB expression on NK cells following

treatment with 14G2a is restricted to tumour-infiltrating NK cells with minimal expression observed on the peripheral NK cells in the spleen and blood.

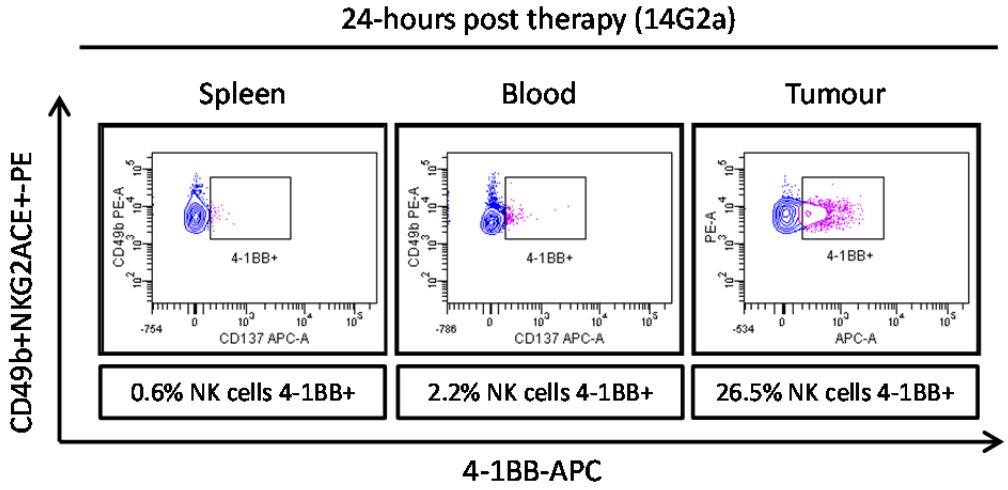

(a)

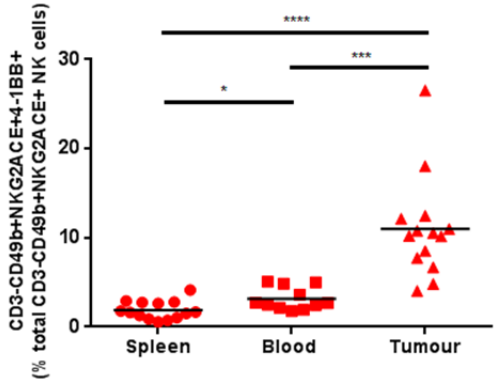

(b)

Figure 4-4. Surface 4-1BB expression of NK cells in the tumour, blood and spleen 24-hours post anti-GD2 mAb therapy. Tumour, blood and spleen samples were harvested from syngeneic A/J mice bearing subcutaneous NXS2 tumours 24-hours post-treatment with 150 µg anti-GD2 (14G2a). The cells were assessed by flow cytometry for surface expression of 4-1BB on CD3-CD49b+NKG2ACE+ NK cells. Flow cytometry profiles showing 4-1BB expression on NK cells harvested from the spleen, blood and tumour respectively (a). Mean 4-1BB+ NK cells as a percentage of the total CD3-CD49b+NKG2ACE+ NK cell population in the spleen (red circles), blood (red squares) and tumour (red triangles), where n = 14 and * p = 0.0104, *** p = 0.0002 and **** p = <0.0001.

4.2.1.3 The effect of dose and route of administration on 4-1BB up regulation 24-hours post anti-GD2 mAb therapy

Figures 4.3 and 4.4 show that surface 4-1BB expression can be specifically induced on tumour-infiltrating NK cells 24-hours post-treatment with 150 µg

of the anti-GD2 14G2a. However, when investigating the effect anti-GD2 plus anti-4-1BB mAb combination therapy has on tumour progression and survival the anti-GD2 mAb will be fractionated, *i.e.* administered as three separate 50 µg doses rather than a single 150 µg dose, to more closely resemble the therapeutic strategy applied in the clinic, and provide a more pro-longed exposure.to antibody.

Consequently it was necessary to confirm whether equivalent 4-1BB surface expression could be induced on tumour-infiltrating NK cells with this dosing regimen. The data in figure 4.5 (a) shows that the mean percentage of 4-1BB+ tumour-infiltrating NK cells observed post-treatment with anti-GD2 remains consistent within the dose range tested (50–150 µg). This suggests that the fractionated treatment schedule proposed for administration of anti-GD2 mAb is also likely to achieve an up regulation of 4-1BB expression by the tumour-infiltrating NK cells.

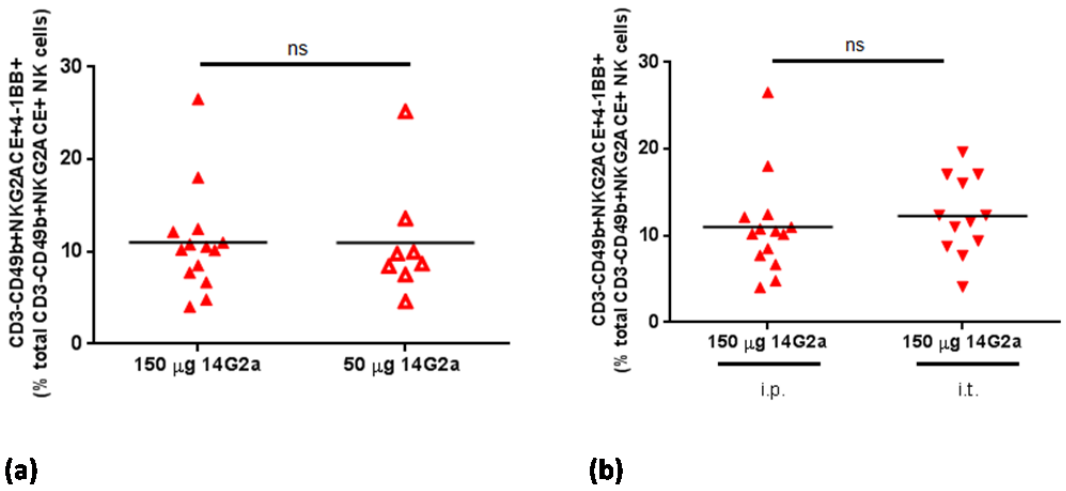

Figure 4-5. The percentage of 4-1BB+ tumour-infiltrating NK cells observed 24-hours post-anti-GD2 mAb following a reduction in dose or altered route of administration. A/J mice bearing subcutaneous NXS2 tumours were treated with either 150 μg or 50 μg 14G2a via the i.p. route. After 24-hours tumours were harvested and processed for flow cytometry assessment and tumour infiltrating CD3-CD49b+NKG2ACE+ NK cells were assessed for surface expression of 4-1BB. Mean 4-1BB+ NK cells as a percentage of the total CD3-CD49b+NKG2ACE+ NK cell population, where n = 14 (150 μg 14G2a) (red triangles) and n = 8 (50 μg 14G2a) (red open triangles) (a). Additional A/J mice bearing subcutaneous NXS2 tumours were treated with 150 μg 14G2a administered i.p. or i.t., 24-hours post-treatment tumours were harvested and processed for flow cytometry assessment and tumour infiltrating CD3-CD49b+NKG2ACE+ NK cells were assessed for surface expression of 4-1BB. Mean 4-1BB+ NK cells as a percentage of the total CD3-CD49b+NKG2ACE+ NK cell population, where n = 14 (150 μg 14G2a i.p.) (red triangles) and n = 12 (150 μg 14G2a i.t.) (red inverted triangles).

Additionally, it was hypothesized that direct administration of 14G2a into the tumour (i.t.) rather than systemically (i.p) may be a more effective means of achieving 4-1BB up regulation on tumour infiltrating NK cells. However, figure 4.5 (b) shows that direct administration of 14G2a into the tumour at this dose does not significantly alter the percentage of 4-1BB+ NK cells compared to systemic administration.

4.2.1.4 4-1BB surface expression by tumour infiltrating T cells 24-hours post antibody therapy

Induction of 4-1BB surface expression is normally considered a marker of T cell activation. Consequently, it was important to determine whether 4-1BB expression was induced on tumour-infiltrating T cells post antibody therapy. Figure 4.6 shows that tumour-infiltrating T cells are readily detected in the subcutaneous NXS2 tumours harvested from A/J mice.

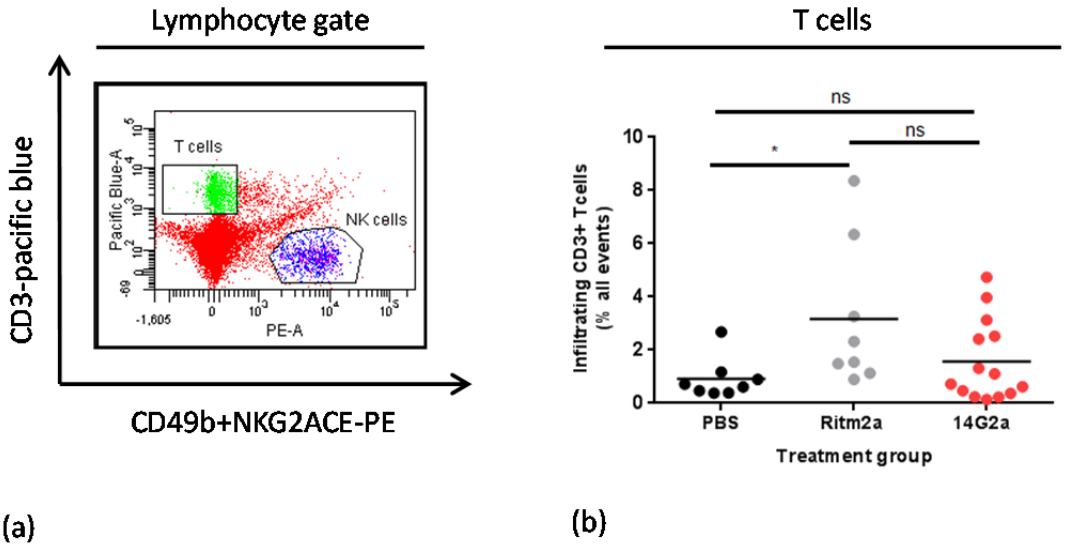

Figure 4-6. Tumour-infiltrating T cells can be identified and enumerated by flow cytometry. Tumour infiltrating T cells were identified and enumerated by passing the events in the lymphocyte gate through the pacific blue channel to identify CD3+ T cells (a). Infiltrating CD3+ T cells as a percentage of all events in mice treated with vehicle alone (PBS) (black circles), 150 µg irrelevant isotype control (Ritm2a) (grey circles), or 150 µg anti-GD2 (14G2a) (red circles) (b), where n = 8 for PBS and Ritm2a treated mice respectively and n = 14 for 14G2a treated mice, ns = not significant and * p = 0.0416.

Figure 4.6 (b) shows that the number of CD3+ T cells is not significantly higher in mice receiving anti-GD2 (14G2a) compared to vehicle alone (PBS). Surprisingly, there is a significant difference between the mice receiving the irrelevant isotype control (Ritm2a) compared to vehicle alone (PBS). This difference is likely to be due to the two mice that had particularly high CD3+ T cell counts (6 and 8 % of all events) skewing the mean for this treatment group. As shown in figure 4.2 (b) these two mice also had particularly high infiltrating NK cell counts (around 2 % of all events) compared to the rest of their cohort but this increase was not enough to make a significant difference.

In order to identify the CD4+ and CD8+ T cell subsets the CD3+ T cell population was passed through the APC-Cy7 channel to identify both the CD3+CD8+ events and the CD3+CD8- events, which were assumed to be CD4+. Representative flow cytometry profiles are shown in figure 4.7 (a). Whilst the overall CD3+ T cell population is not significantly increased post treatment with 14G2a, it is clear from the data in figure 4.7 (b) and (c) that the relative proportions of CD3+CD8- and CD8+ T cells as a percentage of the total CD3+ T cell population are altered in response to anti-GD2 therapy. Figure 4.7 (b) shows a modest but significant reduction in the mean CD3+CD8- population (the majority of which were assumed to be CD4+) for

mice treated with 14G2a compared to mice treated with PBS or Ritm2a. Conversely, figure 4.7 (c) shows a small but significant increase in the mean CD8+ T cell population for mice treated with 14G2a compared to PBS or Ritm2a treated mice.

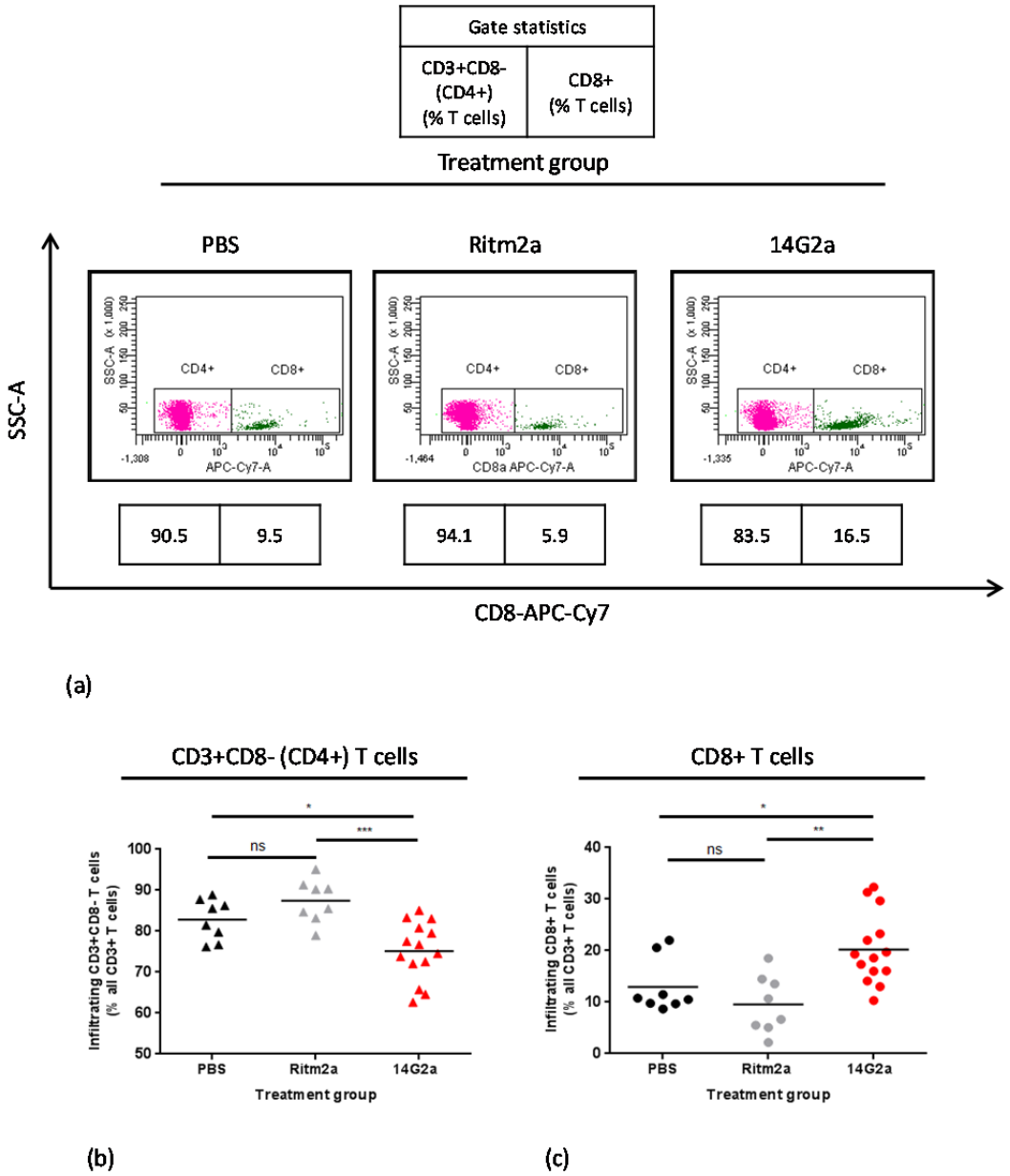

Figure 4-7. CD3+CD8- (CD4+) and CD8+ T cell subsets as a percentage of the total tumour-infiltrating T cell population 24-hours post mAb therapy. Tumour infiltrating CD3+T cells obtained from A/J mice bearing subcutaneous NXS2 tumours were assessed by flow cytometry for surface expression of CD8 24-hours post-therapy. Representative flow cytometry profiles showing both the CD3+CD8+ and CD3+CD8- (CD4+) T cell populations recovered from PBS, Ritm2a and 14G2a treated mice respectively (a). Gate labels and statistics are shown in separate tables for clarity. Mean CD3+CD8- T cells as a percentage of total CD3+ T cells harvested from mice treated with vehicle alone (PBS) (black triangles), 150 µg irrelevant isotype control (Ritm2a) (grey triangles), or 150 µg anti-GD2 (14G2a) (red triangles) (b), where n = 8 for PBS and Ritm2a treated mice and n = 14 for 14G2a treated mice, * p = 0.0145 and *** p = 0.0004. Mean CD8+ T cells as a percentage of total CD3+ T cells harvested from mice treated with vehicle alone (PBS) (black circles), 150 µg irrelevant isotype control (Ritm2a) (grey circles), or 150 µg anti-GD2 (14G2a) (red circles) (c), where n = 8 for PBS and Ritm2a treated mice and n = 14 for 14G2a treated mice, * p = 0.0171 and ** p = 0.0013.

The CD3+CD8- (CD4+) and CD8+ T cell populations were subsequently passed through the APC channel to look at surface 4-1BB expression. Figure

4.8 shows the CD3+CD8-(CD4+)4-1BB+ and CD8+4-1BB+ 24-hours post-therapy as a percentage of the total CD3+CD8- (CD4+) and CD8+ populations respectively.

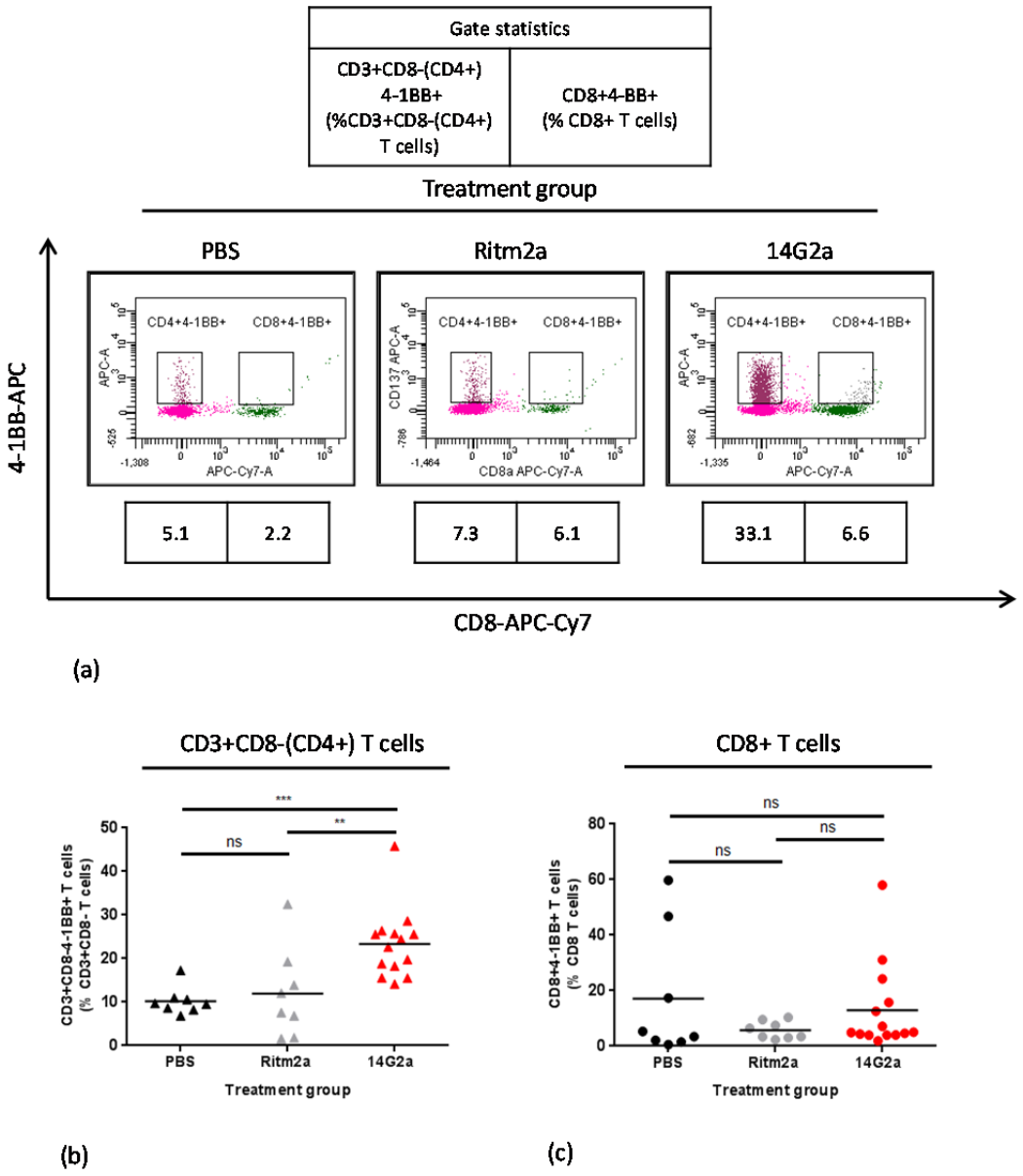

Figure 4-8. 4-1BB expression on the tumour-infiltrating CD3+CD8-(CD4+) and CD8+ T cell subsets 24-hours post mAb therapy. Tumour infiltrating CD3+CD8-(CD4+) and CD8+ T cells obtained from A/J mice bearing subcutaneous NXS2 tumours were assessed by flow cytometry for surface expression of 4-1BB 24-hours post-therapy. Flow cytometry profiles showing both CD3+CD8-(CD4+)4-1BB+ and CD8+4-1BB+ T cells harvested from PBS, Ritm2a and 14G2a treated mice respectively (a). Gate labels and statistics are shown in separate tables for clarity. Mean CD3+CD8-(CD4+)4-1BB+ T cells as a percentage of total CD3+CD8-(CD4+) T cells harvested from mice treated with vehicle alone (PBS) (black triangles), 150 µg irrelevant isotype control (Ritm2a) (grey triangles), or 150 µg anti-GD2 (14G2a) (red triangles) (b), where n = 8 for PBS and Ritm2a treated mice and n = 14 for 14G2a treated mice, ** p = 0.0086 and *** p = 0.0004. Mean CD8+4-1BB+ T cells as a percentage of total CD8+ T cells harvested from mice treated with vehicle alone (PBS) (black circles), 150 µg irrelevant isotype control (Ritm2a) (grey circles), or 150 µg anti-GD2 (14G2a) (red circles) (c), where n = 8 for PBS and Ritm2a treated mice and n = 14 for 14G2a treated mice.

Surface 4-1BB expression was significantly increased on tumour infiltrating CD3+CD8- T cells (the majority of which were assumed to be CD4+) 24-hours post-treatment with 14G2a. Figure 4.8 (b) shows on average 23 % of the total CD3+CD8- (CD4+) population was found to be 4-1BB+ post-treatment, compared to 10 and 12 % of the total CD4+ population following treatment with PBS or Ritm2a respectively. Figure 4.8 (c) shows 4-1BB expression on CD8+ tumour-infiltrating T cells is more variable and there was no significant difference in surface 4-1BB expression by CD8+ T cells between the treatment groups.

In keeping with the observations made in figure 4.4 in relation to 4-1BB expression and tumour-infiltrating NK cells, increased 4-1BB surface expression on T cells following treatment with 14G2a appears to be restricted to the tumour-infiltrating T cells, with surface 4-1BB expression on the T cells found in the spleen and blood remaining negligible. Figure 4.9 shows surface 4-1BB expression on CD3+CD8-(CD4+) and CD8+ T cells harvested from the tumour, blood and spleen of NXS2 tumour bearing A/J mice 24-hours post-treatment with 14G2a. Taken together the data in figure 4.8 (b) shows that 4-1BB expression is induced on tumour-infiltrating CD3+CD8- T cells (the majority of which were assumed to be CD4+) in response to treatment with 14G2a and figure 4.9 (b) confirms that 4-1BB expression is restricted to the tumour-infiltrating CD3+CD8-(CD4+) T cells within the first 24-hours post-treatment. Whilst figure 4.8 (c) showed there was no significant difference in 4-1BB expression by tumour-infiltrating CD8+ T cells between the treatment groups, figure 4.9 (c) shows 4-1BB expression by tumour infiltrating CD8+ T cells is significantly increased relative to the CD8+ T cells in the spleen and blood. However, based on the results shown in figure 4.8 (c) this is unlikely to be a consequence of antibody treatment. 4-1BB surface expression was also assessed on T cells recovered from the blood and spleens of mice receiving either PBS or Ritm2a and found to be negligible (data not shown).

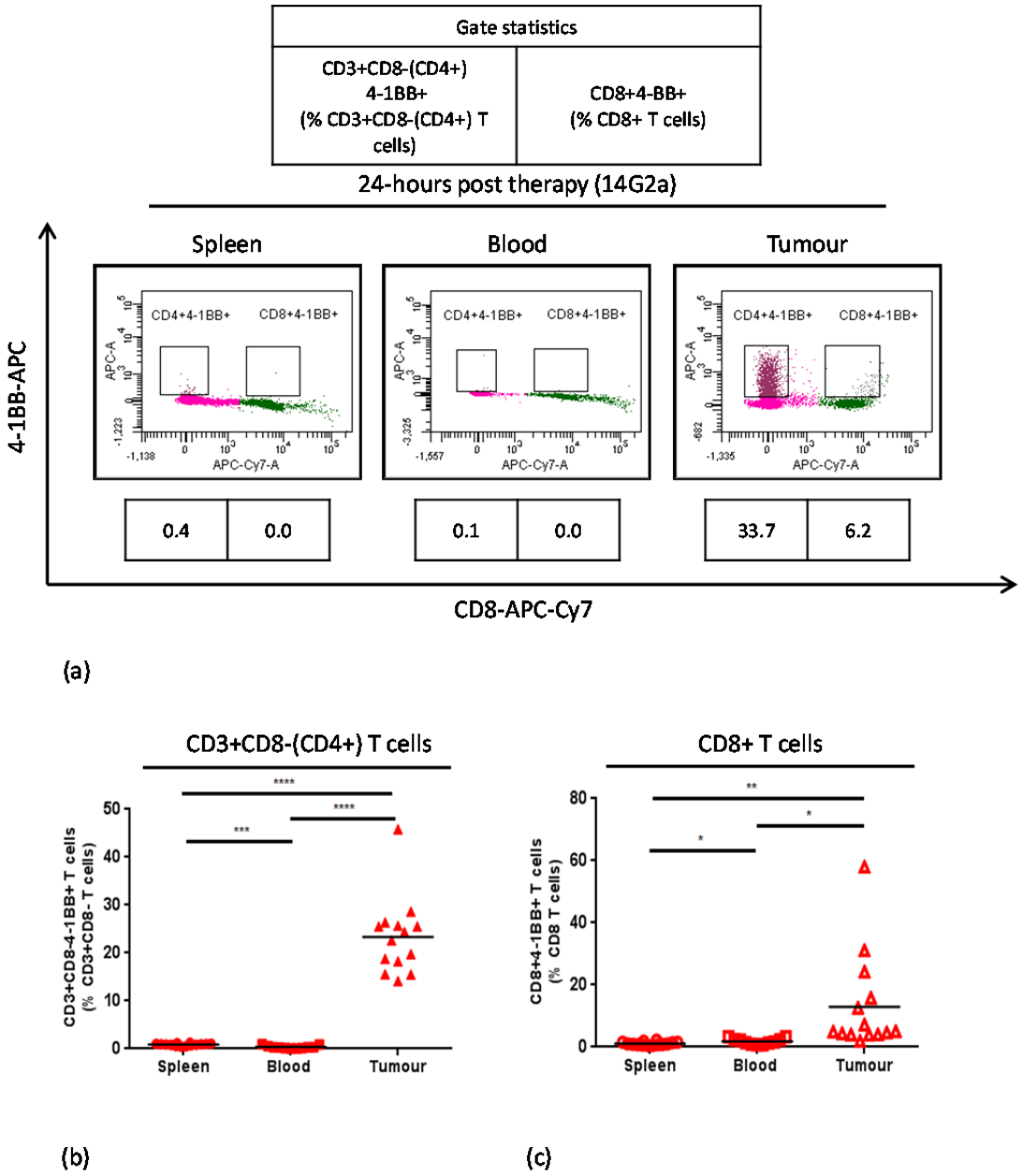

Figure 4-9. 4-1BB expression on CD3+CD8-(CD4+) and CD8+ T cell subsets in the tumour, blood and spleen 24-hours post-anti-GD2 mAb therapy. Tumour, blood and spleen samples were harvested from syngeneic A/J mice bearing subcutaneous NXS2 tumours 24-hours post-treatment with 150 µg anti-GD2 (14G2a). The cells were assessed by flow cytometry for surface expression of 4-1BB on CD3+CD8- (CD4+) and CD3+CD8+ T cells. Flow cytometry profiles showing 4-1BB expression on CD3+CD8-(CD4+) and CD8+ T cells harvested from the spleen, blood and tumour respectively (a). Mean CD3+CD8-(CD4+)4-1BB+ events as a percentage of the total CD3+CD8-(CD4+) T cell population in the spleen (red circles), blood (red squares) and tumour (red triangles), where n =14 and *** p = 0.0001 and **** p = <0.0001 (b). Mean CD8+4-1BB+ events as a percentage of the total CD8+ T cell population in the spleen (red open circles), blood (red open squares) and tumour (red open triangles), where n = 14 and * p = < 0.05 and ** p = 0.0086 (c).

4.2.1.5 Identifying tumour-infiltrating regulatory T cells among the tumour cell population

The data in figure 4.7 shows that regardless of treatment the CD3+CD8- T cell subset (the majority of which are assumed to be CD4+) account for the majority of all tumour-infiltrating CD3+ T cells, with mean CD3+CD8-(CD4+) T cell counts ranging from 75-87 % of the total T cell population (figure 4.6 b). A high proportion of tumour-infiltrating T cells has been attributed to both favourable and poor prognosis depending on the T cell subtype present. The immunosuppressive nature of Tregs has been linked to poor prognosis. Since the purpose of these experiments was to characterise the NK and T cell populations within the immune infiltrate of NXS2 tumour bearing mice, with or without treatment with anti-GD2, an additional flow cytomtery panel was included specifically to determine the proportion of CD4+ tumour infiltrating T cells that could be characterised as Tregs. Representative flow cytometry profiles illustrating the gating strategy used to identify tumour-infiltrating Tregs are shown in figure 4.10. The same strategy was also applied to identify Tregs in the blood and spleen of tumour bearing mice.

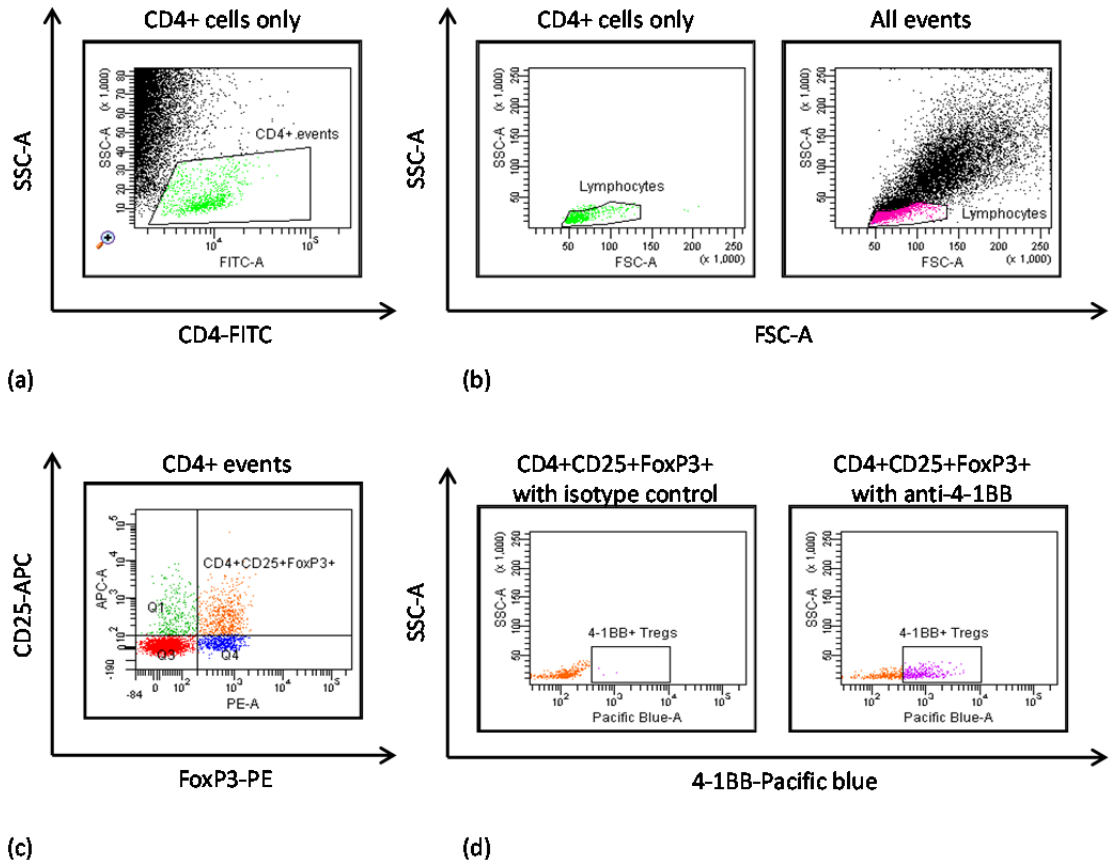

Figure 4-10. Example gating strategy used to identify tumour-infiltrating Tregs in subcutaneous NXS2 tumours harvested from syngeneic A/J mice. A representative flow cytometry profile illustrating CD4+ T cells (a). The CD4+ T cells were used to position the lymphocyte gate (b). The CD4+ events in the lymphocyte gate were passed through the APC and PE channels to identify the CD4+CD25+FoxP3+ Tregs (c). To position the 4-1BB gate two separate FACS tubes were prepared containing the anti-CD4-FITC, anti-CD25-APC, anti-FoxP3-PE mAb plus either a hamster IgG isotype control, or the anti-4-1BB-pacific blue (d).

The tumour-infiltrating Tregs as a percentage of the total CD4+ T cell population for each treatment group are shown in figure 4.11. There was no statistically significant difference in the number of tumour infiltrating Tregs as a percentage of the total CD4+ T cell population between the treatment groups, with mean values recorded as 23.18 %, 19.96 % and 19.27 % for mice treated with vehicle alone (PBS), irrelevant isotype control (Ritm2a) and anti-GD2 (14G2a) respectively.

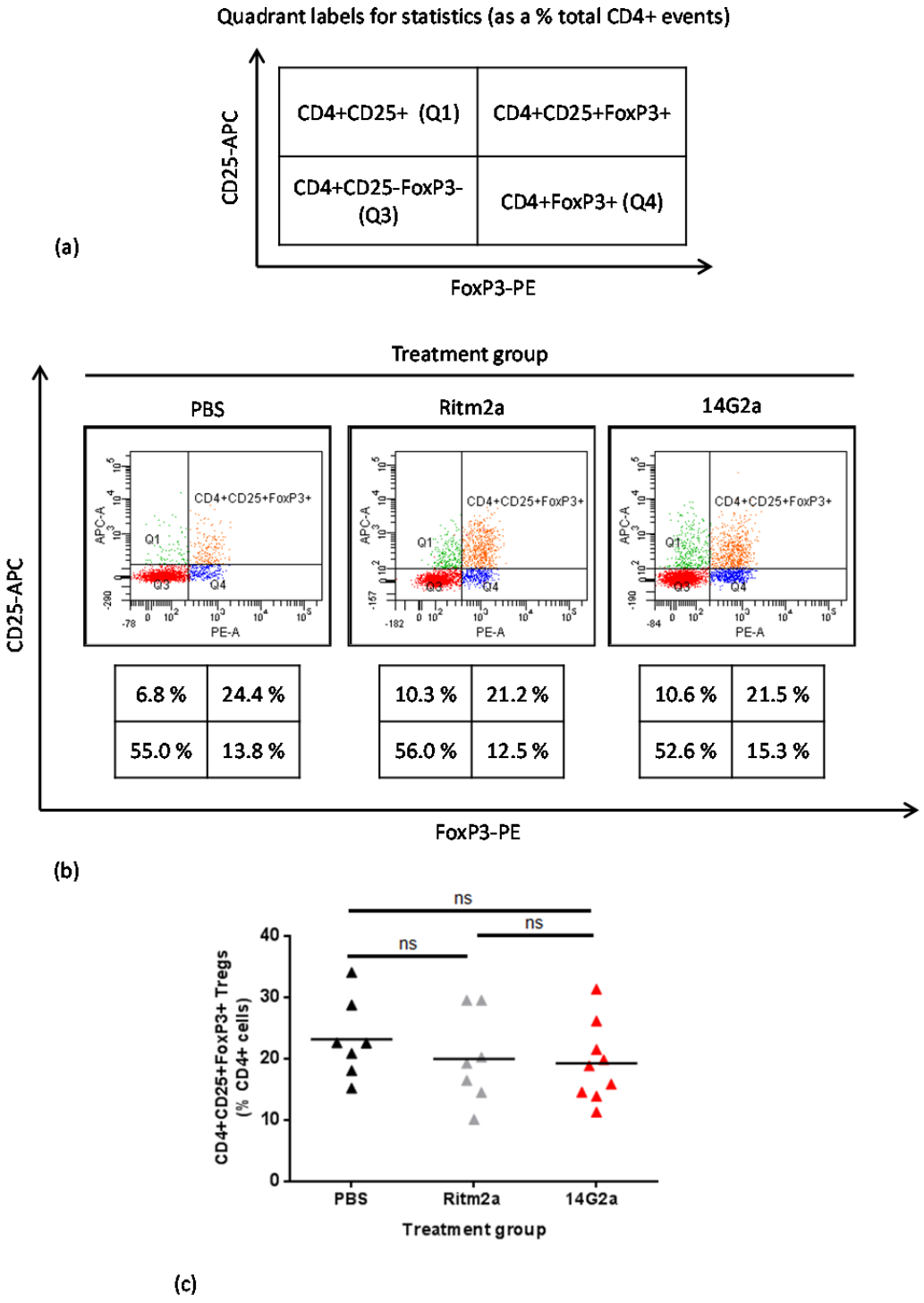

Figure 4-11. Tumour-infiltrating Tregs as identified and enumerated by flow cytometry. Tumour infiltrating Tregs were identified and enumerated by passing the CD4+ events in the lymphocyte gate through the APC and PE channels to identify CD4+CD25+FoxP3+ Tregs. A schematic illustrating the quadrant labels that apply to the individual quadrant statistics displayed beneath each flow cytometry profile for clarity (a). A representative flow cytometry profile for each treatment group showing infiltrating Tregs in tumour samples harvested 24-hours post-treatment (b). Mean tumour infiltrating Tregs classified as CD4+CD25+FoxP3+ as a percentage of the total CD4+ T cell population for mice treated with vehicle alone (PBS) (black triangles), 150 µg irrelevant isotype control (Ritm2a) (grey triangles) and 150 µg anti-GD2 (14G2a) (red triangles) (c), where n = 7 for PBS and Ritm2a treated mice respectively and n = 9 for 14G2a treated mice, ns = not significant.

4.2.1.6 4-1BB surface expression by tumour infiltrating T cells 24-hours post antibody therapy

Regulatory T cells reportedly constitutively express the co-stimulatory molecule 4-1BB on their surface, which could have implications when administering anti-4-1BB mAb therapy, therefore the tumour infiltrating Tregs were co-stained with anti-4-1BB. Figure 4.12 shows the level of 4-1BB surface expression.

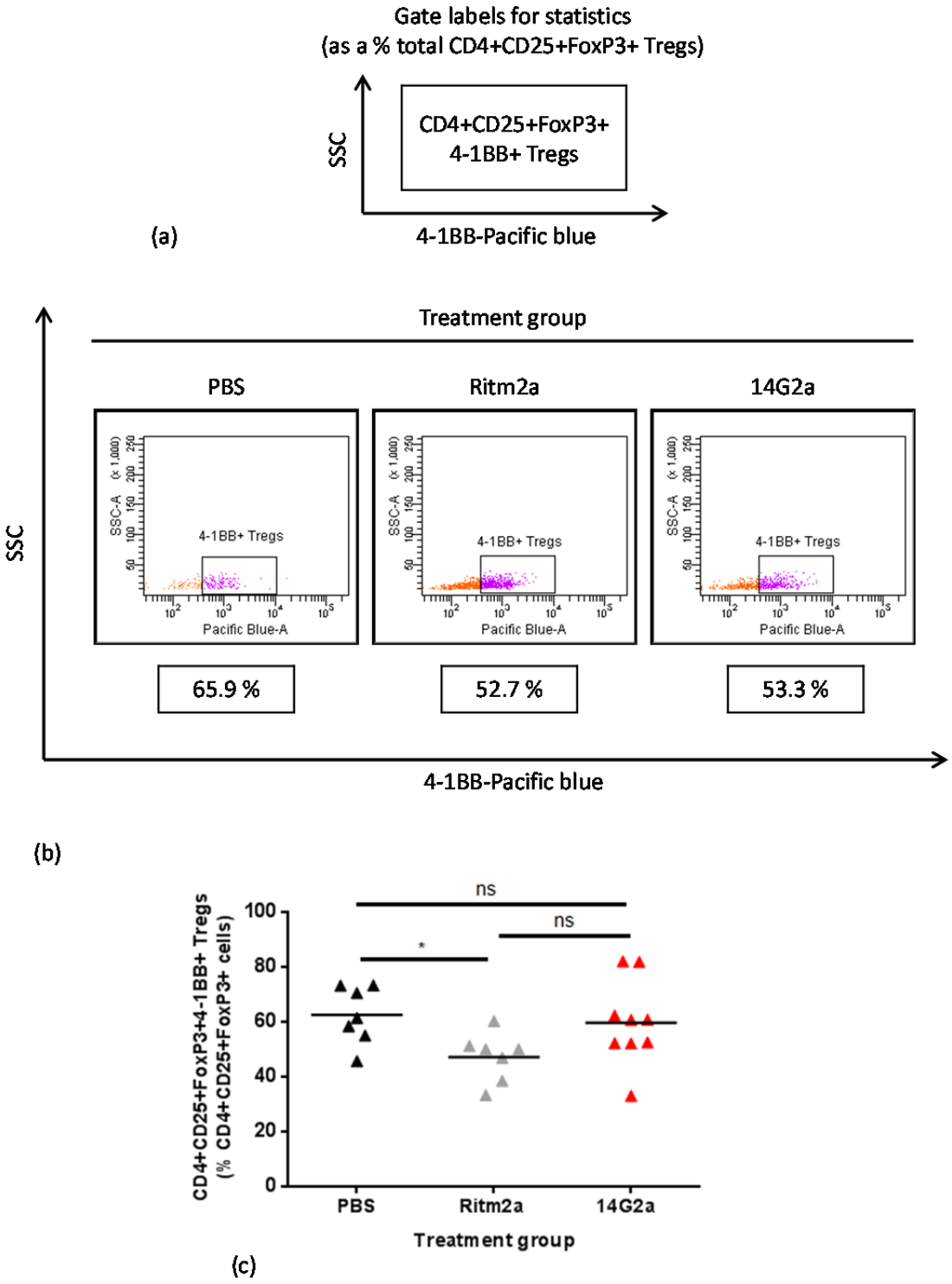

Figure 4-12. 4-1BB expression on tumour-infiltrating Tregs 24-hours post-mAb therapy. Tumour infiltrating Tregs obtained from A/J mice bearing subcutaneous NXS2 tumours were assessed by flow cytometry for surface expression of 4-1BB 24-hours post-therapy. A schematic illustrating the gate labels that apply to the individual gate statistics displayed beneath each flow cytometry profile for clarity (a). Flow cytometry profiles showing the 4-1BB+CD4+CD25+FoxP3+ Tregs harvested from PBS, Ritm2a and 14G2a treated mice respectively (b). Mean 4-1BB+CD4+CD25+FoxP3+ Tregs as a percentage of total CD4+CD25+FoxP3+ Tregs harvested from mice treated with vehicle alone (PBS) (black triangles), 150 µg irrelevant isotype control (Ritm2a) (grey triangles), or 150 µg anti-GD2 (14G2a) (red triangles) (b), where n = 7 for PBS and Ritm2a treated mice and n = 9 for 14G2a treated mice, ns = not significant and * p = 0.0118.

Figure 4.12 demonstrates that on average greater than 50% of the tumour-infiltrating Tregs are positive for 4-1BB surface expression. However, there is no significant difference in the mean percentage of 4-1BB+CD4+CD25+FoxP3+ Tregs following treatment with 14G2a compared to treatment with PBS or Ritm2a.

Whilst there was no difference in the number of tumour-infiltrating Tregs recovered from mice receiving PBS, Ritm2a, or 14G2a, figure 4.13 shows that Tregs are more abundant in the tumours harvested from these mice than the blood or spleen. Additionally, figure 4.14 shows that a disproportionally high percentage of tumour-infiltrating Tregs express surface 4-1BB compared to Tregs in the blood and spleen. This was observed for all mice regardless of treatment group and not restricted to mice that had been treated with anti-GD2 mAb, suggesting that 4-1BB is endogenously expressed on the surface of tumour-infiltrating Tregs, rather than induced in response to antibody therapy.

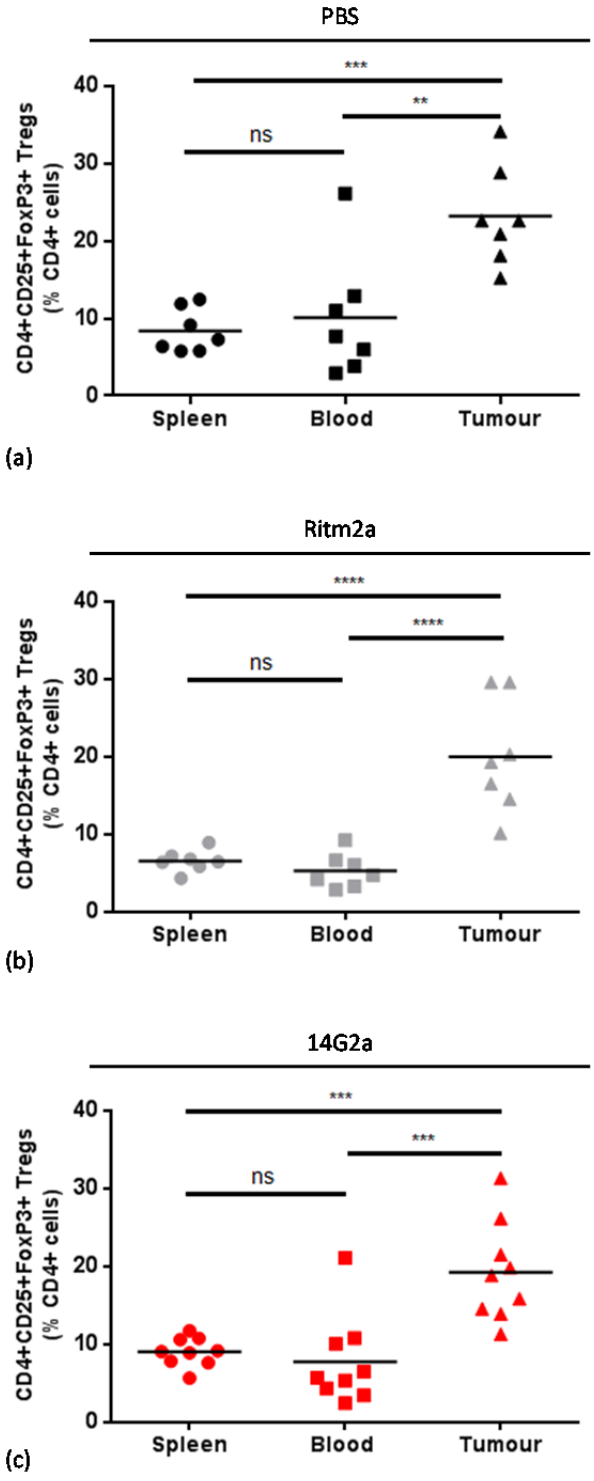

Figure 4-13. Tregs as a proportion of the CD4+ T cell population recovered from the tumour, blood and spleen of tumour bearing mice 24-hours post mAb therapy. Tregs as a percentage of the total CD4+ T cell population in the spleen (black circles), blood (black squares) and tumour (black triangles) of mice treated with vehicle alone (PBS) (a), where n = 7, ns = not significant, ** p = 0.0053 and *** p = 0.0001; or the spleen (grey circles), blood (grey squares) and tumour (grey triangles) of mice treated with irrelevant isotype control mAb (Ritm2a) (b), where n = 7, ns = not significant, *** p = 0.0005 (tumour vs spleen) and *** p = 0.0003 (tumour vs blood); or the spleen (red circles), blood (red squares) and tumour (red triangles) of mice treated with 150 µg anti-GD2 mAb (14G2a) (c), where n = 9, ns = not significant, *** p = 0.0003 (tumour vs spleen) and *** p = 0.0010 (tumour vs blood).

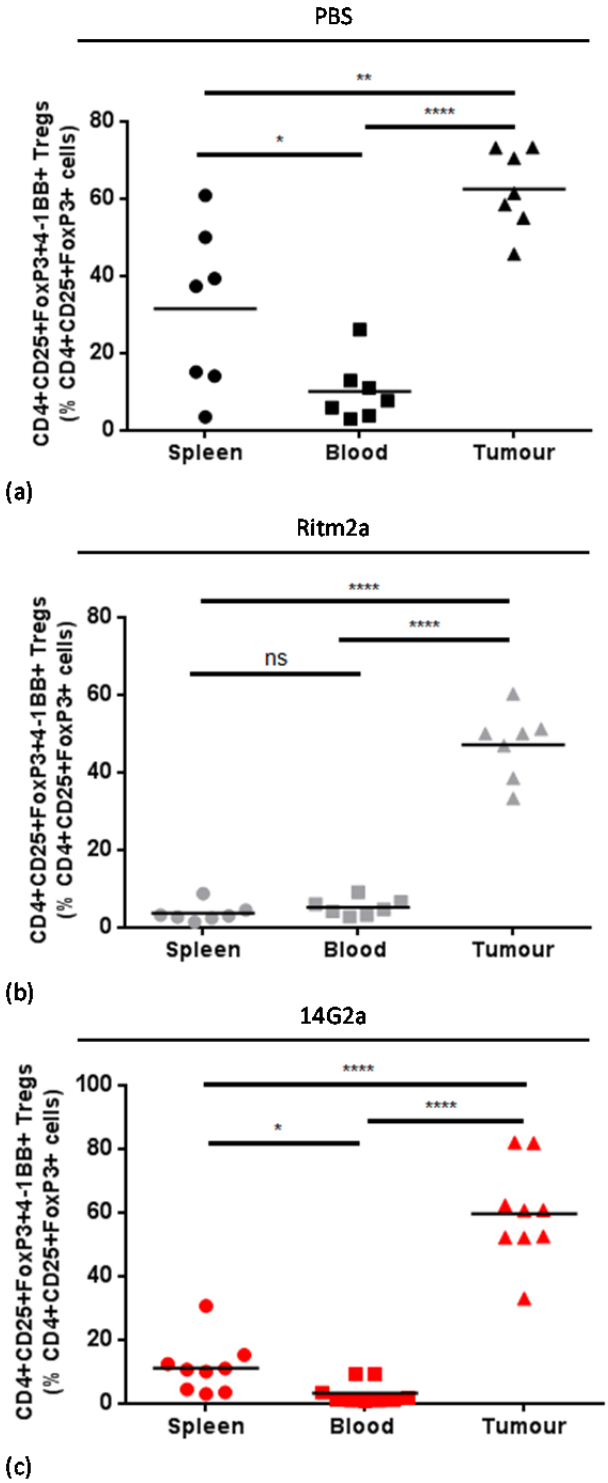

Figure 4-14. 4-1BB+ Tregs recovered from the tumour, blood and spleen of tumour bearing mice 24-hours post mAb therapy. Tregs obtained from the tumour, blood and spleen samples were assessed for surface expression of 4-1BB. The mean percentage of 4-1BB+ Tregs in the spleen (black circles), blood (black squares) and tumour (black triangles) of mice treated with vehicle alone (PBS) (a), where n = 7, * p = 0.0270, ** p = 0.0044 and **** p = <0.0001; or the spleen (grey circles), blood (grey squares) and tumour (grey triangles) of mice treated with 150 µg irrelevant isotype control mAb (Ritm2a) (b), where n = 7, ns = not significant and **** p = <0.0001; or the spleen (red circles), blood (red squares) and tumour (red triangles) of mice treated with 150 µg anti-GD2 mAb (14G2a) (c), where where n = 9, ns = not significant, * p = 0.0182 and **** = p < 0.0001.

To summarise the results presented in figures 4.3 through to 4.14 surface expression of the co-stimulatory molecule 4-1BB can be detected on tumour-infiltrating NK cells 24-hours post anti-GD2 mAb therapy; however, peripheral blood and splenic NK cells harvested from the same tumour bearing mice do not express surface 4-1BB. Additionally, 4-1BB expression levels remain negligible on tumour-infiltrating and peripheral NK cells harvested from mice treated with vehicle alone, or an irrelevant isotype matched control mAb, suggesting that both the target antigen and the anti-GD2 mAb are required in order to induce 4-1BB expression. 4-1BB surface expression was also significantly increased on tumour-infiltrating CD4+ T cells 24-hours post anti-GD2 mAb therapy compared to mice receiving vehicle alone, or irrelevant isotype control mAb. 4-1BB surface expression on tumour-infiltrating CD8+ T cells was comparable between the treatment groups 24-hours post antibody therapy; however, 4-1BB expression on tumour-infiltrating CD8+ T cells was significantly increased relative to peripheral CD8+ T cells and may suggest some endogenous CD8+ T cell activity in the tumour microenvironment. This was also observed for tumour-infiltrating Tregs. More than 50 % of tumour-infiltrating Tregs were observed to express surface 4-1BB, regardless of therapy, a significant increase compared to Tregs recovered from the blood and spleens of these mice.

4.2.2 Exploring the efficacy of anti-GD2 plus anti-4-1BB mAb combination therapy *in vivo* using the syngeneic NXS2 model of neuroblastoma

To explore the efficacy of anti-GD2 plus anti-4-1BB mAb combination therapy *in vivo* using the syngeneic NXS2 model of neuroblastoma it was first necessary to optimise the therapeutic strategy for this model. In all of the *in vivo* experiments performed the anti-GD2 mAb is administered as fractionated doses, rather than a single injection, in order to provide sustained levels of antibody over a longer period of time, thus recapitulating the current therapeutic approach applied in the clinic. The data in figure 4.3 showed that 4-1BB surface expression could be detected on tumour-infiltrating NK cells 24-hours post-administration of anti-GD2 mAb, hence it was decided to administer anti-4-1BB mAb 24-hours after the first dose of anti-GD2, followed by a further two doses of anti-GD2 mAb at 24-hour intervals. The data in figure 4.4 showed that 4-1BB expression was restricted to tumour-infiltrating

NK cells, suggesting the process was dependent on both the presence of the tumour and the anti-GD2 mAb. This observation led to the hypothesis that delaying therapy until the tumour established may be beneficial as there is a greater potential for antigen: antibody: NK cell interaction. However, the rapid growth kinetics for NXS2 *in vivo* means mice are often terminal by day 21, which leaves a fairly narrow therapeutic window. Consequently, the decision was made to test the effectiveness of early versus late therapy in an initial pilot experiment.

4.2.2.1 'Early' versus 'late' therapy

Mice were inoculated with $2x10^6$ NXS2 tumour cells subcutaneously on day 0 and assigned to one of four treatment groups, namely vehicle alone (PBS), anti-GD2 (14G2a) alone, anti-4-1BB (LOB12.3) alone, or anti-GD2+anti-4-1BB (14G2a+LOB12.3). Therapy began either three or eight days post tumour inoculation depending on whether mice had been assigned to the early or late therapy arm. Regular measurements were taken to monitor tumour progression and mice were considered to have reached end point when the mean diameter of the tumour measured 225 mm^2 (see materials and methods section 2.8.2 for further details). The results of this experiment are summarised in figures 4.15 and 4.16.

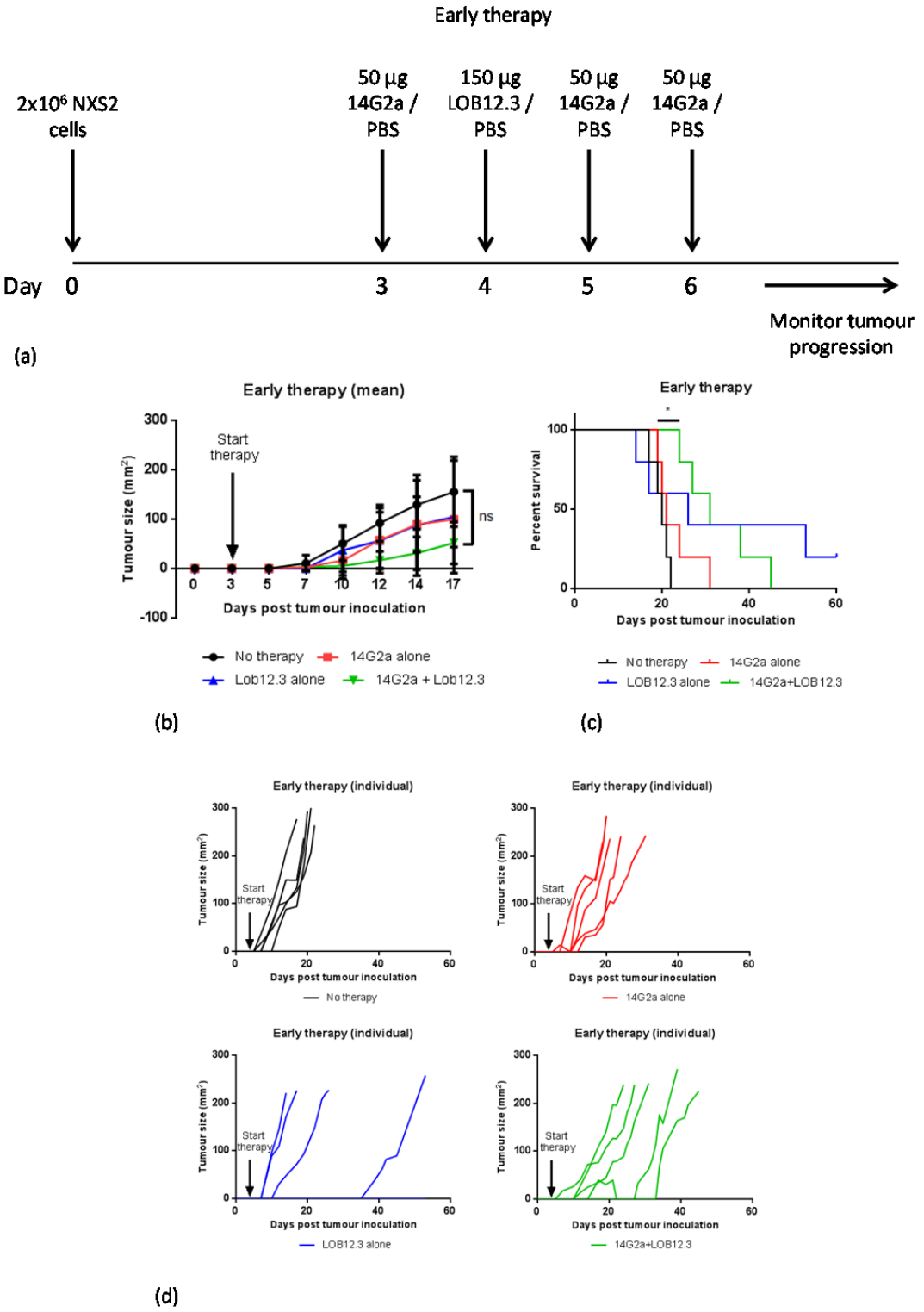

Figure 4-15. Optimising the therapeutic strategy for testing anti-GD2 plus anti-4-1BB mAb therapy in the syngeneic NXS2 neuroblastoma model: 'early' therapy. A/J mice were inoculated with $2x10^6$ NXS2 neuroblastoma cells subcutaneously on the lower back and received therapy (i.p.) according to the schematic schedule shown in (a). Mice (5 per group) were monitored for tumour growth and survival. Mean ± S.D. tumour size (b) and survival (c) for mice receiving vehicle alone (PBS) (black line), anti-GD2 (14G2a) alone (red line), anti-4-1BB (LOB12.3) alone (blue line), or anti-GD2 plus anti-4-1BB (14G2a+LOB12.3) (green line), where ns = not significant and * p = 0.0383. Individual tumour growth curves for all mice across all four treatment groups (d).

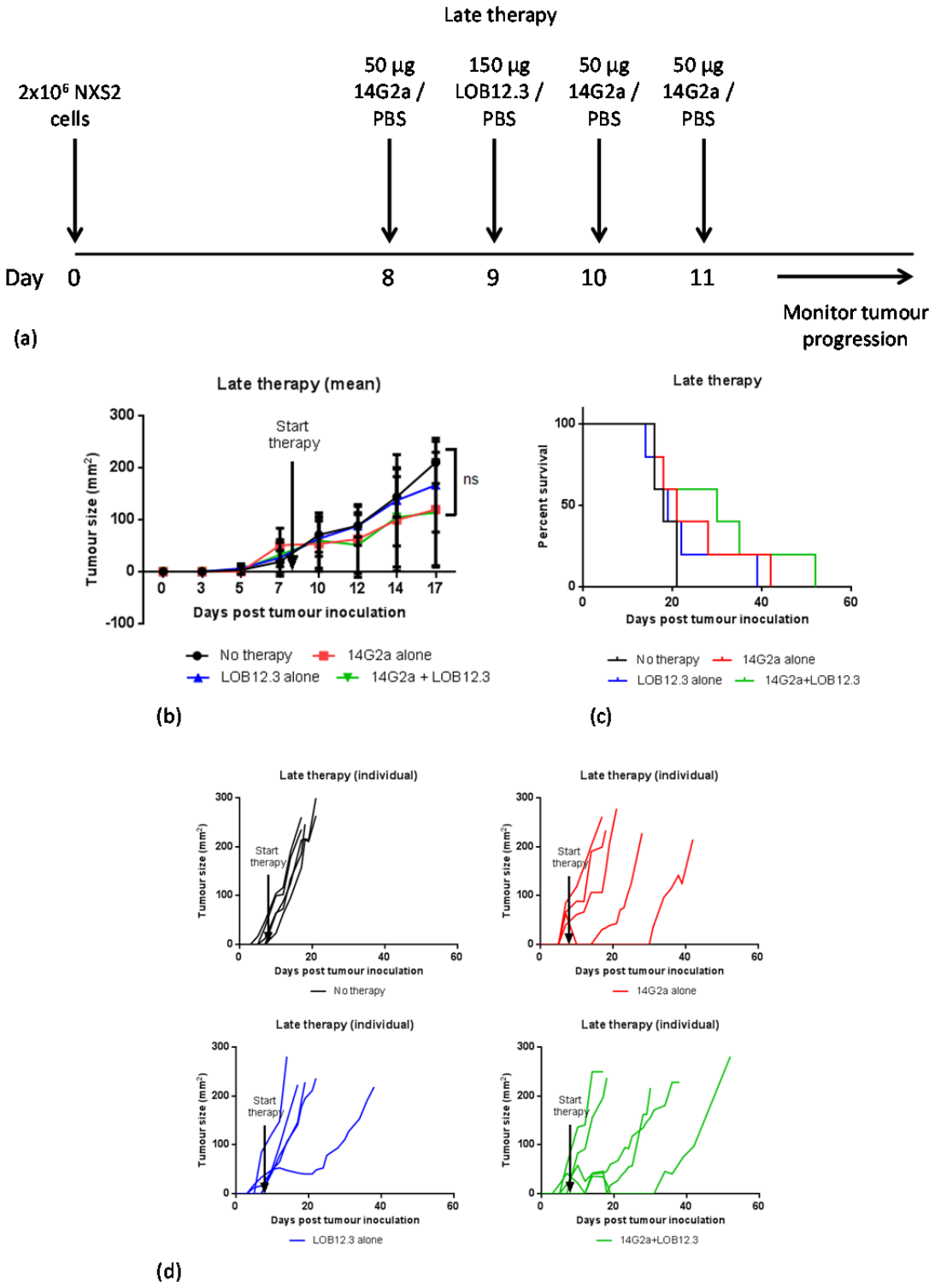

Figure 4-16. Optimising the therapeutic strategy for testing anti-GD2 plus anti-4-1BB mAb therapy in the syngeneic NXS2 neuroblastoma model: 'late' therapy. A/J mice were inoculated with 2x10⁶ NXS2 neuroblastoma cells subcutaneously on the lower back and received therapy (i.p.) according to the schematic schedule shown in (a). Mice (5 per group) were monitored for tumour growth and survival. Mean ± S.D. tumour size (b) and survival (c) for mice receiving vehicle alone (PBS) (black line), anti-GD2 (14G2a) alone (red line), anti-4-1BB (LOB12.3) alone (blue line), or anti-GD2 plus anti-4-1BB (14G2a+LOB12.3) (green line), where ns = not significant. Individual tumour growth curves for all mice across all four treatment groups (d).

Figure 4.15 summarises the results from the early (3 days post-tumour inoculation) treatment regimen. Figure 4.15 (b) shows that there was no significant difference in mean tumour progression between the four treatment groups up until the first mouse reached end point (day 17). However, mean tumour progression for mice receiving the 14G2a+LOB12.3 combination therapy does appear to be the slowest with this treatment group surviving significantly longer than mice receiving 14G2a alone, as shown in figure 4.15 (c). There were concerns regarding the variation in tumour growth kinetics in the early treatment regimen. As shown in figure 4.15 (d) one of the LOB12.3 treated mice (blue lines) failed to develop measurable tumour until day 39 post-inoculation and another mouse in this treatment group failed to develop measurable tumour at all. Whilst this response could be due to the effect of the LOB12.3 therapy, especially as all the mice receiving vehicle alone developed tumour in a uniform manner, it is difficult to make a valid comparison between treatment groups when there are differences in tumour burden at the start of therapy. Delaying therapy until a later time point (8 days post inoculation) did not completely resolve this issue as there were still differences in tumour burden at the start of therapy. The individual growth curves for mice across all four treatment groups, shown in figure 4.16 d) clearly illustrates that several mice did not have measurable tumour at this time point. Overall the results obtained from the late therapy arm of this experiment were similar to the early arm. Figure 4.16 (b) shows that there was no significant difference in mean tumour progression between the four treatment groups up until the first mouse reached end point (day 17) and figure 4.16 (c) shows that the mice receiving 14G2a+LOB12.3 generally survived longer, although the difference was not significant.

Based on the results of this pilot experiment the decision was made to start treatment when the tumours had reached a certain size rather than on a certain day. This strategy would control for the variation in tumour growth kinetics and ensure that all mice had an equivalent tumour burden when starting therapy. A/J mice were inoculated with $2x10^6$ NXS2 cells and tumours were allowed to progress to 50–70 mm^2 before the mice were allocated to a treatment group. The treatment regimen was also amended to include a further 150 µg anti-4-1BB (LOB12.3) to be administered 96-hours post starting therapy to give a longer exposure. The results of this experiment are shown in figure 4.17.

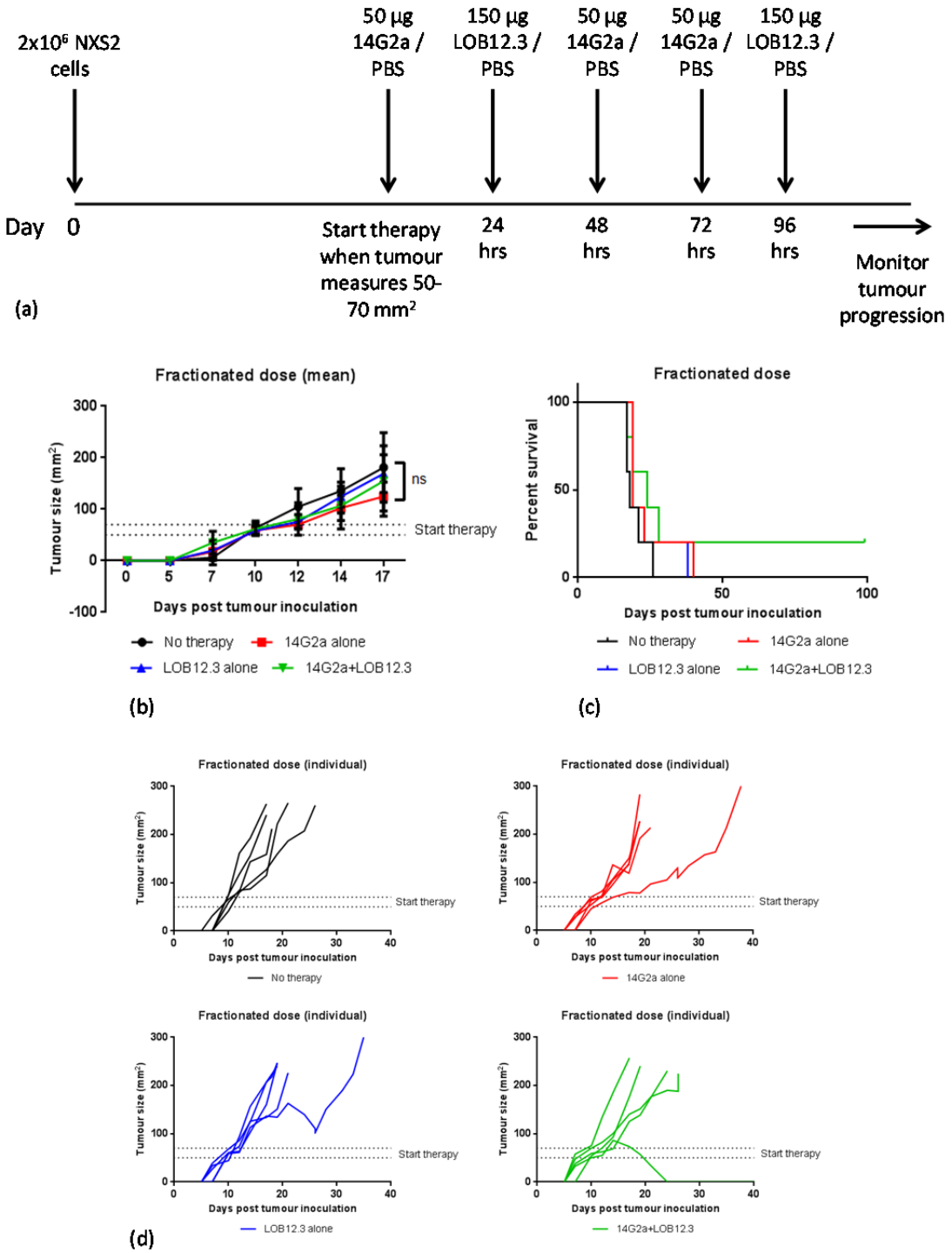

Figure 4-17. Optimising the therapeutic strategy for testing anti-GD2 plus anti-4-1BB mAb therapy in the syngeneic NXS2 neuroblastoma model: 'fractionated' therapy, start date based on tumour burden. A/J mice were inoculated with $2x10^6$ NXS2 neuroblastoma cells subcutaneously on the lower back and received therapy (i.p.) according to the schematic schedule shown in (a). Mice (5 per group) were monitored for tumour growth and survival. Mean ± S.D. tumour size (b) and survival (c) for mice receiving vehicle alone (PBS) (black line), anti-GD2 (14G2a) alone (red line), anti-4-1BB (LOB12.3) alone (blue line), or anti-GD2 plus anti-4-1BB (14G2a+LOB12.3) (green line), where ns = not significant. Individual tumour growth curves for all mice across all four treatment groups (d).

The results in figure 4.17 (b) show that there was no significant difference in mean tumour progression up until the first mouse reached end point (day 17), nor was there a significant difference in survival (figure 4.17 c). However, the individual tumour growth curves is figure 4.17 (d) show that one of the mice receiving 14G2a+LOB12.3 (green lines) rejected tumour and survived tumour free until the end of the experiment.

4.2.2.2 Whole dose versus fractionated therapy

The rationale for giving the therapy in a fractionated regimen was to provide sustained levels of antibody over a longer period of time, thus recapitulating the current therapeutic approach applied in the clinic. However, an additional experiment was set up to test the effectiveness of the combination therapy when administered as a whole dose (*i.e.* 150 µg anti-GD2 followed by 300 µg anti-4-1BB 24-hours later). The results of this experiment are shown in figure 4.18.

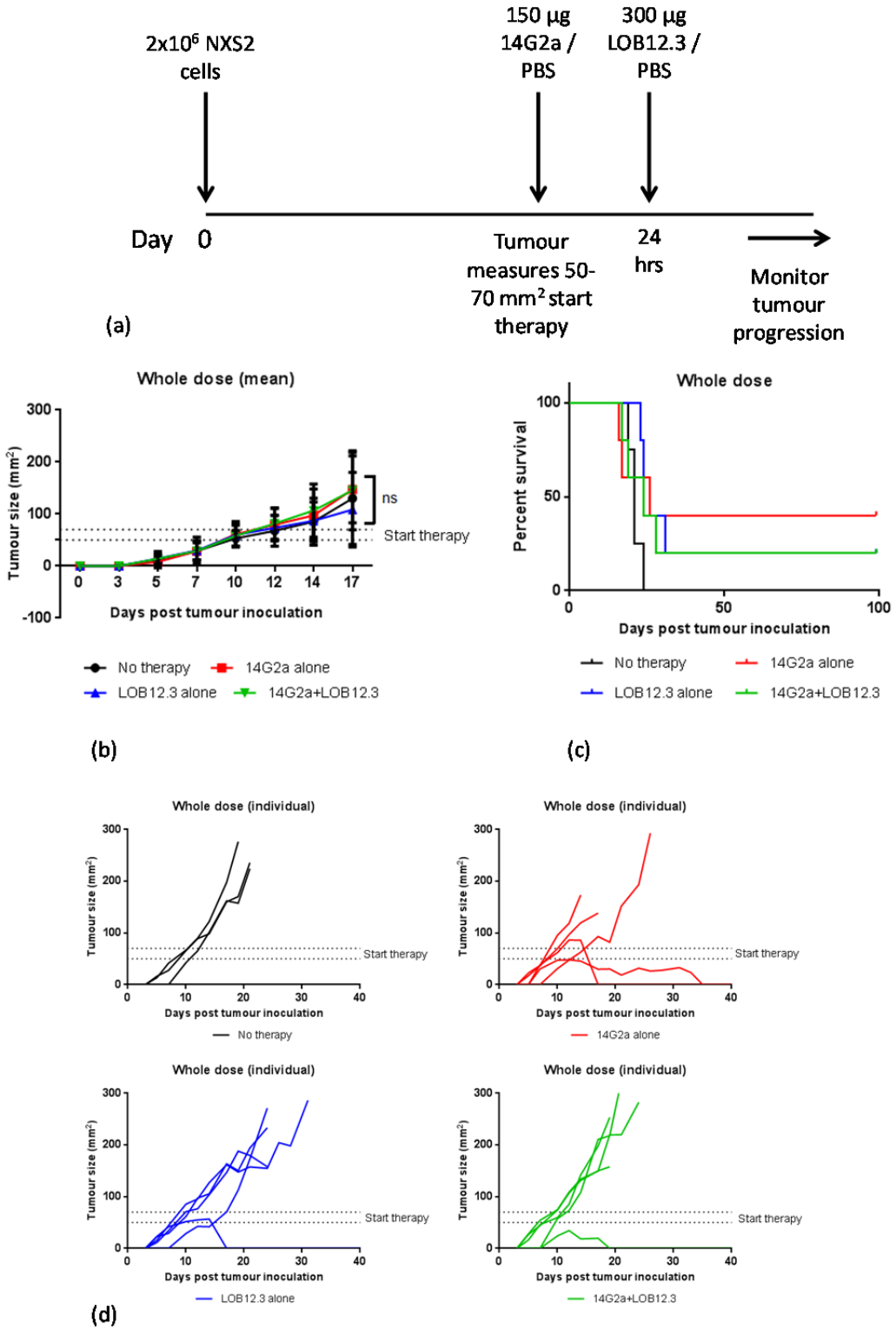

Figure 4-18. Optimising the therapeutic strategy for testing anti-GD2 plus anti-4-1BB mAb therapy in the syngeneic NXS2 neuroblastoma model: 'whole dose' therapy, start date based on tumour burden. A/J mice were inoculated with $2x10^6$ NXS2 neuroblastoma cells subcutaneously on the lower back and received therapy (i.p.) according to the schematic schedule shown in (a). Mice (5 per group) were monitored for tumour growth and survival. Mean ± S.D. tumour size (b) and survival (c) for mice receiving vehicle alone (PBS) (black line), anti-GD2 (14G2a) alone (red line), anti-4-1BB (LOB12.3) alone (blue line), or anti-GD2 plus anti-4-1BB (14G2a+LOB12.3) (green line), where ns = not significant. Individual tumour growth curves for all mice across all four treatment groups (d).

Administering 14G2a+LOB12.3 mAb as a whole dose rather than fractionated over several days made no difference to the mean tumour progression up until the first end point was reached (day 17) or overall survival, as shown in figures 4.18 (b) and (c) respectively. However, figure 4.18 (d) shows that at least one mouse in each of the treatment groups rejected tumour and survived long term.

4.2.2.3 Investigating the effect of anti-GD2+anti-4-1BB mAb using the optimised treatment strategy

Taken together the results in figure 4.15–4.18 suggest that the most effective therapeutic strategy for testing anti-GD2 plus anti-4-1BB mAb in the NXS2 model was the revised fractionated therapy regimen that commenced when tumour burden reached 50–70 mm^2 as per figure 4.17. A direct repeat of this experiment was set up and the combined results (*i.e.* 10 mice per group from two independent experiments) are shown in figure 4.19.

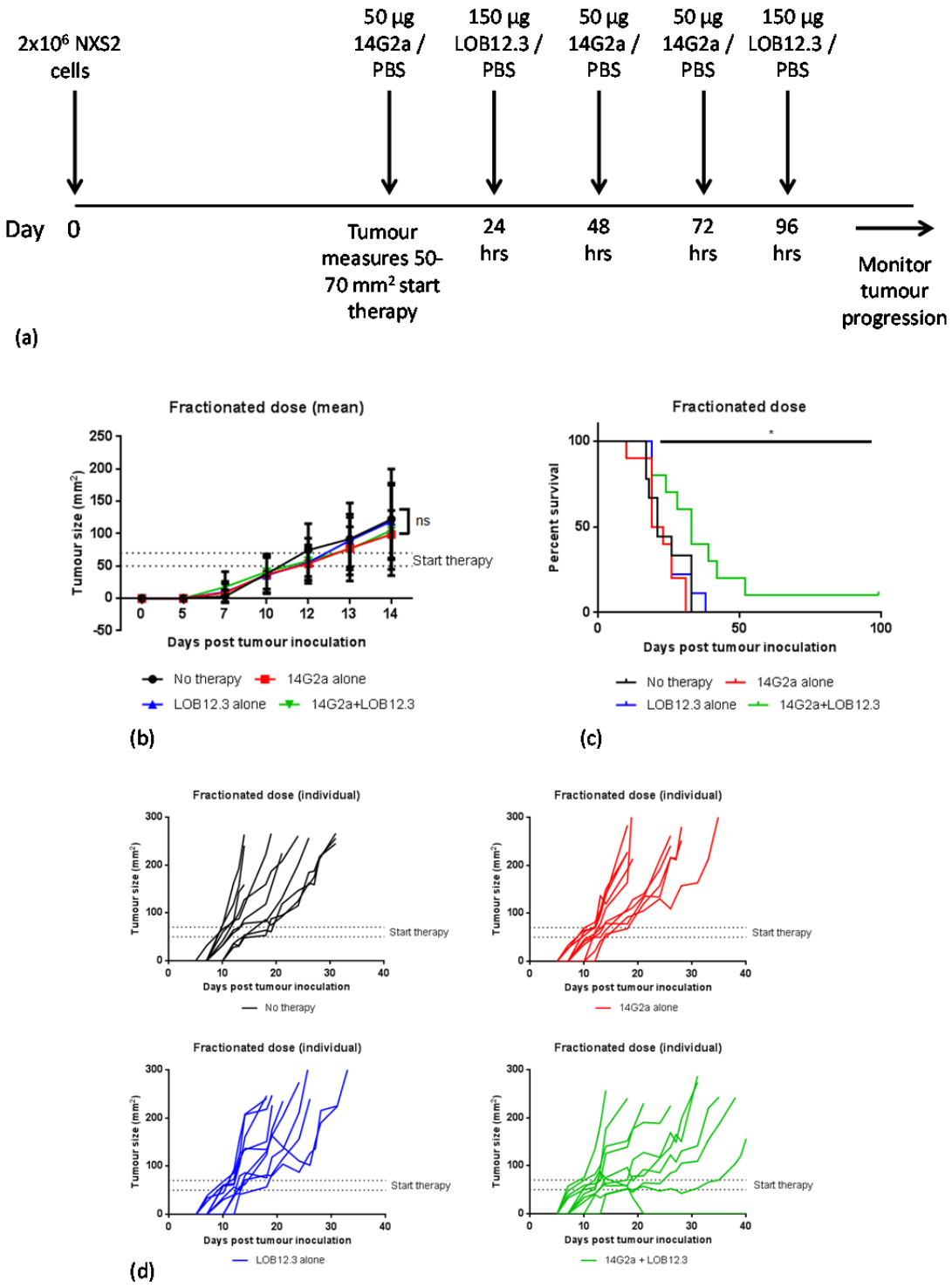

Figure 4-19. Combined data for the optimised fractionated therapeutic strategy (start date based on tumour burden) for testing murine anti-GD2 plus anti-4-1BB *in vivo* using the syngeneic NXS2 neuroblastoma model. A/J mice were inoculated with 2 x 10^6 NXS2 neuroblastoma cells subcutaneously on the lower back and received therapy (i.p.) according to the schematic schedule shown in (a). Mice (10 per group from two independent experiments) were monitored for tumour growth and survival. Mean ± S.D. tumour size (b) and survival (c) for mice receiving vehicle alone (PBS) (black line), anti-GD2 (14G2a) alone (red line), anti-4-1BB (LOB12.3) alone (blue line), or anti-GD2 plus anti-4-1BB (14G2a+LOB12.3) (green line), where ns = not significant and * p = 0.0290. Individual tumour growth curves for all mice across all four treatment groups (d).

The combined results shown in figure 4.19 (b) suggest that there is still no difference in mean tumour progression up until the first end point is reached (day 14). However, figure 4.19 (c) shows that the mice receiving 14G2a+LOB12.3 (green line) have a modest but significant survival advantage over the mice receiving PBS (black line), 14G2a alone (red line), or LOB12.3 alone (blue line). The individual tumour growth curves for the four treatment groups' in figure 4.19 (d) suggest that the 14G2a+LOB12.3 combination therapy (green lines) slows, rather than controls, tumour progression. However, one of the ten mice in this treatment group completely rejected the tumour and remained relapse free for the duration of the experiment.

In summary having optimised the best possible anti-GD2 plus anti-4-1BB mAb treatment strategy to ensure comparable tumour burden between the treatment groups' at the start of therapy, the results obtained suggest that anti-GD2 plus anti-4-1BB combination therapy is more efficacious than either antibody alone. Mice receiving anti-GD2 plus anti-4-1BB demonstrate slower tumour progression, which translates into a modest survival advantage. Anti-GD2 plus anti-4-1BB mAb therapy does not confer the same potent anti-tumour activity that Kohrt *et al.* reported when testing anti-CD20 plus anti-4-1BB mAb therapy in the syngeneic BL3750 lymphoma model (237). However, this is likely to be reflective of the rapid tumour growth kinetics and narrow therapeutic window for therapy in the NXS2 model. To ensure comparable tumour burden between treatment groups in the NXS2 model therapy does not start until around day 8–10, yet the first mice can reach end point as early as day 17. Consequently the disease is well established at the start of therapy and grows rapidly hence it is more difficult to eradicate tumour.

4.2.3 Investigating 4-1BB up regulation on human NK cells cultured with anti-GD2 human neuroblastoma cell lines.

Having demonstrated that significant 4-1BB up regulation can be observed on tumour infiltrating NK cells post anti-GD2 therapy and the enhanced efficacy of anti-GD2 mAb when administered in combination with anti-4-1BB mAb in a syngeneic murine model of neuroblastoma the next logical step was to investigate whether these findings translate to a human model system. The ability to induce surface 4-1BB expression on NK cells following co-culture of human PBMCs with opsonised target cells has been reported in the literature

for a number of tumour cell lines, such as anti-CD20 opsonised lymphoma (237), Herceptin opsonised HER2+ breast cancer (238) and cetuximab opsonised EGFR+ tumour cell lines (239). To investigate whether 4-1BB surface expression could be induced on NK cells co-cultured with anti-GD2 opsonised neuroblastoma cells a time course experiment was set up.

4.2.3.1 Time course for 4-1BB up regulation on NK cells cultured with neuroblastoma target cells

A time course experiment was set up to investigate 4-1BB expression by human NK cells when PBMCs harvested from LRS cones were co-cultured with the chimeric anti-GD2 mAb ch14.18 and the Lan-1 neuroblastoma cell line. The results of this experiment are summarised in figure 4.20.

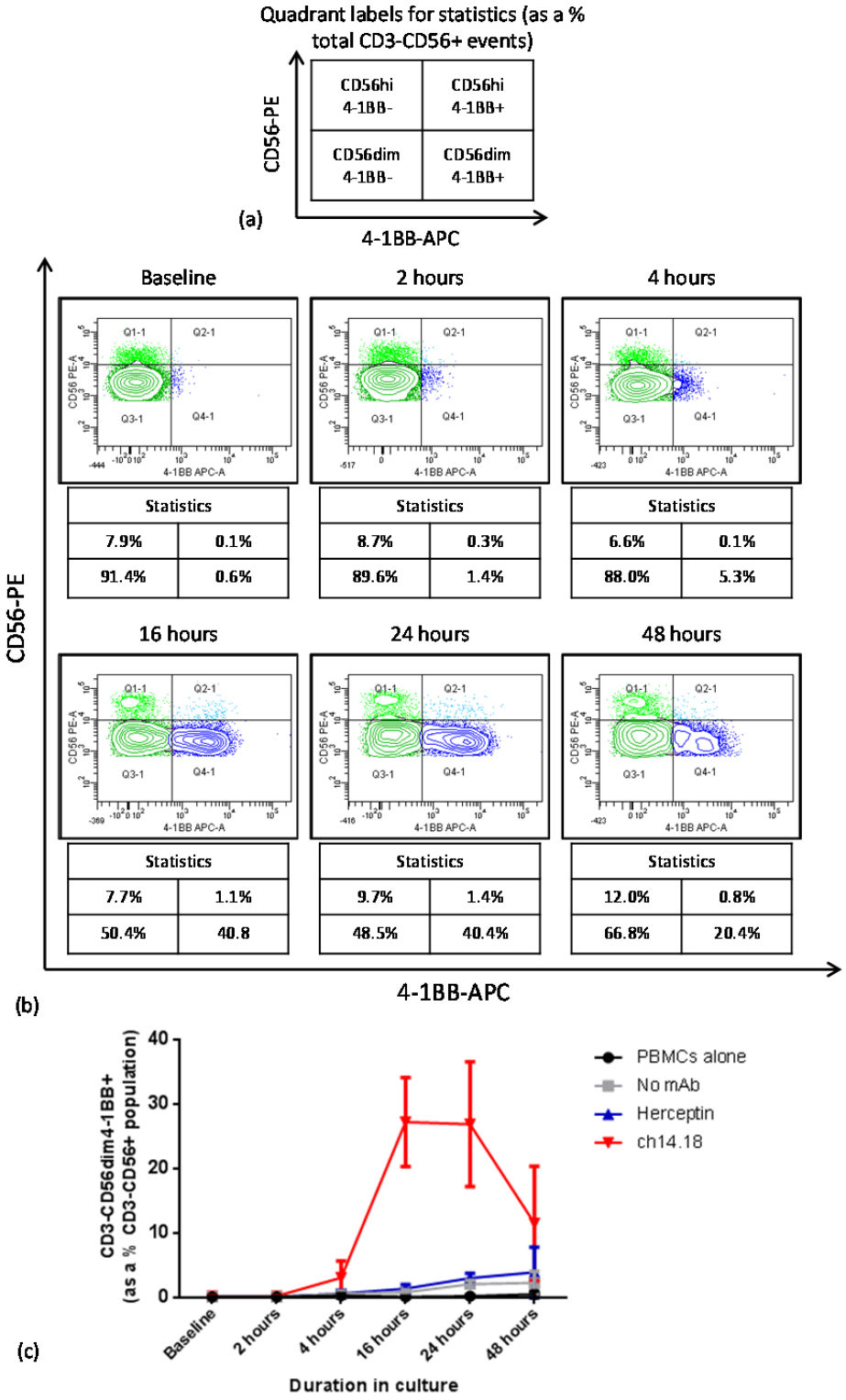

Figure 4-20. Time course for induced 4-1BB surface expression on human NK cells following culture with ch14.18 opsonised LAN-1 cells. PBMCs obtained from three separate LRS cones were analysed by flow cytometry for surface expression of 4-1BB on CD3-CD56+ NK cells at various time points following culture with ch14.18 opsonised LAN-1 cells. A schematic illustrating the quadrant labels that apply to the individual quadrant statistics displayed beneath each flow cytometry profile for clarity (a). A representative contour plot illustrating 4-1BB surface expression of CD3-CD56dim NK cells at each time point (b). Mean CD3-CD56dim4-1BB+ population as a percent total CD3-CD56+ population (c). Data presented as mean + S.D. Where n = 3.

The results presented in figure 4.20 suggest that baseline surface 4-1BB expression by human NK cells is negligible; however, following co-culture with ch14.18 opsonised Lan-1 cells 4-1BB expression is induced within the first 4-hours of culture. Based on the time points tested surface 4-1BB expression has reached its peak by 16-hours and expression persists for at least 8-hours before expression levels start to wane.

4.2.3.2 4-1BB up regulation is dependent on the presence of anti-GD2 mAb and its target

Having confirmed surface 4-1BB expression can be induced on human NK cells following co-culture with anti-GD2 opsonised Lan-1 the next stage was to confirm that the observed 4-1BB up regulation was specifically driven by the anti-GD2 mAb bound to its target and not a consequence of non-specific Fc:FcγR interactions. In these experiments human PBMCs harvested from LRS cones were cultured either alone; with the GD2+ Lan-1 cell line; or the GD2-, CD20+ Raji cell line following treatment with either the irrelevant isotype control mAb Herceptin, the anti-CD20 mAb Rituximab, or ch14.18. The results of these experiments are summarised in figure 4.21.

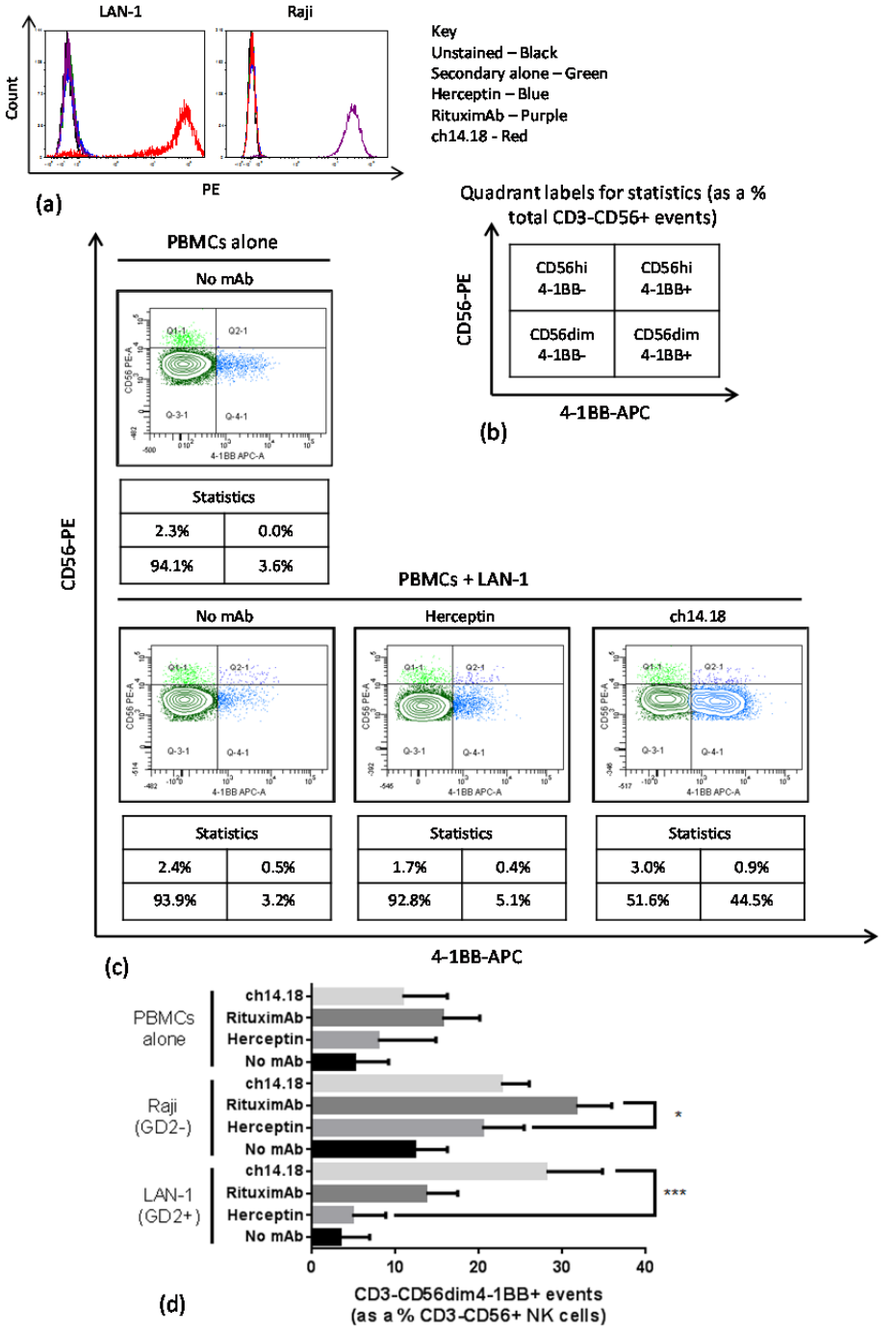

Figure 4-21. 4-1BB up regulation is restricted to NK cells cultured in the presence anti-GD2 opsonised GD2+ Lan-1 cells. PBMCs harvested from LRS cones were analysed by flow cytometry for surface expression of 4-1BB on CD3-CD56+ NK cells following 24-hour culture alone, or with opsonised target cells. GD2 and CD20 surface expression on the GD2+ human neuroblastoma cell line Lan-1 and the GD2-CD20+ human lymphoma cell line Raji, respectively (a). A schematic illustrating the quadrant labels that apply to the individual quadrant statistics displayed beneath each flow cytometry profile for clarity (b). Example flow cytometry profiles illustrating 4-1BB surface expression on the CD56hi and CD56 dim NK cell subsets after 24-hour culture of PBMCs alone or in the presence of the GD2+ neuroblastoma cell line Lan-1, either in the absence of mAb, or following treatment with Herceptin or ch14.18 (c). CD3-CD56dim4-1BB+ events as a percentage of the total CD3-CD56+ NK cell population following culture either alone, or in the presence of the LAN-1 or Raji cells plus ch14.18, Rituximab, or Herceptin (d). Data presented as mean + S.D. where n = 6 (Lan-1) and n = 3 (Raji), * P = 0.0327, *** P = 0.0006.

The surface expression (or lack of) for GD2, CD20 and HER2 by LAN-1 and Raji cells was confirmed by flow cytometry and is shown in figure 4.21 (a). Some representative flow cytometry profiles demonstrating 4-1BB surface expression by PBMCs cultured alone, or alongside Lan-1 cells following treatment with PBS, Herceptin, or ch14.18 are shown in figure 4.21 (c). These profiles clearly demonstrate that when 4-1BB surface expression is only induced when PBMCs are cultured with ch14.18 opsonised Lan-1 cells. Interestingly these profiles also confirm that when 4-1BB expression is induced on NK cells under these circumstances it is restricted to the CD3-CD56dim population, the subset of NK cells associated with potent cytolytic activity. Figure 4.21 (d) confirms that 4-1BB expression is only significantly up regulated by CD3-CD56dim NK cells when PBMCs are cultured with ch14.18 and the GD2+ Lan-1 cells, or Rituximab and CD20+ Raji cells. In the absence of the target antigen, or in the presence of an irrelevant isotype matched control mAb significant 4-1BB up regulation is not observed. Taken together this data suggests that it might be the engagement of FcγRIII (CD16) expressed on NK cells by the Fc portion of a mAb bound to its specific target antigen that triggers 4-1BB surface expression.

4.2.3.3 The effect of the effector: target ratio on 4-1BB expression

The data in figure 4.20 and 4.21 showing 4-1BB surface expression by CD3-CD56dim NK cells was achieved by culturing PBMCs with opsonised targets at an effector: target ratio of 40:1, the same ratio used to induce tumour cell killing in the ADCC assays described in chapter 3. To investigate the effect of effector: target ratio on 4-1BB expression PBMCs were cultured with increasing tumour cell numbers to obtain a range of effector: target ratios. The results of this experiment are shown in figure 4.22.

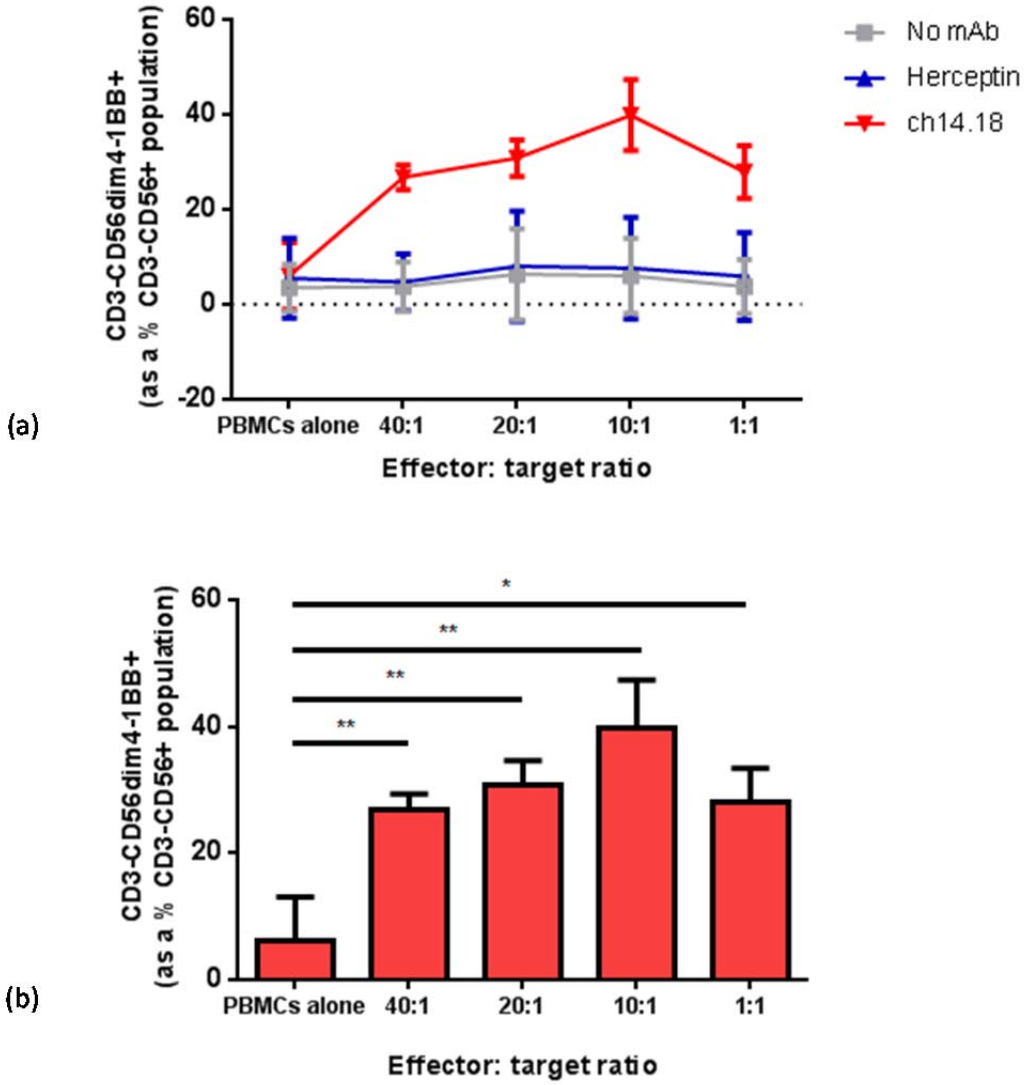

Figure 4-22. 4-1BB surface expression on human NK cells is not significantly enhanced by incubating PBMCs with increasing numbers of LAN-1 neuroblastoma cells and the anti-GD2 mAb ch14.18. PBMCs obtained from three separate LRS cones were analysed by flow cytometry for expression of surface 4-1BB on CD3-CD56dim NK cells after 24-hour culture with increasing numbers of GD2+ LAN-1 cells to obtain a range of effector target ratios. CD3-CD56dim4-1BB+ NK cells as a percentage of the total CD3-CD56+ NK cell population following culture with LAN-1 cells in the absence of mAb (grey squares), plus Herceptin (blue triangles), or plus ch14.18 (red inverted triangles) (a). CD3-CD56dim4-1BB+ NK cells as a percentage of the total CD3-CD56+ NK cell population following culture of PBMCs alone, or in the presence of ch14.18 opsonised LAN-1 at a range of effector : target ratios (b), where * p = 0.0134 and ** p = 0.0046, 0.0058, or 0.0087 respectively.

As previously shown in figure 4.21 (c) and (d) 4-1BB surface expression is only induced when PBMCs are cultured in the presence of both the GD2+ LAN-1 neuroblastoma target cells and the anti-GD2 mAb ch14.18. Figure 4.22 (b) shows that culturing PBMCs in the presence of ch14.18 treated LAN-1 neuroblastoma cells at effector: target ratios ranging from 40:1 up to 1:1 significantly enhances surface 4-1BB expression on CD3-CD56dim NK cells, compared to PBMCs treated with an equivalent dose of ch14.18 but cultured

alone. However, whilst a 10:1 effector: target ratio was associated with the greatest recovery of 4-1BB+ NK cells, there is no significant difference in the percentage of 4-1BB+ NK cells obtained within the range of effector: target ratios tested.

To summarise the results presented in figure 4.20 through to 4.22 surface 4-1BB expression is up regulated by a significant proportion of human NK cells when PBMCs are cultured with anti-GD2 opsonised neuroblastoma targets for a minimum of 16-hours and persists for at least 8-hours. Interestingly, 4-1BB expression is restricted to the CD3-CD56dim subset of NK cells, which are thought to have the greatest cytolytic activity. This observation led to the hypothesis that the anti-GD2 mediated cytolytic activity of NK cells that had been 'pre-activated' following culture in the presence of anti-GD2 opsonised targets to induce 4-1BB up regulation could be enhanced by the addition of anti-4-1BB mAb in *in vitro* ADCC assays.

4.2.3.4 Investigating cytolytic activity of 4-1BB+ NK cells in *in vitro* ADCC assays

A modified version of the calcein release based ADCC assay introduced in chapter three was used to investigate the potential for enhancing anti-GD2 mediated ADCC by 4-1BB+ NK cells though the addition of anti-4-1BB mAb. A schematic illustrating the key stages of this experiment is shown in figure 4.23.

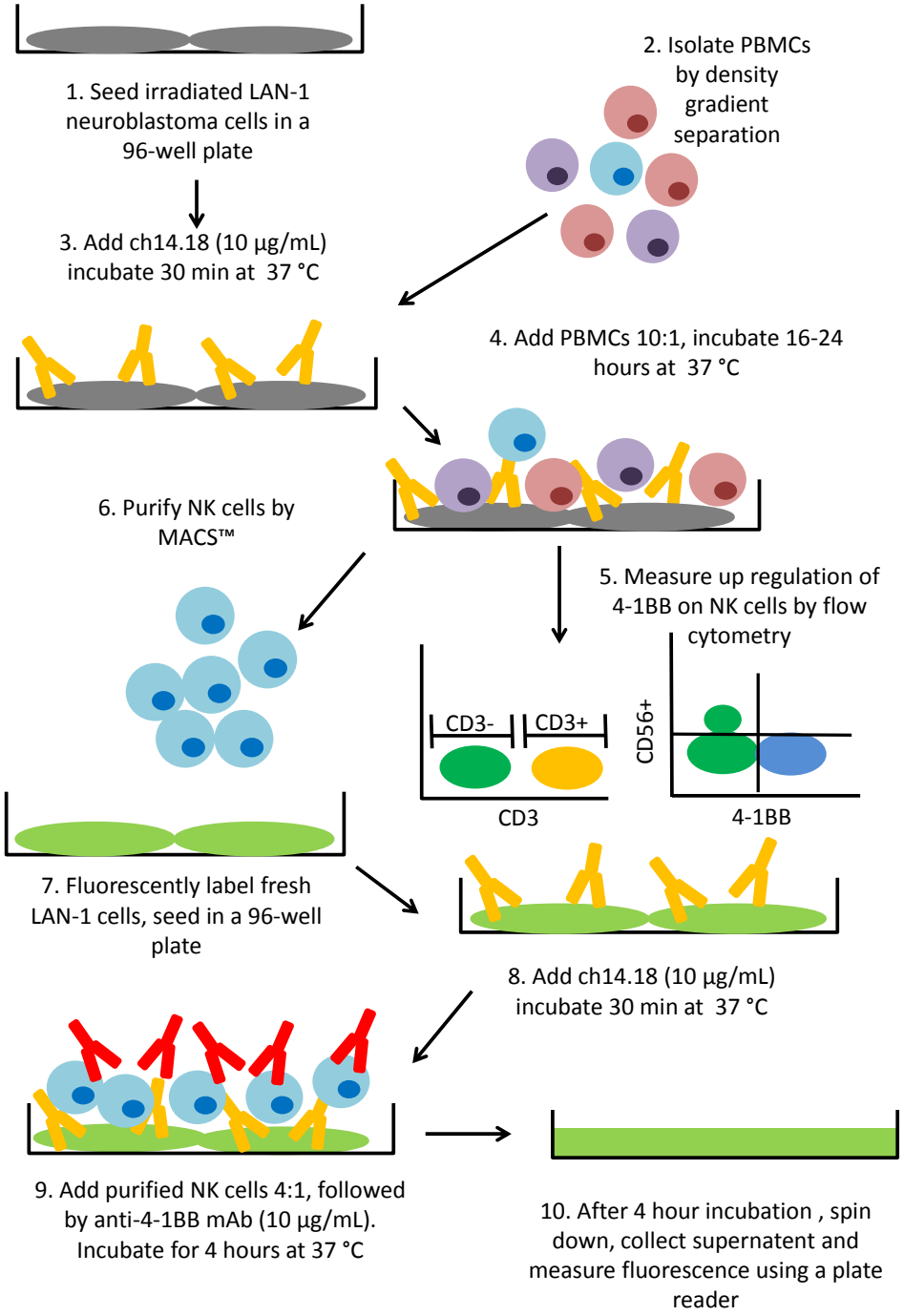

Figure 4-23. Schematic representation of the pre-activation step required to induce 4-1BB surface expression on CD3-CD56dim NK cells and the subsequent recovery process required to obtain a purified 4-1BB+ NK cell population for use in an *in vitro* ADCC assay
For further details see materials and methods section 2.11.1.

To induce 4-1BB surface expression on CD3-CD56dim NK cells PBMCs obtained from healthy volunteers were first incubated with irradiated LAN-1 neuroblastoma cells and the anti-GD2 mAb ch14.18 at an effector target ratio of 10:1 (based on the data in figure 4.22 b) for a minimum of 16-hours (based

on the data in figure 4.20 c). 4-1BB surface expression on CD3-CD56dim NK cells was confirmed by flow cytometry. NK cells, of which the CD3-CD56dim4-1BB+ subset typically comprised 20-30 %, were purified by negative selection (see materials and methods, section 2.4.2) and used as effector cells in the *in vitro* calcein release based assay previously described (see materials and methods, section 2.5.3). PBMCs from the same donor were cultured alone, or in the presence of irradiated LAN-1 cells and an equivalent concentration of Herceptin. These cells were also screened for 4-1BB surface expression before the NK cells were purified and used as effectors in matched ADCC assays. To perform the ADCC assay freshly harvested LAN-1 cells were labelled with calcein-AM as previously described, prior to the addition of either PBS alone (no mAb), Herceptin, or the anti-GD2 mAb ch14.18. NK cells purified from either PBMCs cultured alone (PBMCs alone), PBMCs cultured with LAN-1 cells plus Herceptin (Herceptin), or PBMCs cultured with LAN-1 plus ch14.18 (ch14.18) during the pre-activation step, were added to the opsonised targets along with the agonistic anti-4-1BB mAb (3/28), or an irrelevant isotype matched control (130–1). The cells were incubated for 4-hours after which the supernatant was collected and fluorescence measured. Antibody induced calcein release was calculated as described in materials and methods, section 2.5.2). The results of this experiment are summarised in figure 4.24.

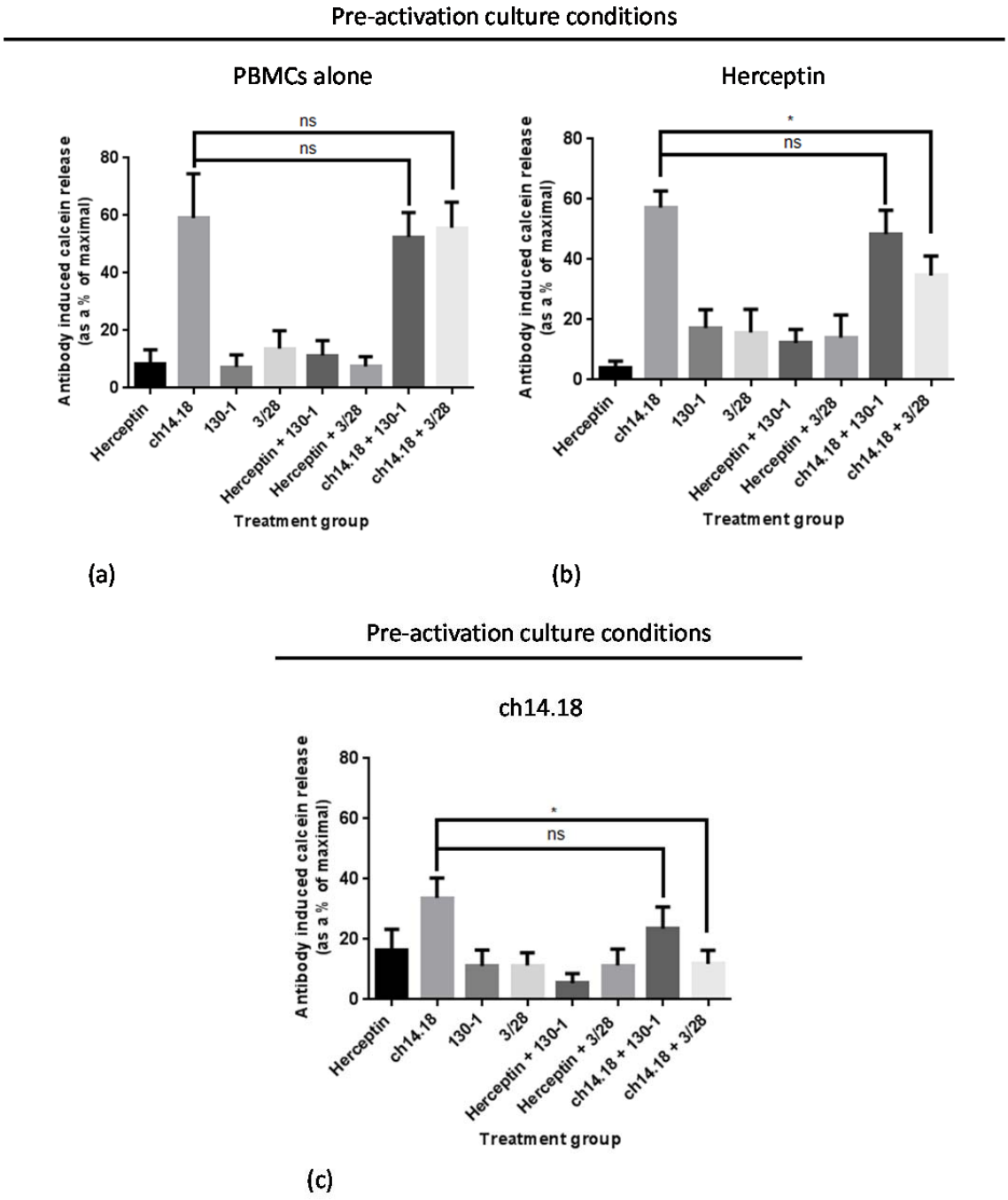

Figure 4-24. Testing the cytolytic activity of 4-1BB+ NK cells in ADCC assays using anti-GD2 mAb +/- anti-4-1BB mAb. PBMCs from three separate donors were cultured alone, or with irradiated LAN-1 neuroblastoma cells, plus Herceptin, or the anti-GD2 mAb ch14.18 for 16-hours to induce 4-1BB expression. NK cells were subsequently purified and used as effector cells in the calcein-release based ADCC assay. Antibody-induced calcein release as a percentage of maximal following ADCC using NK cells purified from PBMCs cultured alone (a), where ns = not significant; with irradiated LAN-1plus Herceptin, where ns = not significant and * p = 0.0179 (b); or with irradiated LAN-1 plus ch14.18, where ns = not significant and * p = 0.0151 (c). All data presented as the mean plus S.D., where n = 3 for the three donors.

Figure 4.24 shows the antibody-induced calcein release as a percentage of maximal. In each case statistical analysis has been performed (see materials and methods, section 2.13) to assess the antibody-induced calcein release as a

percentage of maximal, relative to the level achieved using the anti-GD2 mAb ch14.18 alone. Figure 4.24 (a) shows that when NK cells are obtained from PBMCs cultured alone during the pre-activation step, there is no significant alteration in calcein release when the anti-GD2 mAb ch14.18 is added along with the anti-4-1BB mAb 3/28, or its associated isotype 130-1. Figure 4.24 (b) shows that when NK cells purified from PBMCs cultured with irradiated LAN-1 and Herceptin as used as effectors, there is no significant alteration in calcein release compared to ch14.18 alone, when ch14.18 is added along with 130–1; however, when ch14.18 and 3/28 are added together there is a significant reduction in calcein release. Figure 4.24 (c) shows that when NK cells purified from PBMCs cultured with irradiated LAN-1 and ch14.18 are used as effectors, not only is there is a reduction in the level of calcein release achieved with ch14.18 alone (to around 35 % of maximal, compared to almost 60 % observed in (a) and (b)) but the combined addition of ch14.18 and 3/28 significantly reduces calcein release further still, an effect that is not observed when ch14.18 is added along with 130–1.

4.2.3.5 The effect of pre-activation on FcγRIII (CD16) expression by NK cells

In an attempt to explain the reduction in calcein release in ADCC assays where NK cells purified from PBMCs cultured with irradiated Lan-1 cells and ch14.18, the cells, along with those cultured alone, or with irradiated Lan-1 and Herceptin, were screened by flow cytometry to look at 4-1BB and CD16 surface expression levels. The results of this screening are shown in figure 4.25 and 4.26.

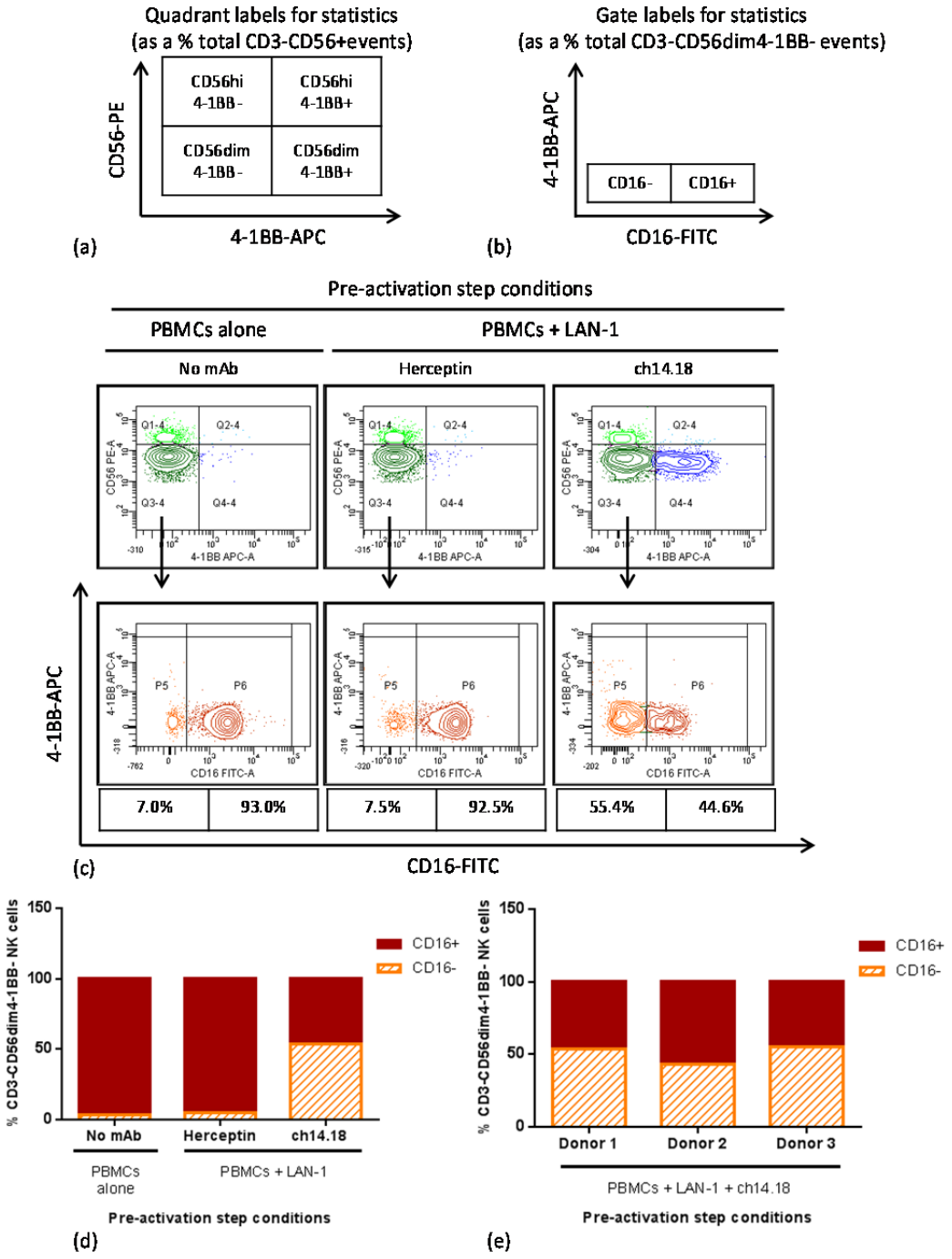

Figure 4-25. CD16 surface expression on CD3-CD56dim-4-1BB- human NK cells following the 16-hour pre-activation step in which PBMCs were cultured alone, or with irradiated LAN-1 neuroblastoma cells plus either Herceptin, or the anti-GD2 mAb ch14.18. PBMCs obtained from leukocyte cones were analysed by flow cytometry for surface expression of CD16 on CD3-CD56dim4-1BB-NK cells after the 16-hour pre-activation step, prior to purifying for use in ADCC assays. Schematics illustrating the quadrant / gate labels that apply to the individual quadrant / gate statistics displayed beneath each flow cytometry profile for clarity (a) and (b). Representative flow cytometry profiles illustrating CD16 surface expression on the CD3-CD56dim4-1BB- subset of NK cells when PBMCs are cultured alone, or with irradiated LAN-1 neuroblastoma cells and either Herceptin or ch14.18 (c). Stacked bar charts illustrating the CD16+ and CD16- events as a percentage of the total CD3-CD56dim4-1BB- NK cells recovered from the PBMCs of one donor when PBMCs were subjected to the different pre-activation conditions (d). Stacked bar charts illustrating the CD16+ and CD16- events as a percentage of the total CD3-CD56dim4-1BB- NK cells recovered from the PBMCs cultured with LAN-1 and ch14.18 for each of the three separate donors.

The CD3-CD56dim4-1BB- NK cell subset, which In the case of the PBMCs cultured alone, or with irradiated LAN-1 neuroblastoma cells plus Herceptin represents almost 90 % of the CD3-CD56+ population was passed through the FITC channel to look at surface CD16. Figure 4.25 (c) reveals for both PBMCs cultured alone, or in the presence of irradiated Lan-1 and Herceptin, around 93 % of the CD3-CD56dim4-1BB- population is CD16+. In contrast when the CD3-CD56dim4-1BB- subset obtained following culture of PBMCs with irradiated LAN-1 and ch14.18 (which represents almost 60 % of the total NK cell population) is passed through the FITC channel to look at CD16 expression, only 45 % of these cells are CD16+, which means more than half of this subset is CD16-. This is shown graphically in figure 4.25 (d). The same trend was observed for all three of the donors', in each case when the CD3-CD56dim4-1BB- subset of NK cells recovered from PBMCs cultured with irradiated LAN-1 and ch14.18 was passed through the FITC channel to assess surface CD16. On average around 50 % of this population was CD16- and this is shown graphically in figure 4.25 (e).

When the CD3-CD56dim4-1BB+ subset NK cells recovered from the PBMCs cultured with irradiated LAN-1 neuroblastoma cells and the anti-GD2 mAb ch14.18 were passed though the FITC channel to assess surface CD16 expression more than 90 % of this subset were found to be CD16- as shown in figure 4.26 (c) and (d).

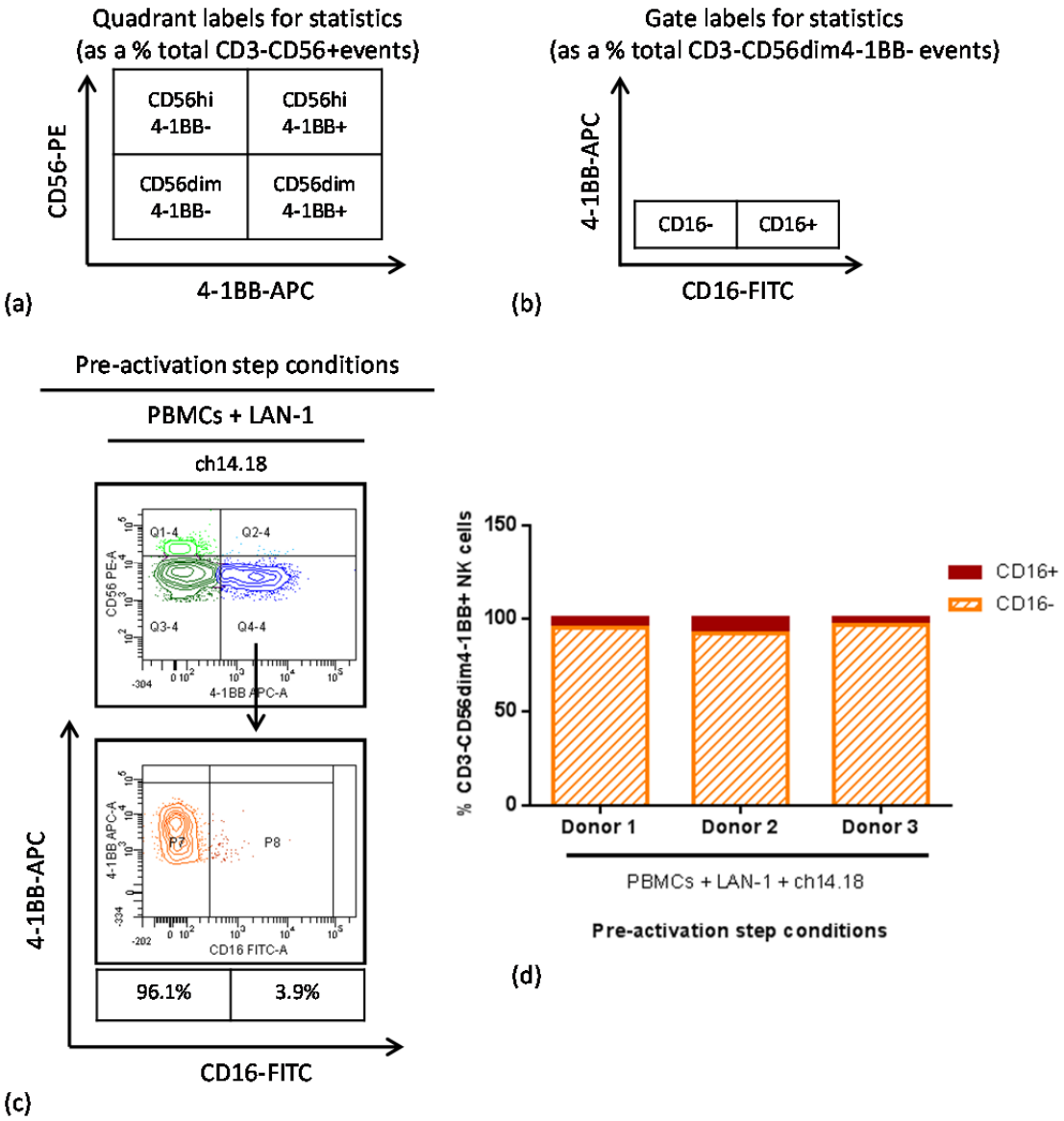

Figure 4-26. CD16 surface expression on CD3-CD56dim-4-1BB- human NK cells following the 16-hour pre-activation step in which PBMCs were cultured with irradiated LAN-1 neuroblastoma cells plus the anti-GD2 mAb ch14.18. PBMCs obtained from leukocyte cones were analysed by flow cytometry for surface expression of CD16 on CD3-CD56dim4-1BB+NK cells after the 16-hour pre-activation step, prior to purifying for use in ADCC assays. Schematics illustrating the quadrant / gate labels that apply to the individual quadrant / gate statistics displayed beneath each flow cytometry profile for clarity (a) and (b). Representative flow cytometry profiles illustrating CD16 surface expression on the CD3-CD56dim4-1BB+ subset of NK cells when PBMCs were are cultured with irradiated LAN-1 neuroblastoma cells and ch14.18 (c). Stacked bar charts illustrating the CD16+ and CD16- events as a percentage of the total CD3-CD56dim4-1BB+ NK cells recovered from the PBMCs of each individual donor (d).

Taken together this data reveals that whilst around 93 % of the CD3-CD56dim NK cells recovered from PBMCs cultured alone, or with irradiated LAN-1 neuroblastoma cells plus Herceptin are CD16+, on average 50 % of the 4-1BB-, and more than 90 % of the 4-1BB+ CD3-CD56dim NK cells recovered from PBMCs cultured with irradiated LAN-1 neuroblastoma cells plus ch14.18 are CD16-, which equates to more than half of the total NK cell population. Since

CD16 plays an integral role in ADCC the loss of surface CD16 on NK cells recovered from PBMCs cultured with irradiated LAN-1 neuroblastoma cells and ch14.18 may contribute to the reduction in ADCC observed in figure 4.24 (c). Following on from this observation as time course experiment was set up to look at the induction of 4-1BB surface expression and the concomitant loss of CD16 when PBMCs were cultured with LAN-1 neuroblastoma cells and the anti-GD2 mAb ch14.18. The results of this experiment are shown in figure 4.27.

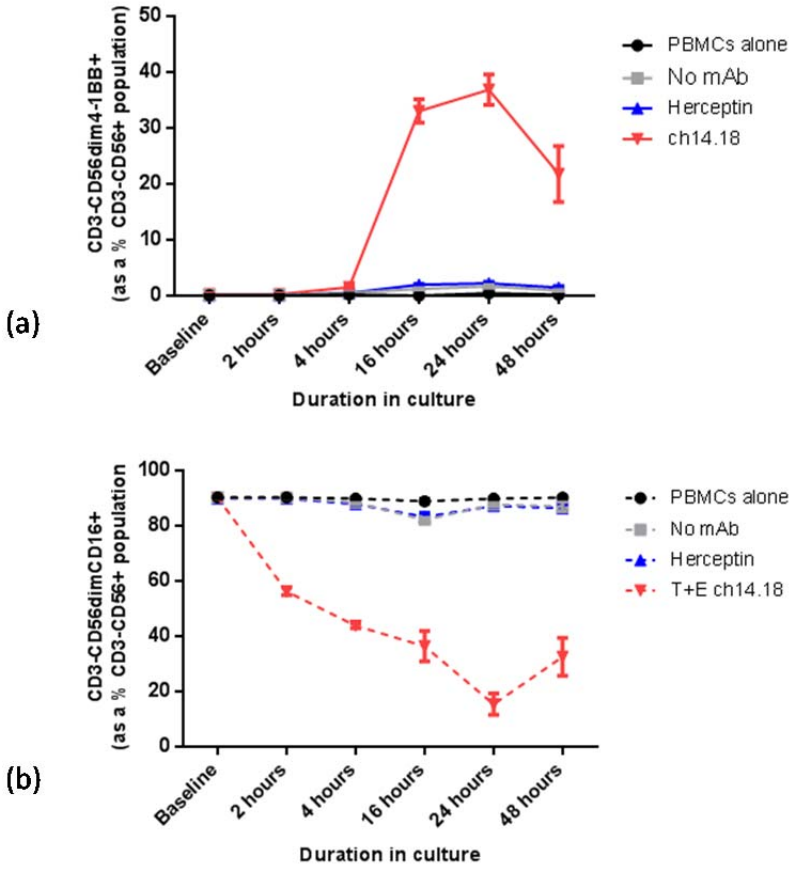

Figure 4-27. Time course for induced 4-1BB surface expression and loss of surface CD16 on human NK cells following culture with ch14.18 opsonised LAN-1 cells. PBMCs obtained from two separate leukocyte cones were analysed by flow cytometry for surface expression of 4-1BB and CD16 on CD3-CD56dim NK cells at various time points following culture of PBMCs alone (black circles), or in the presence of LAN-1 neuroblastoma cells plus PBS alone (no mAb) (grey squares), Herceptin (blue triangles), or ch14.18 (red inverted triangles). Mean (of triplicate repeats) ± S.E.M. CD3-CD56dim4-1BB+ population as a percent total CD3-CD56+ population (a). Mean (of triplicate repeats) ± S.E.M. CD3-CD56dimCD16+ population as a percent total CD3-CD56+ population (b). Representative example of one of two repeats using PBMCs from two independent donors.

The results in figure 4.27 clearly show that when surface 4-1BB expression by CD3-CD56dim NK cells peaks (in this case at 24 hours) (figure 4.27 a), surface CD16 expression by this same subset of NK cells is at its lowest (figure 4.27

b), which may affect *in vitro* NK cell function in terms of ADCC, a process that is dependent on Fc engagement of surface CD16.

4.3 Chapter discussion

Anti-4-1BB mAb is a particularly interesting candidate as an adjuvant for enhancing the efficacy of anti-GD2 mAb due to 4-1BB expression, either constitutive or after activation, on a range of effector subtypes, such as T cells, Tregs, NK cells, macrophages and neutrophils, all of which have been implicated in the immune response to neuroblastoma. Additionally, anti-4-1BB mAb themselves have demonstrated potent anti-tumour activity, in numerous syngeneic murine models of cancer (230-234), through the generation of tumour-specific CTL responses. The first evidence that 4-1BB could be induced on NK cells was provided in 1998 (229). However, it was the subsequent discovery that 4-1BB up regulation could be induced on NK cells following FcγR triggering that led Levy and co-workers to formulate their hypothesis that the efficacy of anti-CD20 mAb, such as rituximab could be enhanced when administered in combination with anti-4-1BB mAb. The rationale being that anti-CD20 exerts its effect, at least in part, via ADCC, a process that is dependent on the engagement of FcγRIII (CD16) and will therefore induce 4-1BB up regulation by NK cells, the subsequent ligation of the 4-1BB molecule by an anti-4-1BB mAb will enhance NK cell killing augmenting the efficacy of rituximab. Levy *et al.* have since demonstrated that this novel combinatorial approach enhances the efficacy of several direct targeting mAb, including rituximab, Herceptin and cetuximab, both *in vitro* and *in vivo* using syngeneic and human xenotransplanted models (237-239). As mentioned at the beginning of the chapter the success of the work carried out by Levy's group (published by Kohrt *et al.*) has provided strong support for our hypothesis that the efficacy of anti-GD2 mAb can be enhanced when administered in combination with anti-4-1BB, which has been explored in this chapter.

Using the syngeneic murine NXS2 model of neuroblastoma I have demonstrated that significant up regulation of the co-stimulatory molecule 4-1BB is observed on tumour-infiltrating NK cells specifically following treatment with anti-GD2 mAb. Additionally, I have shown that syngeneic A/J mice bearing established NXS2 tumours receiving anti-GD2 plus anti-4-1BB mAb have

slower tumour progression resulting in a significant survival advantage over mice receiving either antibody alone. However, although statistically significant, the benefit of combining anti-GD2 and anti-4-1BB in this model appears fairly modest. There may be several reasons for this. Firstly, the rapid tumour growth kinetics of the chosen model results in a narrow therapeutic window. Although optimised as much as possible, within the practical limits of the project, it may be that the tumour load was too high at the start of treatment to allow an adequate therapeutic response. Several different timing strategies were tested and it appears that there is a very fine balance between starting therapy too soon, when there is insufficient tumour antigen, and too late, when there is inadequate time for the therapy to work. The kinetics of tumour growth is slower in patients and the therapeutic window may therefore be more favourable, consequently timing may be less critical. Secondly, the anti-tumour activity of the direct targeting anti-GD2 mAb in this model may be less NK cell dependent than those tested by Levy and co-workers in other models. Data presented in chapter three demonstrated that anti-GD2 mAb therapy was not completely abrogated in tumour bearing mice that had been NK cell-depleted, suggesting that other mechanisms may be involved. Hence the effect of augmenting NK cell mediated therapy in this model may be less pronounced. Thirdly, the anti-4-1BB mAb used in this investigation may not be comparable to the anti-4-1BB mAb used by Levy *et al.* The two mAb are different clones and may therefore bind different epitopes and exhibit different agonistic activity. Furthermore, our in house anti-4-1BB mAb is a rat IgG1 isotype, whereas the one used by Levy *et al.* is a rat IgG2a. Preliminary BIACore data obtained in our lab suggests that rat IgG1 and IgG2a mAb are similar in that they both bind FcγRIII and FcγRIIB; however, the IgG1 mAb may have higher affinity for FcγRIII and may therefore be more likely to delete 4-1BB positive cells. A large proportion of the tumour-infiltrating Tregs were observed to be 4-1BB positive and it is possible that part of the observed therapeutic effect was due to Treg deletion. Of course this also means that the 4-1BB positive NK cells may be targets for deletion but given the reasonably low number of 4-1BB positive NK cells in the tumour microenvironment the effect is likely to be more subtle. One of the attractions of anti-4-1BB as an adjuvant for anti-GD2 mAb therapy is its effect on T cells, particularly CTLs and the potential for generating long term tumour-specific immunity. Ideally this potential would have been explored in this project, using splenocytes

harvested from mAb treated mice and measuring their ability to produce IFN-γ when stimulated with tumour antigen *in vitro*, unfortunately this was not possible as long term survival was rarely achieved.

The mechanisms by which anti-4-1BB mAb enhance the efficacy of direct targeting mAb, such as anti-GD2, are likely to be many and varied, and ligation of 4-1BB+ NK cells can promote a multitude of immune responses. For example Levy *et al.* have demonstrated that 4-1BB+ NK cells have an increased capacity to lyse target cells by ADCC when direct targeting mAb are coupled with anti-4-1BB (237-239). Although, this is in contrast to other reports suggesting that 4-1BB ligation enhances NK cell proliferation and IFN-γ production but their cytolytic activity remains unaltered (225). 4-1BB+ NK cells have also been shown to have a crucial role in the generation of tumour-specific CTL responses (225, 229). The effects of anti-4-1BB mAb when administered along with anti-GD2 mAb *in vivo* are unlikely to be confined to 4-1BB+ NK cells. Levy *et al.* reported that more than 60 % of intratumoral macrophages were 4-1BB+ in the syngeneic BL3750 lymphoma model and although this was not augmented in response to anti-CD20 mAb therapy it is plausible that these macrophages may be activated by anti-4-1BB and contribute to the therapeutic effect of the combined mAb therapy (237). Evidence for the involvement of both NK cells and macrophages in the initial response to anti-CD20 plus anti-4-1BB mab therapy was provided when depletion of either subtype was shown to correspond with an abrogation of therapy. Interestingly, CD8 T cell depletion had no effect on initial tumour regression but 40 % of the CD8 T cell depleted mice relapsed 70 days post tumour-inoculation and eventually succumbed to their tumour burden. This observation suggests that there may be potential for anti-GD2 plus anti-4-1BB mAb strategies to achieve the ultimate goal of immunotherapy and generate tumour-specific long term immunity and warrants further investigation.

In addition to investigating the efficacy of anti-GD2 plus anti-4-1BB mAb *in vivo* attempts were made to explore the efficacy of the combination therapy *in vitro* using human PBMCs from healthy donors and human neuroblastoma cell lines. Clear 4-1BB up regulation was observed on human NK cells, specifically the CD56dim subset, which is associated with the most potent cytolytic activity. Perhaps surprisingly, these cells appeared to exhibit reduced cytolytic activity when used as effector cells in ADCC assays. When human PBMCs were

co-cultured with anti-GD2 opsonised LAN-1 cells to induce 4-1BB expression and NK cells subsequently purified for use in ADCC assays it was noted that the level of killing achieved with the anti-GD2 mAb ch14.18 was reduced compared to control experiments. The most obvious explanation for the reduction in ADCC was the observed loss of FcγRIII (CD16) by NK cells cultured under the pre-activation conditions required to induce 4-1BB expression. Since engagement of CD16 by the Fc portion of the mAb bound to its target is essential to elicit ADCC it was not surprising that the cytolytic activity of these NK cell was reduced. Levy *et al.* have recorded similar observations, although they do not report a loss of ADCC (238). However, they do comment that particularly high effector target ratios were required (100:1 NK: target) in some cases in order to achieve ADCC, which they attribute to a loss of NK cell fitness brought on by the extended period in culture without exogenous cytokines (237). Consequently, it may be possible to recover ADCC to equivalent levels observed in the control conditions by supplementing the PBMCs with IL-2 in the pre-activation step, which may have an added benefit of further augmenting 4-1BB expression, or repeating the experiment at much higher effector: target ratios.

Paradoxically the addition of agonistic anti-4-1BB mAb appeared to have a largely inhibitory effect on anti-GD2 mediated cytolytic activity in ADCC assays in which effector cells had been pre-activated to induce 4-1BB expression. This has not been reported in the literature yet was consistently observed in repeated experiments. Since this observation was confined to samples to which the anti-4-1BB mAb had been added a possible explanation is that the cells were on the verge of exhaustion and this extra stimulus was sufficient to tip the balance and lead to the cessation of cytolytic activity. By the time the 4-1BB+ NK cells were used in ADCC assays they had already been subjected to extended periods in culture in the presence of irradiated, opsonised targets. It has been documented that irradiated cells express, so called damage-associated molecular patterns (DAMPs) (273) that can trigger immune responses. Consequently, the combined effect of antibody-induced and DAMP-induced activation for pro-longed periods may have contributed to NK cell exhaustion. This may be another reason why Levy *et al.* used such high effector: target ratios to achieve killing.

In summary the data presented in this chapter provides the first evidence that anti-GD2 mAb induces significant up regulation of the co-stimulatory molecule 4-1BB, which is restricted to tumour-infiltrating NK cells *in vivo* using the syngeneic murine NXS2 model. Additionally, this effect can be replicated *in vitro* using human model systems, where interestingly 4-1BB expression is restricted to the CD56dim NK cell subset, reported to have the greatest cytolytic activity. It also demonstrates for the first time that sequential administration of anti-GD2 plus anti-4-1BB mAb has a synergistic effect, which leads to slowed tumour progression and significantly, albeit modestly, enhances survival of syngeneic A/J mice bearing established NXS2 tumours.

Chapter 5: Characterising the TH-MYCN transgenic mouse model of neuroblastoma

5.1 Chapter introduction

The TH-MYCN transgenic mouse model of neuroblastoma is one of just two murine models of neuroblastoma that permits study of GD2 targeting immunotherapies in fully immunocompetent mice, the other being the syngeneic NXS2 model which has been used extensively throughout this investigation. The TH-MYCN transgenic mouse model was developed by Weiss *et al.* in 1997 (241). These mice have been genetically engineered to overexpress MYCN in neuroectodermal cells derived from the neural crest and subsequently develop tumours within several months of birth (241). Amplification of the proto-oncogene MYCN, which was originally isolated from neuroblastoma cells (274, 275), is one of the best characterised genetic aberrations in neuroblastoma and correlates with advanced disease (6, 7). MYCN, which is located on chromosome 2p24, encodes the transcription factor N-Myc, belonging to the Myc family of DNA binding basic region/helix-loop-helix/leucine zipper (bHLHZip) proteins. Other members of this family include C-Myc and L-Myc. The Myc family proteins heterodimerise with the bHLHZip protein Max to form a transcription factor complex that binds to specific E-box DNA motifs (5'-CANNTG-3') and activates transcription of a variety of genes involved in a range of cellular functions, including cell growth and proliferation, metabolism, apoptosis and differentiation (276-279). N-myc usually binds the E-box motifs CATGTG and CAACTG; however, when N-Myc is amplified is becomes less specific and will also bind CATTTG and CATCGT (280). The rat tyrosine hydroxylase (TH) promoter was used to target human MYCN expression to the developing neuroblasts of the neural crest. This promoter is active in the migrating cells of the neural crest during early development and has been shown to direct expression of chloramphenicol acetyl transferase to both the sympathetic ganglia and the adrenal gland (which is derived from the neural crest) where neuroblastoma tumours commonly arise (281). Clinical presentation can vary among mice, some present with thoracic tumours, or large palpable abdominal tumours, whereas

others display signs of progressive paralysis of the lower extremities (241). The TH-MYCN model closely resembles human neuroblastoma as the tumours arise in the abdomen and thorax, with some mice showing signs of spinal cord involvement, these mice were subsequently found to have abdominal, or thoracic paraspinous masses, with tumour tracking along the peripheral nerves and encasing the spinal cord (241). Tumorigenesis is affected by gene dosage and mice homozygous for the MYCN transgene develop tumours with increased incidence and decreased latency (241). The developing tumours also share a number of the same histological features and chromosomal aberrations seen in human neuroblastoma (241). However, there are a number of limitations associated with this model, for example tumours rarely metastasize to the bone marrow, the time to tumour presentation can be variable and tumour penetrance is poor on some genetic backgrounds (282). Despite the limitations the TH-MYCN transgenic mouse model is one of the most useful pre-clinical models of neuroblastoma (282) and has been used extensively in numerous areas of neuroblastoma research, including basic biology and therapeutic studies, contributing to some key publications in the field (283). The TH-MYCN transgenic mouse model may represent a more physiologically relevant model of neuroblastoma, due to both its spontaneous nature (tumours develop endogenously within several months of birth) and its clinical presentation, which recapitulates many of the features of human disease (282). Another key feature of the model is that it facilitates study of both endogenous anti-tumour immune responses, as well as the immune response to anti-GD2 mAb based treatment strategies. Despite considerable interest surrounding immunotherapy as part of the standard treatment for high risk neuroblastoma, and the relatively unique ability of the TH-MYCN transgenic mouse model to facilitate study of anti-tumour immune responses, there is little evidence in the literature to suggest that the model has been utilised in this way. One of the main objectives and key novel aspects of this investigation is the characterisation of the model in preparation for the study of anti-GD2 mAb based therapeutic strategies. Part of this work will involve the characterisation of the endogenous immune response to tumour, as it is anticipated changes in the immune composition will provide a suitable end point for assessing response to therapy, as well as establishing a method of recapitulating the MRD setting in preparation for the study of anti-GD2 mAb based therapeutic strategies.

5.2 Results

5.2.1 Tumour penetrance in TH-MYCN transgenic mice

Tumour penetrance in the TH-MYCN transgenic mouse model is strain dependent and Weiss *et al.* reported that 129S/v mice demonstrate increased penetrance compared to the C57/B6J and FBN/N strains (241). Tumours arise at a much higher frequency in 129/SvJ mice, with approximately 33 % of heterozygotes and 100 % homozygotes developing tumours (282), compared to just 5 % and 20 % of C57/B6J mice at 3 and 6 months respectively (241). Consequently, the TH-MYCN transgenic mice in this facility are maintained on the 129/SvJ background. The decreased latency observed in homozygotes (241) renders mice at risk of developing tumour before they are fully immunocompetent, hence the preference for heterozygotes (TH-MYCN+/-) in this study. Congenic female 129/SvJ were bred with males carrying a single copy of the TH-MYCN transgene and the offspring were screened to detect the presence of the TH promoter. Abdominal tumours can be physically detected in these mice at around 9–13 weeks; however, tumour formation can be detected as early as 6 weeks when imaging techniques, such as MRI and ultrasound are employed (282). These techniques are not currently available in this facility; therefore transgenic mice were regularly examined for palpable abdominal masses. Once a palpable tumour has been detected untreated mice typically survive for approximately one week before they are deemed to have reached end point. Routinely, this decision was made independently by an experienced animal technician based on the size of the tumour and other visual signs of discomfort or distress. Figure 5.1 is a Kaplan-Meier curve, which demonstrates the time to terminal tumour burden for TH-MYCN transgenic +/- mice in comparison to congenic 129/SvJ mice.

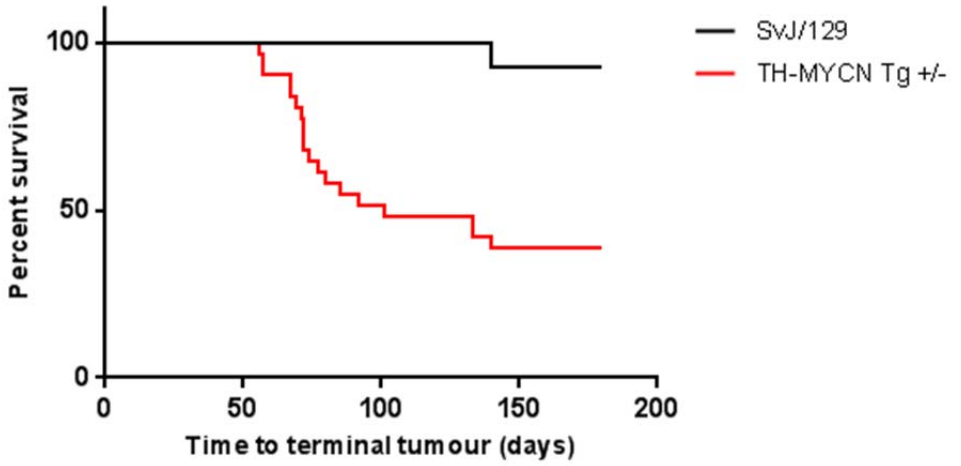

Figure 5-1. Kaplan-Meier curve of TH-MYCN +/- transgenic mice compared to congenic 129/SvJ. Congenic 129/SvJ female mice were bred with males carrying a single copy of the TH-MYCN transgene. Offspring were screened to detect the TH-promoter, thus confirming transgenic status. Transgenic mice were monitored from birth until terminal tumour burden, at which point the tumour bearing mouse was culled. TH-MYCN transgenic (Tg) +/- mice (n = 33) (red line) present with an increased incidence of spontaneous tumour and diminished survival compared to congenic 129/SvJ mice (n = 42) (black line), where p = < 0.0001 following a Log rank test.

The data in figure 5.1 demonstrates that approximately 50 % of the TH-MYCN transgenic +/- mice develop tumour and these mice are typically terminal between 60 and 100 days. Due to space constraints a 180 day cut off was put in place and mice failing to develop tumour within this time frame were routinely culled. It has been reported in the literature that tumour bearing TH-MYCN transgenic mice can undergo spontaneous regression. Teitz *et al.* reported that 10 % of TH-MYCN tumour bearing mice exhibited clear signs of tumour growth arrest between eight and ten weeks, which persisted for approximately two weeks, eventually resulting in complete regression of tumour based on MRI and ultrasound imaging (282). Since these imaging techniques are not available in this facility to support such observations we can only postulate that some of the mice that did not present with tumour may have developed tumour early on that was too small to detect by palpating and subsequently went on to regress fully.

5.2.2 The physical presentation of tumour

The TH-MYCN transgenic mouse model closely recapitulates many of the clinical features of human neuroblastoma, hence physical tumour presentation can vary (241). However, with the exception of one mouse, that presented with shortness of breath due to tumour in the thoracic cavity, the tumour bearing

mice typically present with large palpable abdominal tumours, involving the adrenal gland, kidney and occasionally the spinal cord. Figure 5.2 demonstrates the typical location and size of tumours TH-MYCN transgenic +/- mice have presented with.

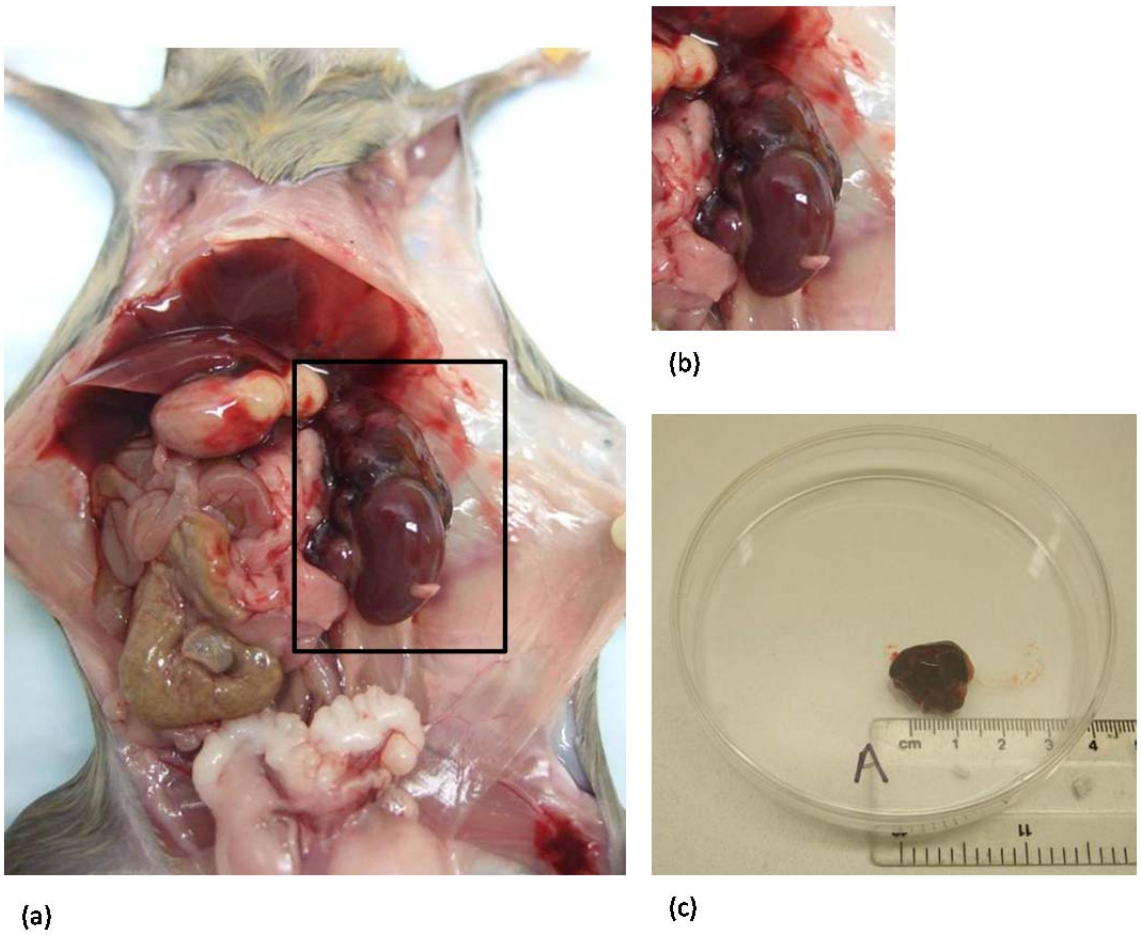

Figure 5-2. Location and size of tumour arising in a TH-MYCN transgenic +/- mouse. An 80 day old male TH-MYCN +/- transgenic mouse was culled upon presentation of terminal tumour. The location of the tumour *in situ* is shown in (a), a close up view from the same image, shown in (b), clearly demonstrates the adrenal gland and kidney involvement. Terminal tumours typically measure approximately 1 cm^2 as shown in (c).

5.2.3 GD2 expression on TH-MYCN +/- transgenic mouse tumours

The tumours harvested from TH-MYCN transgenic +/- mice have been screened for surface GD2 expression. The tumours were screened using the FITC conjugated anti-GD2 mAb 14G2a. Surface GD2 expression on TH-MYCN tumours was compared to subcutaneous NXS2 tumours harvested from syngeneic A/J mice. Surface GD2 expression on TH-MYCN and NXS2 tumours *ex vivo* is shown in figure 5.3.

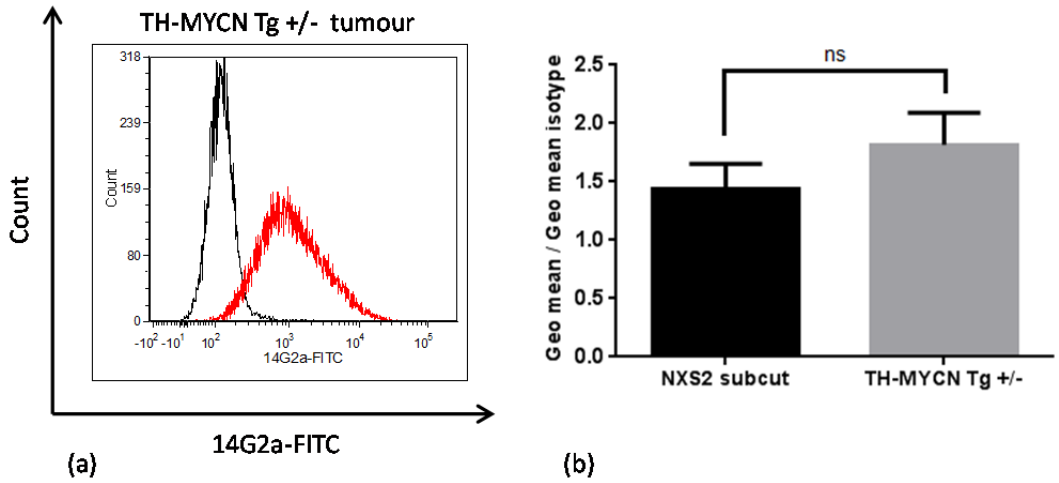

Figure 5-3. Surface GD2 expression on tumours harvested from TH-MYCN transgenic +/- mice and syngeneic A/J mice bearing subcutaneous NXS2 tumours Surface GD2 expression was quantified using the FITC conjugated anti-GD2 mAb 14G2a-FITC and assessed by flow cytometry. A representative flow cytometry histogram shows the mean fluorescence intensity (MFI) obtained using both an irrelevant isotype matched control PK136 (black line), or 14G2a-FITC (red line) for a tumour harvested from a TH-MYCN transgenic +/- mouse (a). The mean fold change relative to the isotype control for tumours harvested from three A/J mice versus three TH-MYCN transgenic +/- mice (b) error bars = S.D, ns = not significant.

The level of surface GD2 expression by three separate tumours harvested from TH-MYCN transgenic +/- mice was found to be comparable to GD2 expression by three separate subcutaneous NXS2 tumours harvested from syngeneic A/J mice. However, the shape of the histogram shown in figure 5.3 suggests that GD2 expression is more uniform on the tumours harvested from TH-MYCN +/- transgenic mice compared to the NXS2 cell line, which has been observed to drift (see figure 3.1).

5.2.4 The immune infiltrate in TH-MYCN transgenic mouse tumour microenvironment

Three multicolour flow cytometry panels were developed to facilitate analysis of NK cell and T cell populations in the tumour microenvironment and spleens harvested from TH-MYCN transgenic +/- mice, compared to spleens of congenic 129/SvJ mice.

5.2.4.1 Tumour infiltrating NK cells

The NK cell panel comprised of fluorescently conjugated antibodies specific for the following surface antigens CD3; CD49b; NKG2ACE; CD11b and CD27. Murine NK cells were characterised as CD3-CD49b+NKG2ACE+ as previously shown in figure 4.2 and this population was subsequently analysed for surface

expression of the integrin CD11b and tumour necrosis factor receptor CD27. Mature murine NK cells can be identified based on their expression of CD11b (284) and further subdivided based on their expression of CD27 (285). CD11b+CD27- NK cells are said to be terminally differentiated (33); however, immature CD11b- NK cells pass through a CD27+ stage as they start to differentiate (286). Mature CD11b+ NK cells that are also CD27+ are reportedly more reactive in terms of cytolytic capacity, cytokine production and proliferation than the mature CD11b+ NK cells that are CD27- (285, 286), which may be explained by the higher proportion of the inhibitory receptor Ly49s on the CD11b+CD27- subset (33). Figure 5.4 illustrates the proportion of NK cells and their different phenotypes detected in the tumour and spleens of TH-MYCN transgenic +/- tumour bearing mice relative to the spleen of congenic 129/SvJ mice.

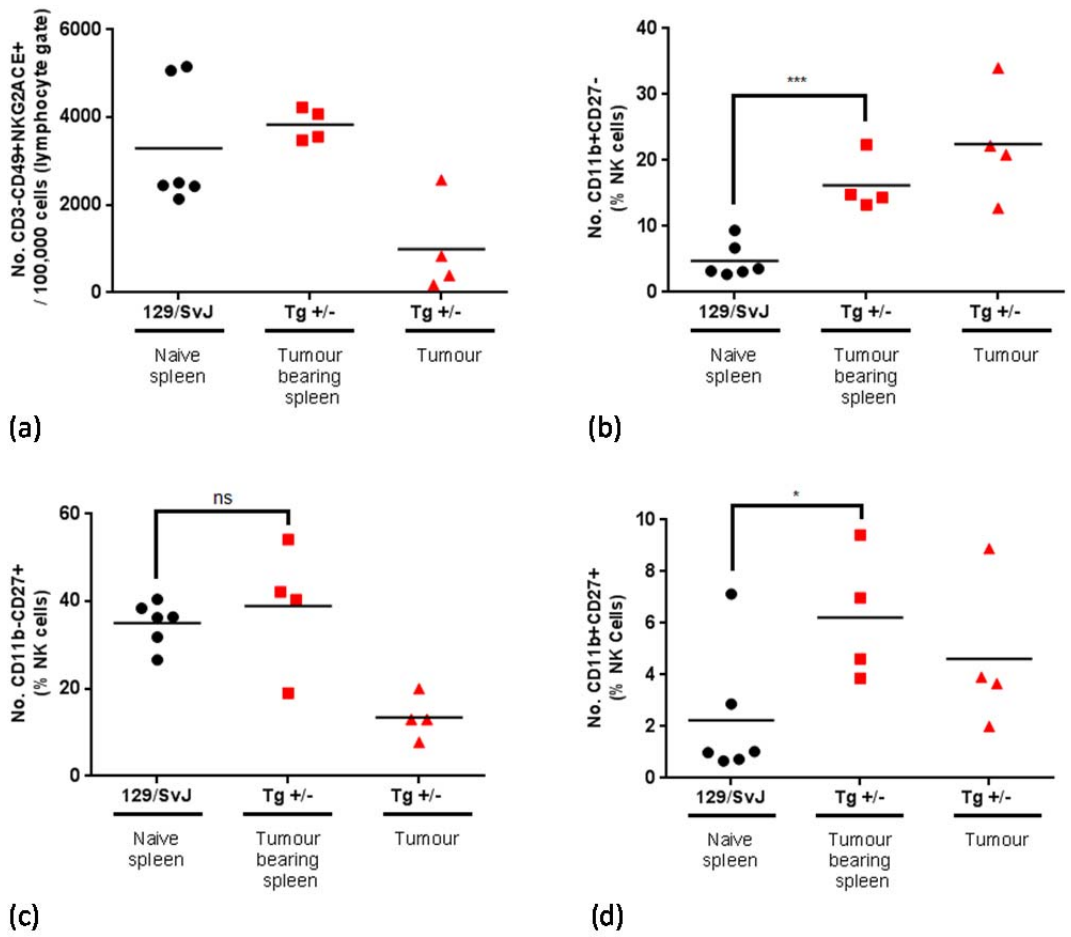

Figure 5-4. Quantification of NK cells in the tumour microenvironment and spleen of TH-MYCN transgenic +/- tumour bearing mice compared to the spleens of congenic 129/SvJ mice. The number of CD3-CD49b+NKG2ACE+ events normalised to 100,000 cells in the lymphocyte gate (a). The percentage of NK cells detected with the CD11b+CD27- phenotype (b), where *** p = 0.0007 following an unpaired t test. The percentage of NK cells detected with the CD11b-CD27+ phenotype (c), where ns = not significant following an unpaired t test. The percentage of NK cells with the CD11b+CD27+ phenotype (d), where * p = 0.0403 following an unpaired t test. Each graph shows congenic 129/SvJ mouse spleens (black circles) n = 6, TH-MYCN transgenic +/- mouse spleens (red squares) and matched tumours (red triangles) n = 4.

Figure 5.4 (a) demonstrates that tumour infiltrating NK cells make up around 1 % of the total number of cells in the lymphocyte gate. Figure 5.4 (b) shows that more than 20 % of these tumour infiltrating NK cells have a terminally differentiated (CD11b+CD27-) phenotype, Additionally, the proportion of NK cells with a terminally differentiated phenotype is significantly higher in the spleens of tumour bearing TH-MYCN transgenic +/- mice relative to congenic 129/SvJ mice. Figure 5.4 (c) shows that around 14 % of the NK cells in the tumour microenvironment have an immature CD11b-CD27+ phenotype and are therefore in the process of differentiating. Figure 5.4 (d) shows that a small proportion of the tumour infiltrating NK cells (approximately 4 %) have the more functionally active CD11b+CD27+, this subset is also significantly

increased in the spleens of the tumour bearing TH-MYCN transgenic +/- mice relative to congenic 129/SvJ mice. The remainder of the NK cells were immature CD11b-CD27-.

5.2.4.2 Tumour infiltrating T cells

The T cell panel comprised of fluorescently conjugated antibodies specific for the following surface antigens CD3; TCRβ; TCRγδ; CD8; CD62L; CD44. Murine T cells were characterised as CD3+ as previously shown in 4.2, this population was subsequently assessed for surface expression of TCRβ, or γδ. The CD3+TCRβ+ cells were subsequently analysed for CD8 and cells that CD3+TCRβ+CD8- were assumed to be CD4+, as shown in figure 4.6. The CD3+TCRβ+CD8-(CD4+) and CD8+ T cell subsets were then analysed for surface expression of CD62L and CD44 to enumerate both effector memory and central memory T cell subsets. Figure 5.5 illustrates the T cell subsets that could be identified using this panel of antibodies.

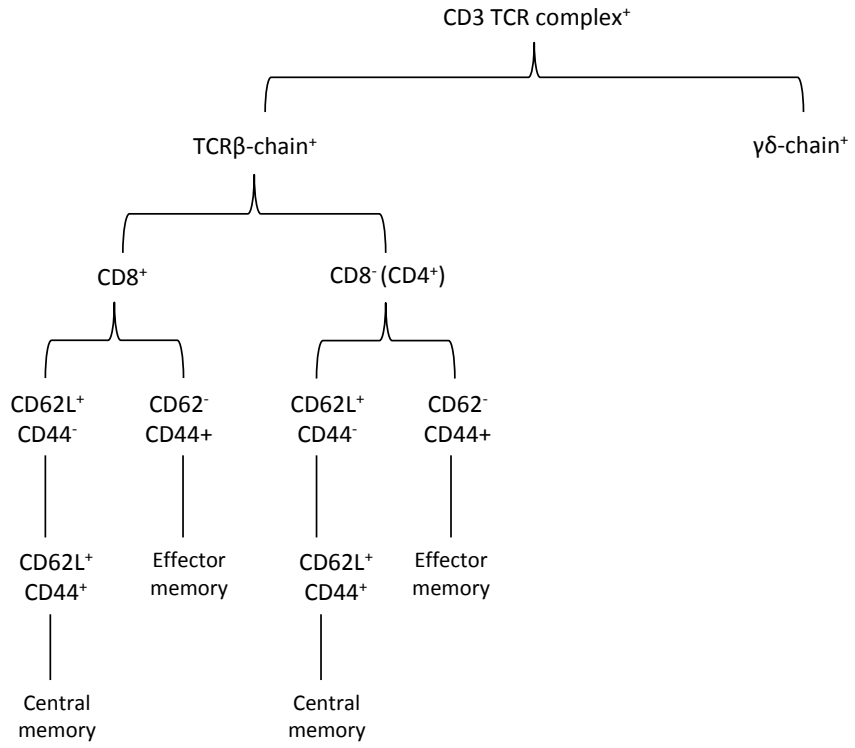

Figure 5-5. The T cell subsets that could be identified using the multi-colour T cell antibody panel.

The CD3+ T cells were initially characterised as CD3+TCRβ+ T cells and CD3+TCR γδT cells as shown in figure 5.6.

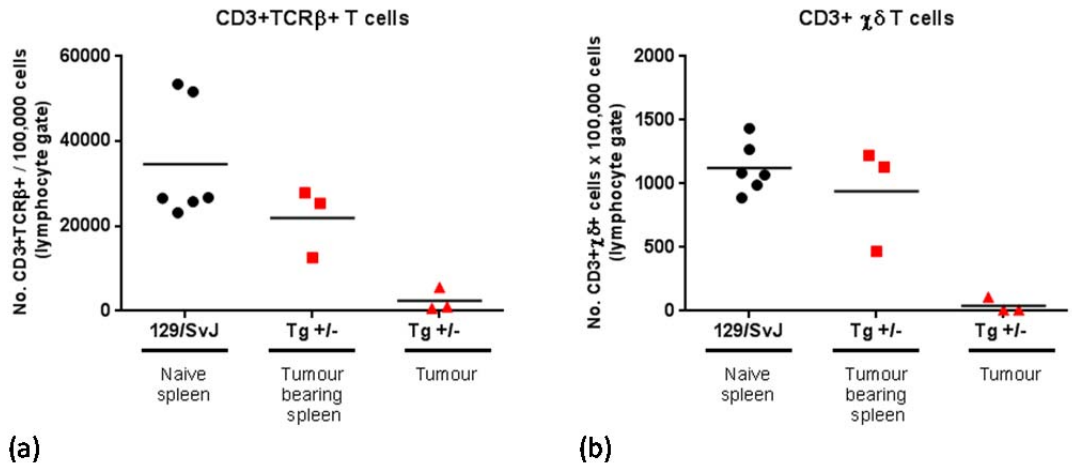

Figure 5-6. Quantification of TCRβ and TCR γδ T cells in the tumour microenvironment and spleen of TH-MYCN transgenic +/- tumour bearing mice compared to the spleens of congenic 129/SvJ mice. The number of CD3+TCRβ+ events normalised to 100,000 cells in the lymphocyte gate (a). The number of CD3+TCRγδ+ events normalised to 100,000 cells in the lymphocyte gate (b). Each graph shows congenic 129/SvJ mouse spleens (black circles) n = 6, TH-MYCN transgenic +/- mouse spleens (red squares) and matched tumours (red triangles) n = 3.

Figure 5.6 (a) demonstrates that tumour infiltrating CD3+TCRβ+ T cells comprise around 3 % of the total number of cells in the lymphocyte gate and that CD3+TCRβ+ T cells appear to be reduced in spleens of tumour bearing TH-MYCN +/- transgenic mice compared to congenic 129/SvJ mice. Figure 5.6 (b) shows that TCRγδ T cells can be detected in the tumour microenvironment immune infiltrate but they comprise less than 0.05 % of the total population in the lymphocyte gate and make up about 1 % of the cells in the lymphocyte gate in the spleens of both tumour bearing TH-MYCN +/- transgenic mice and congenic 129/SvJ mice.

The CD3+TCRβ+ events were subsequently divided into the CD8- (the majority of which were assumed to be CD4+) and CD8+ subsets and assessed for surface expression on CD62L and CD44, based on the expression of these surface markers the T cells were characterised as CD62+CD44-, effector memory, or central memory, as demonstrated in figure 5.5. The results of this phenotypic characterisation are shown in figures 5.7 and 5.8 for the CD8-(CD4+) and CD8+ T cell respectively. In each sample approximately 10 % of the CD8-(CD4+) and CD8+ T cells were characterised as CD62L- and CD44-. Due to the low number of γδ T cells this subset was not subjected to further analysis.

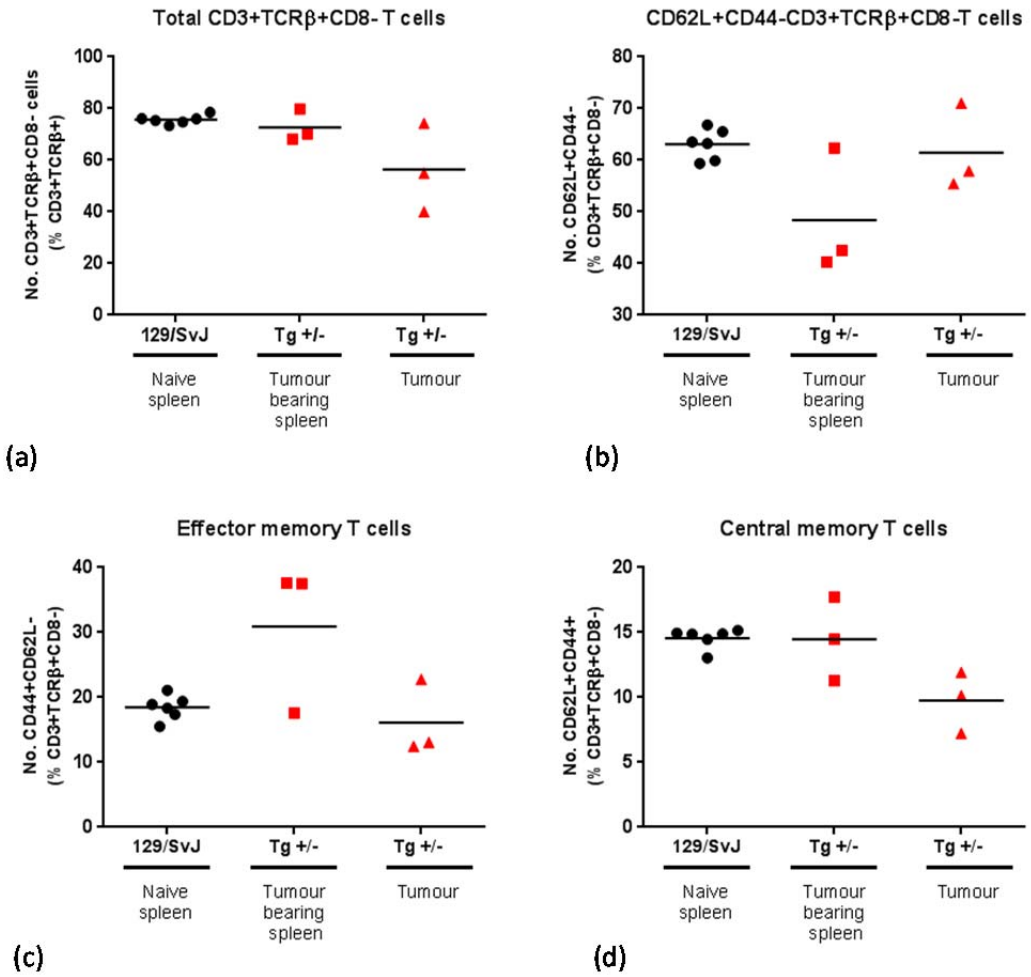

Figure 5-7. Quantification of CD8-(CD4+) T cells in the tumour microenvironment and spleen of TH-MYCN transgenic +/- tumour bearing mice compared to the spleens of congenic 129/SvJ mice. The number of CD8-(CD4+) cells as a percent of the total number of CD3+TCRβ+ T cells (a). CD62L+CD44-CD8-(CD4+) T cells as a percentage of the total CD8- T cells (b). Effector memory CD8-(CD4+) T cells as a percentage of the total CD8- T cells (c). Central memory CD8-(CD4+) T cells as a percentage total CD8- T cells. Each graph shows congenic 129/SvJ mouse spleens (black circles) n = 6, TH-MYCN transgenic +/- mouse spleens (red squares) and matched tumours (red triangles) n = 3.

Figure 5.7 (b) shows that around 60 % of the CD8-(CD4+) T cells that can be detected in the tumour microenvironment of TH-MYCN +/- transgenic mice have a CD62L+CD44- phenotype and correspondingly these mice have fewer CD62LCD44-CD8-(CD4+) T cells in the spleen when compared to congenic 129/SvJ mice. Both effector memory (figure 5.7 c) and central memory (figure 5.7 d) CD8-(CD4+) subsets can also be detected in the tumour microenvironment, and tumour bearing TH-MYCN +/- transgenic mice appear to have a higher percentage of effector memory CD8-(CD4+) T cells in the spleen compared to congenic 129/SvJ.

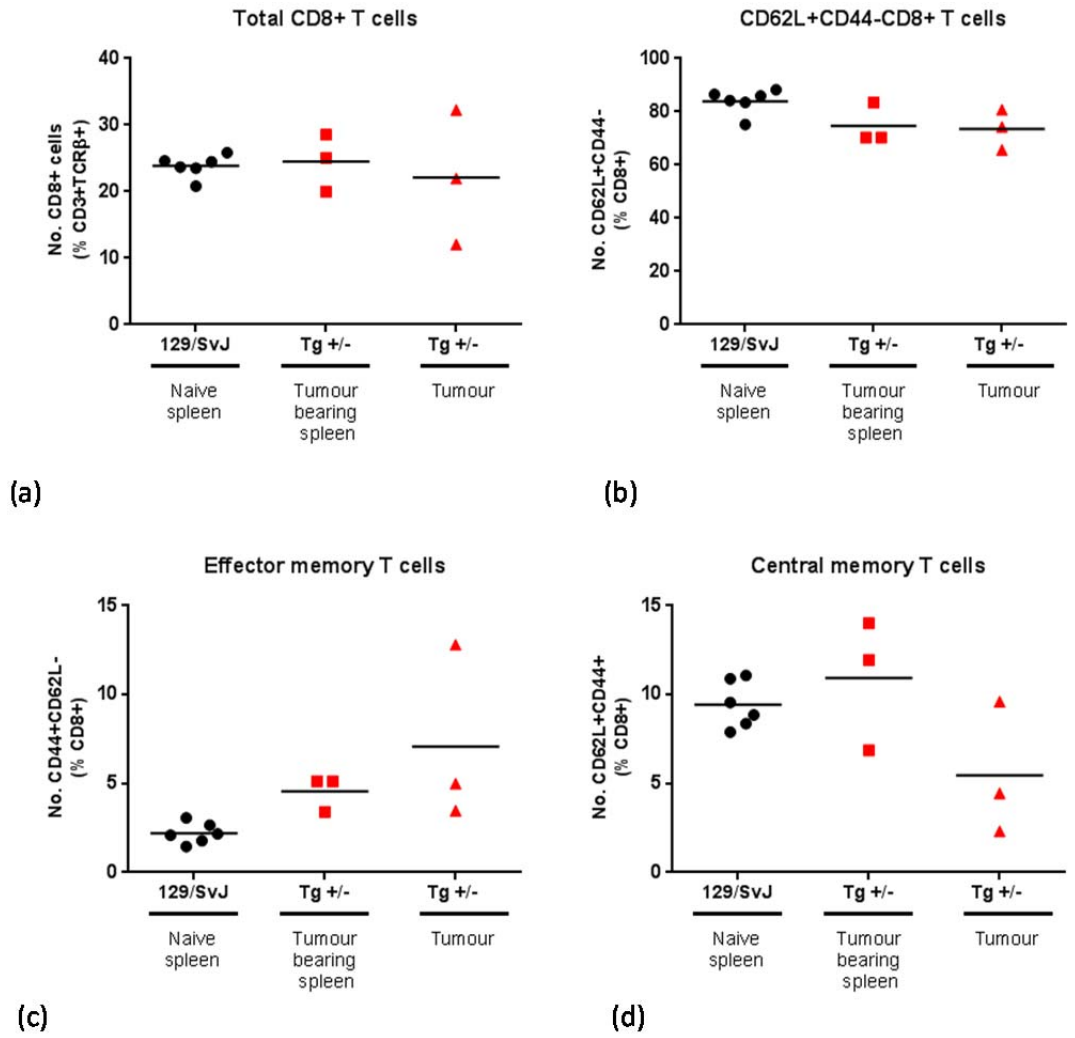

Figure 5-8. Quantification of CD8+ T cells in the tumour microenvironment and spleen of TH-MYCN transgenic +/- tumour bearing mice compared to the spleens of congenic 129/SvJ mice. The number of CD8+ cells as a percent of the total number of CD3+TCRβ+ T cells (a). CD62+CD44-CD8+ T cells as a percentage of the total CD8+ T cells (b). Effector memory CD8+ T cells as a percentage of the total CD8+ T cells (c). Central memory CD8+ T cells as a percentage total CD8+ T cells. Each graph shows congenic 129/SvJ mouse spleens (black circles) n = 6, TH-MYCN transgenic +/- mouse spleens (red squares) and matched tumours (red triangles) n = 3.

Figure 5.8 (b) shows that around 80 % of the CD8+ T cells that can be detected in the tumour microenvironment of TH-MYCN +/- transgenic mice have a CD62L+CD44- phenotype and these mice have slightly less CD62L+CD44- CD8+ T cells in the spleen when compared to congenic 129/SvJ mice. Both effector memory (figure 5.8 c) and central memory (figure 5.8 d) CD8+ subsets can also be detected in the tumour microenvironment, and tumour bearing TH-MYCN +/- transgenic mice appear to have a higher percentage of both memory CD4+ T cells in the spleen compared to congenic 129/SvJ. However, ideally further tumour and spleen samples need to be assessed using the T cell antibody panel to confirm these observations and facilitate statistical analysis.

5.2.4.3 Tumour infiltrating Tregs

Tumour infiltrating Tregs were also assessed in the TH-MYCN +/- transgenic mice. Figure 5.9 illustrates the Treg population as a percentage of the CD4+ T cells in tumour microenvironment and spleens of TH-MYCN +/- transgenic mice relative to congenic 129/SvJ spleens.

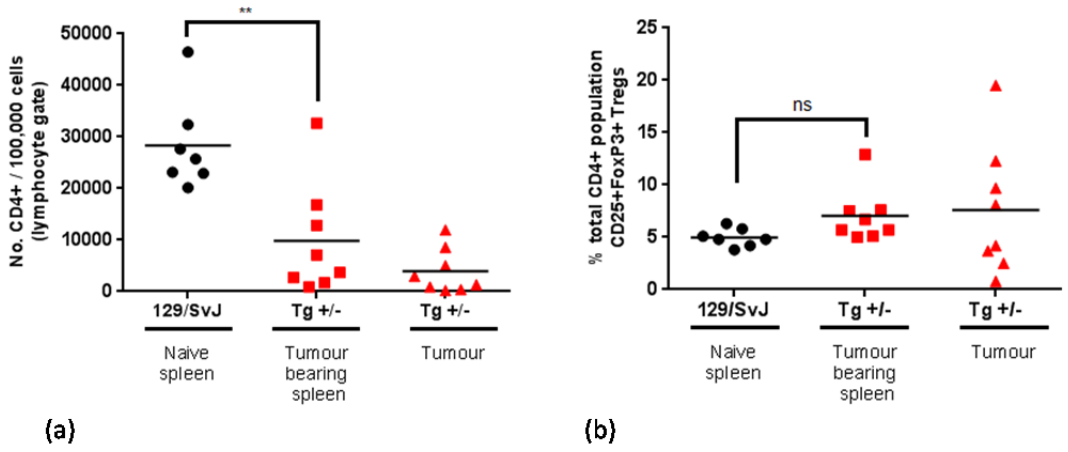

Figure 5-9. Quantification of Tregs in the tumour microenvironment and spleen of TH-MYCN transgenic +/- tumour bearing mice compared to the spleens of congenic 129/SvJ mice. The number of CD4+ cells as per 100,000 events in the lymphocyte gate (a), ** p = 0.0033 following an unpaired t test. The percentage of these CD4+ T cells that possess the CD25+FoxP3 Treg phenotype (b), where ns = not significant following an unpaired t test. Each graph shows congenic 129/SvJ mouse spleens (black circles) n = 7, TH-MYCN transgenic +/- mouse spleens (red squares) and matched tumours (red triangles) n = 8.

Figure 5.9 (a) shows that the number of CD4+ T cells as a percentage of the total number of cells in the lymphocyte gate is significantly reduced in the spleens of tumour bearing TH-MYCN +/- transgenic mice compared to congenic 129/SvJ and in the tumour microenvironment approximately 5 % of the cells that fall in the lymphocyte gate are CD4 %. Around 6–7 % of the CD4+ T cells in the tumour microenvironment are positive for the CD4+CD25+FoxP3+ Treg phenotype; however, there is no significant difference between the Treg populations (as a percentage of the CD4+ Tcells) in the spleens of tumour bearing TH-MYCN +/- transgenic mice compared to congenic 129/SvJ mice.

5.2.5 Establishing a model of MRD in TH-MYCN +/- transgenic tumour bearing mice

In the clinical setting anti-GD2 mAb based therapies are only administered once the bulk of the tumour has been eradicated by surgery, chemotherapy

and/ or radiotherapy *i.e.* in the MRD setting in order to maintain disease remission and reduced the risk of relapse. Therefore to investigate anti-GD2 mAb based therapeutic strategies in a setting that more closely recapitulates MRD it was first necessary to reduce the bulk of the tumour. To achieve this it was necessary to identify a sub-optimal dose of chemotherapy, which when administered to tumour bearing TH-MYCN +/- transgenic mice would be sufficient to reduce tumour burden without being curative, thus creating a therapeutic window during which time immunotherapy could be administered. The chemotherapeutic agent of choice was cyclophosphamide, based on published data that demonstrates the susceptibility of TH-MYCN transgenic mouse tumours to this drug (287) and the potential for beneficial immune effects, such as Treg depletion (288, 289). Upon tumour presentation TH-MYCN +/- transgenic mice were treated with varying doses of cyclophosphamide and monitored closely for signs of re-presentation. A Kaplan-Meier plot demonstrating time to tumour re-presentation in TH-MYCN +/- transgenic treated with cyclophosphamide is shown in figure 5.10

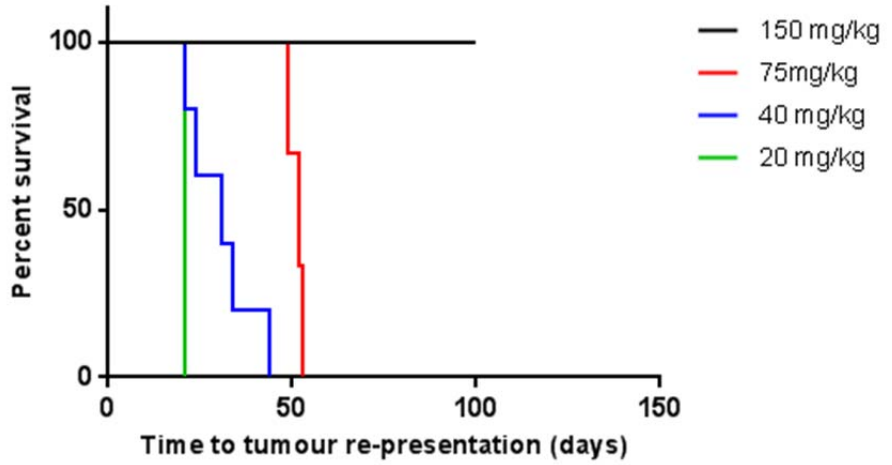

Figure 5-10. Kaplan-Meier curve of tumour bearing TH-MYCN +/- transgenic mice following treatment with various doses of cyclophosphamide. Upon presentation with palpable tumour mice were treated (i.p.) with cyclophosphamide ranging from 150 to 20 mg/kg and monitored for tumour regression and subsequent re-presentation, where n = 2 (150 mg/kg), n = 3 (75 mg/kg), n = 5 (40 mg/kg) and n = 1 (20 mg/kg).

Figure 5.10 shows that when cyclophosphamide was administered as single dose of 150 mg/kg (one third of the reported curative dose (287)), mice survived in excess of 100 days. The dose was subsequently reduced to 75, then 40 and finally 20 mg/kg. The sub-optimal dose taken forward was 40 mg/kg as on average mice survived one month prior to re-presenting and

ultimately succumbing to their tumour burden, providing a suitable therapeutic window for the administration of immunotherapy and sufficient time to extend survival before the 100 day cut off.

5.2.6 Testing the effect of anti-GD2 mAb +/- anti-4-1BB with and without cyclophosphamide pre-treatment

A pilot study was performed to determine whether anti-GD2 mAb +/- anti-4-1BB would be effective at pro-longing survival of tumour bearing TH-MYCN +/- transgenic mice and establish proof of principle for this combinatorial approach in a MRD setting. Each antibody was tested both alone and in combination with cyclophosphamide. Figure 5.11 is a series of Kaplan-Meier curves demonstrating survival of tumour bearing mice following treatment with cyclophosphamide (CPM) alone, the anti GD2 mAb 14G2a alone, the anti-4-1BB mAb LOB12.3 alone, or combinations thereof.

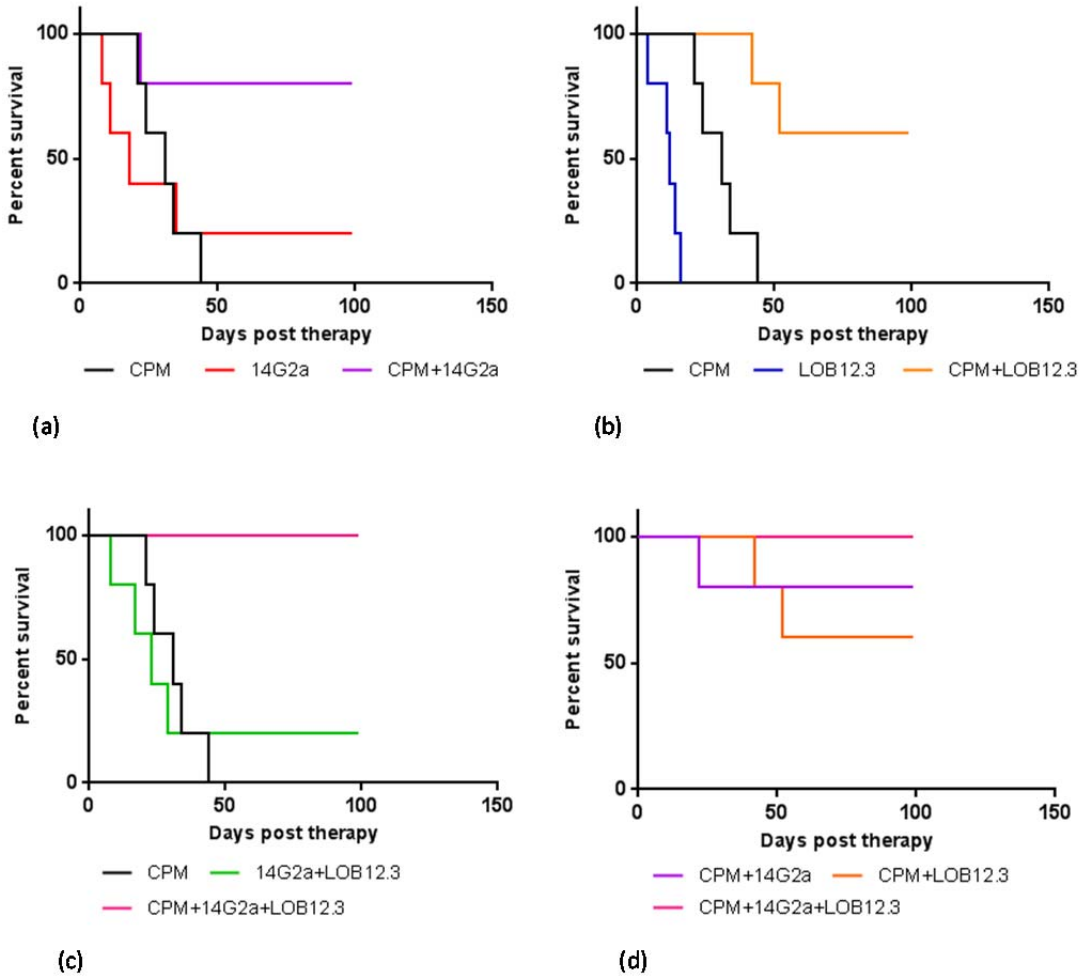

Figure 5-11. Kaplan-Meier curve for tumour bearing TH-MYCN +/- transgenic mice following treatment with cyclophosphamide (CPM) alone, anti-GD2 (14G2a) alone, or anti-4-1BB (LOB12.3), or combinations thereof. Upon presentation with palpable tumour mice were treated (i.p.) with either 40/mg/kg CPM alone, or 150 µg mAb as described and subsequently monitored for tumour regression and re-presentation. Where n = 5 per group and survival was by Log rank tests. Mice received CPM, or 14G2a, or CPM followed by 14G2a 24-hours later (a), where CPM vs 14G2a not significant, CPM vs CPM+14G2a * p = 0.0269 and CPM+14G2a vs 14G2a * p = 0.0127; Mice received CPM, or LOB12.3, or CPM followed by LOB12.3 24-hours later (b), where CPM vs LOB12.3 ** p = 0.0018, CPM vs CPM+LOB12.3 * p = 0.0064 and CPM+LOB12.3 vs LOB12.3 * p = 0.0018;Mice received CPM alone, CPM + 14G2a followed by LOB12.3 24 hours later, or 14G2a alone followed by LOB12.3 24-hours later (c), where CPM vs 14G2a+LOB12.3 not significant, CPM vs CPM+14G2a+LOB12.3 ** p = 0.0018 and CPM+14G2a+LOB12.3 vs 14G2a+LOB12.3 ** p = 0.0133; Combined data obtained for mice receiving CPM + 14G2a, or CPM + LOB12.3, or CPM + 14G2a + LOB12.3 (d), where ns = not significant.

Figure 5.11 (a) shows that the combination of CPM+14G2a was more effective than either agent when administered alone, with 80 % of tumour bearing mice treated surviving 100 days without re-presentation of tumour, as confirmed by autopsy. However, there was no significant difference in survival between mice treated with CPM alone and those treated with 14G2a, with 100 % and 80 % of mice re-presenting and succumbing to tumour respectively. Figure 5.11 (b) shows that the combination of CPM+LOB12.3 was more effective than either

agent when administered alone, with 60 % of tumour bearing mice treated surviving 100 days without re-presentation of tumour, as confirmed by autopsy. Additionally mice treated with CPM alone survived significantly longer than mice treated with LOB12.3 alone, although 100 % of mice in each group eventually re-presented with and succumbed to tumour. Figure 5.11 (c) shows that the combination of CPM+14G2a+LOB12.3 was more effective than either CPM or 14G2a+LOB12.3 when administered alone. CPM+14G2a+LOB12.3 was the most effective therapy combination with 100 % of mice tumour bearing mice treated surviving 100 days without re-presentation of tumour, as confirmed by autopsy. However, there was no significant difference in survival between mice treated with CPM alone and those treated with 14G2a+LOB12.3, with 100 % and 80 % of mice re-presenting and succumbing to tumour respectively. Finally, figure 5.11 (d) compares the effect of CPM+14G2a, CPM+LOB12.3 and CPM+14G2a+LOB12.3, confirming that in a situation whereby mice have been pre-treated with cyclophosphamide in order to recapitulate the MRD setting the combined mAb therapy 14G2a+LOB12.3 is the most effective with 100 % mice surviving 100 days post mAb treatment.

5.3 Chapter discussion

The TH-MYCN transgenic mouse model is considered to be one of the most useful pre-clinical models of neuroblastoma (282) but little has been explored in the context of immunotherapy. However, the initial characterisation work presented in this chapter confirms that the TH-MYCN transgenic mouse model shows considerable promise as a candidate model for the study of immunotherapy. Around 50 % of TH-MYCN +/- transgenic mice housed in this facility develop tumour within 60–100 days of birth, allowing them sufficient time to develop a fully competent immune system. In our hands the tumour bearing mice routinely present with a palpable abdominal mass and often shown signs of adrenal gland, kidney and spinal cord involvement, thus recapitulating several features of human disease (282). The spontaneous nature of tumour development, which typically occurs within 100 days of birth, allows for the concomitant formation of the tumour microenvironment in an orthotopic location, hence the TH-MYCN tumour microenvironment is potentially more physiologically relevant than the microenvironment formed alongside subcutaneous tumours in the syngeneic NXS2 model.

Flow cytometry assessment has confirmed that it is possible to recover several tumour-infiltrating lymphocyte subsets of clinical relevance, all of which have been reported in neuroblastoma patients. Although further tumour samples need to be assessed, particularly for the T cell panel, to establish baseline levels for these subsets. It is anticipated changes in tumour-infiltrating lymphocyte composition, for example an increase in the number of functionally mature NK cells, or the presence of higher proportions of effector memory cells, will provide a suitable end point for monitoring response to immunotherapy.

In terms of suitability for investigating anti-GD2 targeting immunotherapies the TH-MYCN tumours demonstrate comparable surface GD2 expression to NXS2 subcutaneous tumours *ex vivo*. Additionally, preliminary data suggests it is possible to simulate an MRD setting by administering sub-optimal doses of chemotherapy, thus more closely replicating the clinical setting in which anti-GD2 mAb based therapies are only administered once the bulk of the tumour has been eradicated and providing a therapeutic window within which to study anti-GD2 targeting immunotherapy. The data presented in this chapter demonstrates that administration of 40 mg/kg cyclophosphamide alone was sufficient to extend survival by approximately one month before mice succumbed to tumour, and survival was significantly enhanced when cyclophosphamide was administered in combination with anti-GD2 mAb. Eighty percent of mice receiving this combination therapy survived 100 days post-treatment at which point they were culled and found to be tumour free, as confirmed by autopsy. Interestingly, the combination of cyclophosphamide and anti-4-1BB mAb was found to have a synergistic effect in terms of survival. Agonistic anti-4-1BB mAb have been shown to eradicate tumour in a number of syngeneic murine models (230-234); however, TH-MYCN +/- transgenic mice treated with anti-4-1BB mAb alone survived on average 12 days post-treatment. Yet when administered along with the established sub-optimal dose of cyclophosphamide, 60 % of tumour bearing mice survived for 100 days post-therapy at which time they were observed to be tumour free. A possible explanation for this apparent synergy may be attributed to cyclophosphamide both in terms of its cytotoxic and potential immune effects. Cyclophosphamide is converted into its active metabolites aldophosphamide and phosphamide mustards in the liver, these metabolites bind DNA thus preventing replication and trigger cell death. Cyclophosphamide has a direct

tumoricidal effect and which may provide sufficient tumour antigen to prime an anti-tumour immune response, which is augmented by anti-4-1BB. Additionally, whilst high doses of cyclophosphamide causes lymphoablation, low doses (in the region of 20-150 mg/kg) have been shown in animal models to selectively target Tregs, inducing their apoptosis and decreasing proliferation (288, 289). The selective depletion of Tregs, which have a natural immunosuppressive activity and promote tolerance to self-antigens has been shown to promote tumour rejection in syngeneic murine models of neuroblastoma (153), therefore it is possible that the combined action of cyclophosphamide induced Treg depletion and anti-4-1BB induced T cell activation is responsible for tumour rejection and prolonged survival of these mice. The greatest therapeutic benefit was observed following administration of cyclophosphamide alongside anti-GD2 and anti-4-1BB mAb. One hundred percent of tumour bearing TH-MYCN +/- transgenic mice survived 100 days post-therapy and remained tumour free. The therapeutic effect was perhaps due to the combined action of NK cell mediated ADCC, which may have been enhanced by anti-4-1BB mAb, plus T cell activation and Treg depletion, all of which warrant investigation.

In summary the data presented in this chapter confirms that the TH-MYCN transgenic mouse model is a viable option for the study of anti-GD2 based immunotherapeutic strategies. Preliminary studies suggest that when such agents are administered alongside chemotherapy in order to more closely recapitulate the MRD setting, anti-GD2 based immunotherapeutic regimens have the potential to promote tumour rejection and significantly pro-long survival. Additionally, the endogenous nature of tumour development permits the study of a more physiologically relevant tumour microenvironment, compared to syngeneic models, and the design of meaningful immune monitoring based end points for assessing response to therapy.

Chapter 6: Final discussion and future work

6.1 Discussion

The overall aims of this investigation were two-fold, firstly I set out to explore the immune response to tumour and characterise the effector mechanisms responsible for anti-GD2 mAb therapy; secondly I set out to explore the potential of anti-GD2 plus anti-4-1BB mAb to provide a more efficacious, less toxic immunotherapeutic regimen for the treatment of high risk neuroblastoma. A thorough understanding of the effector mechanisms that may be engaged when the anti-GD2 mAb binds its target cell is crucial for the rational design of improved immunotherapeutic strategies. Although the majority of clinical trials of anti-GD2 mAb therapy have included the cytokines IL-2 and / or GM-CSF, the inclusion of these agents is associated with considerable toxicity. Moreover, these cytokines may not necessarily be the most effective means of enhancing effector function. There are likely to be multiple mechanisms that contribute to the *in vivo* efficacy and the observed therapeutic effect in patients. Consequently when looking for suitable adjuvants to enhance the efficacy of anti-GD2 mAb the most successful candidates are likely to be those with the potential to promote a range of effector mechanisms. Anti-4-1BB mAb is a particularly interesting candidate as an adjuvant for enhancing the efficacy of anti-GD2 mAb due to 4-1BB expression, either constitutive or after activation, on a range of effector subtypes, which suggests that the mAb may promote a widespread effect. These include enhanced proliferation, cytolytic activity and IFN-γ production by NK cells, increased IL-2 production by CD4+ T cells and the generation of CTL responses resulting in long term tumour-specific immunity. Anti-4-1BB mAb may prove to be less toxic that some of the cytokine based adjuvants as limited constitutive expression means the effects of such mAb will be largely limited to activated cells.

In chapter three I present mechanistic data which provides some of the first *in vitro* evidence in support of anti-GD2 mediated phagocytosis as a mechanism of action for anti-GD2 mAb driven anti-tumour activity, in addition to the well-established mechanism of NK cell mediated ADCC. Initial depletion experiments suggest that both macrophages and NK cells may contribute to

the therapeutic effect of anti-GD2 mAb in mice bearing metastatic like disease as neither depletion of macrophages nor NK cells alone was sufficient to completely abrogate therapy. Both intra-tumoral macrophages and NK cells express, or can be induced to express, 4-1BB (237) hence any anti-tumour activity these effector cells have *in vivo* may be enhanced upon administration of anti-4-1BB mAb.

In chapter four data obtained using the syngeneic NXS2 model of neuroblastoma provides the first evidence that 4-1BB up regulation is induced on tumour-infiltrating NK cells following treatment with anti-GD2 mAb. Additionally, sequential administration of anti-GD2 plus anti-4-1BB mAb can slow tumour growth and significantly, albeit modestly, increase survival compared to mice treated with either mAb alone. The applicability of this to human NK cells is then explored with the aim of ultimately translating this combinatorial approach to a novel clinical therapy. Clear 4-1BB up regulation is also observed on human NK cells, specifically the CD56dim subset thought to have the most potent cytolytic activity, following culture with anti-GD2 opsonised neuroblastoma cell lines. However, paradoxically, this appears to translate into reduced *in vitro* effector function in ADCC assays. This may be due to the observed reduction in CD16 expression by the NK cells and their potential exhaustion due to prolonged exposure to activatory stimuli in the pre-activation step. Further work is required to investigate whether NK cell cytolytic activity can be recovered by using increased effector: target ratios as reported by Levy *et al.* (237). Additionally, it might be preferential to perform the pre-activation step with non-irradiated targets to reduce the potential for exhaustion. It would also be interesting to repeat these assays with the human IgG4 anti-4-1BB mAb that is currently in clinical trials, as this is the mAb Levy *et. al*. have used for *in vitro* work throughout their investigations.

Throughout this thesis the limitations of existing murine neuroblastoma models are discussed. Many early studies employed immunodeficient human xenograft models. However, an immunocompetent model is needed to assess the multiple immunological effector mechanisms that are likely to be at play *in vivo*. Although the syngeneic NSX2 model is immunocompetent, a number of limitations were identified in this project which limits it applicability to pre-clinical assessment of anti-GD2 immunotherapies. For example low GD2 expression and poor NK effector function in A/J mice. Additionally, the rapid

kinetics of tumour growth mean that the endogenous response likely to be very different to patients, in which a spontaneous tumour has slowly grown over months. The kinetics of the model also meant it was difficult to achieve a period of stability / minimal residual disease during which an immunotherapy can be examined. Chapter 5 attempts to address these issues by exploring and developing a new model for this purpose. In recent years, the TH-MYCN model has been widely used for pre-clinical assessment of novel small molecule and chemotherapy agents, but has been relatively underexplored in the context of immunotherapy. In the first instance, I explore the endogenous immune response to tumour in these mice. I provide evidence of tumour-infiltrating NK and T cell subsets, all of which have been reported in neuroblastoma patients. As in patients, evidence of immune regulatory mechanisms, such as Tregs are observed. The TH-MYCN transgenic mice present with spontaneous tumours, which in this facility are only clinically detectable (by palpation) at relatively advanced stage. Therefore I explored how relatively low dose chemotherapy (cyclophosphamide) could be used to temporarily control tumour growth, and provide a 'window' in which immunotherapy can be explored. This may also have the advantage of favourably skewing the immune microenvironment by depleting Tregs. Having successfully established that cyclophosphamide could be used to achieve a MRD model in this way, I was able to perform preliminary experiments exploring the efficacy of anti-GD2 and anti-4-1BB, both alone and in combination. I found that the greatest therapeutic benefit was observed following administration of cyclophosphamide alongside anti-GD2 and anti-4-1BB mAb with 100 % of treated mice surviving 100 days post-therapy and remaining tumour free. Although this data is based on relatively small numbers of mice (limited by availability of mice developing spontaneous tumours), this provides exciting data to expand and hopefully take forward towards clinical translation.

6.2 Future work

6.2.1 Exploring the role of macrophages in anti-GD2 mAb therapy

The data presented in chapter three provided some *in vitro* and *in vivo* evidence to suggest that both macrophages and NK cells may contribute to the anti-tumour effects of anti-GD2 mAb therapy. As mentioned previously work in ongoing within the group to fully investigate both the role of macrophages

in anti-GD2 mAb therapy and also the influence their phenotype has on response to therapy (*i.e.* by skewing macrophages towards an M1- or M2-like phenotype and testing their ability to phagocytose neuroblastoma targets. Meanwhile, confocal microscopy is being employed to confirm the results obtained in the *in vitro* phagocytosis assays. Additional depletion experiments need to be repeated to fully investigate the relative contributions of macrophages and NK cells to anti-GD2 mAb therapy. Moreover, since neither macrophage nor NK cell depletion was sufficient to completely abrogate therapy it would be interesting to incorporate a 'double-depleted' group in this experiments.

6.2.2 Exploring the potential for the generation of secondary T cell responses.

The potential for generating long term tumour specific immunity is one of the reasons anti-4-1BB mAb is such an attractive candidate adjuvant to anti-GD2 therapy. This is an area I was eager to explore further had sufficient numbers of long term survivors been obtained. Measuring IFN-γ production by splenocytes harvested from long term survivors and stimulated with tumour antigen *in vitro* is a relatively straightforward method of investigating secondary immune responses. The data obtained so far suggests it may be difficult to obtain sufficient numbers of mice to perform these experiments using the syngeneic NXS2 model. However, there are other syngeneic models that may permit investigations into the potential for this mAb combination to promote long term CTL responses outside of the neuroblastoma setting. These include the GD2+ EL4 lymphoma model, which is syngeneic with C57Bl/6 mice, additionally we have access to a CT26 colon carcinoma cell line that has been stably transfected with GD2 and is syngeneic with Balb/c mice. These models may provide a suitable starting point for establishing proof of principle and warrant further investigation.

6.2.3 Investigation the mechanisms of action responsible for anti-GD2 plus anti-4-1BB therapy in the TH-MYCN model

The preliminary data presented in chapter five demonstrated that long term survival could be achieved when tumour bearing mice were treated with cyclophosphamide and anti-GD2 plus anti-4-1BB mAb. Cyclophosphamide has

a direct tumoricidal effect, and may provide sufficient tumour antigen to prime an anti-tumour immune response, which is augmented by anti-4-1BB, yet it also has the potential to selectively deplete Tregs at low doses. Further work is therefore required to dissect the mechanisms at play. Mice could be treated and culled at various time points to look at the effect cyclophosphamide has on tumour infiltrating Tregs. Additionally, it might be possible to look for secondary immune responses following treatment with high and low doses of cyclophosphamide plus a fixed dose of anti-4-1BB mAb therapy to test the effect of antigenic load on the generation of secondary responses. Moreover, it would be interesting to test the combination mAb therapy alongside different chemotherapeutic agents that perhaps don't confer the same immunological benefits through the depletion of Tregs. Finally, since a number of immune cell types of clinical relevance were identifiable in the tumour microenvironment of tumour bearing TH-MYCN transgenic mice it might be feasible to set up immune monitoring studies that mimic those applied in the clinical setting. This would facilitate investigation into immune responses generated following therapy, such end points would be reasonably easy to obtain (by bleeding mice at set times points pre- and post-therapy) and may have direct translational relevance that could be used to aid the design of a clinical trial in which to test this novel combinatorial approach.

Bibliography

1. International Society of Paediatric Oncology European Neuroblastoma Research Network.
2. Evans, A. E. 1980. *Advances in neuroblastoma research*. Raven Press, New York.
3. Brodeur, G. M., R. C. Seeger, A. Barrett, F. Berthold, R. P. Castleberry, G. D'Angio, B. De Bernardi, A. E. Evans, M. Favrot, A. I. Freeman, and et al. 1988. International criteria for diagnosis, staging, and response to treatment in patients with neuroblastoma. *J Clin Oncol* 6: 1874-1881.
4. Brodeur, G. M., J. Pritchard, F. Berthold, N. L. Carlsen, V. Castel, R. P. Castelberry, B. De Bernardi, A. E. Evans, M. Favrot, F. Hedborg, and et al. 1993. Revisions of the international criteria for neuroblastoma diagnosis, staging, and response to treatment. *J Clin Oncol* 11: 1466-1477.
5. Cohn, S. L., A. D. Pearson, W. B. London, T. Monclair, P. F. Ambros, G. M. Brodeur, A. Faldum, B. Hero, T. Iehara, D. Machin, V. Mosseri, T. Simon, A. Garaventa, V. Castel, and K. K. Matthay. 2009. The International Neuroblastoma Risk Group (INRG) classification system: an INRG Task Force report. *J Clin Oncol* 27: 289-297.
6. Brodeur, G. M., R. C. Seeger, M. Schwab, H. E. Varmus, and J. M. Bishop. 1984. Amplification of N-myc in untreated human neuroblastomas correlates with advanced disease stage. *Science* 224: 1121-1124.
7. Seeger, R. C., G. M. Brodeur, H. Sather, A. Dalton, S. E. Siegel, K. Y. Wong, and D. Hammond. 1985. Association of multiple copies of the N-myc oncogene with rapid progression of neuroblastomas. *N Engl J Med* 313: 1111-1116.
8. Ikeda, H., T. Iehara, Y. Tsuchida, M. Kaneko, J. Hata, H. Naito, M. Iwafuchi, N. Ohnuma, H. Mugishima, Y. Toyoda, M. Hamazaki, J. Mimaya, S. Kondo, K. Kawa, A. Okada, E. Hiyama, S. Suita, and H. Takamatsu. 2002. Experience with International Neuroblastoma Staging System and Pathology Classification. *Br J Cancer* 86: 1110-1116.
9. Rubie, H., O. Hartmann, J. Michon, D. Frappaz, C. Coze, P. Chastagner, M. C. Baranzelli, D. Plantaz, H. Avet-Loiseau, J. Benard, O. Delattre, M. Favrot, M. C. Peyroulet, A. Thyss, Y. Perel, C. Bergeron, B. Courbon-Collet, J. P. Vannier, J. Lemerle, and D. Sommelet. 1997. N-Myc gene amplification is a major prognostic factor in localized neuroblastoma: results of the French NBL 90 study. Neuroblastoma Study Group of the Societe Francaise d'Oncologie Pediatrique. *J Clin Oncol* 15: 1171-1182.
10. Perez, C. A., K. K. Matthay, J. B. Atkinson, R. C. Seeger, H. Shimada, G. M. Haase, D. O. Stram, R. B. Gerbing, and J. N. Lukens. 2000. Biologic variables in the outcome of stages I and II neuroblastoma treated with surgery as primary therapy: a children's cancer group study. *J Clin Oncol* 18: 18-26.
11. Evans, A. E., J. H. Silber, A. Shpilsky, and G. J. D'Angio. 1996. Successful management of low-stage neuroblastoma without adjuvant therapies: a comparison of two decades, 1972 through 1981 and 1982 through 1992, in a single institution. *J Clin Oncol* 14: 2504-2510.

12. Matthay, K. K., J. G. Villablanca, R. C. Seeger, D. O. Stram, R. E. Harris, N. K. Ramsay, P. Swift, H. Shimada, C. T. Black, G. M. Brodeur, R. B. Gerbing, and C. P. Reynolds. 1999. Treatment of high-risk neuroblastoma with intensive chemotherapy, radiotherapy, autologous bone marrow transplantation, and 13-cis-retinoic acid. Children's Cancer Group. *N Engl J Med* 341: 1165-1173.
13. Sidell, N. 1982. Retinoic acid-induced growth inhibition and morphologic differentiation of human neuroblastoma cells in vitro. *J Natl Cancer Inst* 68: 589-596.
14. Abemayor, E. 1992. The effects of retinoic acid on the in vitro and in vivo growth of neuroblastoma cells. *The Laryngoscope* 102: 1133-1149.
15. Reynolds, C. P., P. F. Schindler, D. M. Jones, J. L. Gentile, R. T. Proffitt, and P. A. Einhorn. 1994. Comparison of 13-cis-retinoic acid to trans-retinoic acid using human neuroblastoma cell lines. *Prog Clin Biol Res* 385: 237-244.
16. Melino, G., C. J. Thiele, R. A. Knight, and M. Piacentini. 1997. Retinoids and the control of growth/death decisions in human neuroblastoma cell lines. *Journal of neuro-oncology* 31: 65-83.
17. Zage, P. E., M. Kletzel, K. Murray, R. Marcus, R. Castleberry, Y. Zhang, W. B. London, and C. Kretschmar. 2008. Outcomes of the POG 9340/9341/9342 trials for children with high-risk neuroblastoma: a report from the Children's Oncology Group. *Pediatr Blood Cancer* 51: 747-753.
18. Pearson, A. D., C. R. Pinkerton, I. J. Lewis, J. Imeson, C. Ellershaw, and D. Machin. 2008. High-dose rapid and standard induction chemotherapy for patients aged over 1 year with stage 4 neuroblastoma: a randomised trial. *Lancet Oncol* 9: 247-256.
19. Matthay, K. K., J. B. Atkinson, D. O. Stram, M. Selch, C. P. Reynolds, and R. C. Seeger. 1993. Patterns of relapse after autologous purged bone marrow transplantation for neuroblastoma: a Childrens Cancer Group pilot study. *J Clin Oncol* 11: 2226-2233.
20. Boon, T., P. G. Coulie, and B. Van den Eynde. 1997. Tumor antigens recognized by T cells. *Immunol Today* 18: 267-268.
21. Gray, J. C., and J. A. Kohler. 2009. Immunotherapy for neuroblastoma: turning promise into reality. *Pediatr Blood Cancer* 53: 931-940.
22. Anderson, K. V., L. Bokla, and C. Nusslein-Volhard. 1985. Establishment of dorsal-ventral polarity in the Drosophila embryo: the induction of polarity by the Toll gene product. *Cell* 42: 791-798.
23. Medzhitov, R., P. Preston-Hurlburt, and C. A. Janeway, Jr. 1997. A human homologue of the Drosophila Toll protein signals activation of adaptive immunity. *Nature* 388: 394-397.
24. Rock, F. L., G. Hardiman, J. C. Timans, R. A. Kastelein, and J. F. Bazan. 1998. A family of human receptors structurally related to Drosophila Toll. *Proc Natl Acad Sci U S A* 95: 588-593.
25. Akira, S., and H. Hemmi. 2003. Recognition of pathogen-associated molecular patterns by TLR family. *Immunol Lett* 85: 85-95.
26. Jerne, N. K. 1955. The Natural-Selection Theory of Antibody Formation. *Proc Natl Acad Sci U S A* 41: 849-857.
27. Burnet, F. M. 1976. A modification of Jerne's theory of antibody production using the concept of clonal selection. *CA: a cancer journal for clinicians* 26: 119-121.
28. Edelman, G. M. 1973. Antibody structure and molecular immunology. *Science* 180: 830-840.

29. Han, W., J. Mou, J. Sheng, J. Yang, and Z. Shao. 1995. Cryo atomic force microscopy: a new approach for biological imaging at high resolution. *Biochemistry* 34: 8215-8220.
30. Nimmerjahn, F., and J. V. Ravetch. 2008. Fcgamma receptors as regulators of immune responses. *Nat Rev Immunol* 8: 34-47.
31. Nimmerjahn, F., and J. V. Ravetch. 2006. Fcgamma receptors: old friends and new family members. *Immunity* 24: 19-28.
32. Di Santo, J. P. 2006. Natural killer cell developmental pathways: a question of balance. *Annu Rev Immunol* 24: 257-286.
33. Inngjerdingen, M., L. Kveberg, C. Naper, and J. T. Vaage. 2011. Natural killer cell subsets in man and rodents. *Tissue Antigens* 78: 81-88.
34. Ljunggren, H. G., and K. Karre. 1990. In search of the 'missing self': MHC molecules and NK cell recognition. *Immunol Today* 11: 237-244.
35. Karre, K., H. G. Ljunggren, G. Piontek, and R. Kiessling. 1986. Selective rejection of H-2-deficient lymphoma variants suggests alternative immune defence strategy. *Nature* 319: 675-678.
36. Vivier, E., S. Ugolini, D. Blaise, C. Chabannon, and L. Brossay. 2012. Targeting natural killer cells and natural killer T cells in cancer. *Nat Rev Immunol* 12: 239-252.
37. Cerwenka, A., and L. L. Lanier. 2001. Natural killer cells, viruses and cancer. *Nat Rev Immunol* 1: 41-49.
38. Kim, S., J. Poursine-Laurent, S. M. Truscott, L. Lybarger, Y. J. Song, L. Yang, A. R. French, J. B. Sunwoo, S. Lemieux, T. H. Hansen, and W. M. Yokoyama. 2005. Licensing of natural killer cells by host major histocompatibility complex class I molecules. *Nature* 436: 709-713.
39. Bix, M., N. S. Liao, M. Zijlstra, J. Loring, R. Jaenisch, and D. Raulet. 1991. Rejection of class I MHC-deficient haemopoietic cells by irradiated MHC-matched mice. *Nature* 349: 329-331.
40. Liao, N. S., M. Bix, M. Zijlstra, R. Jaenisch, and D. Raulet. 1991. MHC class I deficiency: susceptibility to natural killer (NK) cells and impaired NK activity. *Science* 253: 199-202.
41. Hoglund, P., C. Ohlen, E. Carbone, L. Franksson, H. G. Ljunggren, A. Latour, B. Koller, and K. Karre. 1991. Recognition of beta 2-microglobulin-negative (beta 2m-) T-cell blasts by natural killer cells from normal but not from beta 2m- mice: nonresponsiveness controlled by beta 2m- bone marrow in chimeric mice. *Proc Natl Acad Sci U S A* 88: 10332-10336.
42. Raulet, D. H., and R. E. Vance. 2006. Self-tolerance of natural killer cells. *Nat Rev Immunol* 6: 520-531.
43. Joncker, N. T., and D. H. Raulet. 2008. Regulation of NK cell responsiveness to achieve self-tolerance and maximal responses to diseased target cells. *Immunol Rev* 224: 85-97.
44. Wu, M. F., and D. H. Raulet. 1997. Class I-deficient hemopoietic cells and nonhemopoietic cells dominantly induce unresponsiveness of natural killer cells to class I-deficient bone marrow cell grafts. *J Immunol* 158: 1628-1633.
45. Johansson, M. H., C. Bieberich, G. Jay, K. Karre, and P. Hoglund. 1997. Natural killer cell tolerance in mice with mosaic expression of major histocompatibility complex class I transgene. *J Exp Med* 186: 353-364.
46. Johansson, M. H., and P. Hoglund. 2004. Low number of H-2Dd-negative haematopoietic cells in mixed bone marrow chimeras convey in vivo tolerance to H-2Dd-negative cells but fail to prevent resistance to H-2Dd-negative leukaemia. *Scand J Immunol* 59: 71-78.

47. Chan, C. J., M. J. Smyth, and L. Martinet. 2014. Molecular mechanisms of natural killer cell activation in response to cellular stress. *Cell death and differentiation* 21: 5-14.
48. Lanier, L. L. 2008. Up on the tightrope: natural killer cell activation and inhibition. *Nat Immunol* 9: 495-502.
49. Doherty, P. C., and R. M. Zinkernagel. 1975. H-2 compatibility is required for T-cell-mediated lysis of target cells infected with lymphocytic choriomeningitis virus. *J Exp Med* 141: 502-507.
50. Bevan, M. J. 1976. Cross-priming for a secondary cytotoxic response to minor H antigens with H-2 congenic cells which do not cross-react in the cytotoxic assay. *J Exp Med* 143: 1283-1288.
51. Neefjes, J., M. L. Jongsma, P. Paul, and O. Bakke. 2011. Towards a systems understanding of MHC class I and MHC class II antigen presentation. *Nat Rev Immunol* 11: 823-836.
52. Neefjes, J. J., and H. L. Ploegh. 1988. Allele and locus-specific differences in cell surface expression and the association of HLA class I heavy chain with beta 2-microglobulin: differential effects of inhibition of glycosylation on class I subunit association. *Eur J Immunol* 18: 801-810.
53. Hughes, E. A., C. Hammond, and P. Cresswell. 1997. Misfolded major histocompatibility complex class I heavy chains are translocated into the cytoplasm and degraded by the proteasome. *Proc Natl Acad Sci U S A* 94: 1896-1901.
54. Stumptner-Cuvelette, P., and P. Benaroch. 2002. Multiple roles of the invariant chain in MHC class II function. *Biochim Biophys Acta* 1542: 1-13.
55. Heath, W. R., G. T. Belz, G. M. Behrens, C. M. Smith, S. P. Forehan, I. A. Parish, G. M. Davey, N. S. Wilson, F. R. Carbone, and J. A. Villadangos. 2004. Cross-presentation, dendritic cell subsets, and the generation of immunity to cellular antigens. *Immunol Rev* 199: 9-26.
56. Heath, W. R., and F. R. Carbone. 2001. Cross-presentation in viral immunity and self-tolerance. *Nat Rev Immunol* 1: 126-134.
57. den Haan, J. M., S. M. Lehar, and M. J. Bevan. 2000. CD8(+) but not CD8(-) dendritic cells cross-prime cytotoxic T cells in vivo. *J Exp Med* 192: 1685-1696.
58. Bachem, A., S. Guttler, E. Hartung, F. Ebstein, M. Schaefer, A. Tannert, A. Salama, K. Movassaghi, C. Opitz, H. W. Mages, V. Henn, P. M. Kloetzel, S. Gurka, and R. A. Kroczek. 2010. Superior antigen cross-presentation and XCR1 expression define human CD11c+CD141+ cells as homologues of mouse CD8+ dendritic cells. *J Exp Med* 207: 1273-1281.
59. Crozat, K., R. Guiton, V. Contreras, V. Feuillet, C. A. Dutertre, E. Ventre, T. P. Vu Manh, T. Baranek, A. K. Storset, J. Marvel, P. Boudinot, A. Hosmalin, I. Schwartz-Cornil, and M. Dalod. 2010. The XC chemokine receptor 1 is a conserved selective marker of mammalian cells homologous to mouse CD8alpha+ dendritic cells. *J Exp Med* 207: 1283-1292.
60. Jongbloed, S. L., A. J. Kassianos, K. J. McDonald, G. J. Clark, X. Ju, C. E. Angel, C. J. Chen, P. R. Dunbar, R. B. Wadley, V. Jeet, A. J. Vulink, D. N. Hart, and K. J. Radford. 2010. Human CD141+ (BDCA-3)+ dendritic cells (DCs) represent a unique myeloid DC subset that cross-presents necrotic cell antigens. *J Exp Med* 207: 1247-1260.
61. Poulin, L. F., M. Salio, E. Griessinger, F. Anjos-Afonso, L. Craciun, J. L. Chen, A. M. Keller, O. Joffre, S. Zelenay, E. Nye, A. Le Moine, F. Faure, V. Donckier, D. Sancho, V. Cerundolo, D. Bonnet, and C. Reis e Sousa.

2010. Characterization of human DNGR-1+ BDCA3+ leukocytes as putative equivalents of mouse CD8alpha+ dendritic cells. *J Exp Med* 207: 1261-1271.

62. Kovacsovics-Bankowski, M., and K. L. Rock. 1995. A phagosome-to-cytosol pathway for exogenous antigens presented on MHC class I molecules. *Science* 267: 243-246.
63. Shen, L., L. J. Sigal, M. Boes, and K. L. Rock. 2004. Important role of cathepsin S in generating peptides for TAP-independent MHC class I crosspresentation in vivo. *Immunity* 21: 155-165.
64. Saveanu, L., O. Carroll, M. Weimershaus, P. Guermonprez, E. Firat, V. Lindo, F. Greer, J. Davoust, R. Kratzer, S. R. Keller, G. Niedermann, and P. van Endert. 2009. IRAP identifies an endosomal compartment required for MHC class I cross-presentation. *Science* 325: 213-217.
65. Rodriguez, A., A. Regnault, M. Kleijmeer, P. Ricciardi-Castagnoli, and S. Amigorena. 1999. Selective transport of internalized antigens to the cytosol for MHC class I presentation in dendritic cells. *Nature cell biology* 1: 362-368.
66. Levy, F., L. Burri, S. Morel, A. L. Peitrequin, N. Levy, A. Bachi, U. Hellman, B. J. Van den Eynde, and C. Servis. 2002. The final N-terminal trimming of a subaminoterminal proline-containing HLA class I-restricted antigenic peptide in the cytosol is mediated by two peptidases. *J Immunol* 169: 4161-4171.
67. Shen, X. Z., S. Billet, C. Lin, D. Okwan-Duodu, X. Chen, A. E. Lukacher, and K. E. Bernstein. 2011. The carboxypeptidase ACE shapes the MHC class I peptide repertoire. *Nat Immunol* 12: 1078-1085.
68. Ackerman, A. L., C. Kyritsis, R. Tampe, and P. Cresswell. 2005. Access of soluble antigens to the endoplasmic reticulum can explain cross-presentation by dendritic cells. *Nat Immunol* 6: 107-113.
69. Compeer, E. B., T. W. Flinsenberg, S. G. van der Grein, and M. Boes. 2012. Antigen processing and remodeling of the endosomal pathway: requirements for antigen cross-presentation. *Frontiers in immunology* 3: 37.
70. Gromme, M., F. G. Uytdehaag, H. Janssen, J. Calafat, R. S. van Binnendijk, M. J. Kenter, A. Tulp, D. Verwoerd, and J. Neefjes. 1999. Recycling MHC class I molecules and endosomal peptide loading. *Proc Natl Acad Sci U S A* 96: 10326-10331.
71. Di Pucchio, T., B. Chatterjee, A. Smed-Sorensen, S. Clayton, A. Palazzo, M. Montes, Y. Xue, I. Mellman, J. Banchereau, and J. E. Connolly. 2008. Direct proteasome-independent cross-presentation of viral antigen by plasmacytoid dendritic cells on major histocompatibility complex class I. *Nat Immunol* 9: 551-557.
72. Hoeffel, G., A. C. Ripoche, D. Matheoud, M. Nascimbeni, N. Escriou, P. Lebon, F. Heshmati, J. G. Guillet, M. Gannage, S. Caillat-Zucman, N. Casartelli, O. Schwartz, H. De la Salle, D. Hanau, A. Hosmalin, and C. Maranon. 2007. Antigen crosspresentation by human plasmacytoid dendritic cells. *Immunity* 27: 481-492.
73. Murphy, K. T., P. Walport, M. 2008. *Janeway's Immunobiology*. Garland Science, Taylor & Francis Group, LLC, New York.
74. Smith-Garvin, J. E., G. A. Koretzky, and M. S. Jordan. 2009. T cell activation. *Annu Rev Immunol* 27: 591-619.
75. Gray, J. C., P. W. Johnson, and M. J. Glennie. 2006. Therapeutic potential of immunostimulatory monoclonal antibodies. *Clinical science* 111: 93-106.

76. Riley, J. L., and C. H. June. 2005. The CD28 family: a T-cell rheostat for therapeutic control of T-cell activation. *Blood* 105: 13-21.
77. Bertram, E. M., W. Dawicki, and T. H. Watts. 2004. Role of T cell costimulation in anti-viral immunity. *Semin Immunol* 16: 185-196.
78. Suresh, M., J. K. Whitmire, L. E. Harrington, C. P. Larsen, T. C. Pearson, J. D. Altman, and R. Ahmed. 2001. Role of CD28-B7 interactions in generation and maintenance of CD8 T cell memory. *J Immunol* 167: 5565-5573.
79. Gramaglia, I., A. Jember, S. D. Pippig, A. D. Weinberg, N. Killeen, and M. Croft. 2000. The OX40 costimulatory receptor determines the development of CD4 memory by regulating primary clonal expansion. *J Immunol* 165: 3043-3050.
80. Bertram, E. M., P. Lau, and T. H. Watts. 2002. Temporal segregation of 4-1BB versus CD28-mediated costimulation: 4-1BB ligand influences T cell numbers late in the primary response and regulates the size of the T cell memory response following influenza infection. *J Immunol* 168: 3777-3785.
81. Somersalo, K., N. Anikeeva, T. N. Sims, V. K. Thomas, R. K. Strong, T. Spies, T. Lebedeva, Y. Sykulev, and M. L. Dustin. 2004. Cytotoxic T lymphocytes form an antigen-independent ring junction. *J Clin Invest* 113: 49-57.
82. Monks, C. R., B. A. Freiberg, H. Kupfer, N. Sciaky, and A. Kupfer. 1998. Three-dimensional segregation of supramolecular activation clusters in T cells. *Nature* 395: 82-86.
83. Stinchcombe, J. C., G. Bossi, S. Booth, and G. M. Griffiths. 2001. The immunological synapse of CTL contains a secretory domain and membrane bridges. *Immunity* 15: 751-761.
84. Stinchcombe, J. C., E. Majorovits, G. Bossi, S. Fuller, and G. M. Griffiths. 2006. Centrosome polarization delivers secretory granules to the immunological synapse. *Nature* 443: 462-465.
85. Stemberger, C., K. M. Huster, M. Koffler, F. Anderl, M. Schiemann, H. Wagner, and D. H. Busch. 2007. A single naive CD8+ T cell precursor can develop into diverse effector and memory subsets. *Immunity* 27: 985-997.
86. Kaech, S. M., and E. J. Wherry. 2007. Heterogeneity and cell-fate decisions in effector and memory CD8+ T cell differentiation during viral infection. *Immunity* 27: 393-405.
87. Joshi, N. S., and S. M. Kaech. 2008. Effector CD8 T cell development: a balancing act between memory cell potential and terminal differentiation. *J Immunol* 180: 1309-1315.
88. Kaech, S. M., J. T. Tan, E. J. Wherry, B. T. Konieczny, C. D. Surh, and R. Ahmed. 2003. Selective expression of the interleukin 7 receptor identifies effector CD8 T cells that give rise to long-lived memory cells. *Nat Immunol* 4: 1191-1198.
89. Schluns, K. S., W. C. Kieper, S. C. Jameson, and L. Lefrancois. 2000. Interleukin-7 mediates the homeostasis of naive and memory CD8 T cells in vivo. *Nat Immunol* 1: 426-432.
90. Terabe, M., and J. A. Berzofsky. 2007. NKT cells in immunoregulation of tumor immunity: a new immunoregulatory axis. *Trends Immunol* 28: 491-496.
91. Ezekowitz, R. A., K. Sastry, P. Bailly, and A. Warner. 1990. Molecular characterization of the human macrophage mannose receptor: demonstration of multiple carbohydrate recognition-like domains and phagocytosis of yeasts in Cos-1 cells. *J Exp Med* 172: 1785-1794.

92. Peiser, L., P. J. Gough, T. Kodama, and S. Gordon. 2000. Macrophage class A scavenger receptor-mediated phagocytosis of Escherichia coli: role of cell heterogeneity, microbial strain, and culture conditions in vitro. *Infect Immun* 68: 1953-1963.
93. Flannagan, R. S., V. Jaumouille, and S. Grinstein. 2012. The cell biology of phagocytosis. *Annual review of pathology* 7: 61-98.
94. Chekeni, F. B., and K. S. Ravichandran. 2011. The role of nucleotides in apoptotic cell clearance: implications for disease pathogenesis. *Journal of molecular medicine* 89: 13-22.
95. Kobayashi, N., P. Karisola, V. Pena-Cruz, D. M. Dorfman, M. Jinushi, S. E. Umetsu, M. J. Butte, H. Nagumo, I. Chernova, B. Zhu, A. H. Sharpe, S. Ito, G. Dranoff, G. G. Kaplan, J. M. Casasnovas, D. T. Umetsu, R. H. Dekruyff, and G. J. Freeman. 2007. TIM-1 and TIM-4 glycoproteins bind phosphatidylserine and mediate uptake of apoptotic cells. *Immunity* 27: 927-940.
96. Park, D., A. C. Tosello-Trampont, M. R. Elliott, M. Lu, L. B. Haney, Z. Ma, A. L. Klibanov, J. W. Mandell, and K. S. Ravichandran. 2007. BAI1 is an engulfment receptor for apoptotic cells upstream of the ELMO/Dock180/Rac module. *Nature* 450: 430-434.
97. Park, S. Y., M. Y. Jung, H. J. Kim, S. J. Lee, S. Y. Kim, B. H. Lee, T. H. Kwon, R. W. Park, and I. S. Kim. 2008. Rapid cell corpse clearance by stabilin-2, a membrane phosphatidylserine receptor. *Cell death and differentiation* 15: 192-201.
98. Whiteside, T. L. 2010. Immune responses to malignancies. *J Allergy Clin Immunol* 125: S272-283.
99. Renkvist, N., C. Castelli, P. F. Robbins, and G. Parmiani. 2001. A listing of human tumor antigens recognized by T cells. *Cancer Immunol Immunother* 50: 3-15.
100. Novellino, L., C. Castelli, and G. Parmiani. 2005. A listing of human tumor antigens recognized by T cells: March 2004 update. *Cancer Immunol Immunother* 54: 187-207.
101. Dunn, G. P., A. T. Bruce, H. Ikeda, L. J. Old, and R. D. Schreiber. 2002. Cancer immunoediting: from immunosurveillance to tumor escape. *Nat Immunol* 3: 991-998.
102. Burnet, F. M. 1970. The concept of immunological surveillance. *Prog Exp Tumor Res* 13: 1-27.
103. Dunn, G. P., L. J. Old, and R. D. Schreiber. 2004. The three Es of cancer immunoediting. *Annu Rev Immunol* 22: 329-360.
104. Stutman, O. 1979. Chemical carcinogenesis in nude mice: comparison between nude mice from homozygous matings and heterozygous matings and effect of age and carcinogen dose. *J Natl Cancer Inst* 62: 353-358.
105. Dighe, A. S., E. Richards, L. J. Old, and R. D. Schreiber. 1994. Enhanced in vivo growth and resistance to rejection of tumor cells expressing dominant negative IFN gamma receptors. *Immunity* 1: 447-456.
106. Kaplan, D. H., V. Shankaran, A. S. Dighe, E. Stockert, M. Aguet, L. J. Old, and R. D. Schreiber. 1998. Demonstration of an interferon gamma-dependent tumor surveillance system in immunocompetent mice. *Proc Natl Acad Sci U S A* 95: 7556-7561.
107. Engel, A. M., I. M. Svane, S. Mouritsen, J. Rygaard, J. Clausen, and O. Werdelin. 1996. Methylcholanthrene-induced sarcomas in nude mice have short induction times and relatively low levels of surface MHC class I expression. *APMIS* 104: 629-639.

108. Shankaran, V., H. Ikeda, A. T. Bruce, J. M. White, P. E. Swanson, L. J. Old, and R. D. Schreiber. 2001. IFNgamma and lymphocytes prevent primary tumour development and shape tumour immunogenicity. *Nature* 410: 1107-1111.
109. Smyth, M. J., K. Y. Thia, S. E. Street, D. MacGregor, D. I. Godfrey, and J. A. Trapani. 2000. Perforin-mediated cytotoxicity is critical for surveillance of spontaneous lymphoma. *J Exp Med* 192: 755-760.
110. Smyth, M. J., K. Y. Thia, S. E. Street, E. Cretney, J. A. Trapani, M. Taniguchi, T. Kawano, S. B. Pelikan, N. Y. Crowe, and D. I. Godfrey. 2000. Differential tumor surveillance by natural killer (NK) and NKT cells. *J Exp Med* 191: 661-668.
111. Street, S. E., J. A. Trapani, D. MacGregor, and M. J. Smyth. 2002. Suppression of lymphoma and epithelial malignancies effected by interferon gamma. *J Exp Med* 196: 129-134.
112. Girardi, M., D. E. Oppenheim, C. R. Steele, J. M. Lewis, E. Glusac, R. Filler, P. Hobby, B. Sutton, R. E. Tigelaar, and A. C. Hayday. 2001. Regulation of cutaneous malignancy by gammadelta T cells. *Science* 294: 605-609.
113. Whiteside, T. L. 2008. The tumor microenvironment and its role in promoting tumor growth. *Oncogene* 27: 5904-5912.
114. Reuschenbach, M., M. von Knebel Doeberitz, and N. Wentzensen. 2009. A systematic review of humoral immune responses against tumor antigens. *Cancer Immunol Immunother* 58: 1535-1544.
115. Kiessling, R., E. Klein, and H. Wigzell. 1975. "Natural" killer cells in the mouse. I. Cytotoxic cells with specificity for mouse Moloney leukemia cells. Specificity and distribution according to genotype. *Eur J Immunol* 5: 112-117.
116. Kiessling, R., E. Klein, H. Pross, and H. Wigzell. 1975. "Natural" killer cells in the mouse. II. Cytotoxic cells with specificity for mouse Moloney leukemia cells. Characteristics of the killer cell. *Eur J Immunol* 5: 117-121.
117. Herberman, R. B., M. E. Nunn, and D. H. Lavrin. 1975. Natural cytotoxic reactivity of mouse lymphoid cells against syngeneic acid allogeneic tumors. I. Distribution of reactivity and specificity. *Int J Cancer* 16: 216-229.
118. Herberman, R. B., M. E. Nunn, H. T. Holden, and D. H. Lavrin. 1975. Natural cytotoxic reactivity of mouse lymphoid cells against syngeneic and allogeneic tumors. II. Characterization of effector cells. *Int J Cancer* 16: 230-239.
119. Kim, S., K. Iizuka, H. L. Aguila, I. L. Weissman, and W. M. Yokoyama. 2000. In vivo natural killer cell activities revealed by natural killer cell-deficient mice. *Proc Natl Acad Sci U S A* 97: 2731-2736.
120. Coca, S., J. Perez-Piqueras, D. Martinez, A. Colmenarejo, M. A. Saez, C. Vallejo, J. A. Martos, and M. Moreno. 1997. The prognostic significance of intratumoral natural killer cells in patients with colorectal carcinoma. *Cancer* 79: 2320-2328.
121. Ishigami, S., S. Natsugoe, K. Tokuda, A. Nakajo, X. Che, H. Iwashige, K. Aridome, S. Hokita, and T. Aikou. 2000. Prognostic value of intratumoral natural killer cells in gastric carcinoma. *Cancer* 88: 577-583.
122. Villegas, F. R., S. Coca, V. G. Villarrubia, R. Jimenez, M. J. Chillon, J. Jareno, M. Zuil, and L. Callol. 2002. Prognostic significance of tumor infiltrating natural killer cells subset CD57 in patients with squamous cell lung cancer. *Lung cancer* 35: 23-28.
123. Menon, A. G., C. M. Janssen-van Rhijn, H. Morreau, H. Putter, R. A. Tollenaar, C. J. van de Velde, G. J. Fleuren, and P. J. Kuppen. 2004.

Immune system and prognosis in colorectal cancer: a detailed immunohistochemical analysis. *Lab Invest* 84: 493-501.
124. Bauer, S., V. Groh, J. Wu, A. Steinle, J. H. Phillips, L. L. Lanier, and T. Spies. 1999. Activation of NK cells and T cells by NKG2D, a receptor for stress-inducible MICA. *Science* 285: 727-729.
125. Groh, V., S. Bahram, S. Bauer, A. Herman, M. Beauchamp, and T. Spies. 1996. Cell stress-regulated human major histocompatibility complex class I gene expressed in gastrointestinal epithelium. *Proc Natl Acad Sci U S A* 93: 12445-12450.
126. Groh, V., R. Rhinehart, H. Secrist, S. Bauer, K. H. Grabstein, and T. Spies. 1999. Broad tumor-associated expression and recognition by tumor-derived gamma delta T cells of MICA and MICB. *Proc Natl Acad Sci U S A* 96: 6879-6884.
127. Vetter, C. S., V. Groh, P. thor Straten, T. Spies, E. B. Brocker, and J. C. Becker. 2002. Expression of stress-induced MHC class I related chain molecules on human melanoma. *J Invest Dermatol* 118: 600-605.
128. Wolfel, T., E. Klehmann, C. Muller, K. H. Schutt, K. H. Meyer zum Buschenfelde, and A. Knuth. 1989. Lysis of human melanoma cells by autologous cytolytic T cell clones. Identification of human histocompatibility leukocyte antigen A2 as a restriction element for three different antigens. *J Exp Med* 170: 797-810.
129. Kawakami, Y., R. Zakut, S. L. Topalian, H. Stotter, and S. A. Rosenberg. 1992. Shared human melanoma antigens. Recognition by tumor-infiltrating lymphocytes in HLA-A2.1-transfected melanomas. *J Immunol* 148: 638-643.
130. van der Bruggen, P., C. Traversari, P. Chomez, C. Lurquin, E. De Plaen, B. Van den Eynde, A. Knuth, and T. Boon. 1991. A gene encoding an antigen recognized by cytolytic T lymphocytes on a human melanoma. *Science* 254: 1643-1647.
131. Nagorsen, D., C. Scheibenbogen, F. M. Marincola, A. Letsch, and U. Keilholz. 2003. Natural T cell immunity against cancer. *Clin Cancer Res* 9: 4296-4303.
132. Parmiani, G., C. Castelli, P. Dalerba, R. Mortarini, L. Rivoltini, F. M. Marincola, and A. Anichini. 2002. Cancer immunotherapy with peptide-based vaccines: what have we achieved? Where are we going? *J Natl Cancer Inst* 94: 805-818.
133. Hayakawa, Y., K. Takeda, H. Yagita, L. Van Kaer, I. Saiki, and K. Okumura. 2001. Differential regulation of Th1 and Th2 functions of NKT cells by CD28 and CD40 costimulatory pathways. *J Immunol* 166: 6012-6018.
134. Mantovani, A., T. Schioppa, C. Porta, P. Allavena, and A. Sica. 2006. Role of tumor-associated macrophages in tumor progression and invasion. *Cancer Metastasis Rev* 25: 315-322.
135. Sica, A., T. Schioppa, A. Mantovani, and P. Allavena. 2006. Tumour-associated macrophages are a distinct M2 polarised population promoting tumour progression: potential targets of anti-cancer therapy. *Eur J Cancer* 42: 717-727.
136. Hellstrom, I. E., K. E. Hellstrom, G. E. Pierce, and A. H. Bill. 1968. Demonstration of cell-bound and humoral immunity against neuroblastoma cells. *Proc Natl Acad Sci U S A* 60: 1231-1238.
137. Martin, R. F., and J. B. Beckwith. 1968. Lymphoid infiltrates in neuroblastomas: their occurrence and prognostic significance. *J Pediatr Surg* 3: 161-164.

138. Lauder, I., and W. Aherne. 1972. The significance of lymphocytic infiltration in neuroblastoma. *Br J Cancer* 26: 321-330.
139. Gambini, C., M. Conte, G. Bernini, P. Angelini, A. Pession, P. Paolucci, A. Donfrancesco, E. Veneselli, K. Mazzocco, G. P. Tonini, L. Raffaghello, C. Dominici, A. Morando, F. Negri, A. Favre, B. De Bernardi, and V. Pistoia. 2003. Neuroblastic tumors associated with opsoclonus-myoclonus syndrome: histological, immunohistochemical and molecular features of 15 Italian cases. *Virchows Archiv : an international journal of pathology* 442: 555-562.
140. Pranzatelli, M. R. 1992. The neurobiology of the opsoclonus-myoclonus syndrome. *Clinical neuropharmacology* 15: 186-228.
141. Albert, M. L., and R. B. Darnell. 2004. Paraneoplastic neurological degenerations: keys to tumour immunity. *Nat Rev Cancer* 4: 36-44.
142. Raffaghello, L., M. Conte, E. De Grandis, and V. Pistoia. 2009. Immunological mechanisms in opsoclonus-myoclonus associated neuroblastoma. *European journal of paediatric neurology : EJPN : official journal of the European Paediatric Neurology Society* 13: 219-223.
143. Kinsbourne, M. 1962. Myoclonic encephalopathy of infants. *Journal of neurology, neurosurgery, and psychiatry* 25: 271-276.
144. Rudnick, E., Y. Khakoo, N. L. Antunes, R. C. Seeger, G. M. Brodeur, H. Shimada, R. B. Gerbing, D. O. Stram, and K. K. Matthay. 2001. Opsoclonus-myoclonus-ataxia syndrome in neuroblastoma: clinical outcome and antineuronal antibodies-a report from the Children's Cancer Group Study. *Medical and pediatric oncology* 36: 612-622.
145. Stefanowicz, J., E. Izycka-Swieszewska, E. Drozynska, J. Pienczk, K. Polczynska, P. Czauderna, D. Sierota, E. Bien, T. Stachowicz-Stencel, W. Kosiak, and A. Balcerska. 2008. Neuroblastoma and opsoclonus-myoclonus-ataxia syndrome--clinical and pathological characteristics. *Folia neuropathologica / Association of Polish Neuropathologists and Medical Research Centre, Polish Academy of Sciences* 46: 176-185.
146. Andersen, M. H., I. M. Svane, J. C. Becker, and P. T. Straten. 2007. The universal character of the tumor-associated antigen survivin. *Clin Cancer Res* 13: 5991-5994.
147. Coughlin, C. M., M. D. Fleming, R. G. Carroll, B. R. Pawel, M. D. Hogarty, X. Shan, B. A. Vance, J. N. Cohen, S. Jairaj, E. M. Lord, M. H. Wexler, G. A. Danet-Desnoyers, J. L. Pinkus, G. S. Pinkus, J. M. Maris, S. A. Grupp, and R. H. Vonderheide. 2006. Immunosurveillance and survivin-specific T-cell immunity in children with high-risk neuroblastoma. *J Clin Oncol* 24: 5725-5734.
148. Lampson, L. A., C. A. Fisher, and J. P. Whelan. 1983. Striking paucity of HLA-A, B, C and beta 2-microglobulin on human neuroblastoma cell lines. *J Immunol* 130: 2471-2478.
149. Metelitsa, L. S., O. V. Naidenko, A. Kant, H. W. Wu, M. J. Loza, B. Perussia, M. Kronenberg, and R. C. Seeger. 2001. Human NKT cells mediate antitumor cytotoxicity directly by recognizing target cell CD1d with bound ligand or indirectly by producing IL-2 to activate NK cells. *J Immunol* 167: 3114-3122.
150. Robinson, B. W., R. A. Lake, D. J. Nelson, B. A. Scott, and A. L. Marzo. 1999. Cross-presentation of tumour antigens: evaluation of threshold, duration, distribution and regulation. *Immunol Cell Biol* 77: 552-558.
151. Appleman, L. J., and V. A. Boussiotis. 2003. T cell anergy and costimulation. *Immunol Rev* 192: 161-180.

152. Seeger, R. C. 2011. Immunology and immunotherapy of neuroblastoma. *Semin Cancer Biol* 21: 229-237.
153. Johnson, B. D., W. Jing, and R. J. Orentas. 2007. CD25+ regulatory T cell inhibition enhances vaccine-induced immunity to neuroblastoma. *J Immunother* 30: 203-214.
154. Pearson, K., Taylor, C, Basu, P, Mussai, F, Santilli, G, Sala, A, Anderson, J. 2012. Functionally active myeloid derived suppressor cells (MDSCs) are found within the blood of patients with neuroblastoma. In *8th NCRI Cancer Conference*, BT Convention Centre, Liverpool, UK.
155. Prigione, I., M. V. Corrias, I. Airoldi, L. Raffaghello, F. Morandi, P. Bocca, C. Cocco, S. Ferrone, and V. Pistoia. 2004. Immunogenicity of human neuroblastoma. *Ann N Y Acad Sci* 1028: 69-80.
156. Raffaghello, L., I. Prigione, I. Airoldi, M. Camoriano, I. Levreri, C. Gambini, D. Pende, A. Steinle, S. Ferrone, and V. Pistoia. 2004. Downregulation and/or release of NKG2D ligands as immune evasion strategy of human neuroblastoma. *Neoplasia* 6: 558-568.
157. Groh, V., J. Wu, C. Yee, and T. Spies. 2002. Tumour-derived soluble MIC ligands impair expression of NKG2D and T-cell activation. *Nature* 419: 734-738.
158. Salih, H. R., H. Antropius, F. Gieseke, S. Z. Lutz, L. Kanz, H. G. Rammensee, and A. Steinle. 2003. Functional expression and release of ligands for the activating immunoreceptor NKG2D in leukemia. *Blood* 102: 1389-1396.
159. Kohler, G., and C. Milstein. 1975. Continuous cultures of fused cells secreting antibody of predefined specificity. *Nature* 256: 495-497.
160. Scott, A. M., J. P. Allison, and J. D. Wolchok. 2012. Monoclonal antibodies in cancer therapy. *Cancer Immun* 12: 14.
161. Jones, P. T., P. H. Dear, J. Foote, M. S. Neuberger, and G. Winter. 1986. Replacing the complementarity-determining regions in a human antibody with those from a mouse. *Nature* 321: 522-525.
162. Iannello, A., and A. Ahmad. 2005. Role of antibody-dependent cell-mediated cytotoxicity in the efficacy of therapeutic anti-cancer monoclonal antibodies. *Cancer Metastasis Rev* 24: 487-499.
163. Riechmann, L., M. Clark, H. Waldmann, and G. Winter. 1988. Reshaping human antibodies for therapy. *Nature* 332: 323-327.
164. Marks, J. D., H. R. Hoogenboom, T. P. Bonnert, J. McCafferty, A. D. Griffiths, and G. Winter. 1991. By-passing immunization. Human antibodies from V-gene libraries displayed on phage. *J Mol Biol* 222: 581-597.
165. Winter, G., A. D. Griffiths, R. E. Hawkins, and H. R. Hoogenboom. 1994. Making antibodies by phage display technology. *Annu Rev Immunol* 12: 433-455.
166. Weiner, G. J. 2007. Monoclonal antibody mechanisms of action in cancer. *Immunol Res* 39: 271-278.
167. Masui, H., T. Moroyama, and J. Mendelsohn. 1986. Mechanism of antitumor activity in mice for anti-epidermal growth factor receptor monoclonal antibodies with different isotypes. *Cancer Res* 46: 5592-5598.
168. Nahta, R., and F. J. Esteva. 2006. Herceptin: mechanisms of action and resistance. *Cancer Lett* 232: 123-138.
169. Albanell, J., J. Codony, A. Rovira, B. Mellado, and P. Gascon. 2003. Mechanism of action of anti-HER2 monoclonal antibodies: scientific update on trastuzumab and 2C4. *Adv Exp Med Biol* 532: 253-268.

170. Berard, F., P. Blanco, J. Davoust, E. M. Neidhart-Berard, M. Nouri-Shirazi, N. Taquet, D. Rimoldi, J. C. Cerottini, J. Banchereau, and A. K. Palucka. 2000. Cross-priming of naive CD8 T cells against melanoma antigens using dendritic cells loaded with killed allogeneic melanoma cells. *J Exp Med* 192: 1535-1544.
171. Nouri-Shirazi, M., J. Banchereau, D. Bell, S. Burkeholder, E. T. Kraus, J. Davoust, and K. A. Palucka. 2000. Dendritic cells capture killed tumor cells and present their antigens to elicit tumor-specific immune responses. *J Immunol* 165: 3797-3803.
172. Hoffmann, T. K., N. Meidenbauer, G. Dworacki, H. Kanaya, and T. L. Whiteside. 2000. Generation of tumor-specific T-lymphocytes by cross-priming with human dendritic cells ingesting apoptotic tumor cells. *Cancer Res* 60: 3542-3549.
173. Hilchey, S. P., O. Hyrien, T. R. Mosmann, A. M. Livingstone, J. W. Friedberg, F. Young, R. I. Fisher, R. J. Kelleher, Jr., R. B. Bankert, and S. H. Bernstein. 2009. Rituximab immunotherapy results in the induction of a lymphoma idiotype-specific T-cell response in patients with follicular lymphoma: support for a "vaccinal effect" of rituximab. *Blood* 113: 3809-3812.
174. Cheung, N. K., U. M. Saarinen, J. E. Neely, B. Landmeier, D. Donovan, and P. F. Coccia. 1985. Monoclonal antibodies to a glycolipid antigen on human neuroblastoma cells. *Cancer Res* 45: 2642-2649.
175. Mujoo, K., D. A. Cheresh, H. M. Yang, and R. A. Reisfeld. 1987. Disialoganglioside GD2 on human neuroblastoma cells: target antigen for monoclonal antibody-mediated cytolysis and suppression of tumor growth. *Cancer Res* 47: 1098-1104.
176. Schulz, G., D. A. Cheresh, N. M. Varki, A. Yu, L. K. Staffileno, and R. A. Reisfeld. 1984. Detection of ganglioside GD2 in tumor tissues and sera of neuroblastoma patients. *Cancer Res* 44: 5914-5920.
177. Svennerholm, L., K. Bostrom, P. Fredman, B. Jungbjer, A. Lekman, J. E. Mansson, and B. M. Rynmark. 1994. Gangliosides and allied glycosphingolipids in human peripheral nerve and spinal cord. *Biochim Biophys Acta* 1214: 115-123.
178. Zhang, S., C. Cordon-Cardo, H. S. Zhang, V. E. Reuter, S. Adluri, W. B. Hamilton, K. O. Lloyd, and P. O. Livingston. 1997. Selection of tumor antigens as targets for immune attack using immunohistochemistry: I. Focus on gangliosides. *Int J Cancer* 73: 42-49.
179. Kramer, K., W. L. Gerald, B. H. Kushner, S. M. Larson, M. Hameed, and N. K. Cheung. 1998. Disialoganglioside G(D2) loss following monoclonal antibody therapy is rare in neuroblastoma. *Clin Cancer Res* 4: 2135-2139.
180. Cheung, N. K., H. Lazarus, F. D. Miraldi, C. R. Abramowsky, S. Kallick, U. M. Saarinen, T. Spitzer, S. E. Strandjord, P. F. Coccia, and N. A. Berger. 1987. Ganglioside GD2 specific monoclonal antibody 3F8: a phase I study in patients with neuroblastoma and malignant melanoma. *J Clin Oncol* 5: 1430-1440.
181. Saarinen, U. M., P. F. Coccia, S. L. Gerson, R. Pelley, and N. K. Cheung. 1985. Eradication of neuroblastoma cells in vitro by monoclonal antibody and human complement: method for purging autologous bone marrow. *Cancer Res* 45: 5969-5975.
182. Cheung, N. K., I. Y. Cheung, A. Canete, S. J. Yeh, B. Kushner, M. A. Bonilla, G. Heller, and S. M. Larson. 1994. Antibody response to murine anti-GD2 monoclonal antibodies: correlation with patient survival. *Cancer Res* 54: 2228-2233.

183. Cheresh, D. A., J. Rosenberg, K. Mujoo, L. Hirschowitz, and R. A. Reisfeld. 1986. Biosynthesis and expression of the disialoganglioside GD2, a relevant target antigen on small cell lung carcinoma for monoclonal antibody-mediated cytolysis. *Cancer Res* 46: 5112-5118.
184. Mujoo, K., T. J. Kipps, H. M. Yang, D. A. Cheresh, U. Wargalla, D. J. Sander, and R. A. Reisfeld. 1989. Functional properties and effect on growth suppression of human neuroblastoma tumors by isotype switch variants of monoclonal antiganglioside GD2 antibody 14.18. *Cancer Res* 49: 2857-2861.
185. Kowalczyk, A., M. Gil, I. Horwacik, Z. Odrowaz, D. Kozbor, and H. Rokita. 2009. The GD2-specific 14G2a monoclonal antibody induces apoptosis and enhances cytotoxicity of chemotherapeutic drugs in IMR-32 human neuroblastoma cells. *Cancer Lett* 281: 171-182.
186. Handgretinger, R., P. Baader, R. Dopfer, T. Klingebiel, P. Reuland, J. Treuner, R. A. Reisfeld, and D. Niethammer. 1992. A phase I study of neuroblastoma with the anti-ganglioside GD2 antibody 14.G2a. *Cancer Immunol Immunother* 35: 199-204.
187. Murray, J. L., J. E. Cunningham, H. Brewer, K. Mujoo, A. A. Zukiwski, D. A. Podoloff, L. P. Kasi, V. Bhadkamkar, H. A. Fritsche, R. S. Benjamin, and et al. 1994. Phase I trial of murine monoclonal antibody 14G2a administered by prolonged intravenous infusion in patients with neuroectodermal tumors. *J Clin Oncol* 12: 184-193.
188. Uttenreuther-Fischer, M. M., C. S. Huang, R. A. Reisfeld, and A. L. Yu. 1995. Pharmacokinetics of anti-ganglioside GD2 mAb 14G2a in a phase I trial in pediatric cancer patients. *Cancer Immunol Immunother* 41: 29-36.
189. Gillies, S. D., K. M. Lo, and J. Wesolowski. 1989. High-level expression of chimeric antibodies using adapted cDNA variable region cassettes. *J Immunol Methods* 125: 191-202.
190. Barker, E., B. M. Mueller, R. Handgretinger, M. Herter, A. L. Yu, and R. A. Reisfeld. 1991. Effect of a chimeric anti-ganglioside GD2 antibody on cell-mediated lysis of human neuroblastoma cells. *Cancer Res* 51: 144-149.
191. Handgretinger, R., K. Anderson, P. Lang, R. Dopfer, T. Klingebiel, M. Schrappe, P. Reuland, S. D. Gillies, R. A. Reisfeld, and D. Neithammer. 1995. A phase I study of human/mouse chimeric antiganglioside GD2 antibody ch14.18 in patients with neuroblastoma. *Eur J Cancer* 31A: 261-267.
192. Simon, T., B. Hero, A. Faldum, R. Handgretinger, M. Schrappe, D. Niethammer, and F. Berthold. 2004. Consolidation treatment with chimeric anti-GD2-antibody ch14.18 in children older than 1 year with metastatic neuroblastoma. *J Clin Oncol* 22: 3549-3557.
193. Yu, A. L., A. L. Gilman, M. F. Ozkaynak, W. B. London, S. G. Kreissman, H. X. Chen, M. Smith, B. Anderson, J. G. Villablanca, K. K. Matthay, H. Shimada, S. A. Grupp, R. Seeger, C. P. Reynolds, A. Buxton, R. A. Reisfeld, S. D. Gillies, S. L. Cohn, J. M. Maris, and P. M. Sondel. 2010. Anti-GD2 antibody with GM-CSF, interleukin-2, and isotretinoin for neuroblastoma. *N Engl J Med* 363: 1324-1334.
194. Pession, A., A. Prete, F. Locatelli, S. Pierinelli, A. L. Pession, R. Maccario, E. Magrini, B. De Bernardi, P. Paolucci, and G. Paolucci. 1998. Immunotherapy with low-dose recombinant interleukin 2 after high-dose chemotherapy and autologous stem cell transplantation in neuroblastoma. *Br J Cancer* 78: 528-533.

195. Schwinger, W., V. Klass, M. Benesch, H. Lackner, H. J. Dornbusch, P. Sovinz, A. Moser, G. Schwantzer, and C. Urban. 2005. Feasibility of high-dose interleukin-2 in heavily pretreated pediatric cancer patients. *Ann Oncol* 16: 1199-1206.
196. Slart, R., A. L. Yu, T. L. Yaksh, and L. S. Sorkin. 1997. An animal model of pain produced by systemic administration of an immunotherapeutic anti-ganglioside antibody. *Pain* 69: 119-125.
197. Xiao, W. H., A. L. Yu, and L. S. Sorkin. 1997. Electrophysiological characteristics of primary afferent fibers after systemic administration of anti-GD2 ganglioside antibody. *Pain* 69: 145-151.
198. Dutcher, J., M. B. Atkins, K. Margolin, G. Weiss, J. Clark, J. Sosman, T. Logan, F. Aronson, and J. Mier. 2001. Kidney cancer: the Cytokine Working Group experience (1986-2001): part II. Management of IL-2 toxicity and studies with other cytokines. *Med Oncol* 18: 209-219.
199. Munn, D. H., and N. K. Cheung. 1987. Interleukin-2 enhancement of monoclonal antibody-mediated cellular cytotoxicity against human melanoma. *Cancer Res* 47: 6600-6605.
200. Kushner, B. H., and N. K. Cheung. 1989. GM-CSF enhances 3F8 monoclonal antibody-dependent cellular cytotoxicity against human melanoma and neuroblastoma. *Blood* 73: 1936-1941.
201. Munn, D. H., and N. K. Cheung. 1989. Antibody-dependent antitumor cytotoxicity by human monocytes cultured with recombinant macrophage colony-stimulating factor. Induction of efficient antibody-mediated antitumor cytotoxicity not detected by isotope release assays. *J Exp Med* 170: 511-526.
202. Main, E. K., L. A. Lampson, M. K. Hart, J. Kornbluth, and D. B. Wilson. 1985. Human neuroblastoma cell lines are susceptible to lysis by natural killer cells but not by cytotoxic T lymphocytes. *J Immunol* 135: 242-246.
203. Lode, H. N., R. Xiang, T. Dreier, N. M. Varki, S. D. Gillies, and R. A. Reisfeld. 1998. Natural killer cell-mediated eradication of neuroblastoma metastases to bone marrow by targeted interleukin-2 therapy. *Blood* 91: 1706-1715.
204. Delgado, D. C., J. A. Hank, J. Kolesar, D. Lorentzen, J. Gan, S. Seo, K. Kim, S. Shusterman, S. D. Gillies, R. A. Reisfeld, R. Yang, B. Gadbaw, K. B. DeSantes, W. B. London, R. C. Seeger, J. M. Maris, and P. M. Sondel. 2010. Genotypes of NK cell KIR receptors, their ligands, and Fcgamma receptors in the response of neuroblastoma patients to Hu14.18-IL2 immunotherapy. *Cancer Res* 70: 9554-9561.
205. Venstrom, J. M., J. Zheng, N. Noor, K. E. Danis, A. W. Yeh, I. Y. Cheung, B. Dupont, R. J. O'Reilly, N. K. Cheung, and K. C. Hsu. 2009. KIR and HLA genotypes are associated with disease progression and survival following autologous hematopoietic stem cell transplantation for high-risk neuroblastoma. *Clin Cancer Res* 15: 7330-7334.
206. Tarek, N., J. B. Le Luduec, M. M. Gallagher, J. Zheng, J. M. Venstrom, E. Chamberlain, S. Modak, G. Heller, B. Dupont, N. K. Cheung, and K. C. Hsu. 2012. Unlicensed NK cells target neuroblastoma following anti-GD2 antibody treatment. *J Clin Invest* 122: 3260-3270.
207. Cheung, N. K., R. Sowers, A. J. Vickers, I. Y. Cheung, B. H. Kushner, and R. Gorlick. 2006. FCGR2A polymorphism is correlated with clinical outcome after immunotherapy of neuroblastoma with anti-GD2 antibody and granulocyte macrophage colony-stimulating factor. *J Clin Oncol* 24: 2885-2890.

208. Raffaghello, L., D. Marimpietri, G. Pagnan, F. Pastorino, E. Cosimo, C. Brignole, M. Ponzoni, and P. G. Montaldo. 2003. Anti-GD2 monoclonal antibody immunotherapy: a promising strategy in the prevention of neuroblastoma relapse. *Cancer Lett* 197: 205-209.
209. June, C. H., J. A. Ledbetter, P. S. Linsley, and C. B. Thompson. 1990. Role of the CD28 receptor in T-cell activation. *Immunol Today* 11: 211-216.
210. Kwon, B. S., and S. M. Weissman. 1989. cDNA sequences of two inducible T-cell genes. *Proc Natl Acad Sci U S A* 86: 1963-1967.
211. Kwon, B. S., C. A. Kozak, K. K. Kim, and R. T. Pickard. 1994. Genomic organization and chromosomal localization of the T-cell antigen 4-1BB. *J Immunol* 152: 2256-2262.
212. Schwarz, H., K. Arden, and M. Lotz. 1997. CD137, a member of the tumor necrosis factor receptor family, is located on chromosome 1p36, in a cluster of related genes, and colocalizes with several malignancies. *Biochemical and biophysical research communications* 235: 699-703.
213. Zhou, Z., S. Kim, J. Hurtado, Z. H. Lee, K. K. Kim, K. E. Pollok, and B. S. Kwon. 1995. Characterization of human homologue of 4-1BB and its ligand. *Immunol Lett* 45: 67-73.
214. Alderson, M. R., C. A. Smith, T. W. Tough, T. Davis-Smith, R. J. Armitage, B. Falk, E. Roux, E. Baker, G. R. Sutherland, and W. S. Din. 1994. Molecular and biological characterization of human 4-1BB and its ligand. *Eur J Immunol* 24: 2219-2227.
215. Pollok, K. E., Y. J. Kim, Z. Zhou, J. Hurtado, K. K. Kim, R. T. Pickard, and B. S. Kwon. 1993. Inducible T cell antigen 4-1BB. Analysis of expression and function. *J Immunol* 150: 771-781.
216. Vinay, D. S., and B. S. Kwon. 2011. 4-1BB signaling beyond T cells. *Cellular & molecular immunology* 8: 281-284.
217. Goodwin, R. G., W. S. Din, T. Davis-Smith, D. M. Anderson, S. D. Gimpel, T. A. Sato, C. R. Maliszewski, C. I. Brannan, N. G. Copeland, N. A. Jenkins, and et al. 1993. Molecular cloning of a ligand for the inducible T cell gene 4-1BB: a member of an emerging family of cytokines with homology to tumor necrosis factor. *Eur J Immunol* 23: 2631-2641.
218. Pollok, K. E., Y. J. Kim, J. Hurtado, Z. Zhou, K. K. Kim, and B. S. Kwon. 1994. 4-1BB T-cell antigen binds to mature B cells and macrophages, and costimulates anti-mu-primed splenic B cells. *Eur J Immunol* 24: 367-374.
219. Shuford, W. W., K. Klussman, D. D. Tritchler, D. T. Loo, J. Chalupny, A. W. Siadak, T. J. Brown, J. Emswiler, H. Raecho, C. P. Larsen, T. C. Pearson, J. A. Ledbetter, A. Aruffo, and R. S. Mittler. 1997. 4-1BB costimulatory signals preferentially induce CD8+ T cell proliferation and lead to the amplification in vivo of cytotoxic T cell responses. *J Exp Med* 186: 47-55.
220. Cannons, J. L., P. Lau, B. Ghumman, M. A. DeBenedette, H. Yagita, K. Okumura, and T. H. Watts. 2001. 4-1BB ligand induces cell division, sustains survival, and enhances effector function of CD4 and CD8 T cells with similar efficacy. *J Immunol* 167: 1313-1324.
221. Lee, H. W., S. J. Park, B. K. Choi, H. H. Kim, K. O. Nam, and B. S. Kwon. 2002. 4-1BB promotes the survival of CD8+ T lymphocytes by increasing expression of Bcl-xL and Bfl-1. *J Immunol* 169: 4882-4888.
222. Chu, N. R., M. A. DeBenedette, B. J. Stiernholm, B. H. Barber, and T. H. Watts. 1997. Role of IL-12 and 4-1BB ligand in cytokine production by CD28+ and CD28- T cells. *J Immunol* 158: 3081-3089.
223. Wen, T., J. Bukczynski, and T. H. Watts. 2002. 4-1BB ligand-mediated costimulation of human T cells induces CD4 and CD8 T cell expansion,

cytokine production, and the development of cytolytic effector function. *J Immunol* 168: 4897-4906.
224. Cooper, D., P. Bansal-Pakala, and M. Croft. 2002. 4-1BB (CD137) controls the clonal expansion and survival of CD8 T cells in vivo but does not contribute to the development of cytotoxicity. *Eur J Immunol* 32: 521-529.
225. Wilcox, R. A., K. Tamada, S. E. Strome, and L. Chen. 2002. Signaling through NK cell-associated CD137 promotes both helper function for CD8+ cytolytic T cells and responsiveness to IL-2 but not cytolytic activity. *J Immunol* 169: 4230-4236.
226. Futagawa, T., H. Akiba, T. Kodama, K. Takeda, Y. Hosoda, H. Yagita, and K. Okumura. 2002. Expression and function of 4-1BB and 4-1BB ligand on murine dendritic cells. *Int Immunol* 14: 275-286.
227. Zheng, G., B. Wang, and A. Chen. 2004. The 4-1BB costimulation augments the proliferation of CD4+CD25+ regulatory T cells. *J Immunol* 173: 2428-2434.
228. Melero, I., W. W. Shuford, S. A. Newby, A. Aruffo, J. A. Ledbetter, K. E. Hellstrom, R. S. Mittler, and L. Chen. 1997. Monoclonal antibodies against the 4-1BB T-cell activation molecule eradicate established tumors. *Nat Med* 3: 682-685.
229. Melero, I., J. V. Johnston, W. W. Shufford, R. S. Mittler, and L. Chen. 1998. NK1.1 cells express 4-1BB (CDw137) costimulatory molecule and are required for tumor immunity elicited by anti-4-1BB monoclonal antibodies. *Cell Immunol* 190: 167-172.
230. Ye, Z., I. Hellstrom, M. Hayden-Ledbetter, A. Dahlin, J. A. Ledbetter, and K. E. Hellstrom. 2002. Gene therapy for cancer using single-chain Fv fragments specific for 4-1BB. *Nat Med* 8: 343-348.
231. Taraban, V. Y., T. F. Rowley, L. O'Brien, H. T. Chan, L. E. Haswell, M. H. Green, A. L. Tutt, M. J. Glennie, and A. Al-Shamkhani. 2002. Expression and costimulatory effects of the TNF receptor superfamily members CD134 (OX40) and CD137 (4-1BB), and their role in the generation of anti-tumor immune responses. *Eur J Immunol* 32: 3617-3627.
232. Miller, R. E., J. Jones, T. Le, J. Whitmore, N. Boiani, B. Gliniak, and D. H. Lynch. 2002. 4-1BB-specific monoclonal antibody promotes the generation of tumor-specific immune responses by direct activation of CD8 T cells in a CD40-dependent manner. *J Immunol* 169: 1792-1800.
233. Kim, J. A., B. J. Averbook, K. Chambers, K. Rothchild, J. Kjaergaard, R. Papay, and S. Shu. 2001. Divergent effects of 4-1BB antibodies on antitumor immunity and on tumor-reactive T-cell generation. *Cancer Res* 61: 2031-2037.
234. Murillo, O., A. Arina, S. Hervas-Stubbs, A. Gupta, B. McCluskey, J. Dubrot, A. Palazon, A. Azpilikueta, M. C. Ochoa, C. Alfaro, S. Solano, J. L. Perez-Gracia, B. O. Oyajobi, and I. Melero. 2008. Therapeutic antitumor efficacy of anti-CD137 agonistic monoclonal antibody in mouse models of myeloma. *Clin Cancer Res* 14: 6895-6906.
235. Melero, I., S. Hervas-Stubbs, M. Glennie, D. M. Pardoll, and L. Chen. 2007. Immunostimulatory monoclonal antibodies for cancer therapy. *Nat Rev Cancer* 7: 95-106.
236. Lin, W., C. J. Voskens, X. Zhang, D. G. Schindler, A. Wood, E. Burch, Y. Wei, L. Chen, G. Tian, K. Tamada, L. X. Wang, D. H. Schulze, D. Mann, and S. E. Strome. 2008. Fc-dependent expression of CD137 on human NK cells: insights into "agonistic" effects of anti-CD137 monoclonal antibodies. *Blood* 112: 699-707.

237. Kohrt, H. E., R. Houot, M. J. Goldstein, K. Weiskopf, A. A. Alizadeh, J. Brody, A. Muller, R. Pachynski, D. Czerwinski, S. Coutre, M. P. Chao, L. Chen, T. F. Tedder, and R. Levy. 2011. CD137 stimulation enhances the antilymphoma activity of anti-CD20 antibodies. *Blood* 117: 2423-2432.
238. Kohrt, H. E., R. Houot, K. Weiskopf, M. J. Goldstein, F. Scheeren, D. Czerwinski, A. D. Colevas, W. K. Weng, M. F. Clarke, R. W. Carlson, F. E. Stockdale, J. A. Mollick, L. Chen, and R. Levy. 2012. Stimulation of natural killer cells with a CD137-specific antibody enhances trastuzumab efficacy in xenotransplant models of breast cancer. *J Clin Invest* 122: 1066-1075.
239. Kohrt, H. E., A. D. Colevas, R. Houot, K. Weiskopf, M. J. Goldstein, P. Lund, A. Mueller, I. Sagiv-Barfi, A. Marabelle, R. Lira, E. Troutner, L. Richards, A. Rajapaska, J. Hebb, C. Chester, E. Waller, A. Ostashko, W. K. Weng, L. Chen, D. Czerwinski, Y. X. Fu, J. Sunwoo, and R. Levy. 2014. Targeting CD137 enhances the efficacy of cetuximab. *J Clin Invest* 124: 2668-2682.
240. Lode, H. N., R. Xiang, N. M. Varki, C. S. Dolman, S. D. Gillies, and R. A. Reisfeld. 1997. Targeted interleukin-2 therapy for spontaneous neuroblastoma metastases to bone marrow. *J Natl Cancer Inst* 89: 1586-1594.
241. Weiss, W. A., K. Aldape, G. Mohapatra, B. G. Feuerstein, and J. M. Bishop. 1997. Targeted expression of MYCN causes neuroblastoma in transgenic mice. *EMBO J* 16: 2985-2995.
242. Brunner, K. T., J. Mauel, J. C. Cerottini, and B. Chapuis. 1968. Quantitative assay of the lytic action of immune lymphoid cells on 51-Cr-labelled allogeneic target cells in vitro; inhibition by isoantibody and by drugs. *Immunology* 14: 181-196.
243. Zaritskaya, L., M. R. Shurin, T. J. Sayers, and A. M. Malyguine. 2010. New flow cytometric assays for monitoring cell-mediated cytotoxicity. *Expert review of vaccines* 9: 601-616.
244. van Rooijen, N., and R. van Nieuwmegen. 1984. Elimination of phagocytic cells in the spleen after intravenous injection of liposome-encapsulated dichloromethylene diphosphonate. An enzyme-histochemical study. *Cell Tissue Res* 238: 355-358.
245. Van Rooijen, N., and A. Sanders. 1994. Liposome mediated depletion of macrophages: mechanism of action, preparation of liposomes and applications. *J Immunol Methods* 174: 83-93.
246. van Rooijen, N., A. Sanders, and T. K. van den Berg. 1996. Apoptosis of macrophages induced by liposome-mediated intracellular delivery of clodronate and propamidine. *J Immunol Methods* 193: 93-99.
247. Fleisch, H. A. 1997. Bisphosphonates: preclinical aspects and use in osteoporosis. *Ann Med* 29: 55-62.
248. van Rooijen, N., N. Kors, and G. Kraal. 1989. Macrophage subset repopulation in the spleen: differential kinetics after liposome-mediated elimination. *J Leukoc Biol* 45: 97-104.
249. Van Rooijen, N., N. Kors, M. vd Ende, and C. D. Dijkstra. 1990. Depletion and repopulation of macrophages in spleen and liver of rat after intravenous treatment with liposome-encapsulated dichloromethylene diphosphonate. *Cell Tissue Res* 260: 215-222.
250. Greene, L. A., W. Shain, A. Chalazonitis, X. Breakfield, J. Minna, H. G. Coon, and M. Nirenberg. 1975. Neuronal properties of hybrid neuroblastoma X sympathetic ganglion cells. *Proc Natl Acad Sci U S A* 72: 4923-4927.

251. Seeger, R. C., S. A. Rayner, A. Banerjee, H. Chung, W. E. Laug, H. B. Neustein, and W. F. Benedict. 1977. Morphology, growth, chromosomal pattern and fibrinolytic activity of two new human neuroblastoma cell lines. *Cancer Res* 37: 1364-1371.
252. Tumilowicz, J. J., W. W. Nichols, J. J. Cholon, and A. E. Greene. 1970. Definition of a continuous human cell line derived from neuroblastoma. *Cancer Res* 30: 2110-2118.
253. Wu, Z. L., E. Schwartz, R. Seeger, and S. Ladisch. 1986. Expression of GD2 ganglioside by untreated primary human neuroblastomas. *Cancer Res* 46: 440-443.
254. Alvarez-Rueda, N., A. Desselle, D. Cochonneau, T. Chaumette, B. Clemenceau, S. Leprieur, G. Bougras, S. Supiot, J. M. Mussini, J. Barbet, J. Saba, F. Paris, J. Aubry, and S. Birkle. 2011. A monoclonal antibody to O-acetyl-GD2 ganglioside and not to GD2 shows potent anti-tumor activity without peripheral nervous system cross-reactivity. *PLoS One* 6: e25220.
255. Imai, M., C. Landen, R. Ohta, N. K. Cheung, and S. Tomlinson. 2005. Complement-mediated mechanisms in anti-GD2 monoclonal antibody therapy of murine metastatic cancer. *Cancer Res* 65: 10562-10568.
256. Weischenfeldt, J., and B. Porse. 2008. Bone Marrow-Derived Macrophages (BMM): Isolation and Applications. *CSH Protoc* 2008: pdb prot5080.
257. Beers, S. A., R. R. French, H. T. Chan, S. H. Lim, T. C. Jarrett, R. M. Vidal, S. S. Wijayaweera, S. V. Dixon, H. Kim, K. L. Cox, J. P. Kerr, D. A. Johnston, P. W. Johnson, J. S. Verbeek, M. J. Glennie, and M. S. Cragg. 2010. Antigenic modulation limits the efficacy of anti-CD20 antibodies: implications for antibody selection. *Blood* 115: 5191-5201.
258. Meinhardt, K., I. Kroeger, A. Abendroth, S. Muller, A. Mackensen, and E. Ullrich. 2012. Influence of NK cell magnetic bead isolation methods on phenotype and function of murine NK cells. *J Immunol Methods* 378: 1-10.
259. Whyte, A. L., and S. C. Miller. 1998. Strain differences in natural killer cell-mediated immunity among mice: a possible mechanism for the low natural killer cell activity of A/J mice. *Immunobiology* 199: 23-38.
260. Hank, J. A., J. E. Surfus, J. Gan, P. Jaeger, S. D. Gillies, R. A. Reisfeld, and P. M. Sondel. 1996. Activation of human effector cells by a tumor reactive recombinant anti-ganglioside GD2 interleukin-2 fusion protein (ch14.18-IL2). *Clin Cancer Res* 2: 1951-1959.
261. Zhang, H., S. Zhang, N. K. Cheung, G. Ragupathi, and P. O. Livingston. 1998. Antibodies against GD2 ganglioside can eradicate syngeneic cancer micrometastases. *Cancer Res* 58: 2844-2849.
262. Kim, Y. U., T. Kinoshita, H. Molina, D. Hourcade, T. Seya, L. M. Wagner, and V. M. Holers. 1995. Mouse complement regulatory protein Crry/p65 uses the specific mechanisms of both human decay-accelerating factor and membrane cofactor protein. *J Exp Med* 181: 151-159.
263. Takizawa, H., N. Okada, and H. Okada. 1994. Complement inhibitor of rat cell membrane resembling mouse Crry/p65. *J Immunol* 152: 3032-3038.
264. Chen, S., T. Caragine, N. K. Cheung, and S. Tomlinson. 2000. Surface antigen expression and complement susceptibility of differentiated neuroblastoma clones. *Am J Pathol* 156: 1085-1091.
265. Biedler, J. L., B. A. Spengler, T. D. Chang, and R. A. Ross. 1988. Transdifferentiation of human neuroblastoma cells results in coordinate

loss of neuronal and malignant properties. *Prog Clin Biol Res* 271: 265-276.
266. Spengler, B. A., D. L. Lazarova, R. A. Ross, and J. L. Biedler. 1997. Cell lineage and differentiation state are primary determinants of MYCN gene expression and malignant potential in human neuroblastoma cells. *Oncology research* 9: 467-476.
267. Bennett, B., L. J. Old, and E. A. Boyse. 1964. The Phagocytosis of Tumor Cells in Vitro. *Transplantation* 2: 183-202.
268. Munn, D. H., and N. K. Cheung. 1990. Phagocytosis of tumor cells by human monocytes cultured in recombinant macrophage colony-stimulating factor. *J Exp Med* 172: 231-237.
269. Rushfeldt, C., B. Sveinbjornsson, R. Seljelid, and B. Smedsrod. 1999. Early events of hepatic metastasis formation in mice: role of Kupffer and NK-cells in natural and interferon-gamma-stimulated defense. *The Journal of surgical research* 82: 209-215.
270. Vieira, P., and K. Rajewsky. 1988. The half-lives of serum immunoglobulins in adult mice. *Eur J Immunol* 18: 313-316.
271. Osenga, K. L., J. A. Hank, M. R. Albertini, J. Gan, A. G. Sternberg, J. Eickhoff, R. C. Seeger, K. K. Matthay, C. P. Reynolds, C. Twist, M. Krailo, P. C. Adamson, R. A. Reisfeld, S. D. Gillies, P. M. Sondel, and G. Children's Oncology. 2006. A phase I clinical trial of the hu14.18-IL2 (EMD 273063) as a treatment for children with refractory or recurrent neuroblastoma and melanoma: a study of the Children's Oncology Group. *Clin Cancer Res* 12: 1750-1759.
272. Shusterman, S., W. B. London, S. D. Gillies, J. A. Hank, S. D. Voss, R. C. Seeger, C. P. Reynolds, J. Kimball, M. R. Albertini, B. Wagner, J. Gan, J. Eickhoff, K. B. DeSantes, S. L. Cohn, T. Hecht, B. Gadbaw, R. A. Reisfeld, J. M. Maris, and P. M. Sondel. 2010. Antitumor activity of hu14.18-IL2 in patients with relapsed/refractory neuroblastoma: a Children's Oncology Group (COG) phase II study. *J Clin Oncol* 28: 4969-4975.
273. Vacchelli, E., I. Vitale, E. Tartour, A. Eggermont, C. Sautes-Fridman, J. Galon, L. Zitvogel, G. Kroemer, and L. Galluzzi. 2013. Trial Watch: Anticancer radioimmunotherapy. *Oncoimmunology* 2: e25595.
274. Kohl, N. E., N. Kanda, R. R. Schreck, G. Bruns, S. A. Latt, F. Gilbert, and F. W. Alt. 1983. Transposition and amplification of oncogene-related sequences in human neuroblastomas. *Cell* 35: 359-367.
275. Schwab, M., K. Alitalo, K. H. Klempnauer, H. E. Varmus, J. M. Bishop, F. Gilbert, G. Brodeur, M. Goldstein, and J. Trent. 1983. Amplified DNA with limited homology to myc cellular oncogene is shared by human neuroblastoma cell lines and a neuroblastoma tumour. *Nature* 305: 245-248.
276. Bell, E., L. Chen, T. Liu, G. M. Marshall, J. Lunec, and D. A. Tweddle. 2010. MYCN oncoprotein targets and their therapeutic potential. *Cancer Lett* 293: 144-157.
277. Eilers, M., and R. N. Eisenman. 2008. Myc's broad reach. *Genes Dev* 22: 2755-2766.
278. Larsson, L. G., and M. A. Henriksson. 2010. The Yin and Yang functions of the Myc oncoprotein in cancer development and as targets for therapy. *Exp Cell Res* 316: 1429-1437.
279. Westermark, U. K., M. Wilhelm, A. Frenzel, and M. A. Henriksson. 2011. The MYCN oncogene and differentiation in neuroblastoma. *Semin Cancer Biol* 21: 256-266.
280. Murphy, D. M., P. G. Buckley, K. Bryan, S. Das, L. Alcock, N. H. Foley, S. Prenter, I. Bray, K. M. Watters, D. Higgins, and R. L. Stallings. 2009.

Global MYCN transcription factor binding analysis in neuroblastoma reveals association with distinct E-box motifs and regions of DNA hypermethylation. *PLoS One* 4: e8154.
281. Banerjee, S. A., P. Hoppe, M. Brilliant, and D. M. Chikaraishi. 1992. 5' flanking sequences of the rat tyrosine hydroxylase gene target accurate tissue-specific, developmental, and transsynaptic expression in transgenic mice. *J Neurosci* 12: 4460-4467.
282. Teitz, T., J. J. Stanke, S. Federico, C. L. Bradley, R. Brennan, J. Zhang, M. D. Johnson, J. Sedlacik, M. Inoue, Z. M. Zhang, S. Frase, J. E. Rehg, C. M. Hillenbrand, D. Finkelstein, C. Calabrese, M. A. Dyer, and J. M. Lahti. 2011. Preclinical models for neuroblastoma: establishing a baseline for treatment. *PLoS One* 6: e19133.
283. Chesler, L., and W. A. Weiss. 2011. Genetically engineered murine models--contribution to our understanding of the genetics, molecular pathology and therapeutic targeting of neuroblastoma. *Semin Cancer Biol* 21: 245-255.
284. Kim, S., K. Iizuka, H. S. Kang, A. Dokun, A. R. French, S. Greco, and W. M. Yokoyama. 2002. In vivo developmental stages in murine natural killer cell maturation. *Nat Immunol* 3: 523-528.
285. Hayakawa, Y., and M. J. Smyth. 2006. CD27 dissects mature NK cells into two subsets with distinct responsiveness and migratory capacity. *J Immunol* 176: 1517-1524.
286. Chiossone, L., J. Chaix, N. Fuseri, C. Roth, E. Vivier, and T. Walzer. 2009. Maturation of mouse NK cells is a 4-stage developmental program. *Blood* 113: 5488-5496.
287. Chesler, L., D. D. Goldenberg, R. Collins, M. Grimmer, G. E. Kim, T. Tihan, K. Nguyen, S. Yakovenko, K. K. Matthay, and W. A. Weiss. 2008. Chemotherapy-induced apoptosis in a transgenic model of neuroblastoma proceeds through p53 induction. *Neoplasia* 10: 1268-1274.
288. Ghiringhelli, F., N. Larmonier, E. Schmitt, A. Parcellier, D. Cathelin, C. Garrido, B. Chauffert, E. Solary, B. Bonnotte, and F. Martin. 2004. CD4+CD25+ regulatory T cells suppress tumor immunity but are sensitive to cyclophosphamide which allows immunotherapy of established tumors to be curative. *Eur J Immunol* 34: 336-344.
289. Lutsiak, M. E., R. T. Semnani, R. De Pascalis, S. V. Kashmiri, J. Schlom, and H. Sabzevari. 2005. Inhibition of CD4(+)25+ T regulatory cell function implicated in enhanced immune response by low-dose cyclophosphamide. *Blood* 105: 2862-2868.